Surface Chemistry of Silicon

Hanne Neergaard Waltenburg and John T. Yates, Jr.*

Surface Science Center Department of Chemistry, University of Pittsburgh, Pittsburgh, Pennsylvania 15260

Received November 15, 1994 (Revised Manuscript Received May 2, 1995)

Contents

I. Introduction 1589
II. Reconstructions of Clean Silicon Surfaces 1590
A. Si(100) 1590
B. Si(111) 1592
C. Other Si(*hkl*) Surfaces 1595
III. Hydrogen-Terminated Surfaces 1596
A. Si(100)–H 1596
B. Si(111)–H 1598
C. Decomposition and Desorption of Hydride Species 1599
IV. Group III Adsorbates 1602
A. Si(100) 1602
B. Si(111) 1603
V. Group IV Adsorbates 1604
A. Carbon and Organic Molecules 1604
B. Silicon 1606
C. Germanium 1609
VI. Group V Adsorbates 1610
A. Nitrogen-Containing Species 1610
B. Phosphorus 1615
C. Arsenic 1615
D. Antimony and Bismuth 1617
VII. Group VI Adsorbates 1618
A. Oxygen 1618
B. H_2O on Silicon Surfaces 1620
VIII. Halogens on Silicon Surfaces 1622
A. Chlorine 1622
B. Fluorine, Bromine, and Iodine 1626
C. Abstraction of Halogens by Atomic Hydrogen 1626
IX. Concluding Remarks 1626
Acknowledgments 1626
Appendix 1. Surface Science Measurement Techniques 1626
Appendix 2. Supplementary Bibliography 1628
Hydrogen 1629
Group 1 1632
Group 2 1634
Group 4 1634
Group 5 1634
Group 6 1635
Group 8 1635
Group 9 1636
Group 10 1636
Group 11 1637
Group 12 1639
Group 13 1639
Group 14 1641
Group 15 1646
Group 16 1649
Group 17 1651
Group 18 1653
Rare Earth Metals 1653
Hydrides 1654
Oxides 1657
Nitrides 1661
Phosphides 1661
Silicon Carbide 1662
Halogen Compounds 1662
Semiconductor Films 1664
Organic Molecules 1666
Silicon Compounds 1667
Salts 1669
Special Topics 1669
References 1669

I. Introduction

The surface chemistry of silicon is just beginning to be explored, with the use of modern tools of the surface scientist. Indeed, the unraveling of the surface chemistry of silicon has been one of the most significant driving forces in surface science, resulting in the award of the Nobel prize for the scanning tunneling microscope (STM) in 1986. The excitement of this development persists as the STM is applied as the ultimate probe of surface chemistry.

The understanding and control of silicon surfaces is of great importance in the production of silicon-based electronic devices as well as devices made from other semiconductor materials and constructed on silicon single crystal substrates. In addition to the control of the surface chemistry of etching, doping, and film deposition, it is important to achieve desired mesotropic structures for devices fabricated on silicon single crystal substrates. In this spatial regime, atomic level properties often dictate how this will be done, leading to miniature surface structures with quantum properties dependent on size. As continued reduction in the size of semiconductor devices takes place, surface phenomena will assume an even greater role in achieving this goal.

This review begins with the interesting structural behavior of clean silicon single crystals and then proceeds to the adsorption of elements and compounds on silicon ranging from hydrogen through group VII of the periodic table. Representative examples of the surface chemistry of elements and compounds from each group are provided, with a strong emphasis on thermal processes involving small molecules. For assistance to the reader, Appendix 1 provides a brief summary of selected surface science measurement techniques (and acronyms). In

0009-2665/95/0795-1589$15.50/0

Hanne Neergaard Waltenburg was born in Copenhagen, Denmark, in 1968. From the University of Copenhagen, she received the B.S. degree in chemistry and physics in 1989 and the M.S. degree in chemistry in 1992. She did undergraduate research on oscillating chemical reactions with F. Hynne and P. Graae-Sørensen. Her graduate work with P. J. Møller was in the field of reactions at solid surfaces, with a master thesis on ultrathin copper layers on CaO(100). During her graduate study, she received an ERASMUS (EEC) scholarship to do research for four months at the University of Aix-Marseilles, France. She is currently a Ph.D. student with Professor John T. Yates, Jr., at the University of Pittsburgh, where her research is focusing on the vibrational and thermal properties of adsorbates on semiconductor and metal surfaces.

Professor John T. Yates, Jr., began his research in surface chemistry as a graduate student at MIT. He continued this work from 1963 to 1982 at the National Bureau of Standards. In 1982 he founded the Surface Science Center at the University of Pittsburgh where he was appointed R. K. Mellon Professor. He now holds a joint appointment in the Departments of Chemistry and Physics. Work on metallic, semiconducting, and insulator surfaces is now underway using modern surface measurement techniques. His work with students and postdoctorals is focused on the use of electronic excitation to probe surface phenomena as well as the use of a range of surface vibrational spectroscopies and other methods for understanding surface processes.

addition, a categorized summary of the citations in the literature is given at the end (Appendix 2) for completeness.

II. Reconstructions of Clean Silicon Surfaces

Silicon crystals have the diamond structure, i.e. the atoms are sp^3 hybridized and bonded to four nearest neighbors in tetrahedral coordination. The covalent bonds are 2.35 Å long and each has a bond strength of 226 kJ/mol.[1] Consequently when the crystal is cut or cleaved, bonds are broken, creating dangling bonds at the surface. The number and direction of these dangling bonds will depend on the macroscopic direction of the surface normal, as shown schematically

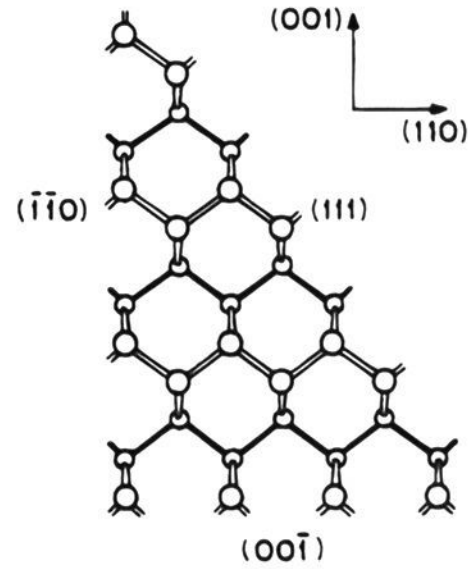

Figure 1. The dangling bond formation on the unreconstructed surfaces of the three low index planes of Si. Each Si atom in the bulk is tetrahedrally bonded to four nearest neighbors. The sizes of the Si atoms are shown to decrease away from the page.[6]

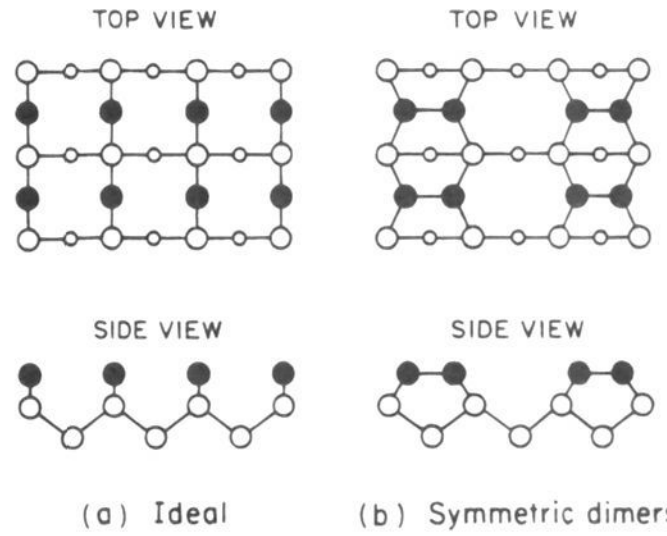

Figure 2. Top and side views of the ideal and reconstructed Si(100) surface.[6]

in Figure 1. The surface energy is lowered by reducing the number of dangling bonds by rebonding, and this leads to a wide variety of surface reconstructions on silicon surfaces. These dangling bonds are the source of the surface chemical activity of silicon surfaces. If they are capped by atomic hydrogen chemisorption, the ability of the surface to react with other potential adsorbate molecules is reduced to zero.[2]

A. Si(100)

The {100} planes have a square unit cell, and each silicon atom below the surface is bonded to two atoms in the plane below and two atoms in the plane above. The structure of the bulk-terminated surface is shown in Figure 2a. Filled circles represent the surface atoms which have two dangling bonds each, open circles represent bulk atoms, and the size of the open circles in the top view decrease with distance from the surface.

1. Nominally Flat Si(100)

The commonly accepted model for the reconstructed Si(100) surface is the dimer model. The first model of this kind was proposed by Schlier and Farnsworth on the basis of their observation of a (2×1) LEED pattern.[3] In this model the density of dangling bonds is decreased by 50% by creation of

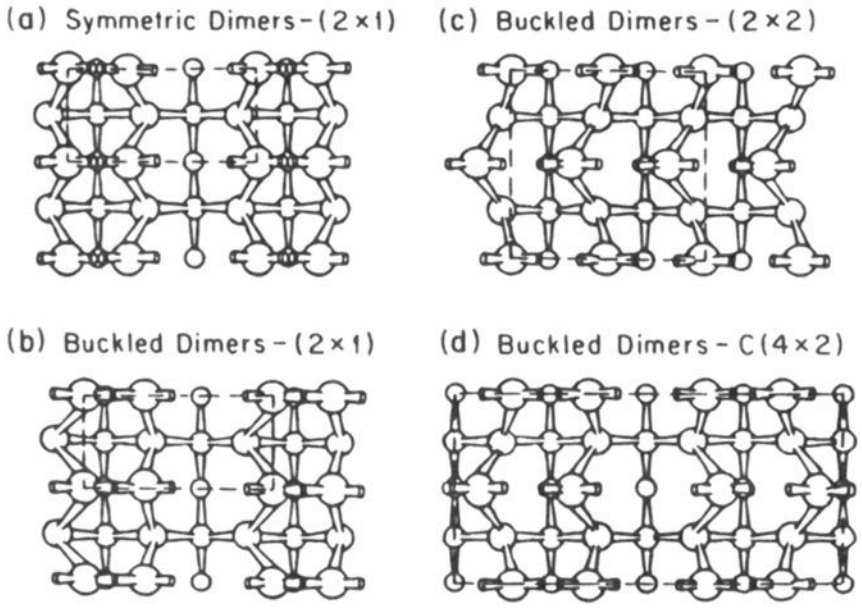

Figure 3. Schematic diagrams for the possible configurations of surface dimers on the reconstructed Si(100) surface.[6]

rows of dimers, where each surface silicon atom bonds to a neighboring atom along the [110] direction using one of its dangling bonds, as shown in Figure 2b. The original model was modified by Levine,[4] and later by Chadi,[5] who proposed that the dimers could be asymmetric. An asymmetric dimer can easily be achieved by pushing one end of the dimer down and pulling the other end up. The discussion leading to acceptance of the dimer model was reviewed by Haneman in 1987[6] together with several other models. Many experiments[7-10] and theoretical calculations[5,11-15] have been devoted to resolving the question of whether the dimers are symmetric or asymmetric (buckled) on perfect regions, and although final agreement has not been reached yet, the majority of the results point toward buckled dimers.

Depending on the relative ordering of the (buckled) dimers, different configurations are obtained as shown in Figure 3. (2×1) structures are expected for symmetric dimers (Figure 3a), and in the case of all dimers buckling in the same direction (Figure 3b). However, the additional lattice strain introduced by dimer buckling is expected to cause adjacent dimers in a row to buckle in opposite directions; two different orderings of these buckled rows are possible. If neighboring dimer rows buckle in the same direction, a local p(2×2) structure is obtained (Figure 3c), while if neighboring dimer rows buckle in opposite directions a local c(4×2) structure is obtained (Figure 3d). Recent calculations[12-15] have indeed shown that buckling lowers the surface energy. The energy is further lowered when the buckling direction alternates along a row,[13-15] and thus the c(4×2) buckled dimers (Figure 3d) were found to be lower in energy by 13.5 kJ/mol dimers relative to symmetric (2×1) dimers.[14,15]

The observation of weak quarter-order streaks in LEED[16] and in He diffraction[17] supports an ordered structure with buckled dimers as shown in Figure 3d. In addition, a phase transition from (2×1) to c(4×2) upon cooling below 200 K has been observed by LEED[18] and STM,[19] indicating that buckled dimers form the stable configuration at low temperature. Landemark et al.[10] found in a recent high-resolution photoemission study that the spectra from the room temperature (2×1) and the low temperature c(4×2) structures are very similar, suggesting that the local structure of the two phases is identical. On the basis of this observation the authors interpreted the c(4×2) to (2×1) phase transition as a loss of long-range ordering.

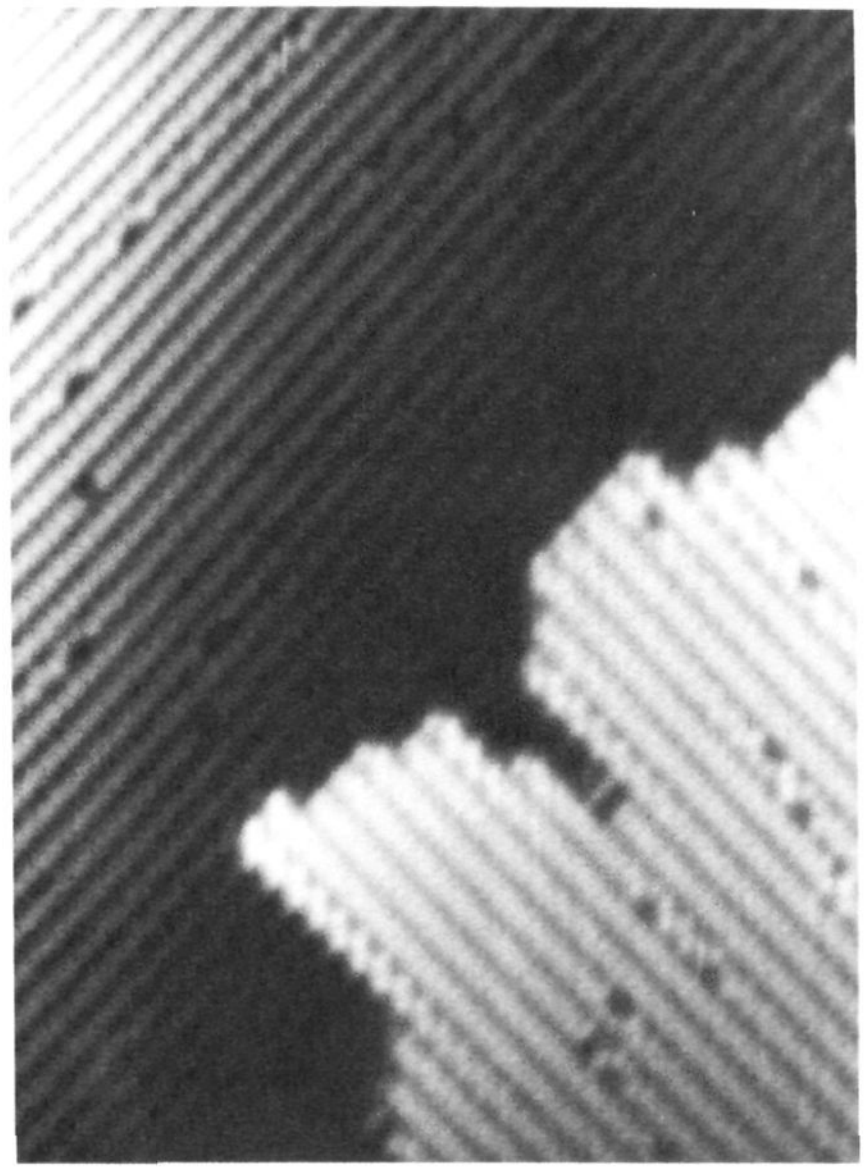

Figure 4. STM image of the clean Si(100)-(2×1) surface recorded at a crystal bias of −1.75 V. Buckled dimers are seen along step edges and near defects. Courtesy of V. Ukraintsev, J. C. Camp, and J. T. Yates, Jr.

A typical STM image from the Si(100)-(2×1) surface is presented in Figure 4, and the presence of parallel rows of symmetric dimers is observed. Furthermore, buckled dimers are seen as zigzag patterns among the symmetric rows (Figure 4). Both p(2×2) and c(4×2) local structures have been observed by STM in areas with buckled dimers.[20] Extensive studies of the Si(100) surface by STM have shown that the fraction of buckled dimers can vary drastically across the surface,[21,22] although buckled dimers are mostly seen along steps or around other surface defects. The observation of predominantly symmetric dimers in room temperature STM images is thus believed to be due to rapid flipping of buckled dimers between different buckling directions in defect-free regions, while the buckling directions are "frozen" near defects.

2. Vicinal Si(100)

Due to the tetrahedral bonding structure of the Si lattice, the direction of the dangling bonds on the (100) surface will rotate by 90° upon crossing a step of single-layer height. Consequently, the dimer rows on consecutive terraces separated by single-layer height steps are perpendicular to each other. Thus, due to the unavoidable presence of steps on any

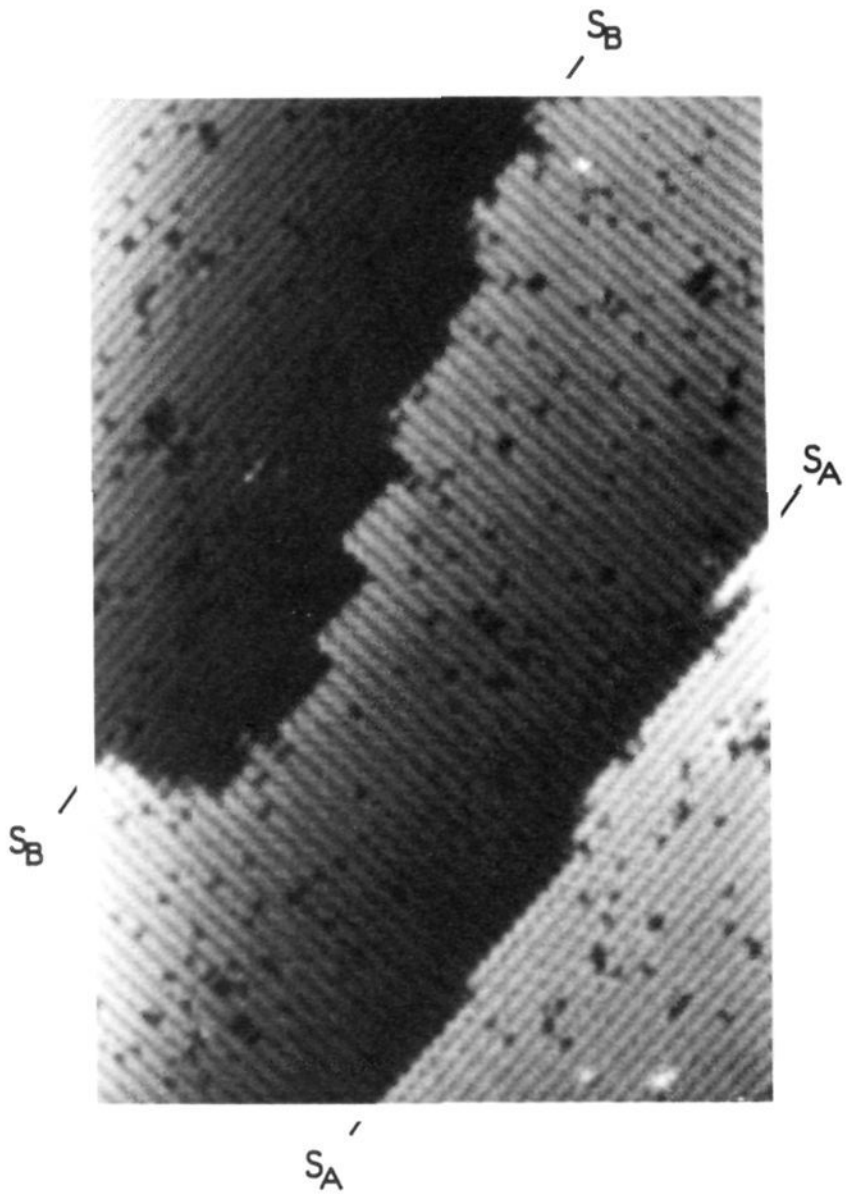

Figure 5. STM image of single atom height stepped Si(100) at a crystal bias of −2.0 V. The difference between the straight S_A and the meandering S_B steps is clearly seen. Courtesy of V. Ukraintsev, J. C. Camp, and J. T. Yates, Jr.

macroscopic crystal, the LEED pattern obtained for nominally flat Si(100) surfaces is a superposition of two identical (2×1) patterns rotated by 90° (strictly speaking a (2×1) and a (1×2) pattern). A STM image of a stepped surface, with the change in dimer row direction on adjacent terraces clearly visible, is shown in Figure 5. By increasing the miscut of the crystal a single-domain LEED pattern can be obtained, indicating that double-layer height steps are created on the surface. Chadi[23] introduced a useful notation to distinguish between the four different possible single and double steps. Single and double steps are denoted by "S" and "D", respectively, and subscripts "A" and "B" indicate the dimerization direction on the upper terrace. "A" is used for upper Si−Si dimer bonds perpendicular (i.e., upper dimer rows parallel) to the step, and "B" for upper dimer bonds parallel (i.e., upper dimer rows perpendicular) to the step. Schematics showing the lowest energy configuration obtained by Chadi[23] are shown in Figure 6, where decreasing circle size corresponds to increasing distance from the surface, and open circles indicate atoms with dangling bonds.

Chadi[23] also calculated the formation energy for the different step structures and found that a S_A step has lower energy. The magnitude of this difference is 40 kJ/mol Si in the step, making S_A steps more stable than S_B. Using the Chadi notation the steps in Figure 5 can be recognized as one S_A and one S_B step, and the S_A step is seen to be straight, whereas the

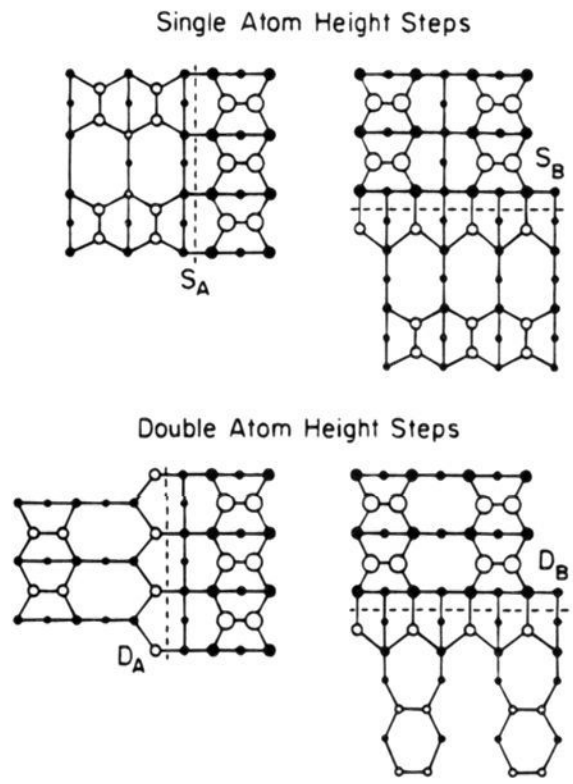

Figure 6. Top views of the step edge structures for single- and double-layer height steps on a Si(100)-(2×1) surface. Open circles indicate top layer atoms with one dangling bond each and the dashed lines mark the step edge position.[23]

S_B step is meandering, and contains S_A segments. This is in agreement with the results of Chadi's calculations, since creation of kinks in a S_B step creates local segments of the energetically favorable S_A step. Furthermore, it should be pointed out that according to calculations by Alerhand et al.[24] and Poon et al.,[25] the anisotropic stress of the (2×1) reconstructed surface would cause a perfectly flat (100) surface to break up into alternating (2×1) and (1×2) domains separated by single height descending and ascending steps, and these steps would all be of the favorable S_A type.

Among the double steps, D_B steps are strongly favored over D_A steps by 47 kJ/mol Si step atoms,[23] consistent with the observation of only D_B steps in STM images of double-stepped crystals. In addition, the formation energy for a D_B step is lower (by 11 kJ/mol Si step atoms) than the sum of the formation energies for one S_A and one S_B step, in agreement with the experimental observation of single domain LEED patterns for high miscut angles. The transformation from a purely single-stepped, through a mixture of single and double steps, to a purely double-stepped structure has been studied by both theory[26−28] and experiments.[29−32] Although there is general agreement that critical angles exist, several different values of these angles have been reported: purely single stepped below 1.5°,[30] 1.37°,[26] and ~1°; purely double stepped above 4.7°,[31] 6°,[32] and 8°.[26,29,30] Furthermore, the distribution between double and single steps is changed in favor of single steps by increasing the temperature.[26,28,31−33]

B. Si(111)

In the [111] direction the silicon crystal has a double-layer structure, with each Si atom having three bonds to atoms in the other layer of the double layer and one bond to an atom in a different double layer (Figure 1). Therefore, depending on where the surface is generated, each atom on the bulk termi-

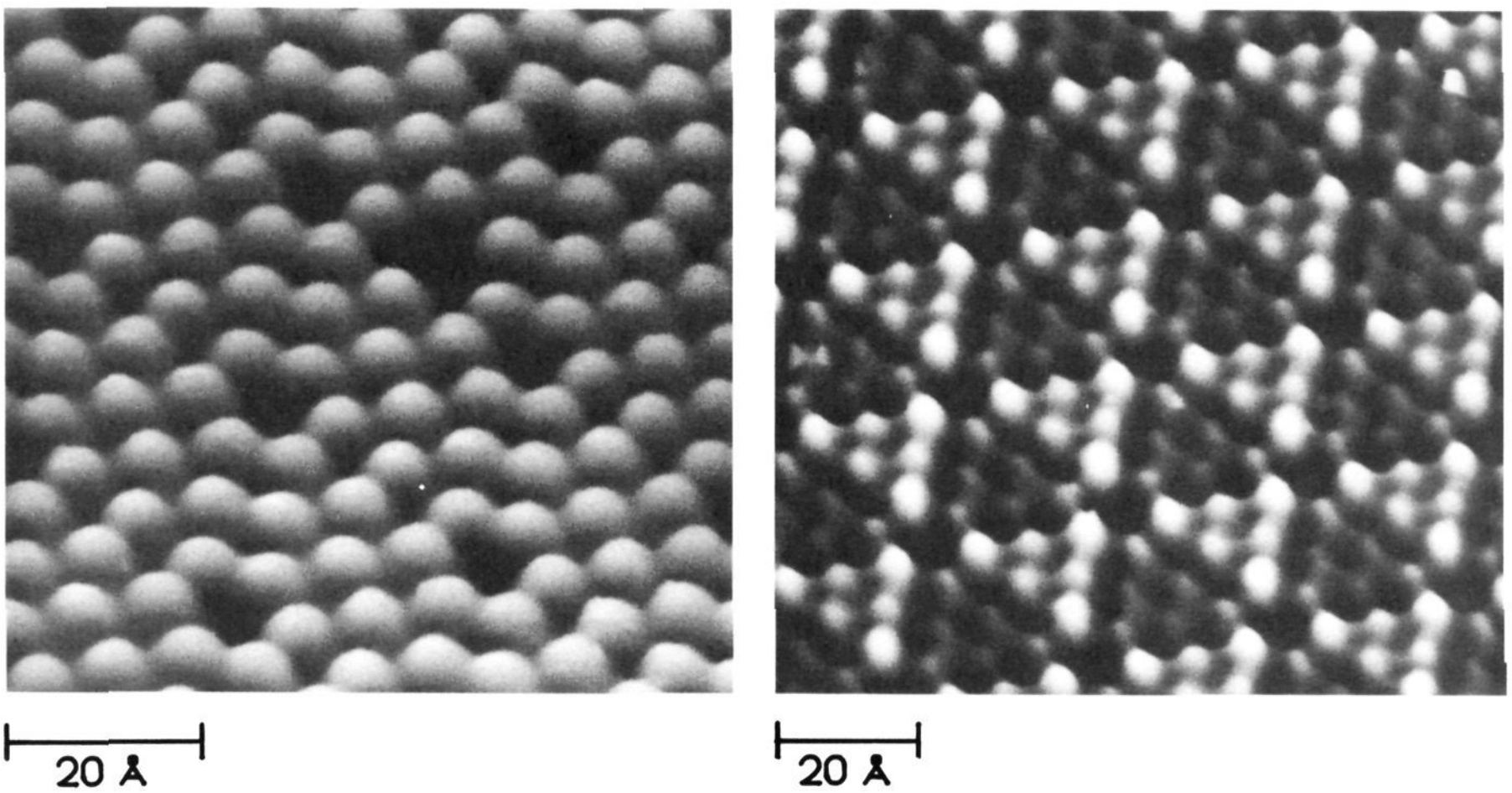

Figure 7. STM topographs of the clean Si(111)-(7×7) surface: (a) unoccupied states imaged at +2.0 V crystal bias, (b) occupied states imaged at −2.0 V crystal bias. The 12 adatoms are clearly visible in both images, and in the occupied state image the stacking fault and differences between corner and center adatoms are also seen. Courtesy of V. Ukraintsev, J. C. Camp, and J. T. Yates, Jr.

nated surface can have either one dangling bond or three dangling bonds. Simple counting of broken bonds would suggest that the structure shown in Figure 1, with one dangling bond per surface atom, would be the energetically favored one. For the Si-(111) surface two very different types of reconstructions have been found for the cleaved and the annealed surface.

1. Annealed Surface—(7×7) Structure

Schlier and Farnsworth reported a (7×7) LEED pattern for the clean Si(111) surface in 1959,[3] and over the next 25 years many structural models were proposed to account for this observation.[6] STM images, as the ones shown in Figure 7, of the (7×7) surface helped in elucidating the structure. Here, images at two tip−crystal bias conditions are shown. The widely accepted structural model is the dimer−adatom−stacking fault (DAS) model proposed by Takayanagi et al. in 1985[34] on the basis of TED results.

As the name indicates the DAS structure is very complex; it involves large displacements of atoms within one (111) double layer and the introduction of 12 adatoms/unit cell on top. The structure is shown in top and side view in Figure 8, and Figure 9 shows the buildup of the structure layer by layer. The structure of the bulk-terminated (111) surface with one dangling bond per surface atom is shown in Figure 9a. The bottom layer of the DAS double layer (the dimer layer) is nearly a normal full layer of atoms each saturating one dangling bond of the bulk layer below (Figure 9b). One atom is missing in each corner of the (7×7) unit cell (i.e. one missing atom per unit cell), creating the "corner holes", which are clearly observed in STM images (Figure 7). The dimer layer is largely unperturbed except for creation of strings of dimers, connecting the missing atoms, along the edge of the (7×7) unit cell and between the two triangular halves of the unit cell (Figure 9b). The dimer atoms have two dangling bonds each, while the rest of the atoms in the dimer layer have three dangling bonds each. These dangling bonds are saturated by the atoms of the upper layer of the double layer (the restatom layer), each of which saturates the dangling bonds of three underlying atoms (Figure 9c). In order to saturate all of the dangling bonds of the dimer layer, the rest layer atoms must occupy stacking fault sites within one of the two triangular subunits and "normal" sites within the other subunit. Differences in the electronic structure introduced by the stacking fault give rise to different contrast for the two subunits in STM images (occupied states, Figure 7b). The resulting surface at this stage has 21 dangling bonds nearly normal to the surface in each of the two subunits. It is impossible to saturate all of these dangling bonds using normal Si units with three dangling bonds pointing down and one dangling bond pointing up (other possible configuration would not eliminate any dangling bonds at all). The best possible solution is six adatoms in each subunit, which occupy sites of a local (2×2) structure (Figure 9d). The dangling bonds of the remaining three rest layer atoms (or restatoms in the conventional short notation) are untouched. The adatoms are divided into two classes according to their position in the subunits: the corner adatoms sit in the corners of the subunits next to the corner

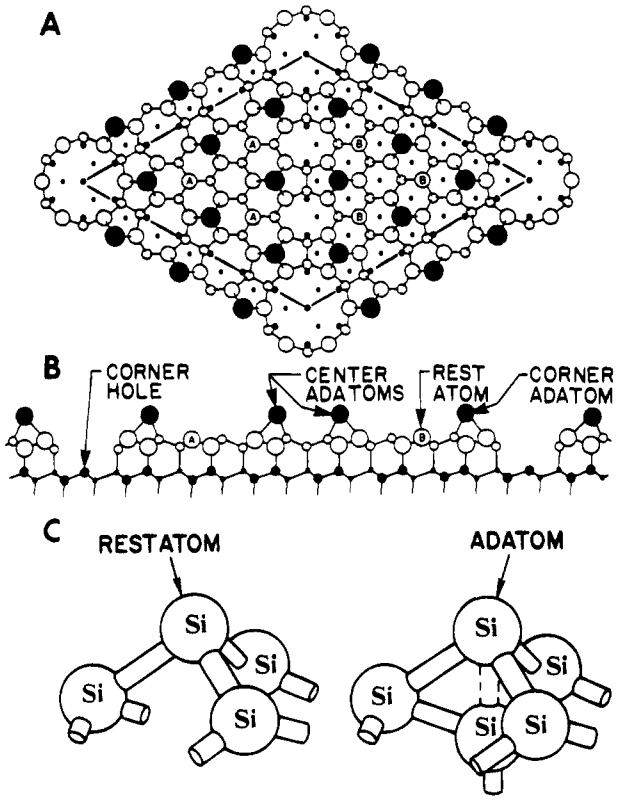

Figure 8. DAS model of the Si(111)-(7×7) surface: (A) Top view, atoms at increasing distances from the surface are indicated by circles of decreasing size. The filled circles denote the adatoms, and circles marked A and B represent the restatoms in the faulted and the unfaulted half, respectively. (B) Side view, cut along the long diagonal of the unit cell. Atoms in the plane of the cut are shown with larger circles than those behind this plane. (C) Details of the bond configurations at restatom and adatom sites.[253]

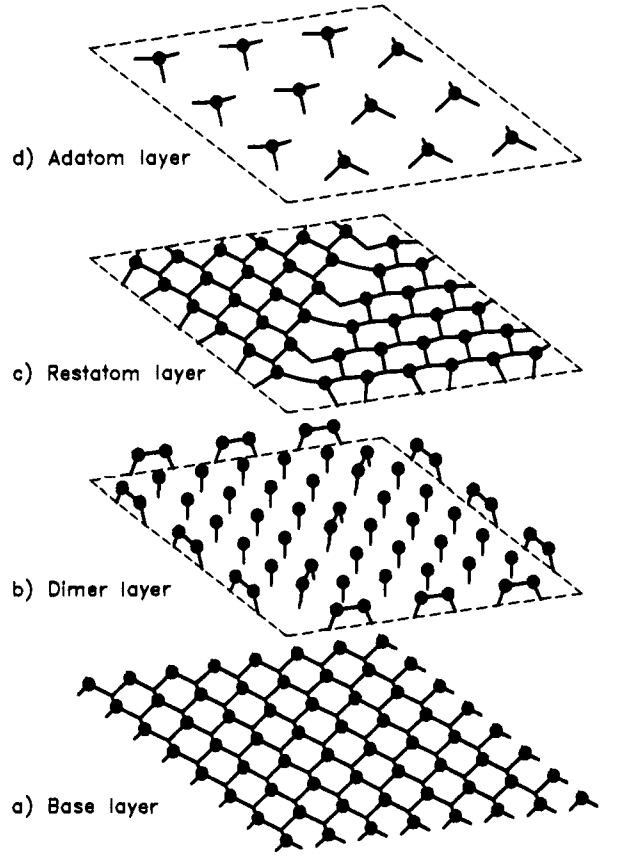

Figure 9. Layer-by-layer construction of the Si(111)-(7×7) structure: (a) (1×1) unreconstructed surface (terminated by a double layer); (b) addition of the bottom layer of the reconstructed double layer, the dimer layer; (c) addition of the second layer of the reconstructed double layer, the restlayer; and (d) introduction of the Si adatoms. The dashed lines show the outline of the (7×7) unit cell for each layer drawn in the plane of the underlying layer.

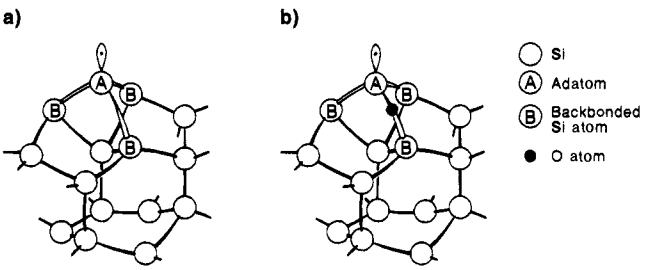

Figure 10. Close-up of strained structures on the Si(111)-(7×7) structure: (a) configuration at adatoms, three adjacent four-membered rings; (b) configuration at adatoms after insertion of an oxygen atom in one of the adatom back-bonds.[39]

holes, and the center adatoms sit in the center of the edges of the subunits. The formation of this structure reduces the number of dangling bonds in the (7×7) unit cell from 49 to 19: $^1/_6$ in each of two holes, $^1/_3$ in each of two holes (making a total of 1 hole in the unit cell), one on each of the adatoms (12 in total), and one on each of six exposed restatoms. Compared to the unreconstructed and the cleaved surface the (7×7) structure has a 4% excess of atoms (48 (dimer layer) + 42 (rest layer) + 12 (adatoms) = 102 compared to 98 for a (7×7) cell of unreconstructed double layer).

The (7×7) structure was later[35-38] shown to be only the most stable of a series of (n×n) (n odd) DAS reconstructions with very similar structures. These other structures can be obtained from the (7×7) structure by eliminating or creating one dimer at a time along the dimer strings, and eliminating or creating corresponding rows of adatoms and restatoms. Furthermore, the formation of the dimer strings and the stacking fault are more important than the introduction of adatoms in terms of lowering the surface energy.[35] The dimer strings dictate the triangular shape as the basic unit of the DAS structures, since this is the only way the dimer strings can be combined without introducing other (less energetically favorable) structures.

The considerable movement of atoms from their normal lattice positions in the unreconstructed surface to the positions in the (7×7) structure results in the surface being highly strained. As can be seen in Figure 1 the basic building blocks of the Si lattice are six-membered Si rings in the chair conformation analogous to one conformation of the cyclohexane molecule. On the other hand, inspection of the DAS model shows five-membered rings on both sides of the dimers (Figure 9b) and three adjacent four-membered rings at each adatom site (Figure 10a). In spite of this the (7×7) structure is very stable and the transformation from the (2×1) cleaved surface (see below) is irreversible. This led Ohdomari[39] to consider the possibility of stabilization by insertion of an O atom in one of the adatom back-bonds,

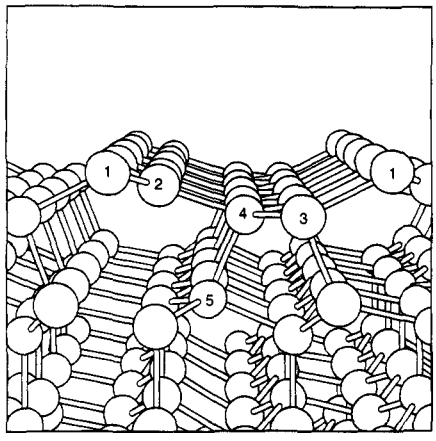

Figure 11. Ball-and-stick model of the Si(111)-(2×1) cleavage surface. Each of the atoms in the upper chain (atoms marked 1 and 2) has one dangling bond, while the atoms in the lower chain (atoms marked 3 and 4) have all bonds saturated.[6]

eliminating two of the three four-membered rings (Figure 10b). It is well known that commercial Si crystals contain a considerable amount of oxygen and in the model of Ohdomari during annealing this oxygen diffuses to the surface, where it accumulates due to the desorption barrier. Cluster calculations by Verwoerd and Osuch[40] showed that the oxygen-modified structure would indeed be very stable.

2. Cleaved Surface—(2×1) Structure

The Si(111) surface structure obtained after cleaving and before annealing is entirely different from the annealed surface. Although the possibility of two different cleaved surfaces (see Figure 1) exists, due to the difficulty of breaking three bonds per atom as compared to one, there is general agreement that the cleave proceeds between the double layers. For the cleaved surface a (2×1) LEED pattern is observed (even by cleavage at close to liquid He temperatures),[6] and STM images[37] show parallel rows of atoms. The commonly accepted model is the π-bonded chain model proposed by Pandey,[41,42] and slightly modified by Northrup and Cohen.[43] As seen in Figure 11, this model contains two layers of chain-bonded atoms: a top layer with one dangling bond per atom (atoms 1 and 2 in Figure 11) and a lower layer with saturated bonds (atoms 3 and 4 in Figure 11). Extensive displacement of the atoms in the surface layers and even further bond breaking is required to obtain this structure. Nevertheless, calculations by Northrup and Cohen[43] showed that the barrier for transition from the bulk terminated to the chain bonded geometry is very low (≤3 kJ/mol Si), and they proposed a pathway for atomic displacements, illustrated in Figure 12. Figure 12 shows a small part of the structure shown in Figure 11, and the numbering of the atoms in the two figures is the same. A layer inversion for the atoms 2 and 4 occurs by concerted bond breaking and bond formation, and concomitantly the dangling bond shifts from atom 4 to atom 2.

Annealing of the (2×1) cleavage structure leads to an irreversible phase transition to the (7×7) structure, and the (5×5) structure has been observed as an intermediate structure in the transformation.[37,38]

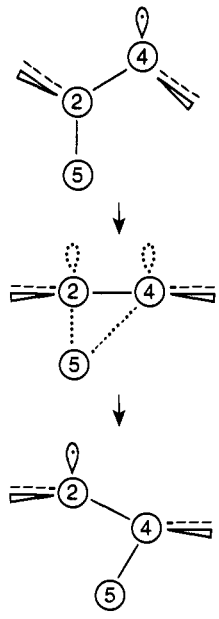

Figure 12. Proposed reaction pathway for the atomic rearrangement during cleaving of Si(111). Partial bonds are shown by dotted lines, and the numbering of the atoms is the same as in Figure 11.

The number density of surface atoms for the (2×1) structure is the same as for the (1×1) structure, and therefore the (7×7) structure has a 4% excess of atoms compared to the (2×1) structure. On the other hand, the (5×5) structure has no excess of atoms (24 (dimer layer) + 20 (restlayer) + 6 (adatoms) = 50, i.e. the same as for a (5×5) cell of the unreconstructed double layer), and it has been speculated that the creation of a (5×5) structure is facilitated by the equal number densities of the (5×5) structure and the (2×1) surface. Only at higher temperatures is the mobility high enough to supply the extra atoms needed for the (7×7) structure.

C. Other Si(*hkl*) Surfaces

Compared to the wealth of structural information available for Si(100) and Si(111) from both experimental and theoretical studies, very little information is available for other Si surfaces. Several different high-index surfaces have been studied,[44-51] but some were found to break up into facets of low-index surfaces. The (211), (113), and (331) surfaces—and the (110) surface—are believed to be smooth surfaces with unique surface structures.[46,48,51] The issue is further complicated by the fact that many of the reconstructions initially reported later turned out to be stabilized by impurities, in particular by Ni.[48,52] It should be mentioned that Ni-induced reconstructions of Si(111) and Si(100), e.g., Si(111)-($\sqrt{19}\times\sqrt{19}$) and Si(100)-(2×n), are also well-known.[53,54]

1. Si(110)

This is the last of the three low-index surfaces for which the creation of dangling bonds is schematically shown in Figure 1. The bulk terminated Si(110) surface consists of zigzag chains of atoms, as shown in Figure 13; each surface atom (large circles) bonds to two other atoms in the surface plane (along the chain), to one atom below the surface (small circles),

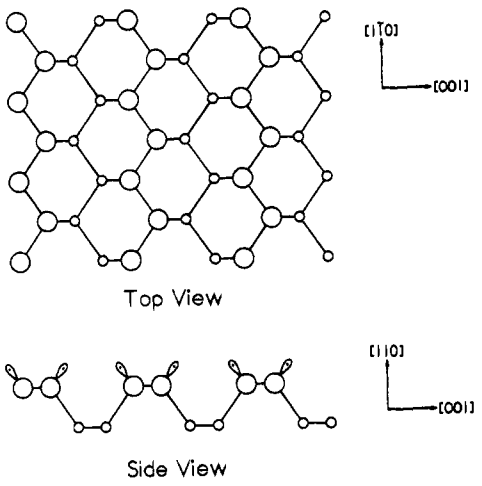

Figure 13. Top and side views of the structure of the unreconstructed Si(110) surface. Each of the upper surface atoms has one dangling bond as shown in the side view.

and has one dangling bond. There is now general agreement from LEED,[52,53,55,56] RHEED, and STM[57] studies that the clean surface reconstructs in a "(16×2)" reconstruction. As for the Si(111) surface, this is a very large surface unit cell, but in contrast to the Si(111), the unit vectors of the reconstruction are not parallel to the fundamental unit vectors. Several similar models have been proposed,[52,55,56,58] all of which have a periodic arrangement of upper and lower terraces as their main element, but none of them has gained broad support.

2. Si(113)

This surface has attracted quite some interest due to its high stability, despite having a high Miller index.[46,47,49,50] The unreconstructed Si(113) surface can be regarded as an alternation of Si(111) and Si(100) terraces, each of which are only one atomic row wide in the direction perpendicular to the steps. Thus the (1×1) unit cell contains one "(111)" atom with one dangling bond and one "(100)" atom with two dangling bonds. Both (3×2) and (3×1) reconstructions have been observed by LEED[46-48] and STM[49,50] (the 3× direction is along the step edge), and the question of whether one of these is more fundamental than the other is still controversial.[49,50] The models proposed for the Si(113) reconstruction[45,50] are based on rebonding of the atoms at the step edges and formation of dimers.

III. Hydrogen-Terminated Surfaces

Just as hydrogen plays a prominent role in the chemistry of carbon in the entire field of organic chemistry, where C−H bonds predominate, the Si−H bond is equally important in the chemistry of silicon. Formation of the Si−H bond on the surface of a silicon crystal provides a high degree of passivation of the surface chemistry of the silicon as a result of reaction with the dangling bond. In the processing of silicon surfaces, the role of the formation and destruction of the surface Si−H bond is often dominant in controlling the processes desired.

The standard method for preparing silicon surfaces involves etching in HF solutions, and after this preparation the surfaces are covered with hydrogen.[59] The hydrogen layer passivates the surface by capping the dangling bonds, creating a fairly stable surface. The preparation and properties of etched surfaces will not be examined here; instead we will focus on the experimental and theoretical efforts devoted to understanding these hydrogen-covered surfaces by studies of single crystal surfaces exposed to atomic hydrogen under vacuum.

The reactivity of molecular hydrogen toward silicon surfaces is very low,[60-62] and hydrogen-terminated surfaces are usually produced by exposure to atomic hydrogen (created by flowing H_2 over a tungsten filament held at ~2000 K or by other methods of activation). As is common practice, atomic hydrogen exposures are expressed in terms of the dose of molecular hydrogen, since the absolute dissociation efficiency on the heated tungsten surface is only poorly defined.[63-65] The flux of atomic hydrogen to the surface also depends on the geometric arrangement of the hydrogen doser, the W filament, and the crystal, and H atoms may be reflected from a cold glass surface if this is needed.[66]

The Si−H bond strength in silanes is ~366 kJ/mol, whereas the Si−Si bond strength in disilane is ~318 kJ/mol.[67] In bulk silicon, the Si−Si bond strength is 226 kJ/mol.[1] On this basis then, on the silicon surface atomic H can result in Si−Si bond breaking as Si−H bonds are energetically preferred. Although the structures of the reconstructed Si(100)-(2×1) and Si(111)-(7×7) are fundamentally different some similarities exist in the interactions with hydrogen. For instance, the surface atoms on both surfaces have at most one dangling bond, but, nevertheless, higher surface hydrides—SiH_2 and SiH_3 species—are often formed, showing that atomic hydrogen is capable of breaking Si−Si bonds. Furthermore, atomic hydrogen has been shown to be a powerful reagent for removing selected chemisorbed species from silicon surfaces, and we will return to this issue later. Abstraction of D atoms during subsequent atomic hydrogen exposure was first reported by Sinniah et al.[68] for Si(100)-(2×1) and by Froitzheim et al.[69] for Si(111)-(7×7). For Si(100)-(2×1), the H atom abstraction reaction was studied in more detail by Naitoh et al.[70] and Koleske et al.[71] using recoil spectroscopy. Koleske et al.[71] also determined the kinetics of the abstraction reaction to be first order with respect to the deuterium coverage with an activation energy of 2.5 ± 0.8 kJ/mol, and concluded that the reaction occurs by a direct abstraction of the surface D by a gas phase H (an Eley−Rideal-type reaction, in which surface accommodation of the incoming reaction partner involving energy exchange with the surface is unnecessary). These studies clearly show that abstraction of H already on the surface by incoming H atoms is a prominent reaction during atomic hydrogen exposure, as Si−H bonds are converted to H−H bonds in a facile manner.

A. Si(100)−H

For the Si(100) surface two different ideal hydrogen terminations were originally proposed.[72] One is the monohydride phase where the dimers are preserved and the dangling bonds—one on each surface atom—

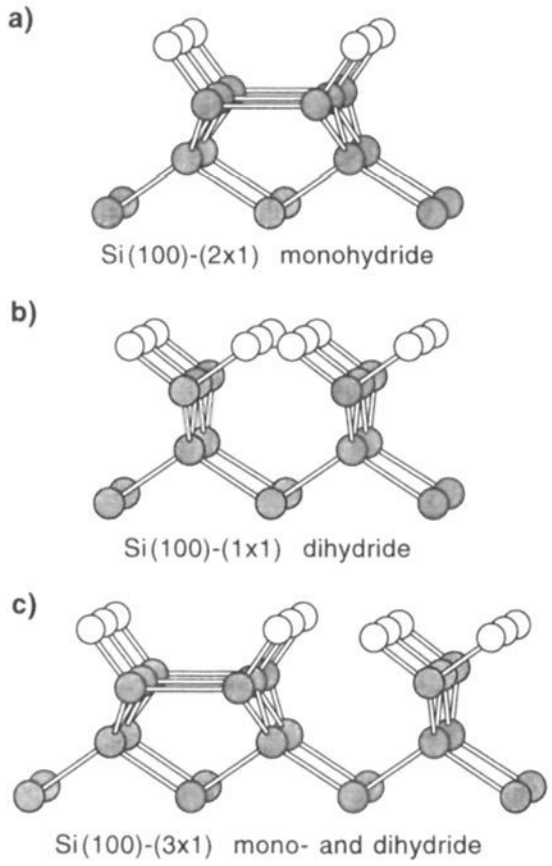

Figure 14. Hydrogen-terminated Si(100) surfaces: (a) monohydride, (2×1) structure; (b) dihydride, (1×1) structure; (c) (3×1) structure.

are capped by hydrogen (Figure 14a), i.e. the (2×1) reconstruction is preserved. The other is the dihydride phase where the dimer bonds are broken, and the two dangling bonds on each surface atom are capped with hydrogen (Figure 14b), leading to a (1×1) structure. Trihydride species on the surface can only be produced at defect sites or by breaking Si−Si backbonds. However, the structure of the hydrogen-covered surface has turned out to be a surprisingly complex function of coverage and adsorption/annealing temperature.[73−76]

The Si(100) monohydride phase is the least controversial, and there is general agreement that it is formed after saturation exposure to atomic hydrogen at a surface temperature of 600 K[72,74−76] or after high exposures at lower temperatures followed by annealing above 575 K.[69,72,73] A (2×1) LEED pattern is observed[73,74] and vibrational spectroscopy, exclusively showing features below 2100 cm^{-1},[69,73,77,78] indicate presence of only the Si−H species. The asymmetric and symmetric Si−H stretches of the H−Si−Si−H monohydride species are observed at 2088 and 2098 cm^{-1}, respectively,[77,78] while the asymmetric and symmetric Si−H stretching modes of SiH_2 (for adsorption at lower temperatures, see below) are observed at 2103 and 2091 cm^{-1}.[73,78]

Hydrogen adsorption at temperatures below the monohydride formation temperature was believed to give the dihydride phase (Figure 14b) at saturation, and indeed a (1×1) LEED pattern is obtained after saturation at 300 K.[72,76] However, an unexpected ordered intermediate structure was reported by Chabal and Raghavachari:[73] the (3×1) structure. This structure was obtained after saturation hydrogen coverage at 400 K, and the IR spectra showed the presence of both monohydride and dihydride species on the surface. Their interpretation involved a structure with alternating rows of monohydrides and dihydrides as shown in Figure 14c. Their observation

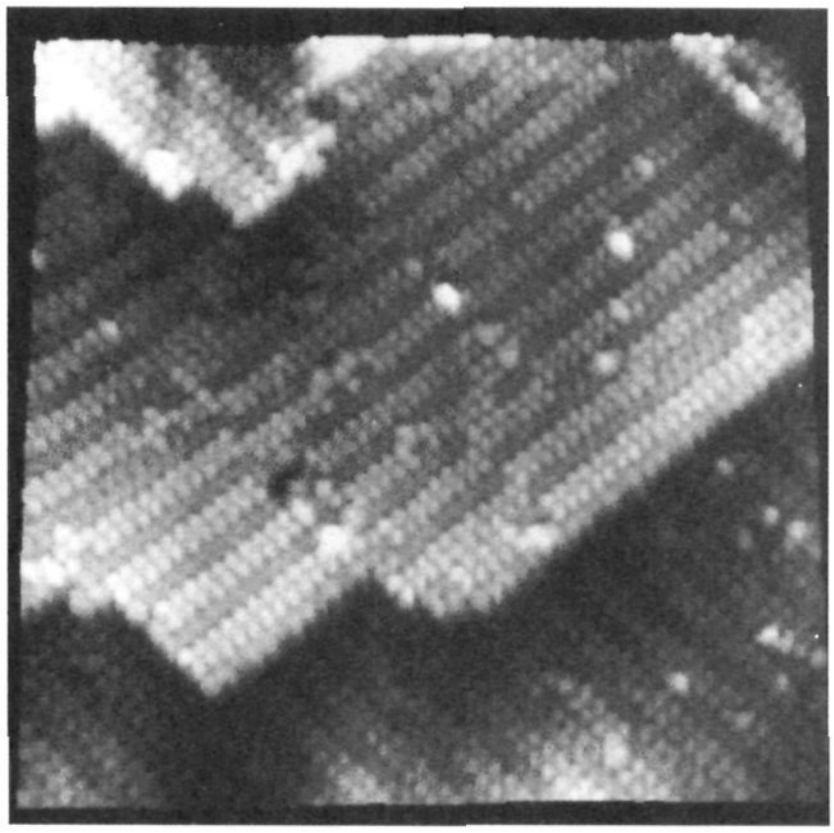

Figure 15. STM image obtained after saturation of Si(100) with atomic hydrogen at 400 K. The image shows the (3×1) structure with alternating rows of bright monohydride dimers and darker dihydrides.[75]

of very similar IR spectra, after saturation at 300 K and at 400 K, lead them to the conclusion that the (1×1) structure is merely a disordered (3×1) phase. However, several studies[74,76,79] showed that the (1×1) phase has a higher saturation coverage (1.9 ML (monolayer)) than the (3×1) phase (1.4 ML). In fact Lu et al.[79] showed by nuclear reaction analysis, NRA, that while the coverage does reach a plateau at ~2.0 ML (after ~5000 langmuir D_2), continued exposure to atomic D increases the coverage further (~3.0 ML after 4×10^5 langmuir D_2), albeit at a much lower rate. This was attributed to etching and facetting. Furthermore, Gates et al.[80] found from combined SSIMS and TPD measurements that at surface temperatures below 500 K, in addition to SiH_2, SiH_3 is also formed, leading to desorption of SiH_4 around 650 K. The SiH_3 coverage is highest for adsorption temperatures between 325 and 375 K, and decreases rapidly for higher adsorption temperatures. Correlating the existence of an extra broad low-temperature H_2 desorption state (we will return to the desorption states from H/Si(100) below) with the desorption of SiH_4, Cheng and Yates[74] showed that surface SiH_3 species are responsible for the (3×1) → (1×1) transition, i.e. the (1×1) phase is a disordered mixture of mono-, di-, and trihydride. These conclusions were confirmed by an STM study by Boland,[75] where STM images of the three different structures were obtained. Following saturation with atomic hydrogen at 600 K, a uniform monohydride structure with the dimer rows preserved were clearly seen. Dimer rows, separated by rows of dihydrides (appearing darker), are also seen in the STM image of the (3×1) structure, shown in Figure 15. It is interesting to note that the step edges are preferentially covered with dihydride species. For the 300 K saturated surface, the STM images showed mainly a disordered structure, although areas with local

Table 1. Structural Evaluations for Si(100) and for Mono- and Dihydride Species on Si(100)

	Si–Si dimer length (Å)	Si–H distance (Å)	Si–Si–H angle (deg)	H-Si–H angle (deg)	ref
clean Si(100)					
TOF-SARS	2.26 ± 0.10				81
SLAB-MINDO calculation	2.13				84
calculation	2.32				85
calculation	2.34				86
bulk Si–Si bond length	2.35				90
monohydride - Si(100)					
TOF-SARS	2.97 ± 0.10	1.2 ± 0.15	133 ± 8		81,82
recoil spectroscopy			110 ± 2		83
SLAB-MINDO calculation	2.37	1.53	110.2		84,87
cluster calculation	2.44	1.51	114.0		88
total-energy calculation	2.40	1.54			89
cluster calculation	2.45				85
SiH_4(g) bond lengths		1.48			91
Si_2H_6(g) bond lengths	2.33	1.49			91
dihydride - Si(100)					
TOF-SARS		1.45 ± 0.12		112 ± 8	82
total-energy calculation		1.50		102	89
SLAB-MINDO calc		1.52		90.2	87

(1×1) dihydride structure were also seen.[75] Observation of etch pits after desorption of hydrogen from the 300 K saturated surface[75] confirms that etching does indeed take place during hydrogen adsorption at this temperature. It should be noted that while the (2×1) and (3×1) phases are unchanged by prolonged exposure to atomic hydrogen at their respective creation temperatures, subsequent atomic hydrogen exposure at 300 K causes conversion to the (1×1) phase.[72,73,75]

The structures for the (2×1) and (1×1) phases—i.e., bond lengths and angles—were determined by Rabalais and co-workers[81,82] by TOF-SARS, detecting the scattered Ar/Ne and recoiled Si and H ions and neutrals resulting from bombardment with keV Ar^+/Ne^+ ions. To enable interpretation, the data for the (1×1) phase was analyzed by neglecting species other than the dihydride. The results (summarized in Table 1) are in agreement with the basic models shown in Figure 14 for the mono- and dihydride phases. Included in Table 1 are also structural parameters obtained from another recoil experiment[83] and from various calculations,[84–89] and bond lengths for bulk silicon,[90] silane, and disilane.[91] Although there are some discrepancies between the actual values, note the general trend that the dimer bond is shorter on the clean surface than on the monohydride surface, supporting the idea of a partial π-bond for the clean surface being broken by hydrogen adsorption.

B. Si(111)–H

The ideal hydrogen-terminated surface of Si(111) has the unreconstructed (1×1) structure with one normally-oriented bond on each surface atom (see Figure 1), and these bonds are capped by hydrogen atoms; this is the structure obtained after chemical treatment of Si(111).[59]

It was recognized early on that although the (1×1) structure is not easily obtained under vacuum conditions, atomic hydrogen exposure on the Si(111)-(7×7) surface introduces major changes in the structure. LEED pictures obtained near saturation show a pattern related to the (7×7) pattern, but all fractional order beams except those connecting the integral order beams and those next to the integral order beams are extinct. This has been termed the "(7×1)" pattern[92] or the δ-(7×7) pattern.[93] Kobayashi et al.[94] studied the surface saturated with atomic hydrogen at ~300 K by HREELS, and found a SiH_x deformation mode attributable to higher hydrides, but unfortunately it was not possible to distinguish between SiH_2 or SiH_3. Using SSIMS, Greenlief et al.[95] were able to make the distinction, and show that, very similar to the Si(100) case, only monohydride is formed for adsorption at 693 K, mono- and dihydride are formed at 543 K, and mono-, di-, and trihydride are formed at 353 K. Even at 353 K the monohydride is still the dominant species with reported di- and trihydride coverages of 8% and 4% of a monolayer, respectively,[95] based on a saturation coverage of 1.25 ± 0.13 ML obtained by NRA.[96] This saturation coverage alone indicates that Si–Si bond breaking occurs, since merely saturating the dangling bonds of the restatoms and adatoms would give a saturation coverage of 0.39 ML (19 dangling bonds in the (7×7) unit cell). ESDIAD and TPD studies by Wallace et al.[97] also indicated the presence of higher hydrides, and in addition, showed that hydrogen from the bulk diffuses to the surface.

Karlsson et al.[98] concluded from their ARPES and LEED study that a monohydride phase is formed within the (7×7) unit cell, and two independent STM studies[99,100] reached similar conclusions. Initial hydrogen exposure leads to saturation of the dangling bonds of the adatoms, i.e. the full (7×7) structure is preserved. In STS spectra, the difference between an unreacted (Figure 16a) and a reacted (Figure 16b) adatom site is clearly seen. The restatoms are not visible in STM images but the difference in STS spectra (Figure 16, parts c and d) reveals that some of the restatoms have also reacted. The peak at −0.8 eV (dangling bond state, Figure 16c) is characteristic for an unreacted restatom site, while this state is not observed for a reacted site (Figure 16d). With increasing hydrogen exposure the back-bonds of the silicon adatoms are broken, and hydrogen saturates both of the new dangling bonds—one on the underlying restlayer and one on the adatom. At low temperature, isolated adatom dihydride and trihydride

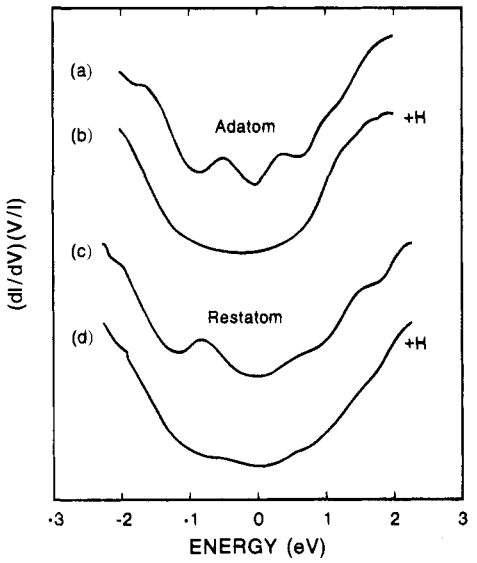

Figure 16. STS spectra of specific sites of the Si(111) surface after submonolayer atomic hydrogen exposure: (a) Unreacted adatom, (b) reacted adatom, (c) unreacted restatom, and (d) reacted restatom.[99]

species were observed by STM,[99] in agreement with the observation of random SiH_3 species in a RHEED study by Ichimiya and Mizuno.[93] At higher temperature, the increased mobility of the adatom species leads to formation of adatom islands[99] accompanied by a hydrogen passivated rest layer. The exact composition and structure of these hydrogenated adatom islands are unknown, but the height as judged from STM images is typically close to the height of a Si(111) double layer. Boland[99] observed no etching of the surface during H exposure, whereas Mortensen et al.[100] invoked the desorption of SiH_4 removing some of the displaced adatoms. The dimer strings along the edges of the (7×7) cell, and therefore also the stacking fault, remain. Before comparing to the reactivity of the dimers on the Si(100) surface, one has to bear in mind that the dimers bordering the Si(111)-(7×7) unit cell do *not* have dangling bonds. The preservation of the dimers and the stacking fault is in agreement with the theory that these are the more fundamental elements of the DAS reconstruction compared to the adatoms.[35] Furthermore, on the clean surface the number of dangling bonds is reduced notably by each adatom saturating the dangling bonds of three restatoms. However, this occurs at the expense of introduction of considerable surface stress. In contrast, the observation of a hydrogen-saturated rest layer shows that it is more favorable to saturate the dangling bonds of the restatoms by hydrogen atoms, with no introduction of surface stress.

Landemark et al.[101] used an interesting approach in an attempt to obtain the ideal Si(111)-(1×1)-H structure: removing the stacking fault by adsorption of In atoms followed by annealing to ~875 K, creating a $(\sqrt{3}\times\sqrt{3})$-In structure. Subsequent hydrogen adsorption resulted in a sharp (1×1) LEED pattern, and photoemission spectra showed the replacement of Si–In bonds by Si–H bonds, with the In forming metallic islands. Unfortunately, a pure H/Si(111) phase cannot be obtained following In desorption, since In is more thermally stable than the H/Si structure, and thus annealing leads to reversal to the $(\sqrt{3}\times\sqrt{3})$-In structure.

That a near ideal (1×1) surface—i.e. a surface without dimers and stacking fault—can after all be obtained by exposure to atomic hydrogen was recently reported by Owman and Mårtenson.[102] They exposed a Si(111)-(7×7) surface to atomic hydrogen at a surface temperature of 650 K. The density of defects on the surface depends strongly on the hydrogen exposure, and an exposure of 5000 langmuir was found to be optimal. STM images of this surface, as the one shown in Figure 17, show that small triangular domains with stacking faults remained on only about 1% of the surface area. For lower exposures stacking faults remain in larger areas, and for higher exposures holes are created in the first bulk layer. This implies that this hydrogen terminated (1×1) surface is not stable under hydrogen exposure. In accordance with previous results,[99,100] islands of displaced adatom species (bright spots in the STM image, Figure 17) are seen on top of the (1×1)-H structure, and they are observed to shrink during the removal of the stacking fault. This is expected since the removal of the stacking fault requires insertion of Si atoms along the dimer strings between the faulted and unfaulted parts of the Si(111)-(7×7) structure. Compared to the bulk-terminated surface, the Si(111)-(7×7) structure with and without adatoms has a 4% excess and a 8% deficiency of atoms, respectively.

C. Decomposition and Desorption of Hydride Species

The thermal desorption of hydrogen from the different hydrogen phases on Si(100) and Si(111) exhibits many similarities as well as some differences. The dominant H_2 desorption feature for all atomic hydrogen exposures and adsorption temperatures is the β_1 state around 800 K,[68,74,95,103] which is the only desorption process seen for low exposures.[68,104] Depending on exposure and adsorption temperature two other H_2 desorption states might also be observed: the β_2 state at ~650 K and the broad β_3 state at 350–550 K.[74,97] For comparison, TPD spectra following atomic hydrogen adsorption on Si(100) and Si(111) at various temperatures are shown in Figures 18 and 19.

Since the β_1 state is the only state observed for adsorption at either lower coverages or higher temperatures, this state has been assigned to H_2 desorption from monohydride species. One would expect desorption from this phase to follow second-order kinetics, but several studies by TPD, LITD, and isothermal desorption have shown, that while this is the case for Si(111)[104,105] and in the limit of very low coverage for Si(100),[106] the desorption from Si(100) at higher coverages follows first-order kinetics instead.[68,105–107] This very surprising result was first reported by Sinniah et al.,[107] who proposed a delocalization model, where hydrogen recombination on the surface occurs via the irreversible excitation of a hydrogen atom to a delocalized state, followed by the reaction of this delocalized H with a localized H to

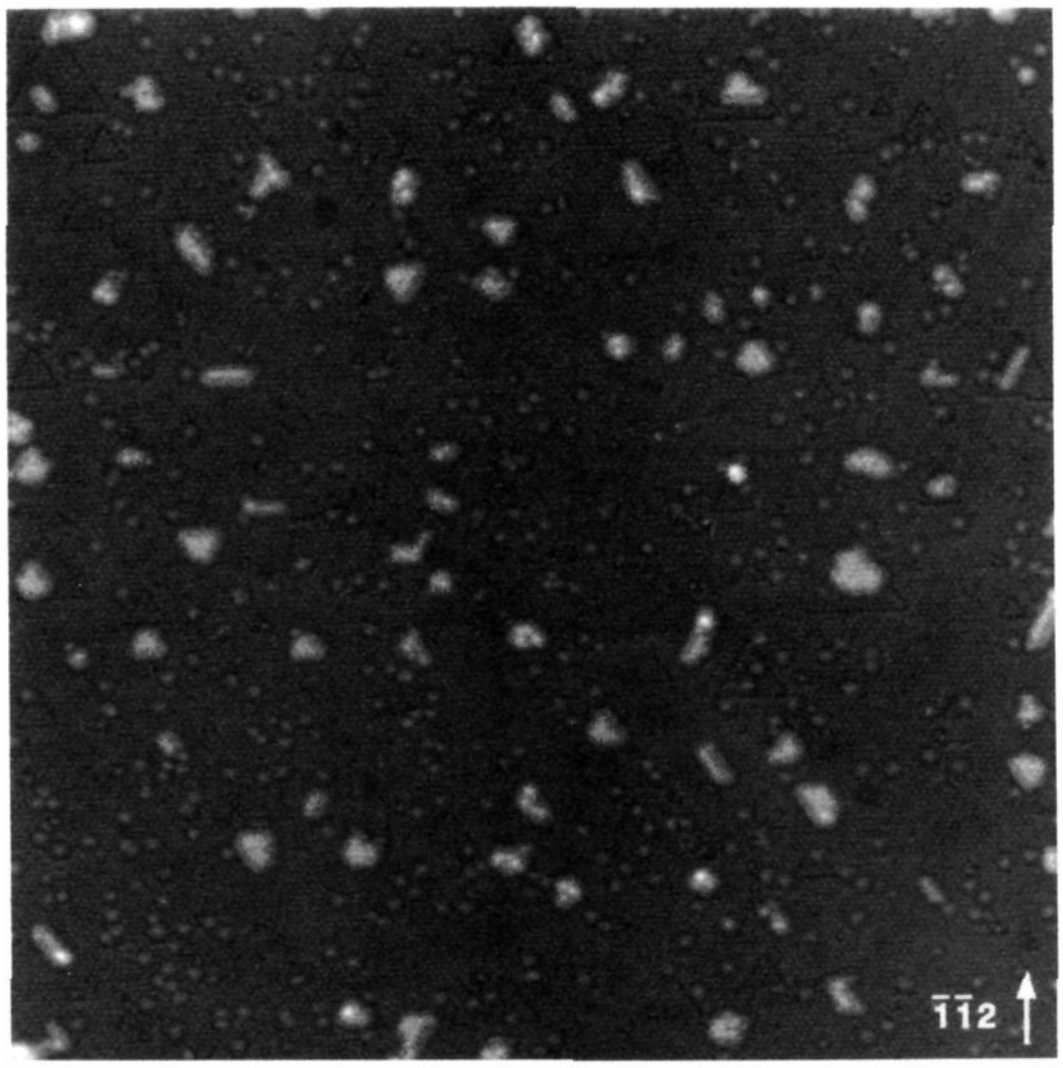

Figure 17. STM image (crystal bias −2.5 V) of a Si(111)-(7×7) surface exposed to 5000 langmuir of hydrogen at a surface temperature of 645 K. The surface shows almost perfect (1×1) ordering; the triangles seen are the remaining stacking faulted subunits.[102]

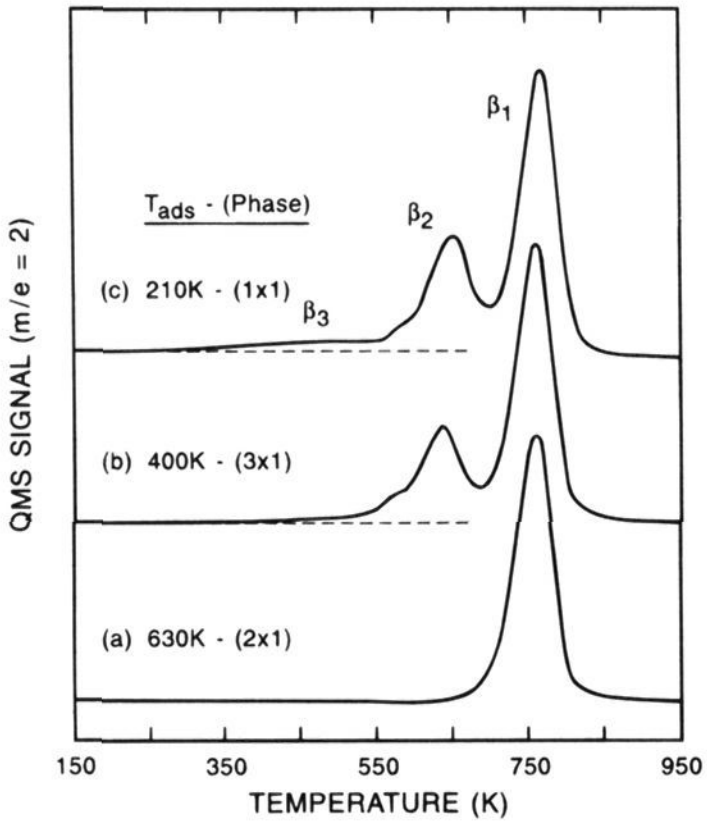

Figure 18. TPD of H_2 desorption from H-saturated Si-(100) at different adsorption temperatures: (a) 630 K, (b) 400 K, (c) 210 K.[74]

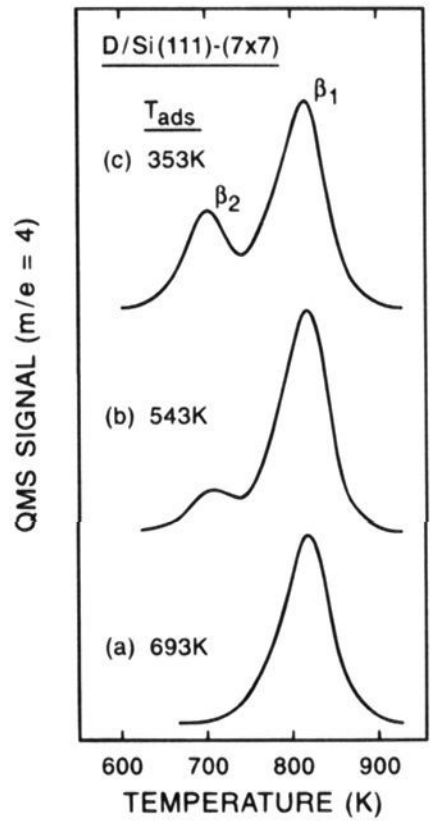

Figure 19. TPD of D_2 desorption from D-saturated Si-(111) at different adsorption temperatures: (a) 693 K, (b) 543 K, (c) 353 K.[95]

form H_2(g). On the other hand, STM studies of the Si(100)-monohydride by Boland[108] have been interpreted in terms of a pairing model similar to the concerted desorption model initially proposed by Wise et al.[105] Hydrogen coverage measurements by Höfer et al.,[106] using SHG measurements during isothermal desorption, has also been interpreted in favor of this model. During the initial stages of adsorption the hydrogen atoms occupy single dangling bonds, but at higher temperatures they tend to pair up on the surface dimers[108] as can be seen in Figure 20. Figure 20a shows a STM image of the Si(100)-(2×1) surface after submonolayer exposure to atomic hydrogen. Supported by the tunneling spectra (Figure 21), the bright ball-like features are assigned to the remaining dangling bond on dimers where one of the dangling bonds has reacted with hydrogen, and this assignment is supported by recent calculations by Uchiyama and Tsukada.[109] The dark features are assigned to dimers where both dangling bonds are

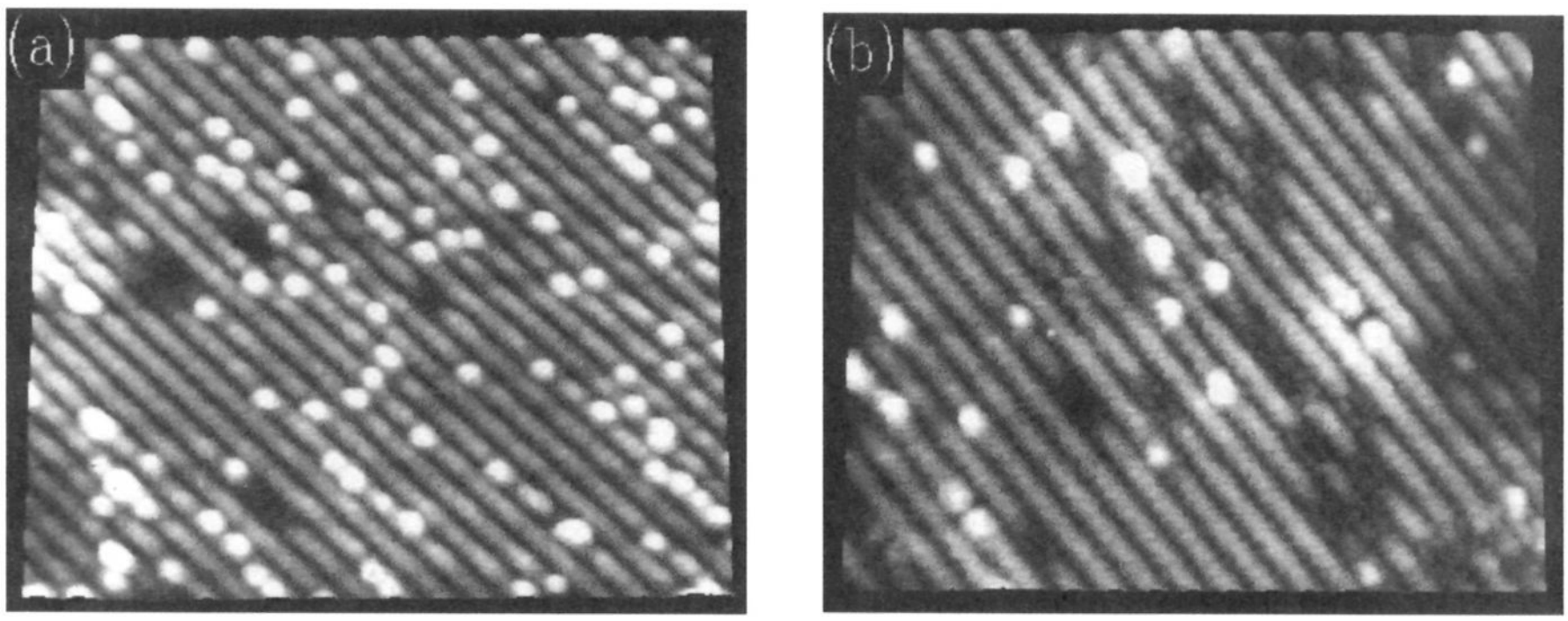

Figure 20. STM of Si(100)-(2×1) with (a) submonolayer coverage of H adsorbed at 295 K, and (b) previous surface following 10 s annealing at 630 K. The areas shown are 180 × 148 Å^2, bias +0.8 V.[389]

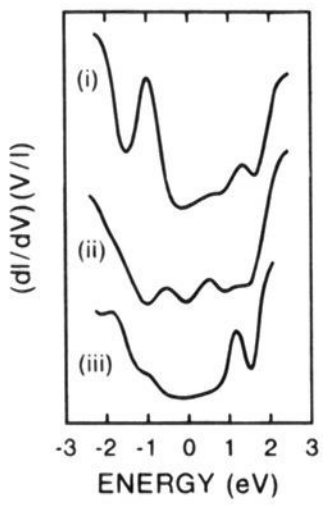

Figure 21. STS spectra of H/Si(100) recorded at (i) unreacted dimer site, (ii) bright ball-like site, and (iii) reacted (dark) dimer site.[389]

capped with hydrogen, giving rise to a hydrogen induced state at 1.2 eV above E_F. After annealing (Figure 20b) the number of ball-like features decreases while the number of fully reacted dimers increases. This pairing is attributed to the energetically favorable π-interaction between two dangling bonds on the same dimer,[110] thereby forcing the hydrogens to pair on other dimers. Figure 21 shows three STS spectra for (i) an unreacted dimer site; (ii) a bright ball-like site; and (iii) a dark reacted dimer site. For the bright ball-like site, two maxima close to E_F are seen, attributed to the bonding and antibonding dangling bond states, respectively. These are the states giving rise to the high tunneling current responsible for the bright appearance in STM images. In contrast, the unreacted and fully reacted sites have no states close to E_F, causing them to appear darker in STM images. The experimental and theoretical estimates of the π-bond stabilization energy, ϵ, for the conversion of unpaired dangling bonds to paired dangling bonds (and therefore also for conversion of unpaired monohydride species to paired monohydride species) span a wide range. On the basis of the STS spectra (Figure 21), Boland estimated ϵ to be 75 kJ/mol,[108] Höfer et al. reported 24 kJ/mol,[106] whereas different theoretical calculations have given values of 21,[85] 4−8,[88] and 31 kJ/mol.[111] Following desorption of small amounts of hydrogen from the saturated Si(100) surface, dangling bonds are again found in pairs, supporting the idea that desorption from the monohydride phase occurs by recombination of hydrogens from the same dimer.

Interestingly, Shane et al.[112] found that the rovibrational state of the H_2 desorbing from the monohydride phase is insensitive to the structural differences between Si(100) and Si(111). Specifically, H_2 is rotationally cold but vibrationally hot, and this result was confirmed for Si(100) by the calculations of Sheng and Zhang.[113] On the basis of these observations, Shane et al.[112,114] proposed that the recombinative desorption of H_2 from Si(100) and Si(111) surfaces occurs through very similar intermediates, which have a dihydride-like structure.

The coverage dependence is more complex for the β_2 state resulting from SiH_2 decomposition,[80] and at least on Si(111), also from SiH_3 decomposition.[95,103] As mentioned above the β_3 state has been uniquely assigned to SiH_3 species on the Si(100) surface,[74] and the same state has been observed from Si(111) for room temperature saturation exposure to atomic hydrogen.[97] It is important to note that a monohydride phase is always obtained after decomposition of the higher hydrides, and for initial coverages > 1 ML the monohydride coverage after annealing may be adjusted to 1 ML by controlled heating.[76] Two different mechanisms can account for this, as originally suggested by Froitzheim et al.;[69] these consider only di- and monohydride, but the arguments can easily be extended to trihydride:

Model I. Initial desorption takes place by removing one hydrogen from each dihydride (trihydride) giving rise to the β_2 (β_3) desorption state. Then, at higher temperatures hydrogen desorbs from the resulting monohydrides.

Model II. Initial desorption (β_2, possibly β_3) removes two hydrogens from the same dihydride (trihydride), yielding monohydride directly from trihy-

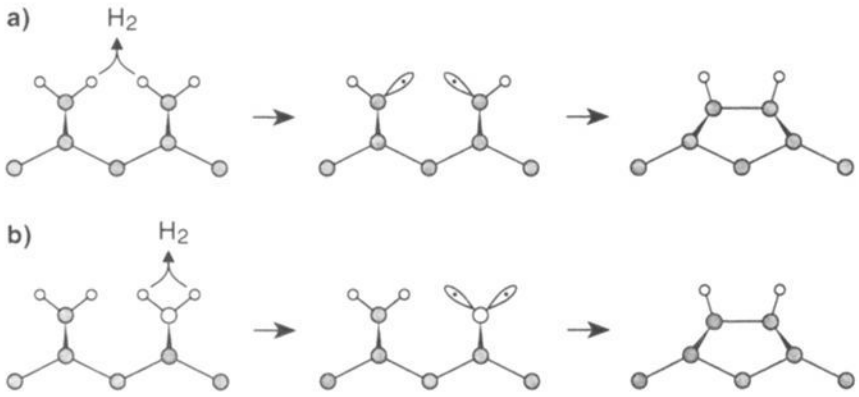

Figure 22. Models of possible desorption mechanisms from higher hydrides on Si(100) (for simplicity shown only for dihydrides): (a) one H atom from each SiH_2; and (b) both H atoms from the same SiH_2.

dride. For dihydride, diffusion occurs from other dihydride sites to fill the created empty sites. As for model I hydrogen desorbs from the resulting monohydride phase at higher temperatures.

The two models are shown schematically in Figure 22, where for clarity only dihydride is shown. This question has not been addressed in detail, but the initial result of the HREELS study by Froitzheim et al.[69] was that model I applies for Si(100)-(2×1) and model II for Si(111)-(7×7). On the other hand, Greenlief et al.[95] found by SSIMS that decomposition of SiH_2 follows second-order kinetics on both surfaces, which suggests model I is operative.

As mentioned above, limited etching also takes place following adsorption at low temperatures, resulting in desorption of silane, SiH_4;[80,97,103] from Si(100), polysilicon hydrides, Si_xH_y, have also been reported.[80] Desorption of SiH_4 is clearly linked to the presence of SiH_3 on the surface,[74,80,103] and thus two channels for depletion of SiH_3 exist: recombination with H to form desorbing SiH_4, or decomposition ultimately resulting in H_2 desorption. The trihydride species is a minority species, with a coverage of a few percent of a monolayer as measured by SSIMS,[95,103] depending on adsorption temperature. No results have been reported for the distribution among the two reaction channels, but for Si(100) a maximum of 4% of the surface hydrogen coverage desorbs as SiH_4, removing about 0.01 ML of Si atoms.[80]

IV. Group III Adsorbates

The elements of group III of the periodic table are important for two applications in silicon technology: they are used as dopants (acceptors) in bulk silicon crystals, and for fabrication of III−V semiconductor films on silicon surfaces.[115,116]

The group III metals (Al, Ga, and In) are solids with vapor pressures suitable for use in evaporation sources, and thus these metals are usually deposited on the clean Si surfaces by evaporation from heated tungsten filaments or Knudsen cells. In device fabrication, compounds such as the organometallics and hydrides are also used, but with organometallics the problem of carbon contamination persists; the use of organometallics is a field in itself and will not be treated here. For boron the usual sources are boron hydrides, and since the sticking coefficient of the simple hydrides is very low,[117] decaborane ($B_{10}H_{14}$) is widely used.

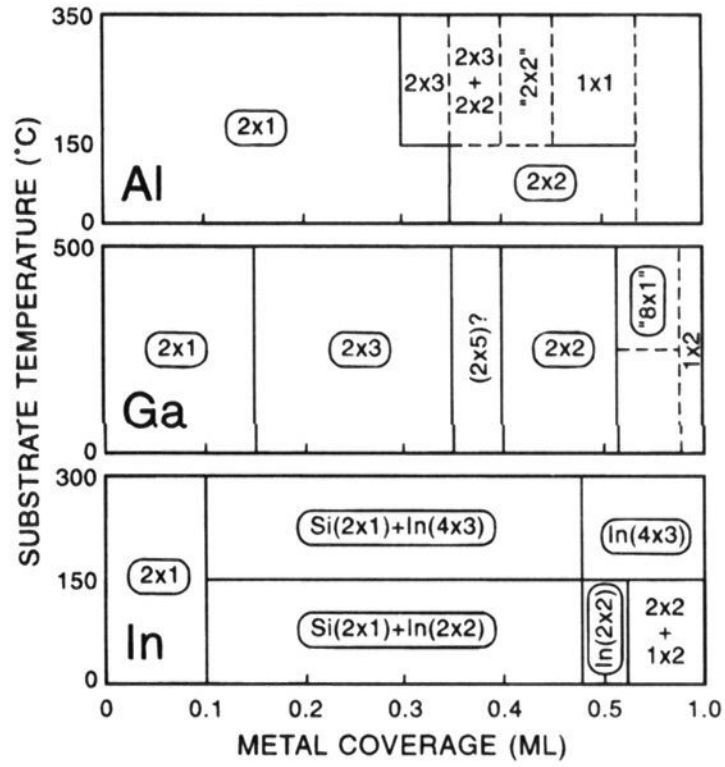

Figure 23. Phase diagrams for the different reconstructions of Si(100) induced by group III metals, as seen by electron diffraction. Phases marked by ovals indicate those also seen in STM studies. Note that the temperature scale is different for the Ga panel, and that the 0.5−1.0 ML coverage region has been compressed.[119]

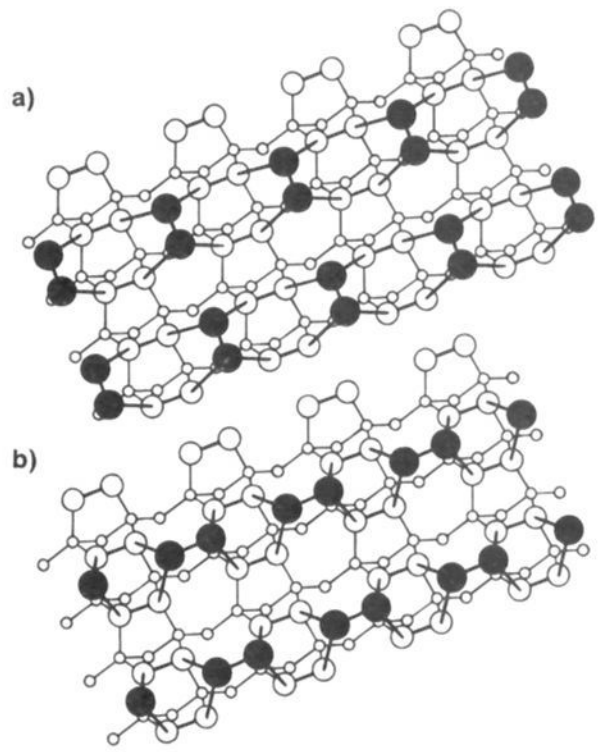

Figure 24. Models for dimer reconstructions of group III metals on Si(100). Note that the Si dimers are intact; adsorbate dimers form in the channels between the Si dimer rows: (a) The original model with adsorbate dimers perpendicular to Si dimers; and (b) the model more recently proposed (for Al) with adsorbate dimers parallel to Si dimers.[119]

A. Si(100)

As seen in the phase diagrams in Figure 23, complex sequences of structures are observed for deposition of Al, Ga, and In on Si(100) depending on coverage and deposition/annealing temperature.[118−123] The (2×2) structure, which is common for all three adsorbates for coverages around 0.5 ML, is the most studied and best understood of these structures. The model shown in Figure 24a was originally proposed on the basis of LEED,[118,121,124] SEM and RHEED,[124] and later confirmed by STM.[53,119,122] In STM images, adsorbate strings were observed to form in directions perpendicular to the Si dimer rows. This was inter-

preted as adsorbate dimers forming in the channels between the Si dimers, saturating the dangling bonds of the Si dimers. In the original model (Figure 24a), the adsorbate dimers were perpendicular to the Si dimers, while Nogami et al.,[119] for Al/Si(100), favored the model in Figure 24b, with the adsorbate dimers parallel to the Si dimers. The model for the (2×3) structure observed for Al and Ga contain the same adsorbate dimer rows as for the (2×2) structure, but here the adsorbate dimer rows are separated by a string of unaffected Si dimers.[119,120] Adsorbate dimers have also been proposed to be involved in some of the other structures observed,[121] but this has not been confirmed.

Gallium and indium have been reported to react more strongly with double-stepped than with nominally flat Si(100) crystals.[125,126] When deposited on a double-stepped crystal at 300 K, the behavior of Ga was identical to that observed for nominally flat crystals.[125] If, however, the surface was annealed after deposition or if Ga was deposited at elevated temperatures (725 K), a strong interaction with the double height steps was observed in STM images. At very low Ga coverages (0.1 ML), kinks developed in the steps or the steps split into single height steps. At higher coverages, step bunching was observed, with Ga dimer rows forming on the large flat terraces between the bunched steps. Similar observations of step bunching and changes in the step directions were made following In adsorption and annealing.[126]

B. Si(111)

As for Si(100) several different reconstructions have been observed for Al and In.[127,128] In general, no ordered structures are observed following deposition of any of the group III elements at temperatures around 300 K. In the submonolayer regime, the most prominent and the best characterized structure is the $(\sqrt{3}\times\sqrt{3})R30°$ structure with a coverage of $^1/_3$ ML. This structure is obtained when several monolayers of the adsorbate are deposited on the Si(111)-(7×7) surface, followed by annealing to 1275 K (B), 925 K (Al and Ga), or 725 K (In).[128−132] In the case of B, Al and In, the $(\sqrt{3}\times\sqrt{3})R30°$ structure has also been reported for deposition of $^1/_3$ ML directly at the annealing temperature.[127,133,134] From studies using several experimental techniques it has been concluded that Al, Ga, and In atoms occupy 3-fold adatom (T_4) sites,[127,131,132,134,135] see Figure 25, while B atoms occupy subsurface substitutional (S_5) sites,[129,130] see Figure 26. The different site observed for B compared to Al, Ga, and In was attributed to the difference in covalent radius. The covalent radius of B is smaller than that of Si, while the others have covalent radii larger than Si. The adsorbates in the T_4 sites saturate all the dangling bonds of the Si surface atoms, and since the group III metals are trivalent, no new dangling bonds are introduced. Lyo et al.[129] found by STS that, although a Si atom occupies the adatom (T_4) position on the boron-modified surface, charge transfer from Si to B leaves the Si dangling bond state for the T_4 adatom unoccupied. Thus the Si(111) surface is expected to be passivated by the adsorption of group III elements, as discussed below.

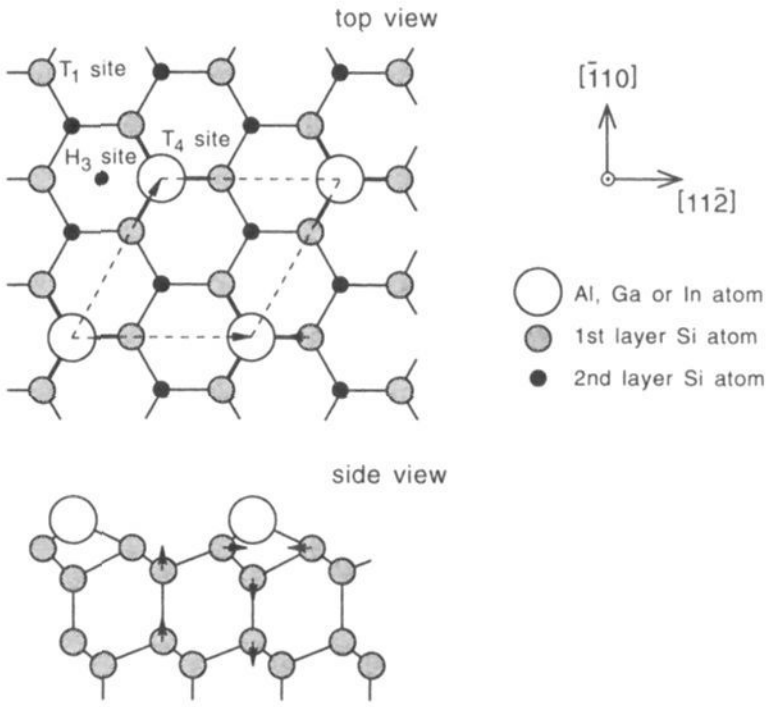

Figure 25. Top and side views of the structure of the $(\sqrt{3}\times\sqrt{3})R30°$ structure observed for Al, Ga, and In on Si-(111). The adsorbate occupies the adatom (T_4) site. Also shown are the two other high symmetry sites, which have been considered: the hollow (H_3) site and the on-top (T_1) site.

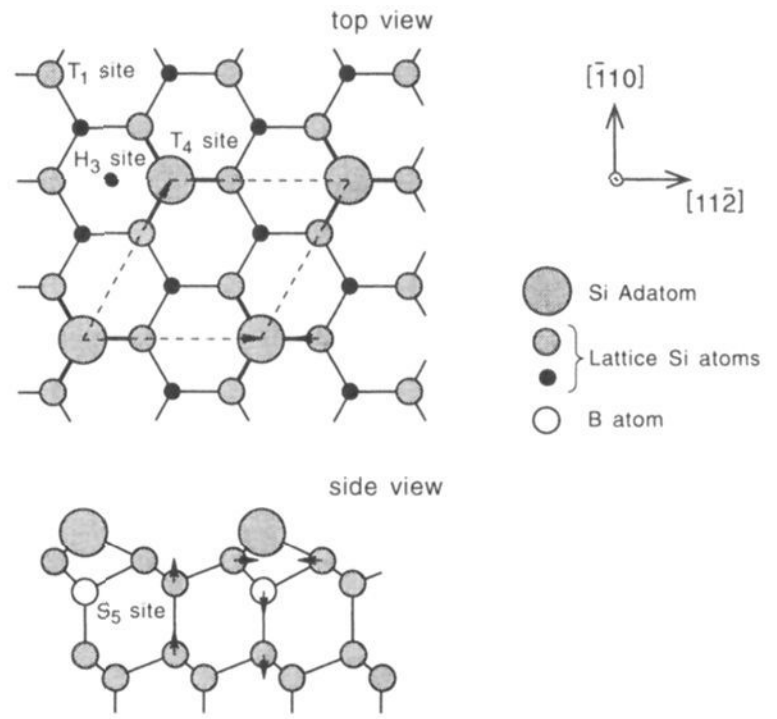

Figure 26. Top and side views of the structure of the $(\sqrt{3}\times\sqrt{3})R30°$ structure observed for B on Si(111). Boron occupies a subsurface (S_5) site.

The thermal decomposition of $B_{10}H_{14}$ on Si(111) was studied in detail by Lyo et al.[129] using STM and by Chen et al.[130] using HREELS and TPD. $B_{10}H_{14}$ adsorbs molecularly,[130] and during decomposition no Si−H bonds form, i.e., the H_2 desorption observed over the temperature range 300−900 K occurs directly from B−H bond breaking. STM images[136] show that the surface is poorly ordered up to the point where the $(\sqrt{3}\times\sqrt{3})R30°$ structure forms after annealing to 1275 K. On the other hand, the $(\sqrt{3}\times\sqrt{3})R30°$ phase is very smooth and well-ordered.[136]

As expected the reactivity of the Si(111) surface is affected by modification with the group III elements. The boron modified surface is far less reactive toward ammonia[136,137] and hydrogen[138] than the clean surface. Ammonia adsorbs and desorbs molecularly,[136,137] in contrast to the dissociation and decomposition observed for the clean surface, as discussed in section

VI.A. For hydrogen, the saturation coverage is lowered significantly and etching is inhibited; no SiH_4 desorption is observed.[138] Surprisingly, the opposite effect is observed for hydrogen on the aluminum-modified surface,[139] where the reactivity for etching is increased. The silane production is increased by a factor of approximately 6, and furthermore the silane desorption temperature is decreased by 300 K. As described in more detail in section III.B, In facilitates the adsorption of atomic hydrogen, forming a (1×1) structure, which is difficult to obtain for hydrogen on the clean surface.

V. Group IV Adsorbates

Silicon shares the diamond crystal structure with its neighbors in group IV of the periodic table, carbon and germanium. Other allotropic forms of carbon, graphite and C_{60}, are less interesting from the electronic device technology standpoint. Diamond, however, has strong possibilities for use as an electronic device material in the future and a review on diamond surface chemistry has just appeared.[140] Ge furthermore has a lattice constant (and covalent radius) very close to that of Si, only 4% larger, while that of C is 34% smaller. Si and C react to form the stoichiometric compound silicon carbide, SiC, while Si and Ge form alloys with various composition, $Si_{1-x}Ge_x$. Both of these products, SiC and $Si_{1-x}Ge_x$, and thin films of diamond, Si itself and Ge on silicon crystals are of technological importance.

A. Carbon and Organic Molecules

The growth of single crystal diamond on Si surfaces is still an elusive goal;[141] in most cases, so-called diamondlike films, polycrystalline films with properties intermediate between graphite and diamond, are obtained. Some of the more promising results have recently been obtained by laser ablation of graphite onto Si(100).[142,143] The significant sp^3 bonding and the high crystallinity (extending over areas as large as 140 × 140 Å^2) obtained even at 300 K have been attributed to the high kinetic energy of the C resulting from laser ablation. Like the diamond surface itself, the thin diamond films are not stable at high temperatures;[143] annealing to 1175 K causes graphitization and formation of silicon carbide.

Recently, the behavior of carbon monoxide on silicon surfaces has been studied and compared to the vast amount of work on CO on transition metal surfaces. Bu and Lin[144] reported that for low exposures (≤10 langmuir) at 100 K, CO does not stick to Si(111), while it adsorbs molecularly on Si(100). HREELS and TPD showed no evidence for any decomposition on Si(100), and molecular desorption was observed around 180 K. Interestingly, Chamberlain et al.[145] found for that for very high exposures (10^4 langmuir), CO also adsorbs on Si(100) at 300 K. Again, the adsorption is molecular, and exclusively molecular desorption is observed around 375 K.

1. Unsaturated Hydrocarbons on Si(100)

Hydrocarbons are important precursor molecules for silicon carbide growth on silicon surfaces. On the clean Si(100) surface, however, the sticking coefficient is zero for hydrocarbons containing single carbon–carbon bonds, even for strained ring compounds such as cyclopropane.[137,146] Thus, attention has turned to hydrocarbons with multiple carbon–carbon bonds, particularly ethylene and acetylene. The interaction of these unsaturated hydrocarbons with Si(100) is particularly interesting, since in this case the interaction of two π-bonded systems is probed. The high reactivity of the C=C double bond with the Si(100) surface was first reported by Bozack et al.[146] for propylene on Si(100), where an initial coverage-independent sticking coefficient near unity was obtained at 120 K.[146] This was also reported for ethylene and acetylene,[147,148] and a typical uptake curve is shown in Figure 27, where the reflected or nonreacted molecules are detected by a mass spectrometer. From the initial independence of the sticking coefficient on coverage and the decrease in sticking coefficient with increasing adsorption temperature, adsorption through a mobile precursor mechanism was proposed.[147,148] Furthermore, the saturation coverage of C_2H_2 and C_2H_4 on Si(100) was determined as 0.75 molecules/Si dimer relative to the perfect surface, which, considering the density of defects on the surface (as observed in STM images), was interpreted as being due to one molecule/Si dimer.[149] Earlier HREELS measurements by Nishijima et al.[150,151] showed that both C_2H_2 and C_2H_4 adsorbed molecularly on Si(100). The model proposed[148] for C_2H_2 and C_2H_4 based on these results was the di-σ model, shown in Figure 28a, where for simplicity only C_2H_2 is shown. In the original model,[150,151] the dimer bond was intact, but later studies by Weinberg and co-workers[148,152,153] postulated that the Si dimer bond is cleaved as Si–C bonds are formed. This model is also in agreement with preservation of the (2×1) LEED pattern following adsorption of ethylene and acetylene.[150,151,154] The C–C stretching mode was observed at 1450[152] and 1100 cm^{-1} [151,153] for adsorbed C_2H_2 and C_2H_4, respectively, compared to 2100, 1600, and 950 cm^{-1} for triple-, double-, and single-bonded carbons. Thus it was concluded that C_2H_2 rehybridizes to sp^2 upon adsorption, and the unusually low C=C vibrational frequency was attributed to interaction between the Si dangling bonds and the rehybridized acetylene

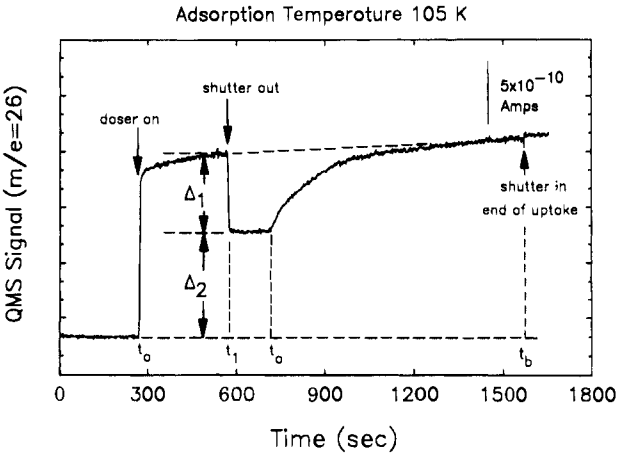

Figure 27. Kinetic uptake measurement of C_2H_2 adsorption on a Si(100) surface at 105 K using a calibrated doser and a QMS detecting the random flux.[148]

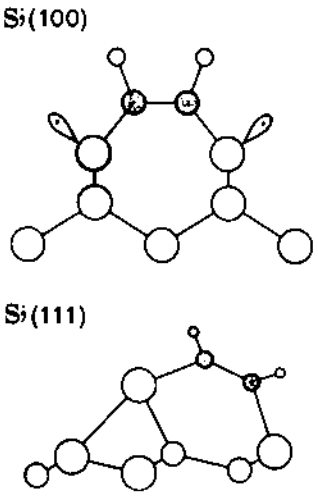

Figure 28. Models for di-σ bonding of C_2H_2. (a) on Si(100): C_2H_2 bonds to the Si dimer atoms through cleavage of the dimer bond (the same model applies to bonding of C_2H_4). (b) On Si(111): C_2H_2 bonds to the dangling bonds of an adatom and a restatom.[148,161]

π-orbital.[152] Similarly, C_2H_4 rehybridizes to near sp^3.[151,153] That the Si dangling bonds are indeed preserved after adsorption of propylene[155] and ethylene[153] is evidenced by the preserved ability to adsorb atomic hydrogen after saturation with the olefin. On the other hand, preadsorbed hydrogen acts as a site blocker, preventing the subsequent adsorption of the olefin.[2,147] The di-σ model is also supported by theoretical studies.[156,157]

Despite the similarity in bonding of C_2H_2 and C_2H_4 to the Si(100) surface, marked differences exist in their thermal behavior. The majority channel for acetylene is dissociation to produce chemisorbed C and H_2(g), with only <5% desorbing molecularly at ~750 K.[148] H_2(g) is evolved at slightly higher temperature than from the hydrogen-covered Si(100) surface, indicating that hydrogen desorption is limited by the C−H bond scission. The carbon left on the surface begins to diffuse into the bulk at temperatures above 800 K. In contrast, ethylene desorbs molecularly at ~550 K, with only approximately 2% of the monolayer undergoing dissociation.[147] This has been attributed to a lower activation energy of C_2H_4 desorption (159 kJ/mol)[147] compared to C_2H_2 (193 kJ/mol),[148] allowing the majority of C_2H_4 to desorb prior to dissociation. An isotopic mixing study by Cheng et al.[158] excluded recombinative desorption: 2 CH_2-(a) — C_2H_4(g) from playing a role in ethylene desorption, showing that ethylene desorbs unimolecularly. A recent study by Widdra et al.[153] showed that the fraction of ethylene decomposing can be increased dramatically by postadsorption of atomic hydrogen. Hydrogen capping of the dangling bonds apparently stabilizes the chemisorbed ethylene on the surface, and, at high hydrogen exposures, induces a conversion of the di-σ bonded ethylene to a mono-σ bonded ethyl species. Thereby the ethylene desorption temperature increased by 100 K, allowing ~60% of the ethylene to decompose.

Recently, the first study of the role of geometrical isomerism in controlling the chemistry of olefin chemisorption and desorption/decomposition has been carried out. Kiskinova and Yates[159] compared *cis*- and *trans*-2-butene on Si(100). These two molecules differ in thermodynamic stability by 4.4 kJ/mol, with the *trans*-isomer being most stable. Both 2-butene molecules adsorb by di-σ chemisorption with similar adsorption kinetics. This indicates that the conformational differences between the two molecules are of little importance in the adsorption kinetics via a mobile precursor process. It is suggested that the molecules preserve their *cis*- and *trans*-forms in the di-σ-bound states on the silicon dimer sites. Upon heating of the saturated 2-butene layers, 25% of the *trans*-butene and 13% of the *cis*-butene undergo decomposition. The steric and related energetic differences in the two chemisorbed butene-derived species are postulated to control the different reactivity, with the more stable *trans*-butene-derived species remaining on the surface to higher temperatures, and therefore being able to undergo more extensive decomposition, compared to the *cis*-derived surface species.

2. Unsaturated Hydrocarbons on Si(111)

Acetylene adsorption has also been studied on the Si(111) surface by both experiment[160,161] and theory.[162,163] The sticking coefficient depends strongly on the surface structure, with an initial sticking coefficient at 300 K of $<10^{-4}$ on the Si(111),[161] compared to >0.5 on the Si(100) surface.[148] By HREELS, Yoshinobu et al.[160] showed that acetylene adsorbs molecularly and rehybridizes to a hybridization state between sp^2 and sp^3. A di-σ model was proposed, but due to the complexity of the Si(111) surface the exact adsorption site could not be determined. Theoretical studies supported the di-σ model,[162,163] but suggested that significant restructuring of the surface was necessary to give dangling bonds with the appropriate separation. However, a recent STM study[161] showed no evidence of rearrangement of Si surface atoms. Instead, a 2:1 preference for reaction at center adatoms compared to corner adatoms was observed. Among the pairs of atoms with dangling bonds in the (7×7) DAS structure, only the restatom−adatom pairs are close enough for reasonable Si−C and C−C bond lengths of a di-σ bonded C_2H_2. And since there are twice as many restatom−adatom pairs involving center adatoms versus corner adatoms, the observed preference for center adatoms is in excellent agreement with di-σ bonding of acetylene between an adatom and a restatom, as shown in Figure 28b. Interestingly, another site preference is also observed for acetylene adsorption on Si(111): the adatoms in the faulted subunits react faster than those in the unfaulted subunits.[161] This site preference could be due to either differences in surface stress or to differences in electronic structure. In either case, the fact that the incoming acetylene is able to sample the surface in order to select the most favorable site indicates either that adsorption occurs by a mobile precursor mechanism, or that reaction occurs with different probabilities for adsorption from the gas on the different sites.

3. Ring Compounds on Si(100) and Si(111)

Recently, studies of ring compounds, cyclohexene and cyclohexadienes,[164,165] as well as aromatic molecules,[165−170] have also been carried out, mainly on Si(111). An interesting difference in the bonding of benzene to Si(100) and Si(111) was reported from HREELS studies by Taguchi et al.[166,168] On both

surfaces, benzene adsorbs molecularly; but on Si(100), benzene is di-σ bonded,[168] while on Si(111), π-bonding is observed.[166] HREELS spectra of benzene on Si(111) display only one C−C stretching mode at 1440 cm^{-1}, close to the frequency observed for gas-phase benzene. In contrast, the spectra from Si(100) display two C−C stretching modes at 1080 and 1595 cm^{-1}, showing the presence of both single and double C−C bonds. The only desorption product observed in TPD is benzene itself,[166,168,170] and the difference in bonding is also evident from the difference in desorption temperatures. On Si(100), benzene is stable up to 450 K, while on Si(111), it is only stable up to 315 K. By sputtering of the Si(111) surface, sites can be created where benzene has a thermal stability similar to that observed on the Si(100) surface.[170] The π-bonded species is believed to be parallel to the surface,[166,170] while the di-σ bonded species is believed to be tilted with respect to the surface plane.[168,169] A tilt angle of 24° was determined from a theoretical study by Craig.[169] Since no H_2(g) or other decomposition products were observed in TPD,[166,168] it was assumed that C was not deposited on the surface.

B. Silicon

Epitaxial Si films are produced either by molecular beam epitaxy (MBE) through deposition of elemental Si or by chemical vapor deposition (CVD) with silicon-containing compounds, mainly silicon hydrides (silanes) and silicon chlorides (chlorosilanes). In the CVD process, the Si crystal is usually held at high temperatures where the unwanted byproducts (hydrogen, etc.) desorb easily.

The surface species obtained after exposure to silanes or chlorosilanes are very similar to the surface species obtained after exposure of the clean surface to hydrogen and chlorine, respectively. Accordingly, in early studies, unambiguous conclusions about the decomposition pathway were hampered by the lack of ability to distinguish adsorbate Si atoms from surface Si atoms. This problem has been alleviated to a certain extent by STM, where a distinction is possible under favorable conditions.

In contrast to the saturated hydrocarbons, silanes with single Si−Si bonds adsorb on Si surfaces with high sticking probability, although the bond strengths of the C−C bond (average experimental value for several small hydrocarbons[171]) and the Si−Si bond (theoretical value for Si_2H_6[67]) are comparable, ~318 kJ/mol. On the other hand, the Si−H bond is somewhat stronger (366 kJ/mol[67]) than the Si−Si bond in disilane. This may be associated with a significantly lower sticking coefficient for SiH_4 compared to Si_2H_6. The silanes adsorb dissociatively, leading to silicon hydride species, SiH_x, on the surface.

1. Adsorption and Decomposition of Silane, SiH_4

The surface reactions of silane on silicon surfaces have been studied in detail by Gates and coworkers.[172-175] Precise determination of the sticking coefficient of silane is difficult due to the unavoidable presence of disilane impurity in silane gas, but using silane gas with less that 4 ppm disilane, a value of

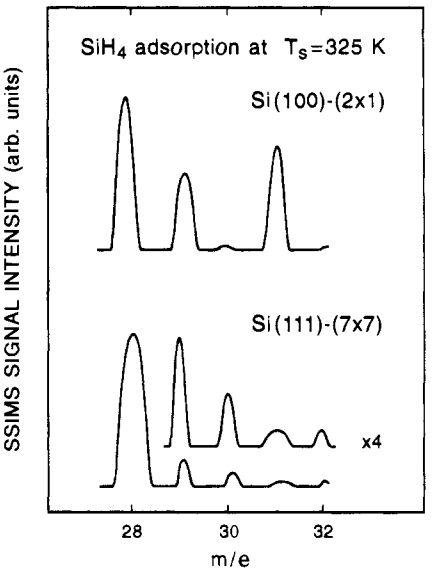

Figure 29. SSIMS spectra from silane adsorbed on Si(100) and Si(111) at 325 K. On Si(100), only SiH_3 and SiH are observed, while on Si(111), mainly SiH_2 and SiH are observed.[174a]

10^{-5} at zero coverage was obtained for both Si(100) and Si(111) at surface temperatures between 375 and 775 K.[173] They proposed that the internal energy of the incoming molecules (i.e., the fraction of the molecules having sufficient energy to overcome the adsorption barrier) is more important than the surface structure in controlling the rate of adsorption.

However, very recently Engstrom et al.[176] found that for higher kinetic energies (~1 eV) the sticking coefficient is much higher, in the range 10^{-2} to 10^{-1}, and is influenced by the surface structure. The sticking coefficient is higher for Si(100)-(2×1) than for Si(111)-(7×7), and additionally, the sticking coefficient for Si(111) increases sharply between 800 and 900 °C, where the (7×7) → (1×1) phase transition occurs. Finally, Engstrom et al.[176] also found that the observed angular dependence of the sticking coefficient could be explained as scaling with energy along the local surface normal of a corrugated surface.

In spite of the identical sticking coefficient, different species are formed on the surface during the adsorption process at ~300 K. SSIMS results,[173,174a] shown in Figure 29, showed that SiH_3 and SiH are formed on Si(100), while SiH_2 and SiH are formed on Si(111). This difference was attributed to the larger distance between the dangling bonds on Si(111) (~7 Å) compared to Si(100) (~2.5 Å), and the following models were proposed:[173] (1) on Si(100), SiH_4 dissociates at adjacent dangling bonds, with SiH_3 bonding to one of the dangling bonds and H bonding to the other; (2) on Si(111), the dissociation occurs at a single dangling bond, where SiH_2 bonds, while H_2(g) is liberated. For adsorption at higher temperatures, SiH_4 dissociates fully upon adsorption, giving SiH(a) and adsorbed H(a).

Following SiH_4 exposure, the only desorption product observed in TPD is H_2.[173,174b] For SiH_4/Si(100), two states were observed identical to the β_1 and β_2 states observed following atomic hydrogen exposure,[174b] and by comparing the TPD areas, a total hydrogen coverage of 0.8 ML from SiH_4 was obtained,

corresponding to 0.4 SiH_4/Si dimer. Interestingly, only a single H_2 desorption state was observed from Si(111), at the same temperature where the β_1 state was observed following atomic hydrogen exposure.[173]

2. Adsorption and Decomposition of Disilane, Si_2H_6

The sticking coefficient for disilane is ~0.5 for both Si(100)[177] and Si(111)[172] at 300 K, and adsorption is dissociative on both surfaces at temperatures above 120 K,[178-185] but molecular adsorption occurs on Si(100) below 90 K.[186] Engstrom et al.[184,185] found that the adsorption probability is very sensitive to the incident translational energy and to surface corrugation. Different models have been proposed for the dissociation process:[187,188]

$$Si_2H_6(g) \rightarrow SiH_2(a) + SiH_4(g) \quad (1)$$

$$Si_2H_6(g) \rightarrow 2SiH_3(a) \quad (2)$$

with the $SiH_x(a)$ species decomposing further at elevated temperatures. Kulkarni et al.[187,189] found that reaction 1 dominates during Si growth on Si(111) at temperatures above 775 K. As for SiH_4, the only desorption product observed in TPD following adsorption at lower temperature is H_2, with peak desorption temperatures identical to those observed after atomic hydrogen exposure.[172,177]

a. Si_2H_6/Si(100). Several groups have studied the deposition of Si films from disilane on Si(100) by XPS[186] and STM,[180,182,183,188] and very interesting results have been obtained from recent detailed STM studies by Hamers and co-workers.[182,188] Several different adsorbate features are observed in STM images after disilane adsorption at 300 K. One type of small bright feature is found midway between two dimers in a single row, away from the center of the dimer row. An adsorbate in this position must have two bonds to the surface, and thus this feature was attributed to SiH_2.[182] A second type of bright feature, appearing slightly larger, is particularly interesting, as it was observed to transform spontaneously to the feature described above over a time scale of minutes. These features were found atop of one of the dimer atoms, and thus they were assigned to SiH_3 terminally bonded to a dangling bond.[188] The third characteristic feature is a dimer with one dark and one bright half, and this is attributed to a dimer with one dangling bond capped by hydrogen[182] (identical to features observed after atomic hydrogen exposure, see section III.A). At high coverage, a large number of $SiH_3(a)$ were observed immediately after adsorption. However, over a time span of a few minutes, the transformation $SiH_3(a) \rightarrow SiH_2(a) + H(a)$ was observed.[188] At low coverages, only the dissociation products $SiH_2(a)$ and H(a) were observed, and the observation of an 1:1 ratio of the numbers of these species excludes adsorption through release of SiH_4(g), reaction 1 above.[188] The higher stability of the $SiH_3(a)$ at higher coverages is probably due to the decreasing number of dangling bond sites available for the further dissociation.

Further decomposition of the $SiH_2(a)$ and creation of new Si dimers occur upon annealing to 470 K.[188] Figure 30a shows models of the new dimer structures

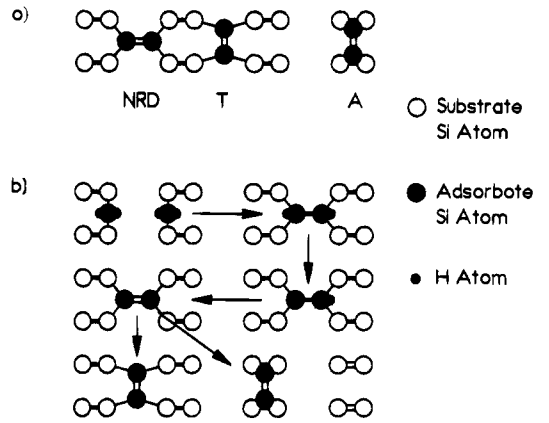

Figure 30. Models for creation of Si dimers following deposition of Si_2H_6 on Si(100)-(2×1) and annealing to 470 K. Dimers with their dangling bonds (π-bond) intact are shown with a double bond: (a) Models for dimer structures observed in STM (NRD, non-rotated dimer (parallel to the underlying dimers)); T, dimer in "trough" site, bonded between two dimer rows; and A, dimer in "atop" site, bonded directly on top of two dimers within a single dimer row) and (b) proposed model for the decomposition of SiH_2, creation of initial nonrotated dimers, which decompose and eventually form rotated dimers.[188]

observed by STM. Ideally, since the Si−Si bond directions rotate by 90° in going from one layer to the next, the dimer direction should also change by 90° when new dimers are formed on top of a dimerized surface. These ideal rotated dimers are observed in two inequivalent positions: on top of the dimer rows (species A in Figure 30a) or in the trough between the dimer rows (species T in Figure 30a). However, nonideal (nonrotated) dimers are also observed, occupying the position between the dimer rows (species NRD in Figure 30a), both with and without attached hydrogens. The presence of nonrotated dimers is surprising, since they are expected to be highly strained, but considering the bonding of the $SiH_2(a)$ species a straightforward model evolves.[188] As shown in Figure 30b, two SiH_2 species next to each other on adjacent dimer rows can easily form a nonrotated dimer by releasing two H atoms. Since the nonrotated dimers are only observed as isolated dimers, not as extended islands,[188] they are considered to be intermediate species. Later, they break up again allowing the individual Si atoms to diffuse over the surface and nucleate into islands of rotated dimers, as shown schematically in Figure 30b. Interestingly, segregated regions are formed on the surface, with the Si atoms deposited from disilane accumulating in hydrogen-free Si islands, while the H atoms are transferred to the substrate Si atoms creating monohydride regions separating the Si islands.[188]

b. Si_2H_6/Si(111). Following adsorption of disilane on Si(111)-(7×7) at 120 K, IR spectra[179,190] show two vibrational modes at 2154 and 2130 cm^{-1} attributed to the symmetric and asymmetric stretching modes of $SiH_3(a)$, respectively. On the other hand, adsorption at 400 K gives only SiH(a) species, characterized by a single stretching mode at 2096 cm^{-1}. From the preferential quenching of the S_2 state (dangling bond state of the restatoms) in UPS spectra (Figure 31), Avouris and Bozso[181] concluded that SiH_3 bonds

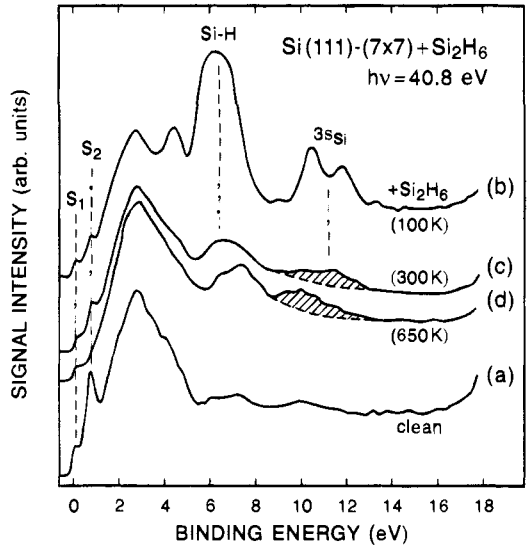

Figure 31. UPS spectrum of (a) clean Si(111)-(7×7), (b) after exposure to 1.5 langmuir of Si_2H_6 at 100 K, (c) after annealing to 300 K, and (d) after annealing to 650 K. Preferential quenching of the S_2 (restatom dangling bond) state is observed, first upon adsorption and further when the adsorbate Si–H bonds are broken by annealing to 650 K.[181]

primarily to the restatoms. The UPS spectrum following disilane adsorption at 100 K (Figure 31b) clearly shows the decrease in intensity of the S_2 state relative to the spectrum of the clean surface (Figure 31a), while the S_1 state (dangling bond state of the adatoms) is unchanged. The remainder of the spectrum is dominated by peaks assignable to physisorbed Si_2H_6. Annealing to 300 K desorbed the molecularly adsorbed Si_2H_6, leaving the Si–H state at 6.5 eV and the $3s_{Si}$ state at 11.5 eV (Figure 31c). The intensity of the S_2 state is unchanged, however, showing that reaction with the restatom dangling bonds occurs already at low temperature. The intensity of the S_2 peak decreases even further after decomposition of the SiH_x species by annealing to 650 K (Figure 31d), showing that the H atoms released bond preferentially to the restatoms. In contrast, on Si(111) surfaces exposed to atomic hydrogen, H atoms bond to both adatom and restatom sites.

3. Adsorption and Decomposition of Chlorosilanes

Several of the chlorinated silicon compounds considered as candidates in CVD growth of silicon films, $SiCl_4$,[191-193] SiH_2Cl_2,[194-196] Si_2Cl_6,[192,197] and $(C_2H_5)_2SiCl_2$,[198] have been studied on clean Si surfaces. Many of the chlorosilanes, however, cannot be used in CVD processes alone, since the primary chlorine-containing desorption product from a chlorine-covered surface is $SiCl_2$. This implies that unless the Cl atoms are removed in a different way (in high-temperature CVD, chlorosilanes are mixed with H_2), the surface will be etched instead, e.g., through the net reaction $SiCl_4 + Si \rightarrow 2SiCl_2$. If H atoms are present on the surface, at least some of the Cl atoms can be desorbed as HCl, and promising silicon deposition results have also been obtained with SiH_2Cl_2,[194,195] and with alternating exposures of Si_2H_6 and Si_2Cl_6.[197]

Similar to the case of the silanes themselves, the sticking coefficient is much higher for chlorinated

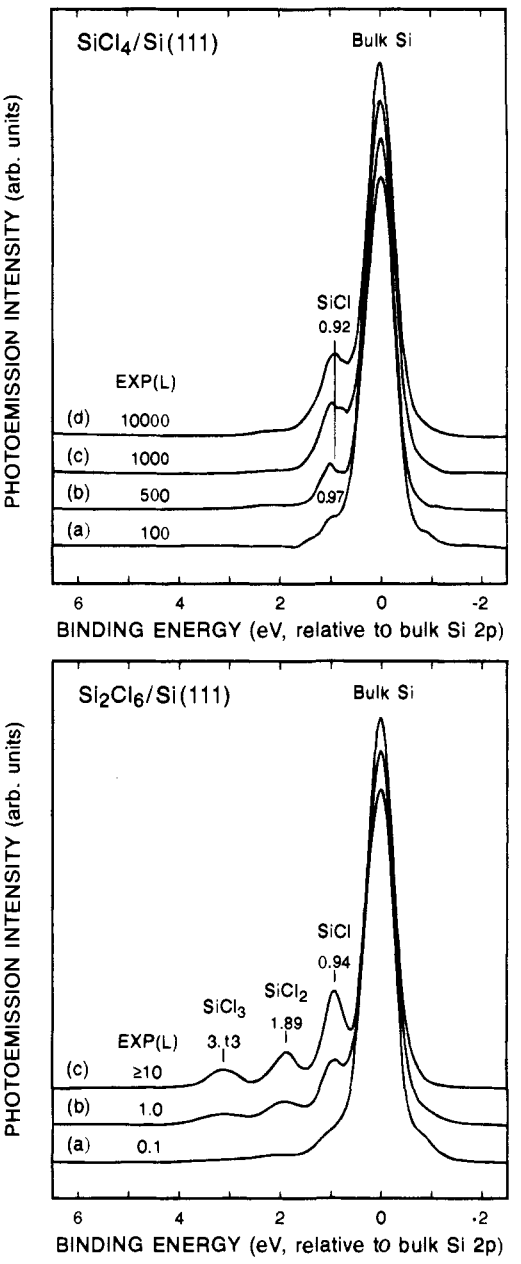

Figure 32. $Si2p_{3/2}$ XPS spectra after exposure of 300 K Si(111)-(7×7) to increasing amounts of $SiCl_4$ and Si_2Cl_6.[192]

silicon compounds containing a Si–Si bond,[192] although there is some discrepancy in the values reported for $SiCl_4$ on Si(111) at 300 K. The LITD results of Gupta et al.[191] yielded a value of 0.1, while Whitman et al.[192] estimated a value ≤0.002 from AES measurements. Both $SiCl_4$ and Si_2Cl_6 adsorb dissociatively, but as seen in the XPS spectra of Figure 32 the dissociation products are different.[192] $SiCl_4$ dissociates fully to monochloride species (Figure 32, top), although it is not clear whether three or four Cl atoms are transferred to substrate Si atoms. On the other hand, a mixture of mono-, di-, and trichloride species are formed from Si_2Cl_6 (Figure 32, bottom). Interestingly, the binding energy shifts for the $SiCl_3$ (+3.13 eV) and $SiCl_2$ (+1.89 eV) species obtained from Si_2Cl_6 are significantly higher than those obtained after chlorine exposure, 2.72 and 1.65 eV, respectively (see section VIII.A and Figure 53). This was attributed to reduced screening for the $SiCl_x$ species sitting on the surface than for similar species

where the Si atom is part of the surface Si layer.[192] Annealing of the Si_2Cl_6 exposed surface to 575 K leads to dissociation of the $SiCl_x$ species, leaving only monochloride on the surface.[192]

A recent study by Gao et al.[193] using TPD, ESDIAD, and HREELS, showed that the behavior of $SiCl_4$ on Si(100) is very different from that on Si(111). At 125 K, molecular monolayer and multilayer adsorption of $SiCl_4$ was observed, and the majority of the $SiCl_4$ desorbs molecularly at temperatures below 200 K. A few percent of a monolayer dissociates during heating, yielding monochloride species on the surface at 673 K, and finally desorbing as $SiCl_2$(g) above 800 K.

4. Deposition of Elemental Silicon

Depending on the surface temperature of the substrate, two basic growth modes are observed in MBE: island growth and growth through step propagation. Island growth, where nucleation occurs on extended terraces, dominates at lower temperatures where the surface diffusion is limited; defect sites often serve as nucleation centers.[199] In most cases, however, bonding at step sites is favored over bonding at terrace sites, and thus at higher temperatures the increased silicon mobility enables all of the incoming atoms to diffuse to the steps. In this case, growth through step propagation, step flow, is obtained.

For deposition of silicon on silicon surfaces, temperatures above 750[200-202] and 875 K[199] are required for initiation of growth by step flow on Si(100) and Si(111), respectively. At lower temperatures, island growth occurs and the islands are partly amorphous at temperatures below ~525 K.[199,203] In the intermediate temperature range the structures of the islands are similar to those of the underlying substrates, i.e., dimer structures on Si(100) and DAS structures on Si(111).

The Si islands observed on Si(100) are strongly anisotropic, a few dimers wide and up to 100 dimers long.[202,204] Mo et al.[205] showed that after annealing the shapes are much more rounded, and thus the anisotropy is a growth phenomenon and not an equilibrium phenomenon. Two other plausible causes for the anisotropy have been considered: anisotropic diffusion and anisotropic accommodation. Although it has been shown by both STM experiments[206] and by theory[207] that surface migration is much faster along the dimer rows than perpendicular to them, other calculations have shown that this would not be sufficient to give anisotropic growth shapes.[208] On the basis of these calculations, the anisotropic shapes were attributed to a much larger kinetic sticking coefficient at the end than at the side of a dimer row.[208] In agreement with this, S_B steps (which consist of dimer row ends, Figure 6) were found to be much better sinks for Si atoms than S_A steps (which consist of dimer row sides, Figure 6).[206] This conclusion was based on the observation of a considerably larger denuded zone (regions from which all the deposited atoms have migrated to the step) around S_B steps than around S_A steps. Furthermore, the S_B steps appeared to be symmetric sinks for atoms coming from the upper and lower terrace, i.e., no large barrier for step crossing exists.[206] This conclusion was drawn from the observation of denuded zones of equal width around steps in the ⟨100⟩ direction. Steps in this direction are at an angle of 45° relative to the dimer rows; thus they consist of alternating sections of S_A and S_B steps, causing all terraces in between to be equivalent.

The structure of the deposited Si layer on Si(111)-(7×7) is highly affected by the surface reconstruction. Even the amorphous clusters obtained for deposition at 300 K grow exclusively within the (7×7) unit cells, leaving the corner holes and the dimers uncovered.[199] The islands formed at a deposition temperature above 650 K display (7×7) reconstruction, and for the majority of the islands, the (7×7) structure on top of the island is in registry with that of the substrate below.[199] In addition, smaller domains with other DAS reconstructions, (5×5) and (9×9), are also observed.

C. Germanium

The interest in germanium interactions with silicon surfaces stems from potential applications of Ge thin film structures and the production of $Si_{1-x}Ge_x$ alloys for electronic device technology. The main interest is obtaining thick films, and Ge hydrides and chlorides are commonly used in chemical vapor deposition (CVD) of Ge on silicon surfaces, but very few studies of the decomposition of these species on clean Si surfaces exist. GeH_4, Ge_2H_6,[209] and $GeCl_4$[210] were all reported to adsorb dissociatively at 300 K and below. By annealing, Cl and H can be removed, as $SiCl_2$ and H_2, respectively, leaving elemental Ge on the surface. Part of the hydrogen desorbs at lower temperature than from clean Si, and this effect can be enhanced by cycles of GeH_4 adsorption and H_2 desorption.[209] This low temperature H_2 was speculated to originate from Ge sites, as the desorption temperature is close to that observed from hydrogen on Ge surfaces.

A full description of the CVD and related processes is beyond the scope of this review, but one aspect of growth of thick films is worth mention. Ge grows on clean Si crystals in the Stranski-Krastanov mode,[211-214] i.e., islands start to form after deposition of only a few Ge layers. This is undesirable from the point of view of obtaining thick homogeneous films, and ways to circumvent this problem have been sought. Good results have been obtained[215-218] by using "surfactants" as originally proposed by Copel et al.[219] Surfactants are defined as species that change the surface energies of the substrate and the adsorbate; in this case, in such a way that island formation is suppressed. Furthermore, in order to obtain uncontaminated films, the surfactant must segregate from the substrate and the adsorbate, always staying on top of the layered structure. Common surfactants in Ge epitaxy on Si are As[219] and Sb,[215,217,218] but Te was also found to be very effective,[216] and pure layer-by-layer Ge growth and high crystallinity were obtained even for thick Ge films. One practical obstacle is that perfect segregation is rarely obtained, and usually small amounts of surfactant must be supplied continuously—meaning that the films are slightly contaminated.

In the growth of the very first layers, the behavior of Ge on Si surfaces mimics that of clean Si surfaces

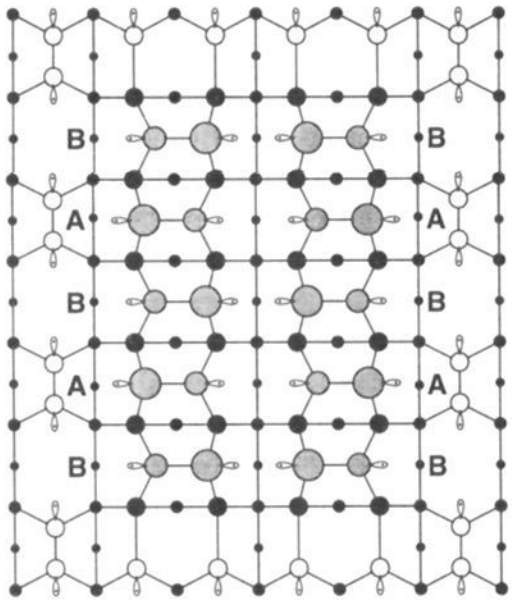

Figure 33. Schematic structure of a Ge island on Si(100) observed by STM. Empty and filled circles indicate Si atoms with and without a dangling bond, respectively. The Ge dimers are buckled; large hatched circles denote up-atoms, and smaller hatched circles denote down-atoms. Note that substrate Si dimer rows meet with Ge dimer up-atoms (positions marked A), and channels between Si dimer rows meet with Ge dimer down-atoms (positions marked B).[220]

closely. For studies of these systems, deposition of elemental Ge from evaporation sources has been employed primarily. Deposition at a crystal temperature of 300 K gives unordered surfaces, and temperatures above 625 K are needed to form ordered structures. On Si(100), Ge dimers are formed,[8,220] and the discussion of symmetric versus buckled dimers extends to this system as well. Figure 33 shows a schematic diagram of a typical Ge island observed by STM[220] during early stages (≤0.2 ML) of the deposition. At least in this low coverage limit, the Ge dimers are buckled, and the correlation *between the buckling direction of the Ge dimers and* the location of the underlying Si dimer rows should be noted.

For Ge deposition on Si(111)-(7×7), DAS structures were observed, but interestingly, the (5×5) structure appeared to be the more stable structure.[211,221] For very low coverages the (7×7) and the (5×5) structures coexisted,[221] but for a coverage of 2 ML, the surface was completely (5×5) reconstructed. After annealing to 975 K or for deposition at this temperature, a (7×7) structure is obtained. Since the DAS reconstructions involve several layers, the question arises of how Ge is distributed among these layers—and whether Si/Ge substitution occurs below the surface. Early studies[211,222] suggested that in particular the high temperature (7×7) structure was a Ge−Si alloy structure, while more recent experimental and theoretical results[223] indicated that Ge adsorption on top is more likely.

VI. Group V Adsorbates

Interactions of species containing elements from group V of the periodic table with silicon surfaces fall into two important classes: (1) incorporation of the group V element in the silicon surface itself, creating a silicon-containing film on top of the silicon crystal; and (2) reaction of the group V element with other species to form thin films on top of the silicon crystal. The first class of reactions has mainly been studied for nitrogen containing species, where the goal is to produce films of technologically important silicon nitride, Si_3N_4, on the surface. Another technologically important product are thin films of *III*-V semiconductors supported on silicon. GaAs[115,116] is the most studied example from the second class.

The vast majority of the work with group V elements has been concerned with nitrogen, and with ammonia in particular, since the reaction of NH_3 with Si surfaces has been used as a prototypical example to study the reactivity of the dangling bonds on silicon surfaces.

A. Nitrogen-Containing Species

The first study of thermal nitridation of silicon surfaces by Heckingbottom and Wood in 1973[224] reported Si_3N_4 production on Si(100), Si(111), and Si(311) by exposure to ammonia and nitrogen gas at elevated temperatures (1073−1373 K). It was already recognized at this point that N_2 gas is far less efficient for silicon nitridation than NH_3, and it has later been confirmed that the sticking coefficient of N_2 is very low. Therefore more recent studies have focused on other nitrogen containing compounds, mainly NH_3 but also NO and lately N_2H_4 and HN_3 (hydrazoic acid), and on nitrogen atoms created by dissociation of N_2. Independent of the reactant gas employed the properties of the Si_3N_4 layer formed are very similar.[225] A new Si(LVV) Auger feature develops at ~84 eV[224−229] in addition to the elemental Si(LVV) AES feature at 92 eV, which shifts down in energy to 90.5 eV after initial nitrogen exposure.[225,227−229] The N(KLL) Auger feature remains fixed in energy at ~368 eV.[224,226−229] Two different ordered structures are formed for silicon nitride on Si(111) depending on the adsorption/annealing temperature, the "8×8" and the quadruplet structures (for films contaminated with small amounts of carbon[228]),[226,228,230,231] whereas no ordered structure has been found for silicon nitride on Si(100).[232] HREELS spectra after annealing to 1240 K show four vibrational loss features at 485, 735, 970, and 1135 cm^{-1}, which further develop into spectra with one intense loss at 970 cm^{-1} and two small features at 485 and 725 cm^{-1} by further annealing to 1350 K.[225,229,231] On the basis of a comparison of HREELS spectra[231] with IR spectra of crystalline and amorphous Si_3N_4, the film obtained after 1350 K annealing is believed to be Si_3N_4. Several studies have indicated that a monolayer of silicon exists on top of the Si_3N_4 film.[225,231,233,234]

Low temperature (≤300 K) growth of Si_3N_4 has been carried out by electron stimulation during[235,236] or following[236] NH_3 adsorption. Bozso and Avouris[235] suggested that the main role of the electrons is to desorb hydrogen from the surface. However, N−H bond breaking is a dominant process in electron-stimulated surface chemistry.[237−239] Using a cycling procedure, alternating NH_3 adsorption and electron irradiation, Tarasova et al.[236] confirmed that the stimulation occurs at the surface and is not due to excitation of NH_3 in the gas phase.

Silicon nitride is removed from the surface by annealing above 1400 K, where desorption of Si_2N occurs.[225,227,232,240]

1. Adsorption of N Atoms

The processes leading from initial Si−N bonding at low temperatures to the ultimate silicon nitride film after annealing can be investigated with the adsorption of N atoms on the surface without interference from other coadsorbed molecular fragments. Unfortunately most studies have been concerned with reaction with atomic nitrogen at high temperatures,[224,226-228] preventing the thermal activation steps at lower temperatures from being probed. For N adsorption on Si(111) at 300 K the HREELS spectra of Edamoto et al.[231] showed two vibrational features at 400 and 820 cm^{-1}, assigned to a near-planar Si_3N structure by comparison to the known structure and vibrational modes of $(SiH_3)_3N$. Bozso and Avouris[241] found by UPS for N on Si(100) that adsorption at 100−300 K removed the dangling bond states of Si, indicating that the dangling bonds are of importance in binding atomic N to Si(100).

2. Adsorption and Decomposition of NH_3

Although the direct thermal nitridation takes place at high temperatures, finding ways to make Si_3N_4 films at low temperatures is an important issue. After intensive studies it has been concluded that NH_3 adsorption is dissociative even at 90 K[235,242-244] and the dissociation products depend on the actual surface structure. Over the years, several models have been proposed for ammonia adsorption on Si(100) and Si(111) at low temperatures including all possible configurations from molecularly adsorbed NH_3,[245] to partially dissociated NH_x species,[241,242,246,247] to full NH_3 dissociation.[235,248-250] Before we turn to these different models and the experimental results supporting them, some common observations for the two surfaces are worth mentioning. On both surfaces it has been reported that the reconstructions, (2×1) and (7×7), respectively, are preserved after the reaction with NH_3,[244,248,251-253] indicating that reaction occurs mainly at existing dangling bond sites without major disruption of the Si surface structure. Specifically, for the Si(100) surface the preservation of the (2×1) structure strongly suggests that the dimer bonds are not broken, i.e. reaction can only take place at the dangling bonds. For adsorption at low temperature, multilayers of molecular NH_3 are adsorbed on top of the initial dissociated layer,[247,248,254-256] and the multilayers are removed by mild annealing (220−350 K depending on physisorbed amount).[248,255]

a. NH_3/Si(100). On the basis of XPS, ISS, UPS,[235,248] and STM[249,250] studies, Avouris and coworkers originally proposed that NH_3 dissociates fully on Si(100) even at 90 K yielding N in subsurface sites and hydrogen capping the dangling bonds in a structure similar to the monohydride phase. They based this conclusion mainly on STM images and UPS spectra following NH_3 adsorption which were very similar to those obtained following atomic H adsorption. In a later photoemission study, Bozso and Avouris[241] reported an N(1s) XPS peak with a binding energy (BE) of 398.5 eV, which they assigned to NH(a), concluding that Si(100) dissociates NH_3 to produce NH(a) at 100 K. From their photoemission studies Bolmont et al.[242,257] also reported only partial dissociation to NH_x species (x = 1, 2), although they favored NH_2 species over NH, despite the reported saturation coverage of ~0.25 ML of N. The presence of NH_2 was confirmed by the HREELS studies of Fujisawa et al.,[246] where stretching (3335 cm^{-1}) and bending (1570 cm^{-1}) modes of Si−NH_2 and Si−H stretching modes (2080 cm^{-1}) were observed after NH_3 adsorption at 300 K. The model proposed by Fujisawa et al.[246] on the basis of these result was that NH_2 and H each saturate one dangling bond of the surface dimer, as shown in Figure 34. The same model was proposed for NH_3 adsorption at 120 K from an independent study by Dresser et al.[247] From the observation of NH_2D as the dominating D-containing species in TPD following coadsorption of D_2 and NH_3, together with a characteristic H^+ ESDIAD pattern attributable to torsional oscillations about the Si−NH_2 bond, it followed that NH_2 was the majority surface species. Furthermore, these workers[247] showed by uptake measurements using a calibrated doser and a QMS that the saturation coverage was one NH_3 (i.e. one NH_2 and one H) per Si dimer. This has later been challenged by Chérif et al.,[252] who reported a saturation coverage of one NH_2 and one H per 2 Si dimers (NH_2 and H occupy bridging positions above the dimers) from uptake measurements on Si(100) surfaces dosed by backfilling the chamber with NH_3. The measurements locating the saturation exposure were made by AES. On the other hand, a theoretical study by Zhou et al.[258] confirmed that the adsorption of NH_3 on Si(100)-(2×1) is dissociative to NH_2 and H each bonded to one of the dangling bonds of the Si dimers as shown in Figure 34. Later studies by HREELS,[259,260] XPS,[254,261] and SSIMS[255] have all confirmed that the dissociation products are NH_2 and H, but the issues of the adsorption site and the saturation coverage are still not fully resolved. Interestingly, Dufour et al.[256] concluded from their very recent XPS study that in addition to NH_2(a) and physisorbed NH_3(s), N(a) and weakly adsorbed NH_3(a) are also present at the Si(100) surface after adsorption at 90 K. On the other hand, this study suggests that after heating to 300 K, exclusively NH_2(a) is found on the surface, as can be seen from the deconvoluted XPS measurements shown in Figure 35a.

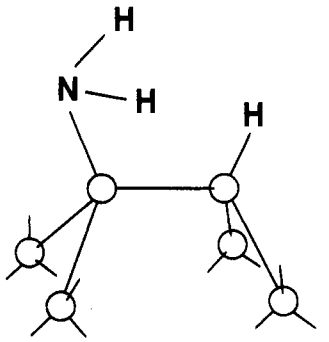

Figure 34. Schematic of the bonding of NH_2 and H, resulting from dissociative adsorption of NH_3, to the dangling bonds of Si(100)-(2×1).[247]

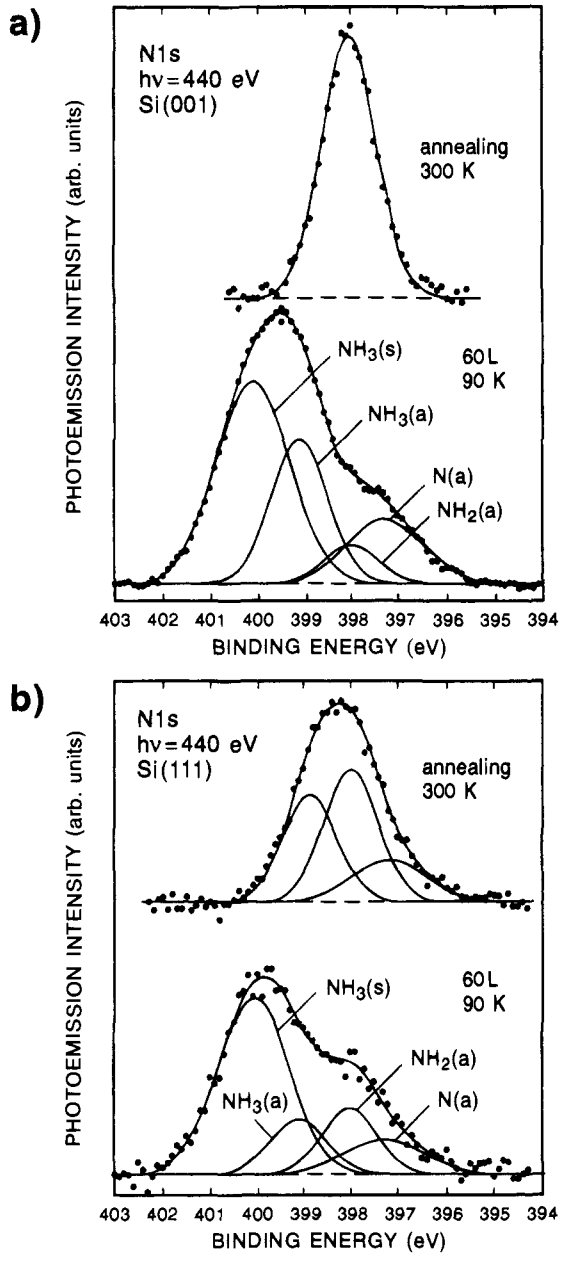

Figure 35. XPS spectra of NH_3 on (a) Si(100) and (b) Si(111). The assignments of the peaks are indicated.[256]

Only a few studies[247,252,262] have been concerned with NH_3 adsorption kinetics, and it was shown that NH_3 adsorbs with a high and constant sticking coefficient almost up to saturation, suggesting that the adsorption occurs by a mobile precursor mechanism.

The next important issue is the further decomposition of the NH_2 resulting from the dissociative adsorption, eventually leading to Si_3N_4 deposition on the surface. Apart from the low temperature (<350 K) desorption of the molecularly adsorbed NH_3 mentioned above, the most prominent thermal desorption state is the H_2 state at ~750 K,[235,247] and in addition, a second NH_3 desorption state is observed at ~625 K.[247] By coadsorption of D and NH_3 Dresser et al.[247] confirmed that the low-temperature NH_3 desorption state is indeed due to desorption of molecularly adsorbed NH_3, since no isotopic mixing is observed for this state. In contrast, isotopic mixing is observed for the high-temperature NH_3 state,

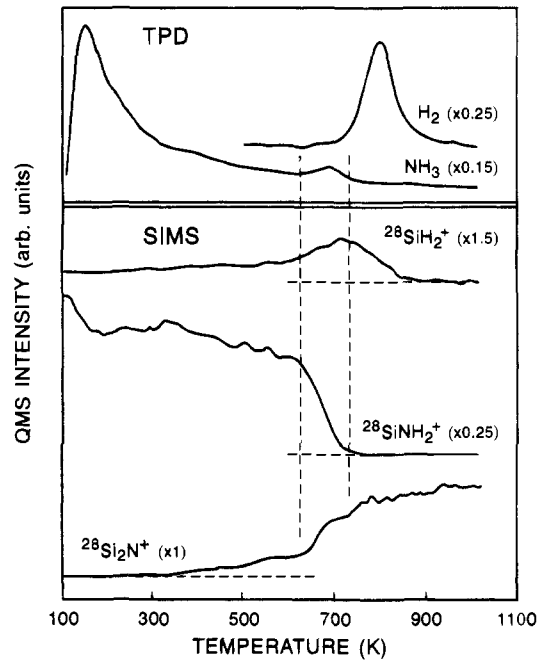

Figure 36. Thermal desorption of H_2 and NH_3 compared to temperature-programmed SSIMS of SiH_2^+, $SiNH_2^+$, and Si_2N^+ for Si(100). The decrease in the $SiNH_2^+$ SSIMS signal is accompanied by increases in Si_2N^+ and SiH^+ signals and by desorption of NH_3. Subsequently the SiH^+ SSIMS signal decreases as H_2 desorption is observed.[255]

indicating that this state arises from recombinative desorption of NH_2 and H(D).[247] Thus the following two reaction channels for NH_2 decomposition on the surface were proposed:[247]

$$NH_2(a) \rightarrow N(a) + 2H(a) \quad (3)$$

$$NH_2(a) + H(a) \rightarrow NH_3(g) \quad (4)$$

The direct decomposition, step 1, of NH_2 to N and H was confirmed by a SSIMS study by Zhou et al.[255] and a HREELS study by Chen et al.,[260] where no evidence for an intermediate NH species was found. Indeed, the intensities of the $SiNH_2$-SSIMS signal[255] and the $SiNH_2$-vibrational mode[260] decrease only slightly up to ~600 K, and then the $SiNH_2$-SSIMS signal decreases rapidly above 630 K, accompanied by increases in SiH- and Si_2N-SSIMS signals and NH_3 desorption;[255] results from SSIMS and TPD are shown in Figure 36. From the relative peak areas for NH_3 and H_2 in the early TPD study,[247] the recombination channel was reported to be the minority channel, whereas a more recent TPD study concluded from a comparison of the amount of H_2 desorption following saturation with atomic hydrogen and with NH_3, respectively, that 73% of the $NH_2(a)$ is depleted by recombination to produce NH_3 at ~600 K.[260]

b. NH_3/Si(111). Although the surface structure of Si(111)-(7×7) is much more complicated than the structure of Si(100)-(2×1), the adsorption of NH_3 on the former surface has been much less controversial. The adsorption was found to be dissociative to produce NH_2 and H at 300 K and below. This was determined from HREELS,[244,260] XPS, UPS,[241] and AES[251] measurements. However, as for Si(100)-(2×1) very recent XPS results by Dufour et al.[256] have been

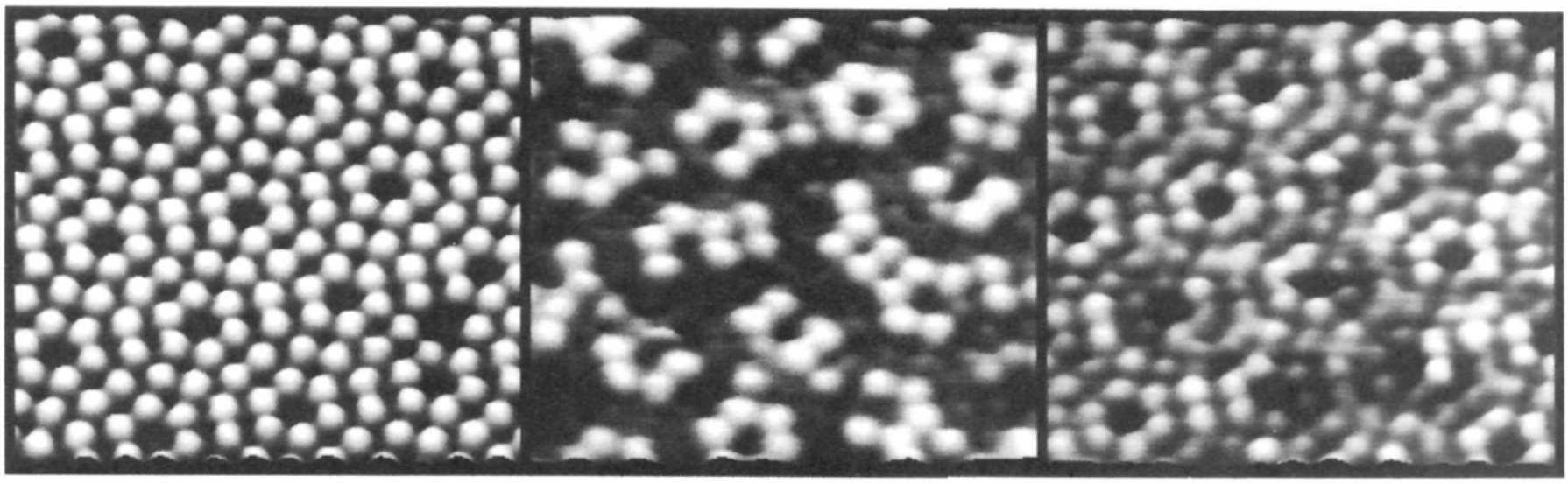

Figure 37. STM topographs of the unoccupied states of Si(111)-(7×7); left, clean (crystal bias = +0.8 V); center, partially reacted with NH_3 (crystal bias = +0.8 V); and right, partially reacted with NH_3 (crystal bias = +3.0 V).[253]

interpreted as revealing the presence of N(a) and weakly adsorbed NH_3(a) at the surface at 90 K in addition to NH_2(a) and physisorbed NH_3(s). In contrast to Si(100), some NH_3(a) and N(a) remain on the surface in addition to NH_2(a) after annealing to 300 K (Figure 35b).

Due to its complicated structure, the Si(111)-(7×7) surface displays several different adsorption sites, and the scanning tunneling microscope has been a powerful tool in elucidating the reactivity of the different sites. Combining STM and STS, Wolkow and Avouris[253] found significant differences in the reactivity of the different kinds of dangling bonds, with the restatoms being more reactive than the adatoms; the center adatoms are more reactive than the corner adatoms. Figure 37 shows STM images of the surface before (Figure 37, left) and after (Figure 37, center and right) reaction with NH_3—the bright features in the images are adatoms. Imaging the partially reacted surface with the same the bias (0.8 V) as the clean surface (Figure 37, center), some adatoms have apparently disappeared—these appear as dark sites. Increasing the bias (+3.0 V, Figure 37, right) causes these adatoms to reappear, although still darker, and the basic (7×7) unit cell is seen to be preserved. As seen in Figure 37, the restatom sites are not prominent features in the STM images, but they can be probed by STS as shown in Figure 38. The curves A are the tunneling spectra over the unreacted restatom sites while the curves B and C are over two types of adatom sites. The difference between the unreacted (Figure 38A, left hand side) and the reacted restatom site (Figure 38A, right hand side) is striking. Clearly, the dominant feature at −0.8 eV due to the occupied dangling bond state for the restatoms on the clean surface has been removed on the reacted surface. In the right panel the solid and the dashed curves B show the spectra for an unreacted and a reacted corner adatom site, respectively, and again a clear difference is observed. Inspection of large numbers of topographs and spectra similar to those in Figures 37 and 38 revealed that when about half the adatoms were still unreacted, no unreacted restatoms remained at all; among the adatoms more unreacted corner adatoms than unreacted center adatoms were found. Furthermore, by comparing curves B and C in the left and right panel of Figure 38, is evident that while the unreacted corner and center adatom sites are different on the clean surface they become very similar on a surface where the restatoms have reacted. Specifically, for the center adatoms the distribution between occupied and unoccupied states is reversed.

As for the Si(100)-(2×1) surface the main thermal desorption feature after NH_3 adsorption on Si(111)-(7×7) is the desorption of hydrogen at ~750 K. Interestingly, no high-temperature NH_3 desorption is observed for Si(111)-(7×7),[263] indicating that some differences exist between the decomposition channels for NH_2(a) on the two surfaces. In the original HREELS study[244] it was proposed that NH_2(a) decomposes directly to N(a) and H(a) as on Si(100), since the expected Si−N−H bending mode (~1170 cm^{-1}) was not observed. However, in a later HREELS study on Si(111), Colaianni et al.[263] assigned the weak mode at 1100 cm^{-1} (which in ref 244 had tentatively been assigned to NH_2) as a δ(NH) mode, indicating that NH(a) exists on the Si(111) surface between 200 and 700 K following NH_3 adsorption at 80 K. This study also showed that the thermal stability of NH_2 depends on the initial NH_3 exposure; for high exposure NH_2 is stable up to 600 K. Similar results were obtained by Koehler et al.[240] using LITD, except for a discrepancy in temperature; in this study NH(a) and NH_2(a) was reported to be stable up to 800 and 700 K, respectively. Thus the following scheme for decomposition of NH_2 on Si(111) was proposed:[260]

$$NH_2(a) \rightarrow NH(a) + H \quad (5)$$

$$NH(a) \rightarrow N(a) + H \quad (6)$$

By comparing usual Si−N bond lengths to the different Si−Si distances on the (7×7) reconstructed surface, Chen et al.[260] recognized that >NH cannot bridge two dangling bond sites. Combining their result with the differences in reactivity of different sites mentioned earlier,[253] they proposed the model shown in Figure 39. Initially NH_2 bonds to the dangling bond of an adatom. Then, during annealing, one of the strained backbonds of the adatom is broken and >NH is inserted into the backbond. Because less strain exists in the Si−Si back-bonds on Si(100) compared to Si(111), adsorbed NH_2 species can exist on Si(100) to higher temperatures where the recombination reaction to produce NH_3 takes place.[260] This is an example of the role of local strain effects in the surface region in controlling surface

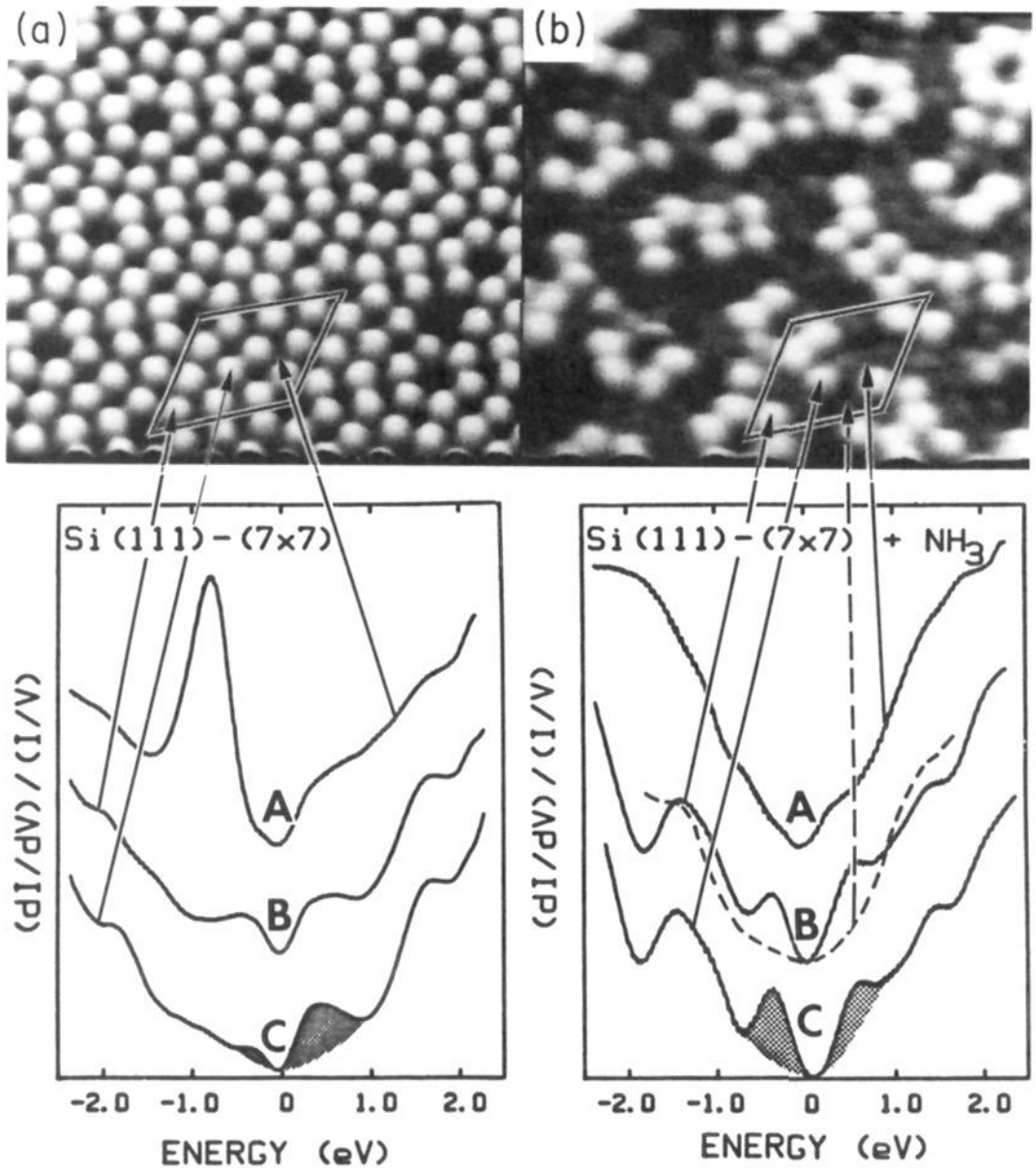

Figure 38. Comparison of STM topographs (top) and atom-resolved tunneling spectra (below) of the clean (left) and NH_3 reacted (right) Si(111)-(7×7) surface. Left: Curve A is for a restatom site, curve B for a corner adatom site, and curve C for a center adatom site of the clean surface. Right: Curve A is for a *reacted* restatom site, curve B (dashed line) is for a *reacted* corner adatom, while curve B (solid line) and curve C are for *unreacted* corner and center adatoms, respectively.[253]

chemistry on covalent solid surfaces. The H atoms bond to the less strained restatom sites (Figure 39), i.e., for each NH_3 adsorbed one adatom dangling bond and one restatom dangling bond is removed. Since there are twice as many adatom sites as restatom sites on the Si(111)-(7×7) surface, this model is in excellent agreement with the STM results.[253]

3. Other Nitrogen-Containing Compounds

The results for adsorption and decomposition of nitric oxide (NO), hydrazine (N_2H_4), and hydrazoic acid (HN_3) on silicon surfaces are far more sketchy than for NH_3, especially for N_2H_4 and HN_3 where the earliest results are only a few years old.[264-266] These three molecules are energetic compared to NH_3, and their decomposition kinetics and routes might be expected to differ from that of NH_3. The relevant ΔG_f° values for the gaseous molecules:[171] NH_3(g): −16.50 kJ/mol; NO(g): +86.62 kJ/mol; N_2H_4(g): +159.39 kJ/mol; and HN_3(g): +328 kJ/mol.

Adsorption of NO on Si(111)-(7×7) was found to yield N and O in on-top sites characterized by vibrational losses around 975 and 820 cm^{-1}, respectively.[229] For NO adsorbed on Si(100) at 90 K, Avouris et al.[248] reported two N(1s) XPS peaks (397.7 and 401.9 eV), attributed to initial dissociatively adsorbed N (low binding energy) followed by the physisorbed multilayer NO (high binding energy). After removal of molecular NO by annealing to 300 K, only O was detected with ISS, which is highly surface sensitive, while both N and O were detected with photoemission and AES, leading to the conclusion that N occupies subsurface sites while O saturates the dangling bonds. Taguchi et al.[267] also found dissociative adsorption for NO adsorption at 300 K by HREELS, attributing the observed losses to Si−O−Si and near-planar Si_3N species. On the other hand, Sasse and co-workers[268-270] found that the NO adsorption at 300 K is molecular with low saturation coverage (~15% of a monolayer by AES), and that dissociation takes place at 550 K. Originally,[269] the low saturation coverage was explained by NO adsorbing exclusively at missing dimer defects, but after further studies[270] electrostatic repulsion was found to be a better explanation with NO bonding to silicon dimers also. The observation of molecular adsorption was supported by their theoretical calculations,[270] whereas a more recent calculation by Fu et al.[271] found adsorption to be dissociative with N and O saturating the dangling bonds.

For N_2H_4 adsorption, Lin and co-workers[264,272] reported N−H bond breaking to occur upon N_2H_4 adsorption at 120 K on Si(111)-(7×7)[264] and on Si(100)-(2×1),[272] upon the basis of the observation of a Si−H stretching mode (2057 cm^{-1}) in HREELS. Simultaneous observation of NH_2, NH, and N−N modes indicates that the adsorbed species are mainly N_2H_x (x = 2, 3). The relatively narrow N(1s) XPS peak, indicating that all N atoms sit in a similar environment, and the high intensity of the N−N

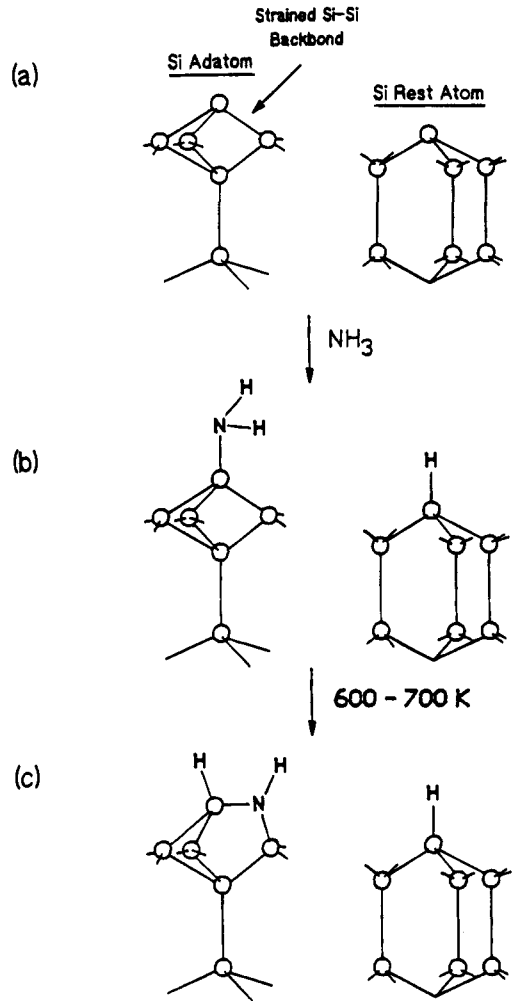

Figure 39. Ball–stick model for the adsorption and decomposition of NH_3 on Si(111)-(7×7).[260]

stretching mode (1129 cm^{-1}) observed by HREELS in the off-specular direction, strongly suggested that the N–N bond was parallel to the surface. Further N–H bond breaking occurred upon annealing, and as for NH_3,[260] NH_2 was more stable on Si(100) than on Si(111).[272] Above 600 K the N–N bond breaks,[264,272] as evidenced by the disappearance of the N–N mode and slight changes in the frequencies of NH_2 and NH modes. For Si(100) it was proposed[272] that upon N–N bond breaking, the Si dimer bond is also broken and NH is inserted into a bridging position between the Si atoms, as shown schematically in Figure 40. Final annealing leads to H_2 desorption and Si_3N_4 formation. Slaughter and Gland[265] studied the nitridation of Si(100) by cycles of NH_3/N_2H_4 adsorption and annealing using AES uptake measurements, and found that N_2H_4 nitrided the surface much more effectively than NH_3.

Hydrazoic acid (HN_3) was first studied by Bu et al.[266] on the less common Si(110) surface and was reported to adsorb molecularly. Following adsorption at 120 K, molecular vibrational modes similar to those obtained for HN_3 in the gas phase were observed, whereas warming to 220 K resulted in dissociation to N_2 and NH. The N_2 was believed[266] to desorb immediately upon formation, while NH dissociated further to give N and H as the surface was annealed from 580 to 800 K. Jonathan et al.[273] studied HN_3 on Si(100) by TPD and reached very

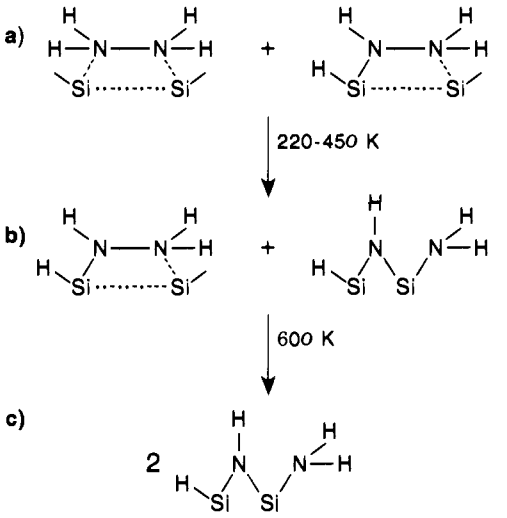

Figure 40. Model for thermal decomposition of N_2H_4 on Si(100) following adsorption at 100 K.[272]

similar conclusions, although they questioned the immediate desorption of N_2, since in their experiment N_2 desorption was only observed above 400 K. The only other desorption product observed was H_2 around 750 K, which is typical for H on silicon, consistent with the result for Si(110) where transfer of H from N to Si is observed.[266] Recently, Chu et al.[274] studied HN_3 adsorption on Si(111)-(7×7) and compared it to Si(100) and Si(110), concluding that the adsorption and decomposition of HN_3 is essentially identical on the three low-index surfaces.

B. Phosphorus

Phosphorus is widely used as bulk dopant in silicon crystals,[275] but the surface reactions of phosphorus-containing species has attracted very little attention. Early studies[16,117,276–279] showed that several different reconstructions exist depending on the adsorption/annealing temperature. In more recent studies, phosphine (PH_3) was reported to adsorb dissociatively as PH_2 and H at $T < 100$ K on Si(111) by Chen et al.[280] and on Si(100) by Colaianni et al.[281] Very similar to the case of NH_3,[260,263] only low-temperature molecular desorption of PH_3 occurs on Si(111), whereas some PH_2 undergoes recombinative desorption to produce PH_3 at 635 K on Si(100). Decomposition of PH_2 occurs on both surfaces during annealing, and ultimately P_2 and H_2 desorption processes are observed.

C. Arsenic

The growth of GaAs and other III–V semiconductors by molecular beam epitaxy is beyond the scope of this review, and a overview of this topic can be found in refs 115 and 116. However, the first step in growth of GaAs on Si surfaces is often the creation of an As monolayer, and some very interesting observations have been made for this process.[282,283] With five valence electrons As (and Sb) prefer a 3-fold coordination with the remaining two electrons occupying a lone-pair orbital; thus the substitution of As for surface Si atoms with dangling bond(s) leads to elimination of one dangling bond per substituted atom. This substitution is not unlikely since the

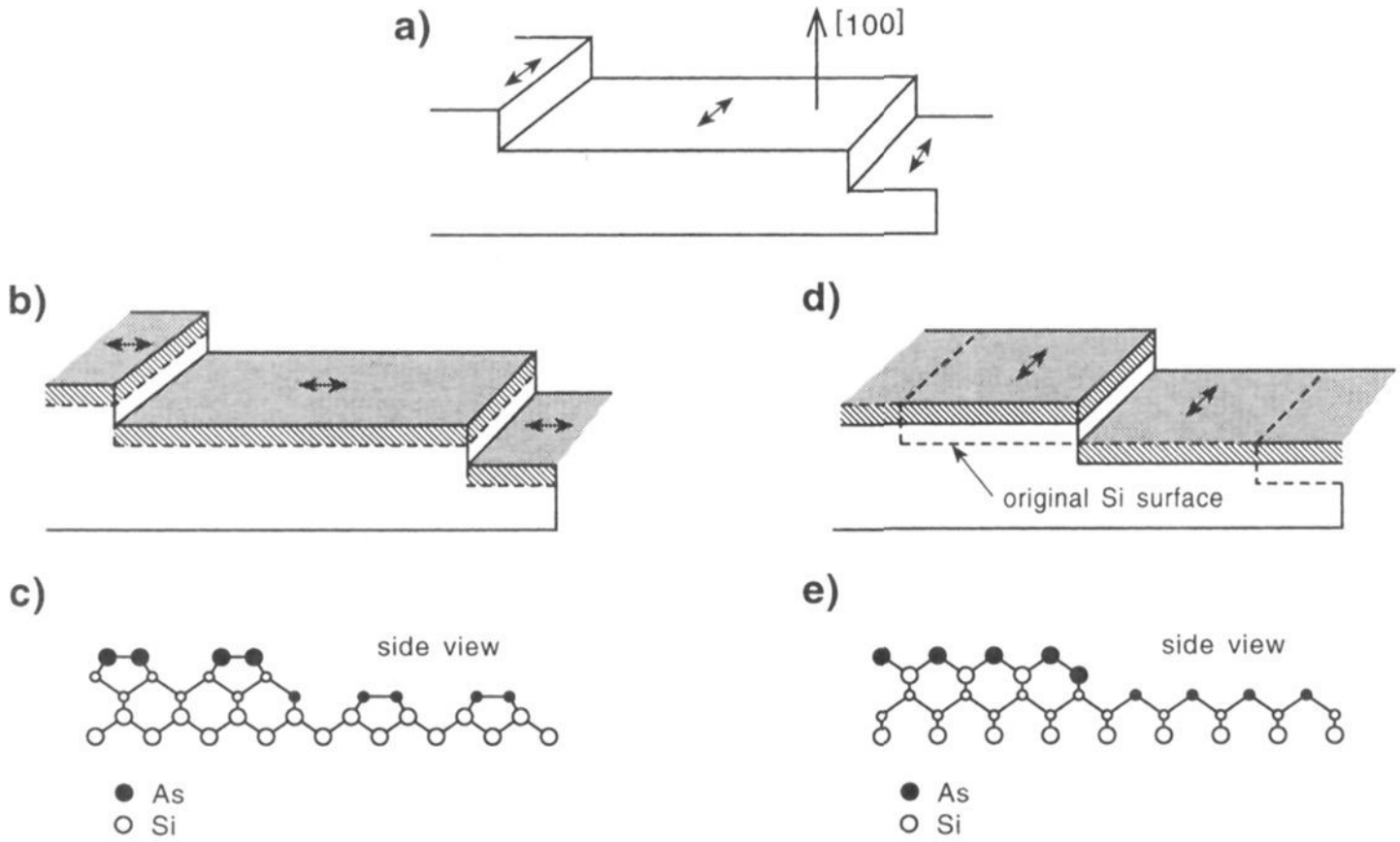

Figure 41. Schematic drawings of step structures (a, b, and d; arrows indicate dimer direction) and dimer arrangement (c and e) for vicinal Si(100) before and after coverage with a monolayer of As. (a) Clean Si(100)4°-(2×1) with dimers parallel to the step edges. Depending on deposition conditions, As deposition leads either to "rotated dimers" as shown in b (step structure) and c (dimer arrangement), or to "nonrotated dimers" as shown in d (step structure) and e (dimer arrangement). (Parts a, b, and d are from ref 286; parts c and d, from ref 287.)

covalent radius of As is within 1% of that of Si.[275] Since the elimination of dangling bonds is the driving force for reconstruction, substitution of As is predicted to change the reconstruction of the surfaces. This is especially true for the Si(111) surface where the atoms in the outermost layer of the unreconstructed surface have one dangling bond each (Figure 9a) and thus substitution of these atoms with As atoms eliminates all of the dangling bonds. Substitution of As is therefore expected to stabilize the unreconstructed surface, creating a Si(111)-(1×1)-As surface. In contrast, on the unreconstructed Si(100) surface, each Si atom has two dangling bonds, and thus substituted As atoms will still have one dangling bond each. These dangling bonds are expected to be eliminated by creation of As dimers, thus giving a Si(100)-(2×1)-As surface with no dangling bonds.

1. As/Si(100)

As expected, As adsorption on Si(100) leads to formation of As dimers, and these dimers has been found to be symmetric by both experiment[283] and theory.[14] On single-domain, double-stepped Si(100), where the Si dimers are parallel to the step edges, it was originally reported[284] that incoming As adsorbs on top of existing dimers, breaking them and creating new As dimers rotated by 90°. This was observed by LEED where the initial (2×1) pattern was transformed to a (1×2) pattern following As adsorption. However, in other cases—under different deposition conditions—the (2×1) structure was preserved after As deposition, meaning that the new As dimers were parallel to the original dimers.[285] Bringans et al.[286] studied this in detail by LEED, STM, and XPS and found that rotated As dimers resulted from initial As deposition on a cold crystal (low mobility), whereas nonrotated dimers resulted from initial As deposition on a hot crystal (high mobility). An interesting model[285] was proposed to account for these observations: under low mobility conditions (Figure 41, parts b and c), As_2 adsorption occurs, whereas under high mobility conditions (Figure 41, parts d and e), the incoming As atoms displace Si atoms in the top layer, and these displaced Si atoms diffuse to the steps. Schematics showing structures of the As layer under the two different conditions are seen in Figure 41. In agreement with this, total energy calculations by Alerhand et al.[287] found D_B steps to be energetically favored for the As-covered surface, as is true also for the clean Si(100) surface, and predicted the formation of nonrotated dimers in equilibrium (high mobility), but rotated dimers in kinetically limited (low mobility) conditions. In a later study by Tromp et al.[288] using LEEM and STM, nonrotated dimers were observed after As deposition at 900 K on Si(100) surfaces with wide, flat terraces separated by single layer steps, suggesting that displacive adsorption takes place also on large terraces. Some islands with rotated dimers (adsorption on top without Si displacement) were also observed within large areas of nonrotated dimers. Step movement was observed during the deposition in agreement with displacement of Si atoms from the terraces, and surface stress relaxation was proposed as the driving force for the displacement. A model for the dimer exchange mechanism on the atomic level was proposed by Yu and Oshiyama[289] and is shown in Figure 42. In this model, initially an As dimer forms on top by breaking two Si dimers (Figure 42b), followed by the As dimer and a pair of Si atoms on one side changing place (Figure 42c). The resulting Si dimer diffuses away (Figure 42d) leaving room for a new As dimer to form on top (Figure 42e). The place change process then repeats with the remaining pair of Si atoms under-

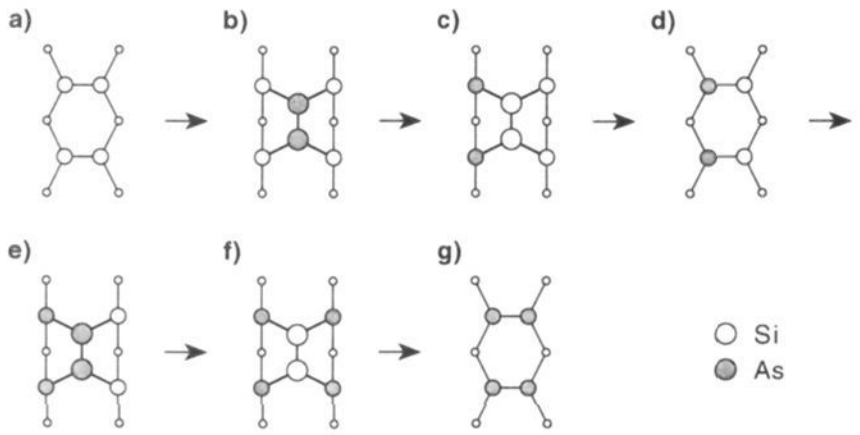

Figure 42. Model for dimer exchange mechanism during As adsorption on Si(100)-(2×1): (a) Si dimers on the clean surfaces; (b) the incoming As atoms break the existing dimers and create a new As dimer on top; (c) the pair of As atoms then exchanges places with a pair of underlying Si atoms; (d) the top Si dimer diffuses away; (e) a new As dimer is formed on top; (f) the place exchange process is repeated; and (g) the top Si dimer diffuses away, leaving two new As dimers parallel to the original Si dimers.[289]

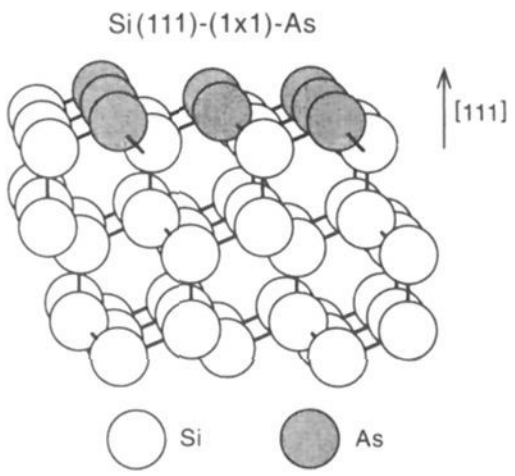

Figure 43. Structural model for arsenic-terminated Si-(111)-(1×1).[290]

neath (Figure 42f), thus having exchanged two Si dimers with two As dimers (Figure 42g).

Tromp et al.[288] also studied the desorption of As from the single-stepped surface at 1073 K. The As islands desorb first, followed by creation of holes in the "nonrotated" As layer. The displacement is then reversed by Si migration, leading to a step structure very similar to that of the initial surface. For the double-stepped surface, annealing to 1073 K has also been reported[284] to lead to As desorption and recovery of the original Si(100)-(2×1) structure.

2. As/Si(111)

Several studies by different experimental techniques (XPS,[282,290] XSW,[291] UPS,[290] LEED,[292] and STM[293]) have shown that As lifts the (7×7) reconstruction of Si(111) leading to a (1×1) structure with As replacing the top half of the Si double layer, i.e., As bonds to three Si atoms (Figure 43). From XSW measurements, Patel et al.[291] found that the As atoms reside 0.17 Å above the ideal unrelaxed positions of the Si lattice. Comparing experiments and theory, Uhrberg et al.[290] confirmed that an As lone-pair state replaced the Si dangling-bond state. This led to a highly stable surface, where no further As adsorption can take place.[282] Furthermore the surface was almost unaffected by high exposures to oxygen and air,[282,290] but was less stable toward atomic H exposure, which has been reported to lead to H bonding to the As layer.[290] The Si(111)-(7×7) reconstruction is recovered by annealing to 1123 K.

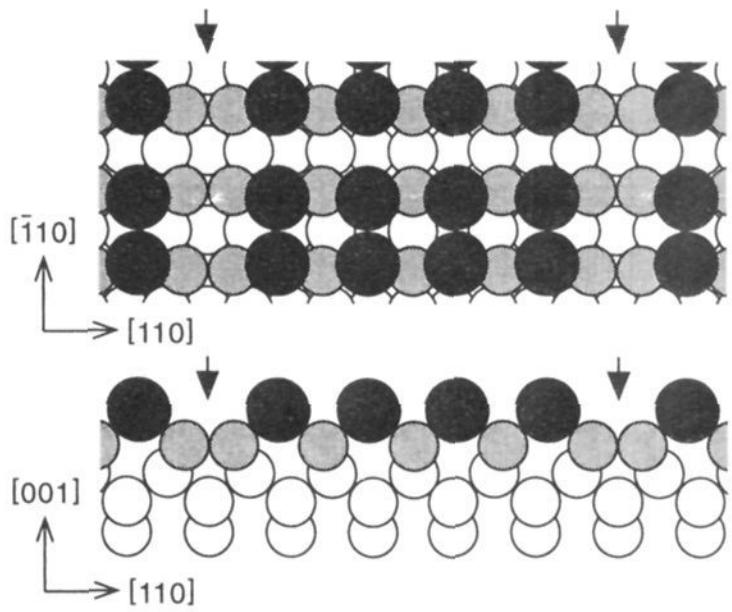

Figure 44. Top and side view of the missing-dimer model for the Si(100)-(2×n)-Bi structure; the missing rows are marked by arrows. For simplicity, the case of $n = 5$ is shown.[295]

D. Antimony and Bismuth

From a bonding point of view, antimony and bismuth atoms have the same prospect of favorable substitution for silicon atoms as arsenic atoms, but the large ratios of their covalent radii to that of silicon are far less promising for substitution.[275,294,295] Although initial studies indicated that the Sb and Bi layers formed were disordered,[296-298] later studies[294,299-301] have reported that dimers do form. STM and SEXAFS studies[294,299,300] found Sb dimers only following annealing to 810 K, and even at this temperature only short rows of dimers formed, and domain boundaries were abundant, giving a less ordered surface than the As/Si(100) surface. However, in a recent transmission ion channeling study,[301] dimers were found after deposition at temperatures between 300 and 820 K. It was proposed that at low temperatures the dimers forms a random array, and only at higher temperatures do they have enough mobility to coalesce and form short rows. The small domain size is probably also the reason for the very faint half-order spots observed in LEED. In contrast to As/Si(100), studies on vicinal surfaces[300] have shown that Sb dimers form exclusively on top of existing Si dimers; no displacive adsorption has been observed. For Bi/Si(100), RHEED investigations by Hanada and Kawai[295] showed a (2×n) structure. The 1/n streaks moved away from the fundamental LEED beams (n increasing from 13 to 5) over the temperature range 530 to 820 K, above the temperature where multilayer Bi desorbs. This was interpreted as a succession of structures with Bi dimers, where every nth dimer in the row is missing, as shown in Figure 44. For Bi/Si(111), a LEED study by Wan et al.[302] found two different phases, both with a ($\sqrt{3}\times\sqrt{3}$)-R30° structure: the α phase occurring at a coverage of $^1/_3$ ML and temperature of 630 K, and the β phase at 1 ML and 570 K. Figure 45 shows the structural models for the two phases, giving the best agreement between calculations and experimental results. It should be noted that these structures for Bi overlayers are very strained compared to the substitutional structure for As on Si(111).

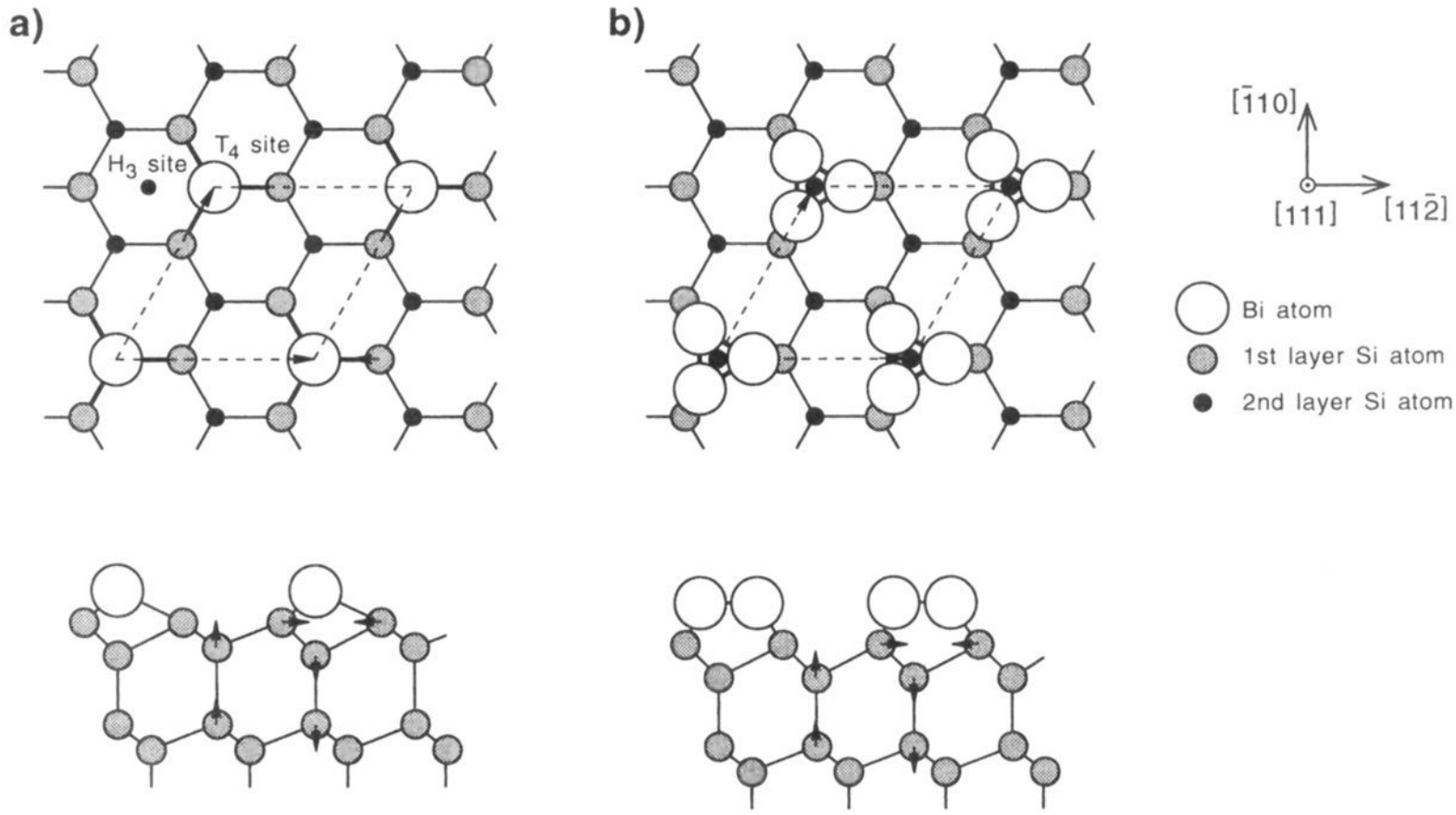

Figure 45. Top and side views of optimized structural models for Bi/Si(111): (a) the α phase obtained for $^1/_3$ ML at 630 K; and (b) the β phase for 1 ML at 570 K.[302]

VII. Group VI Adsorbates

Oxygen is the only representative of group VI of the periodic table for which the interaction with silicon surfaces has been studied in any detail. On the other hand, silicon oxide (SiO_2) films on silicon surfaces and the Si−SiO_2 interface are overwhelmingly well-studied.[303] Oxidized silicon surfaces can be produced by wet oxidation in a chemical etching environment, or by exposure of the clean silicon surface held at elevated temperatures to oxygen or water under vacuum. Silicon oxide films produced by chemical etching are widely used to protect the silicon surface from contamination while it is handled in the atmosphere. Later, the oxide film can easily be removed by annealing, revealing the clean Si surface. Furthermore, SiO_2 films are important as insulator films and as protective coatings against etching in electronic device technology.

A. Oxygen

Interaction of silicon surfaces with oxygen gas can lead to either production of a silicon oxide film on the surface (passive oxidation) or to etching of the surface (active oxidation), depending on surface temperature and oxygen pressure. The two different oxidation processes that can take place are:

$$\text{passive oxidation: } Si(s) + O_2 \rightarrow SiO_2(s) \quad (7)$$

$$\text{active oxidation: } Si(s) + {}^1/_2O_2 \rightarrow SiO(g) \quad (8)$$

The general trend is that active oxidation dominates at high temperatures, while passive oxidation dominates at high oxygen pressures. Lately, the focus has been on understanding the initial stages of the oxidation process, i.e., the interaction of atomic and molecular oxygen with clean Si surfaces, and a review by Engel[304] has recently appeared. N_2O is a common source of atomic oxygen as it dissociates at the surface: $N_2O(g) \rightarrow O(a) + N_2(g)$.[305] Atomic oxygen is also used for oxidation of silicon.[306]

It is well established that O_2 adsorption on both Si(100) and Si(111) is predominantly dissociative at 300 K, and the adsorption occurs by a molecular precursor mechanism.[307−311] The configuration of oxygen in crystalline SiO_2 is a bridging position between two silicon atoms; each silicon atom in turn is surrounded by four oxygen atoms in a tetrahedral configuration in the bulk SiO_2. The bridging site where O is inserted into a Si−Si back-bond is the preferred major adsorption site on silicon surfaces obtained from both experiment[312−318] and theory.[307,316,319] On the other hand the dangling bonds must also be involved in the dissociation process, since hydrogen-covered surfaces have been shown to be nearly inert toward O_2.[309,320]

1. Oxygen/Si(100)

Many conflicting results for the initial oxidation of the Si(100) surface have been reported. A saturation coverage of 1.0 ML was reported from most AES and XPS studies[306,318,320,321] for O_2 adsorption at 300 K, while lower saturation coverages have also been reported.[322] From an atomic oxygen beam study[306] no true saturation was found for atomic oxygen exposure, but the uptake slowed down considerably at a coverage of 2−3 ML. From STM studies,[323] Avouris and Lyo concluded that the initial adsorption occurred predominantly at defect sites.

From theoretical calculations, O_2 is predicted to adsorb dissociatively,[307,319] and Figure 46 shows different adsorption sites that have been considered—except for the dangling bond site, marked 1, oxygen is inserted into a Si−Si bond. Initial adsorption of both molecular and atomic oxygen was found to lead to insertion of O into the dimer bond[307,319,324] (site marked 2 in Figure 46). During this step, the (2×1) reconstruction of the silicon atoms was predicted to be intact since the atoms of the former dimer are

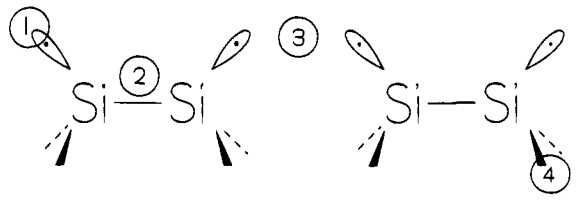

Figure 46. Possible adsorption sites for oxygen on Si(100): (1) dangling bond site; (2) short (dimer) bridge site, dimer bond is broken; (3) long (nondimer) bridge site; and (4) bridge site between first and second layer.

pulled toward each other in the Si−O−Si bridge. At high exposures O also bonds in the remaining surface bridge sites (between the original dimer positions, site 3 in Figure 46) and the two bridging sites become equivalent during this step.[319,324] Insertion of O into the bridge sites between the first and second layer (site 4 in Figure 46) was predicted to occur only at elevated temperatures.[324]

In contrast to the consistent theoretical predictions of well-ordered surface structures, experimental results show a high degree of local disorder. Bu and Rabalais[318] studied adsorption of both molecular and atomic (from N_2O) oxygen by TOF-SARS. The results obtained for the two adsorbates were identical, confirming that O_2 adsorption is dissociative. The results showed that no short-range ordering of the O atoms exists. The results did show, though, that while initially adsorbed oxygen resided above the surface Si atoms, oxygen was also found below the first Si layer in later stages. The STM study by Johnson et al.[321] confirmed that the surface is disordered, and no evidence of the (2×1) reconstruction was observed. Bu and Rabalais[318] also found that the (2×1) LEED pattern was extinct at saturation, while Westermann et al.[320] observed a (2×1) pattern with high background. Yaguchi et al.[322] reported that the (2×1) RHEED pattern was preserved even after exposure to 1500 langmuir of O_2 at 300 K.

2. Oxygen/Si(111)

Little experimental data exist on the sticking coefficient and saturation coverage for oxygen on the Si(111) surface. Gupta et al.[309] and Tikhov et al.[325] reported that the initial sticking coefficient of O_2 on Si(111)-(7×7) decreased with surface temperature, and values around 0.1 at 300 K were reported.[309] Furthermore, the saturation coverage increased with temperature from 0.4 ML at 110 K[309] to 1.0 ML at 750 K.[325]

For O_2 on Si(111), the molecular precursor is metastable, with the reported lifetime ranging from 14 min[308] to several hours.[311] This long lifetime gives a unique possibility to study both the molecular precursor and the stable dissociated species. The lifetime is temperature dependent, and a short annealing to 400 K results in full dissociation.[308,311,315]

Figure 47 shows the adsorption geometries and reaction pathways on Si(111)-(7×7) proposed by Schubert et al.[316] based on extensive studies by STM, STS, UPS, and tight-binding calculations.[310,314-316] Since the (7×7) unit cell is too large for theoretical calculations to be feasible, the calculations where carried out for a (2×2) unit cell (shown as an insert in Figure 47) representing the local symmetry of adatoms and restatoms inside the (7×7) unit cell. Since the adatoms dominate STM images, and the dangling bonds of the restatoms and adatoms give easily identified features in UPS and STS spectra, this model is regarded as a good model, although it ignores the dimer strings and the corner holes. Earlier studies by Höfer et al.[308] characterized the precursor as a species in bridge configuration between dangling bonds. They recognized the *bridge* species shown in Figure 47 as the unstable precursor of a stable dissociated species, and proposed a bridge-bonded species in a less well-defined environment of the oxygen-modified surface as the stable molecular precursor.[308] Schubert et al.[316] calculated the local density of states for several bridged species as well as for the on-top species shown in Figure 47 (*grif*, *para*, and *paul*), and the best agreement with UPS spectra was obtained for the species shown in Figure 47.

For the stable dissociated species, Morgen et al.[312] found only a bridge-bonded atom inserted into the back-bond between the adatom and the atom below (identical to *ins* shown as part of *ins-rest* in Figure 47) to be compatible with their XPS and UPS spectra. Avouris et al.[315] showed by calculation of the local density of states that this species—with the adatom dangling bond intact—would give rise to a bright site image in STM, and bright sites are observed only as minority sites in STM. The majority of the reacted adatom sites appear dark[314,315] and thus a different configuration is required to account for these sites. The local density of states calculations showed that dark sites are obtained for configurations where the adatom dangling bond is capped by oxygen. Saturation of the dangling bond alone (*ad* species) was excluded due to the lack of a plausible pathway leading to this species from the precursor states, and the *ins-ad* species shown in Figure 47 was preferred.

Recent ESDIAD results[311] were also interpreted in favor of the species shown in Figure 47. The desorption of O_2^+ was concentrated in directions close to the surface normal and attributed to an on-top molecular species (*paul* in Figure 47), while the O^+ desorption was evenly distributed in all directions and attributed to a combination of O atoms in the on-top dangling bond site and the bridging site.

3. Decomposition of Oxidized Layers

Very interesting results have been obtained for the decomposition of the oxide layer on silicon surfaces.[326-330] The only decomposition product observed is SiO(g), which desorbs with a coverage-dependent peak temperature around 1000 K. Thus extra Si is needed in the decomposition process:

$$SiO_2 + Si \rightarrow SiO(g) \qquad (9)$$

and on the basis of this alone, the decomposition is expected to require major diffusion in the surface layers. For thick oxide films produced by thermal oxidation (adsorption at above 900 K) or by wet chemical methods, the decomposition was found to be strongly inhomogeneous.[326,327,329,330] Voids (nucleating at defect sites) exposing the clean silicon surface were created in the oxide layer, even for

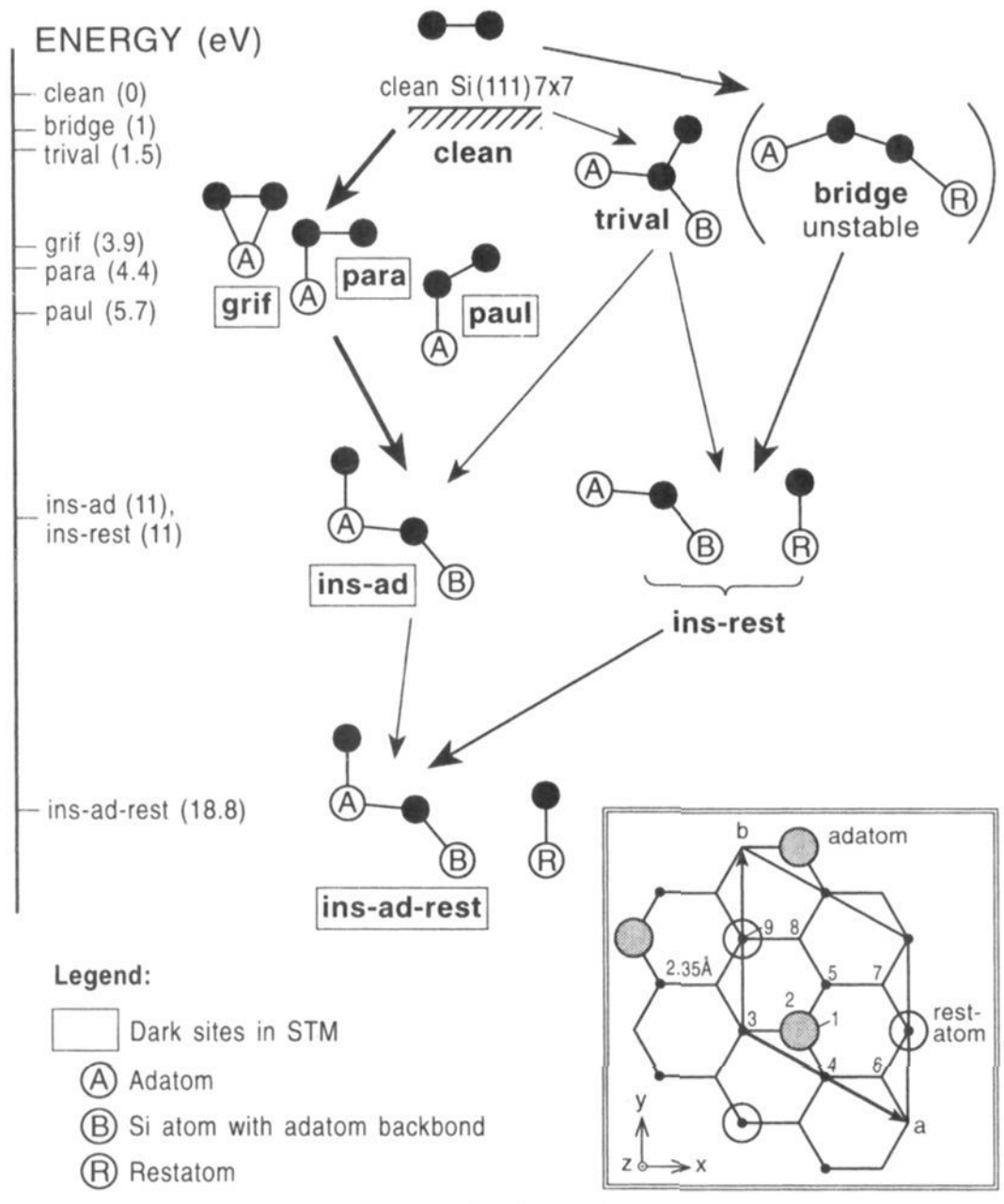

Figure 47. Adsorption geometries and reaction pathways for the oxidation of Si(111). Para, paul, and grif are the metastable molecular precursors. The thickness of the arrows indicates the importance of the corresponding reaction.[316]

initial coverages in the submonolayer range. The exposed Si surface in the bottom of the voids serves as the source of the extra Si needed. Using STM, Johnson et al.[321] observed voids forming also for Si(100) surfaces exposed to O_2 at 300 K. In addition, after complete oxide removal, reconstructions due to dimer vacancies were observed: the c(4×4) and the (2×*n*) reconstruction. The exact structure of the c(4×4) reconstruction is unknown, but it was speculated to involve a complex pattern of dimers in the top and second layer of the Si(100) surface. The (2×*n*) structure is the missing row structure, which is shown in Figure 44 (for Bi dimers). The (2×1) dimer reconstruction is restored by annealing to 1525 K, where Si sublimation occurs.

B. H_2O on Silicon Surfaces

Since H_2O is a relatively simple molecule one might expect that its interaction with silicon would also be uncomplicated, but it has turned out to be very controversial. The results and discussions up to 1987 were reviewed extensively by Thiel and Madey.[331]

One fundamental and controversial issue that has only recently been resolved, is whether H_2O undergoes dissociative or molecular adsorption. Early photoemission studies on both Si(100)[332] and Si(111)[333] were interpreted in terms of molecular adsorption, whereas vibrational studies, by both IR[334] and HREELS,[335] supported dissociative adsorption, through the observation of Si−H and SiO−H stretching modes (Figure 48a). Later PES studies[336−338]—including an angle-resolved study[336]—together with reinterpretation of the old PES data,[338] led to the conclusion that H_2O adsorbs dissociatively to OH and H on both surfaces. Few studies have been under-

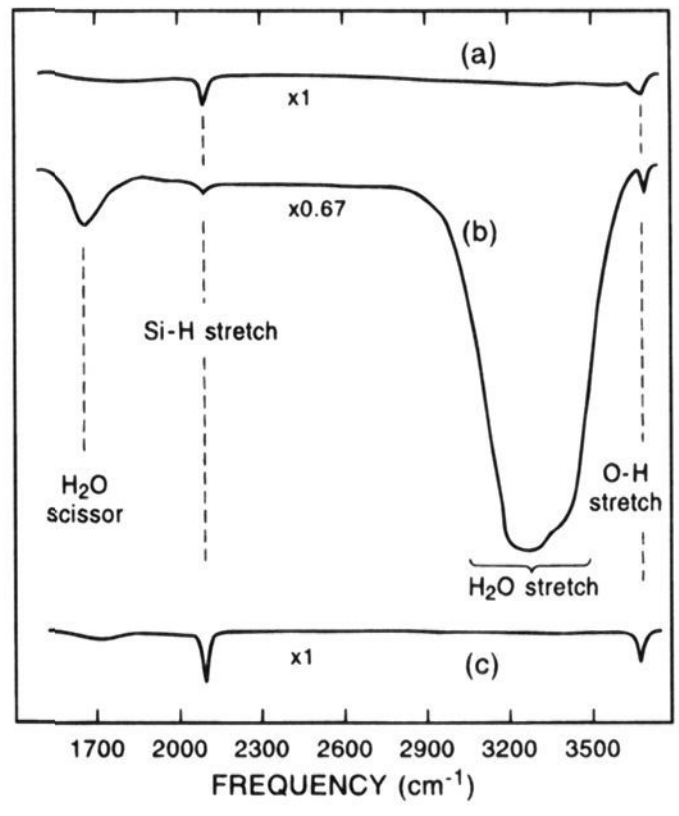

Figure 48. IR spectra after H_2O exposure on Si(100) at 80 K: (a) 0.5 langmuir, (b) 10 langmuir, and (c) 10 langmuir followed by annealing to 280 K. The assignments of the peaks are indicated.[334]

taken on other Si surfaces, but Schaefer et al.[339] reported adsorption of H_2O on the cleaved Si(100)-(2×1) surface to be dissociative.

The adsorption probability is strongly structure dependent, resulting in vastly different sticking coefficients on Si(100) and Si(111).[334,340,341] At room temperature the sticking coefficient on Si(100) is high (near unity) and constant up to saturation, suggesting the involvement of a mobile precursor adsorption mechanism.[340] On the other hand, the sticking coefficient on Si(111) is around 10^{-2} and depends on the H_2O pressure during adsorption.[341] At low temperatures (below 160 K) molecular water may be physisorbed on top of the initial chemisorbed layer (Figure 48a),[334,342,343] as evidenced by the observation of vibrational modes of molecular water in IR (Figure 48b). Figure 48c shows that the chemisorbed layer remained after desorption of the physisorbed layer by annealing to 280 K. LITD results[342] suggested that on Si(111) the physisorbed layer began to form before saturation of the dissociated layer. For Si(100), the saturation coverage in the dissociated layer is reported to be 0.5 ML, i.e. one OH or H per Si surface atom.[344,345]

Recent STM studies[345-347] have led to very interesting results. Reaction does not take place uniformly over the surface, but instead islanding is observed.[345-347] Following initial adsorption of H_2O on Si(100) at 300 K, Chander et al.[345] observed a marked increase in the number of two types of features: dark dimers and dimers with one bright and one dark end. On the clean surface identical features have been interpreted as defects: missing dimers and missing single Si atoms, respectively.[348] Further H_2O adsorption, on the other hand, gave features with atomic resolution in both filled and empty state images, while for the clean surface atomic resolution is only obtained in empty state images.[345,347] The interpretation[345] based on these observations was that the first features are due to molecular water, while the second ones are due to dissociation; thus the first 0.05 ML of H_2O adsorbed molecularly followed by dissociative adsorption up to saturation. This suggests that some of the "defects" normally seen on Si(100) surfaces by STM are in fact impurities in the form of molecularly adsorbed water. This is not unreasonable, since H_2O is always present in the ultrahigh vacuum chamber background gas, and H_2O has a high sticking coefficient. As the H_2O coverage increased, some of the molecular features were converted to dissociated features, while the rest remained, and the latter were speculated to be "true defects". (It should be mentioned that recent theoretical calculations[349] have shown that molecularly adsorbed oxygen will also have the appearence of a "missing dimer defect", and thus some of the observed defects could be due to oxygen adsorption.) Andersohn and Köhler[347] reached similar conclusions and furthermore found that adsorption preferentially occurs on terraces, and steps are saturated in later stages, in agreement with the observations by Avouris and Lyo[346] for Si(111), and with earlier conclusions from IR.[334,350] From IR studies, Chabal[350] originally concluded that H_2O adsorption did not saturate the steps at all, whereas Schröder-Bergen and Ranke[344]

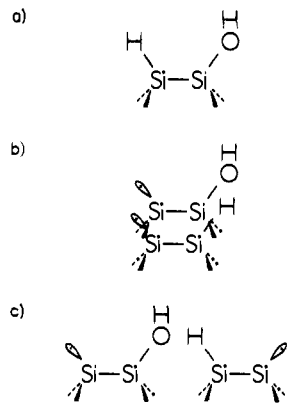

Figure 49. Adsorption of H_2O on Si(100). Schematic of OH and H bonding to adjacent dangling bonds, which is the only reaction observed by STM.

found the saturation coverage to decrease with increasing step density, but attributed this to smaller dangling bond density at steps (as may be seen in Figure 6). On the basis of LEED it had been proposed that the step structure and distribution was changed by water adsorption,[30] but this was not observed in the STM images.[347]

STM images[346,347] also suggest that a very strong site correlation exists. On Si(100), only pairwise saturation of adjacent dangling bonds by OH(a) and H(a) was observed, although not necessarily on the same dimer,[347] as shown schematically in Figure 49. Furthermore, isolated dangling bonds on the nearly saturated surface were very stable against adsorption, supporting the idea that two adjacent dangling bonds are needed for dissociative adsorption. Taken together, these two observations strongly suggest that the dissociative adsorption occurs through a mobile molecular precursor[347] at surface sites presenting adjacent dangling bonds. Interestingly, in images recorded at short time intervals, an apparent oscillation of the features assigned to isolated dangling bonds between the two ends of the dimer was observed. Thus, adsorbed H and OH species on singly occupied dimers are not immobile, they can move to the adjacent unoccupied site. On Si(111), where the Si adatoms are most easily imaged by STM, center adatoms were twice as reactive as corner adatoms.[346] In the DAS model, the closest pairs of atoms with dangling bonds are restatom−adatom pairs, and among these there are twice as many pairs with center adatoms as with corner adatoms (each restatom is surrounded by two center adatoms and one corner adatom). Thus if it is assumed that the adsorption of H_2O occurs at adjacent dangling bonds, those of a restatom and an adatom, one would expect twice as many center adatoms as corner adatoms to react. This is exactly what is observed by STM, strongly suggesting that adsorption of H_2O on Si(111) also occurs at adjacent dangling bond sites. Finally, the observation that preadsorbed hydrogen blocks the adsorption of H_2O,[342] is also in agreement with adsorption occurring at dangling bond sites.

H_2O on Si(100) has been studied by ESDIAD and only the desorption of H^+ in a four-lobe pattern was observed. By comparison to the much lower yield from hydrogen-terminated surfaces, it was concluded that this H^+ originated from OH groups on the

surface.[351-353] The observation of H^+ from the OH groups indicates that the O−H bond is pointing away from the surface (as shown in Figure 49), since H^+ from an O−H bond pointing toward the surface is expected to be neutralized by the surface. On double-stepped Si(100) crystals,[353] the patterns are dominated by two lobes, which are perpendicular to the step edges and therefore perpendicular to the terrace dimer bonds. Thus the O−H bond is tilted away from the vertical plane of the dimer bond. Since the angle of the Si−O bond relative to the surface is unknown, the Si−O−H bond angle cannot be determined from the H^+ beam angle observed in ESDIAD. Recent TOF-SARS results[318] showed two hydrogen positions, one close to the surface and one high above the surface. These were attributed to the hydrogens of Si−H and Si−OH, respectively, and interpreted in favor of the O−H bond pointing away from the surface. The dynamical behavior of the Si−OH moiety has been studied by ESDIAD.[352] H^+ beam broadening effects which are highly anisotropic indicate that the torsional mode about the Si−O bond in Si−OH species is of high amplitude.[352]

For low exposures at low temperature or for H_2O exposures on Si(100) at >200 K, only the decomposition products H_2 and SiO are observed in TPD.[342,343] The SiO desorption temperatures reported for Si(100) and Si(111) surfaces are very similar, 930 and 950 K for Si(100)[343] and Si(111),[342] respectively. The H_2 desorption temperature of 800 K is the same as that of H_2 desorption from hydrogen covered Si surfaces, suggesting that H_2 desorption occurs from Si sites. This is in agreement with results from PES,[340] LITD,[342] and SIMS,[343] which show conversion of the terminally bonded OH species to a bridge bonded oxygen species:

$$\text{Si−OH} \rightarrow \text{Si−O−Si} + \text{Si−H} \qquad (10)$$

On Si(111), the decrease of SiOH and H_2O LITD signals, attributed to direct desorption of SiOH and recombinative desorption of H + OH → H_2O, respectively, showed that this process occurred between 400 and 600 K. On Si(100), the OH species is more stable; although some OH starts to decompose at 300 K, the majority decomposes between 500 and 750 K.[343] For high exposures at low temperature (<200 K), desorption of multilayer H_2O was observed at 170 and 225 K for Si(100)[343] and at 160 K for Si(111).[342] IR spectra (Figure 48c) showed that following high exposures on Si(100) at 80 K and annealing to 300 K, only OH and H was left on the surface.[334]

It is interesting to compare the reactivity toward silicon surfaces of the hydrogen atoms in H_2O to that of atomic and molecular hydrogen. The sticking probability of H_2O is much greater than for molecular hydrogen—which of course could also be related to the lone-pair electrons on the oxygen atom in H_2O—and on Si(100) the sticking probability of H_2O is comparable to that of atomic hydrogen. However, in contrast to atomic hydrogen, the adsorbed hydrogen resulting from dissociation of H_2O is not capable of breaking Si−Si bonds, as evidenced by the persistence of Si(100) dimers and the conservation of the step structure.

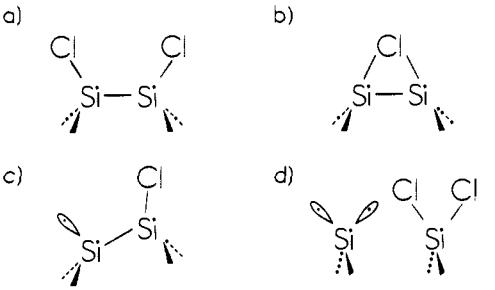

Figure 50. Different proposed bonding configurations for chlorine on Si(100): (a) terminal bonding at dangling bond sites of symmetric dimer, (b) bridging site, (c) terminal bonding at dangling bond of asymmetric dimer, and (d) dichloride species.

VIII. Halogens on Silicon Surfaces

With their preference for formation of single bonds, the halogens are expected to be similar to hydrogen in their interaction with silicon surfaces. The halogens (except iodine), however, are more agressive in terms of etching, and especially chlorine and fluorine are widely used in commercial etching processes, although often in form of chlorinated and flourinated compounds in a plasma.

As is the case with nitrogen in group V, chlorine dominates the studies of halogen chemistry on silicon surfaces.

A. Chlorine

The studies of chlorine on silicon surfaces has been complicated by the use of different chlorine sources: Cl_2 gas itself, or chlorine species from an electrochemical chlorine source. Although the majority of the chlorine from the electrochemical source is molecular, the presence of Cl atoms has also been reported.[354] Recent studies with molecular and atomic chlorine suggest that the reactivities of the two species toward silicon surfaces are different.[355,356]

1. Cl/Si(100)

The question of the adsorption site and saturation coverage of chlorine on Si(100) is controversial and intimately related to the question of buckled or symmetric dimers. There is general agreement from LEED studies[357-362] and RHEED[363] that the (2×1) structure is preserved after adsorption of Cl, although both weakening[359] and strengthening[362] of the half-order spots following adsorption has been reported. Furthermore, it has been reported that Cl_2 adsorbs with high and constant sticking coefficient up to near saturation.[356,359] An early study[363] found a very low saturation coverage, concluding that Cl bonded only to steps and defects, but most later studies[356,359,360] have concluded that the saturation coverage is close to 1.0 ML, i.e. one Cl per surface Si atom. For adsorption of atomic chlorine, Szabó et al.[356] found no true saturation, but the uptake slowed down considerably above ~1.5 ML coverage.

Figure 50 shows the different models that have been proposed for bonding of chlorine to Si(100). Terminal bonding to the dangling bonds of the symmetric dimer (Figure 50a) was first proposed by Thornton et al.[357] on the basis of NEXAFS results,

and ARPES[364] and EELS[363] results were also interpreted in favor of an off-normal Si−Cl bond. This structure was also one of the two structures found by Gao et al.[359,365] in a study combining several experimental techniques and employing adsorption of Cl_2 gas at a Si(100) temperature ≤120 K. Primarily on the basis of the ESDIAD patterns and HREELS spectra shown in Figure 51, these authors concluded that a mixture of a bridging species (Figure 50b) and a terminal species (Figure 50a) exists after adsorption at ~120 K. In the ESDIAD patterns four shoulders or peaks are seen in the directions of the dangling bonds in the two orthogonal (2×1) domains, indicating off-normal Si−Cl bonding in these directions. At low temperature a central Cl^+ beam is also observed, corresponding to a species bonded normal to the surface. The HREELS spectra show a Si−Cl stretching mode at ~600 cm^{-1}, and a 300 cm^{-1} mode which was interpreted as a stretching mode of a bridged Si−Cl−Si species as shown in Figure 50b. As seen in Figure 51, annealing up to 673 K gradually removes the normal Cl^+ ESDIAD beam and the 300 cm^{-1} mode, suggesting that a conversion of the bridging species to a terminal species occurs. Support for this model has come from several calculations,[14,366,367] where both the terminal dangling bond site (Figure 50a) and the bridging site (Figure 50b) are found to be stable sites. All studies found the terminal site to be lowest in energy, but different results for the magnitude of the stabilization have been reported from 145[366] to 93[14] to 12 kJ/mol dimers.[367] The initially asymmetric dimers convert to a symmetric configuration after chlorine adsorption.[14,367] For the bridge-bonded species, one important difference in the theoretical structure[14,366] compared to the experimental structure,[359] is that the theoretical calculations found the Si−Si dimer bond to be broken. The Si−Cl bond length obtained from NEXAFS[357] was 1.95 Å, slightly shorter than theoretical estimates of the bond length for the terminal site: 2.05,[14] 2.16,[366] and 1.97 Å.[367] For the Si−Cl bond angle relative to the surface normal there is also some discrepancy between the experimental value of 25 ± 4° from ESDIAD[359] and the values of 15°,[14] 14.8°,[366] and 21°[367] calculated from the models.

A bridge-bonded species has also been invoked by Boland[368] as a metastable state undergoing tip-induced hopping of chlorine between adjacent sites observed in STM. Two main features were observed after Cl_2 adsorption: dark dimers and bright "balls" on one side of the dimer rows, and these were interpreted as dimers with both or one dangling bond saturated with Cl, respectively. In addition, STM evidence for Cl_2 dissociative adsorption on adjacent Si dimers in the same dimer row was found.

Entirely different conclusions have been reached from other NEXAFS[362] and ESDIAD[358] studies employing an electrochemical source. In these studies the dominant bond direction was found to be close to the surface normal, interpreted as Cl bonding to the dangling bond of the "up-atom" of a buckled dimer (Figure 50c). In the study by Purdie et al.[362] only this species was found after adsorption at 500 K, whereas after adsorption at 300 K evidence for some off-normal bonding was also found. The ESDIAD patterns of Bennett et al.[358] also show contributions from both normal and off-normal species after adsorption at 300 K, but in contrast to the ESDIAD patterns in Figure 51, only a normal Cl^+ beam is observed after annealing to 670 K. Thus, the normal beam was attributed to Cl bonded to a buckled dimer (Figure 50c). To account for the off-normal species at 300 K, in addition to bonding to dangling bonds of a symmetric dimer (Figure 50a), the possibility of dichloride species (Figure 50d) was also proposed. It should be noted that two studies[355,356] have found that polychlorides are formed only after exposure to atomic chlorine, not after exposure to molecular chlorine.

In the ESDIAD study by Bennett et al.,[358] Cl on vicinal Si(100) was also studied. For these surfaces an extra peak in the downstairs direction (perpendicular to the terrace dimers) was also found and attributed to either etching or terminal bonding at step sites. The same downstairs beam was observed by Dohnálek et al.,[369] who favored bonding to a step site, where the presence of a downstairs-tilted dangling bond is in agreement with Chadi's model[23] of double steps (D_B step in Figure 6).

Most studies[356,359,370] have reported that thermal removal of Cl from the Si(100) occurs exclusively by etching—desorption of $SiCl_2$ and $SiCl_4$—although in one study,[361] Cl_2 was observed to desorb at 115 K following very large Cl_2 doses. For small exposures only a high-temperature $SiCl_2$ desorption state is seen,[356,359,361,370] with reported peak temperature varying from 850 K[359] to 950 K,[356,361] and furthermore the peak temperature decreases with increasing initial coverage. With increasing exposure, a $SiCl_4$ desorption state develops at 500 K.[356,359,361,370] For very high exposures, etching is observed at surprisingly low temperature, through the development of several additional $SiCl_4$ desorption states below 200 K.[356,361] These desorption states were first observed by Mendicino and Seebauer[361] after Cl_2 gas exposure, whereas Szabó et al.[356] found that they were only observed for atomic Cl exposure. In molecular beam scattering experiments direct desorption of SiCl has been observed for temperatures above 1073 K.[371]

2. Cl/Si(111)

The results reported for chlorine on Si(111) are far more consistent than those reported for Si(100). After adsorption at temperatures below 300 K the (7×7) structure is preserved as observed by RHEED[363] and LEED.[372] Photoemission results of Schnell et al.[373] obtained after saturation at 300 K showed that $SiCl_3$, $SiCl_2$, and SiCl species are present on the surface (Figure 52 bottom), while after annealing to 673 K only SiCl remains (Figure 52 top). Further coverage-dependent XPS[192] revealed that only SiCl is present for low exposures (Figure 53a), while first $SiCl_2$ and then $SiCl_3$ develop with increasing exposure (Figure 53, parts b and c). The indicated coverages are based on the density of Si(111)-(7×7) restatoms (the reason for this will become apparent from the STM results below) and corresponds to 0.10, 0.52, and 1.62 ML, respectively, in terms of density of the (1×1) surface. Similar results have been reached from LITD,[374] where the $SiCl_2$ and $SiCl_3$

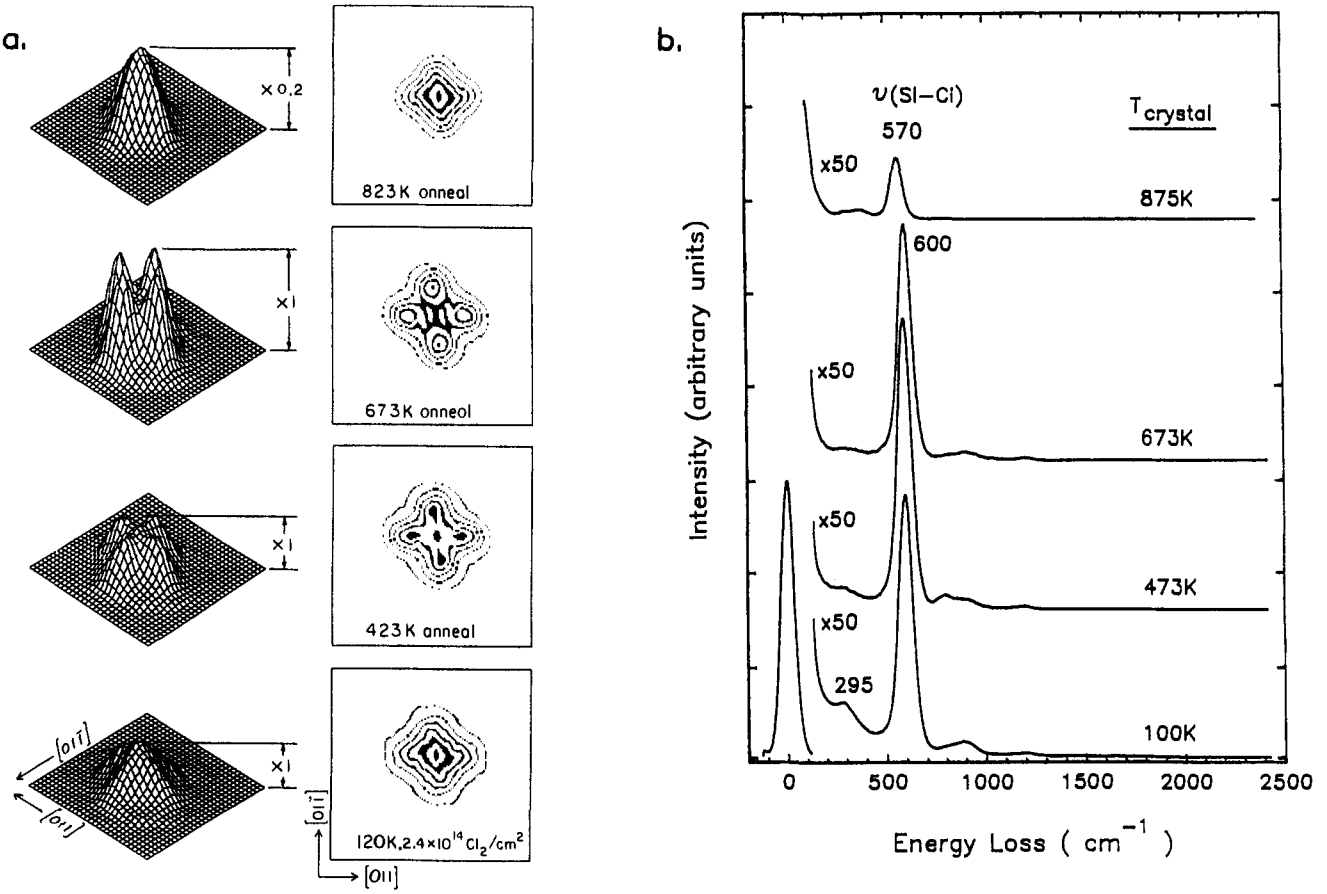

Figure 51. Temperature-dependent Cl^+ ESDIAD (left) and HREELS (right) following Cl_2 adsorption on Si(100)-(2×1) at $T \sim 120$ K. The bottom pattern and spectrum were obtained from the as-deposited surface, and the others were obtained after annealing at the indicated temperature and cooling down to 120 K (ESDIAD)/100 K (HREELS). A 4-fold symmetry is observed in the ESDIAD patterns, due to two Si(100) domains.[359]

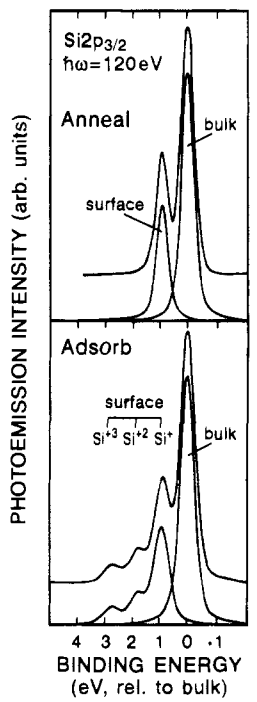

Figure 52. Si2p XPS spectra (after subtraction of $Si2p_{1/2}$ contribution and background) for a saturation chlorine exposure on Si(111)-(7×7) following adsorption at 300 K (bottom) and annealing to 673 K (top).[373]

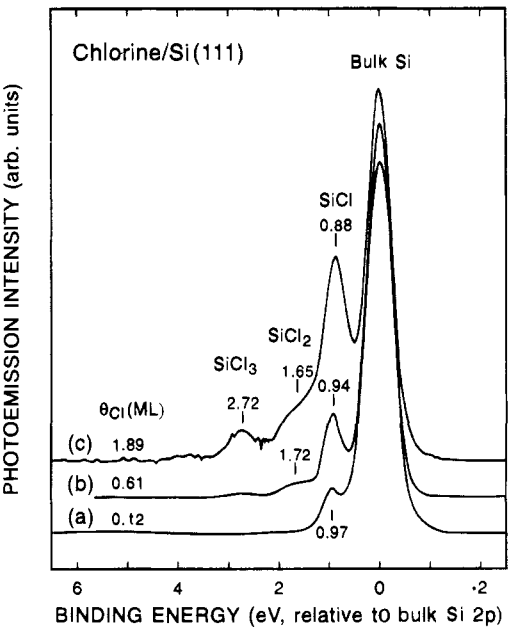

Figure 53. $Si2p_{3/2}$ XPS spectra after exposure of 300 K Si(111)-(7×7) to increasing amounts of chlorine. The indicated chlorine coverages are the ratios of the areas of the Si2p chemically shifted peaks to the SiCl peak obtained after annealing to 673 K.[192]

desorption yields were correlated with the existence of mono-, di-, and trichloride on the surface. $SiCl_2$ was assigned to recombinative desorption of SiCl + Cl → $SiCl_2$, while $SiCl_3$ was assigned to a combination of direct desorption of $SiCl_3$ and recombinative des-

orption of $SiCl_2 + Cl \rightarrow SiCl_2$. Szabó et al.[356] reported a slightly smaller saturation coverage of 1.4 ± 0.1 ML after exposure to molecular chlorine, while as in the case of Si(100) no true saturation was obtained for atomic chlorine exposure, but the uptake slowed down considerably above 1.5 ML. For both atomic and molecular chlorine, the coverage after 800 K annealing was 1.0 ± 0.1 ML. The adsorption site after annealing reported from NEXAFS[357,375] was the atop site with a Si−Cl bond distance of 2.03 Å. ESDIAD results of Yonezawa et al.[372] for a submonolayer Cl coverage indicated that the Si−Cl bond was close to the surface normal, while the authors remarked that Si−Cl bonds with large angles to the surface normal might exist, since they would not be detected in their experimental arrangement. For very low exposures, STM measurements by Boland and Villarrubia[376] indicated that Cl bonds exclusively to the Si adatoms.

In addition to the conversion from a mixture of mono-, di-, and trichloride to pure monochloride, major structural changes occur during annealing of the chlorine-saturated Si(111) surface. STM images[376−378] showed conversion from the (7×7) DAS structure to a (1×1) bulk-like structure. By mild annealing the stages of the lifting of the reconstruction can be studied, and Boland and Villarrubia[377] showed that the first step beginning at 573 K is creation of a surface with (7×7) periodicity but without Si adatoms. As seen in the STM image of Figure 54a, 42 maxima (Si rest layer atoms, compare to Figure 54b) per unit cell were observed, instead of the 12 maxima (Si adatoms) observed for the clean surface (Figure 7). Dimer strings are still observed as troughs on the surface. A few adatoms are still observed within the (7×7) cells in Figure 54 as bright protrusions near corner holes, while the "missing adatoms" are observed as protruding islands in other areas of the surface.[376] Scanning tunneling spectra showed no dangling bond states, confirming that the surface is Cl covered. Close inspection of these and higher resolution STM images also provided striking evidence for the existence of the stacking fault in the DAS structure, in addition to the strong contrast of adjacent halves of the (7×7) unit cell; a line drawn through a row of restatoms in one unit cell falls between the rows in a neighboring unit cell. Continued annealing initiated the removal of the dimer strings, leading to a conversion to extended (1×1) regions.[376] This process appeared to be kinetically limited, and quantitative conversion could only be achieved by long annealing or by dosing chlorine at the annealing temperature. The reaction could be reversed by annealing to still higher temperature, causing loss of Cl.[376] The adatoms from the protrusions were redispersed over the surface, and after heating to 1320 K the (7×7) structure was reestablished. Feltz et al.[378] studied the nucleation of the (1×1) and the (7×7) structures in the (7×7) ↔ (1×1) phase transition induced by adsorption and desorption of Cl at temperatures between 950 and 1030 K. The two processes appear to be reversible in details with the (1×1) structure nucleating on the lower terrace side of steps and at domain boundaries, while the (7×7) structure nucleated at the upper terrace step edges.

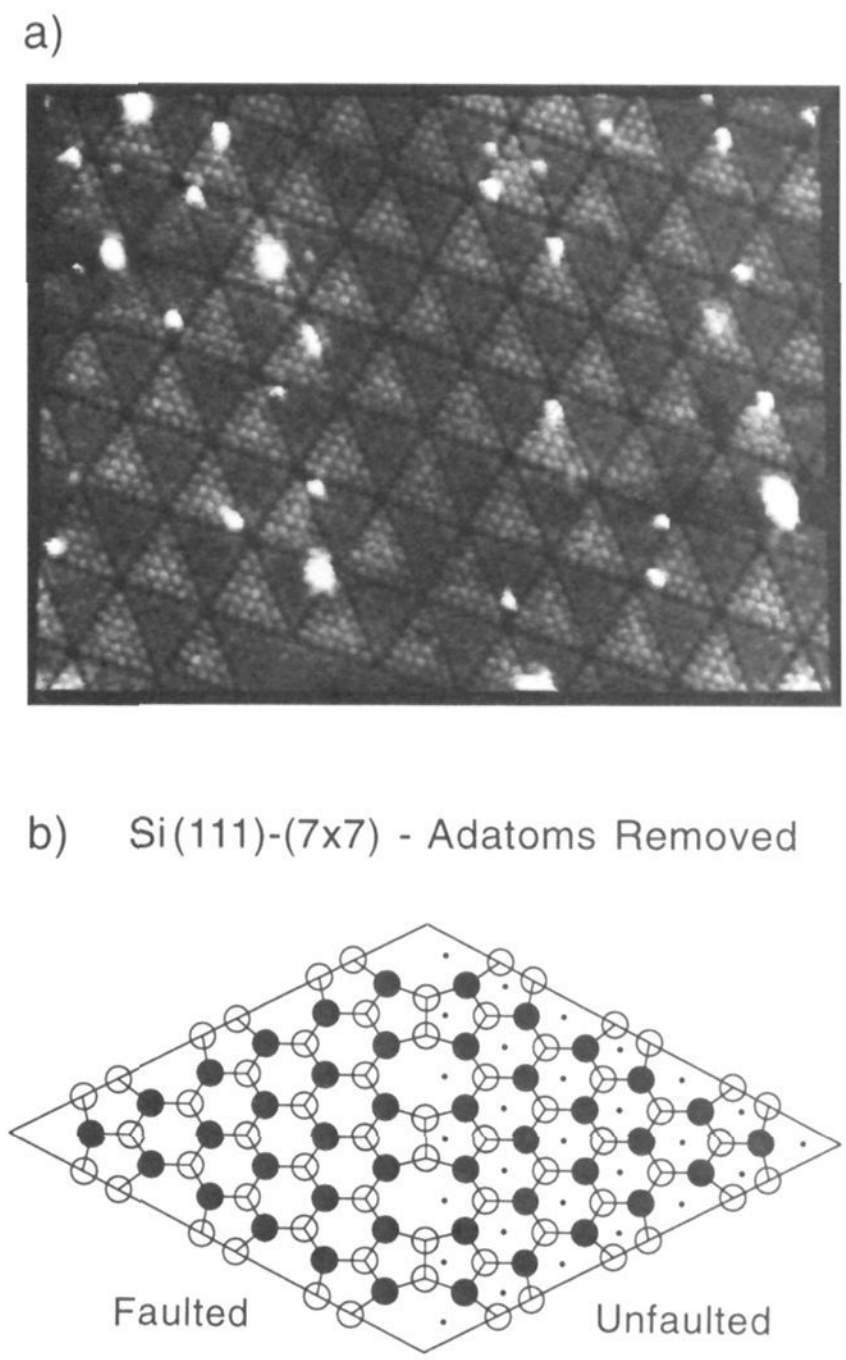

Figure 54. (a) STM image (bias +3 V) of the Si(111) surface after saturation exposure of chlorine and annealing to 743 K for 2 min. The area shown is 88 × 96 Å. (b) Structure of the Si(111)-(7×7) DAS model without the Si adatoms.[377]

As for Si(100), $SiCl_2$ is the only desorption product observed for low coverages on Si(111), and the observed desorption temperature (950 K) is similar to that for Si(100).[192,356,374] For higher coverages, $SiCl_4$ desorption develops, but while Whitman et al.[192] and Szabó et al.[356] reported a $SiCl_4$ desorption temperature of ~600 K, Gupta et al.[374] reported $SiCl_4$ desorption at 950 K. Furthermore, additional $SiCl_2$ desorption occurs around 700 K.[192,374] The 700 K desorption of $SiCl_2$ (and possibly $SiCl_4$) appears to be related to the presence of higher chlorides, since these are not observed on the surface above this temperature.[374] For atomic chlorine exposure, the same low temperature (<200 K) etching as for Si(100) is also observed. The 950 K $SiCl_2$ desorption has been reported to be second order in chlorine coverage,[356,374] and the reported kinetic parameters are in fair agreement: E_{act} = 71 kcal/mol, ν = 90 cm²/s from Gupta et al.[374] and E_{act} = 83 kcal/mol, ν = 2000 cm²/s from Szabó et al.[356] In molecular beam scattering experiments direct desorption of SiCl has been observed for temperatures above 1073 K,[379] as was seen on Si(100).[371]

B. Fluorine, Bromine, and Iodine

Studies of adsorption and desorption of the other halogens are far more scarce that for chlorine, and in particular very little structural data is available. Fluorine[380] and bromine[381] were reported to etch the surface like chlorine, while no etching was observed for iodine, which was reported to desorb as I.[382]

ESDIAD results for adsorption of residual F[358,383] and HF[351] on Si(100) indicated that F bonds to the dangling bonds of the dimers, very similar to the bonding of Cl shown in Figure 50a. The reported bond angles were 36 ± 5°,[383] 29 ± 3°,[351] and 30 ± 5°.[358] Adsorption of molecular and atomic fluorine was studied in detail by Engstrom et al.[380] using molecular beam techniques, XPS, TPD, and LEIS. Molecular fluorine adsorbs dissociatively with an initial sticking coefficient of 0.46 ± 0.02 ML, and rapid adsorption occurs up to apparent saturation at ~1.5 ML after ~20 ML exposure. However, this is followed by a much slower phase of adsorption, which yields a coverage of 3–4 ML after 600 ML exposure. The sticking coefficient for atomic fluorine is initially similar to that of molecular fluorine, but it decreases much more slowly with coverage, and ~400 ML exposure yields a coverage of ~10 ML. The coverage of 1.5 ML[380] is inconsistent with bonding only to the existing dangling bonds of Si(100). Calculations by Wu and Carter[384] showed that while bonding occurs at the dangling bonds up to a coverage of 1.0 ML, beyond this point the dimer bonds are broken and difluoride species form. However, the repulsion between adjacent F atoms creates a barrier for further adsorption at a coverage of 1.5 ML. Recent studies by Ceyer et al.[385] have shown that an F_2 molecule interacting with a Si(100) surface ejects an energetic F atom, which can either desorb or chemisorb elsewhere on the surface.

C. Abstraction of Halogens by Atomic Hydrogen

The halogens can be efficiently removed by bombardment with atomic hydrogen, as has been first reported by Yates and co-workers[386,387] for Cl, Br, and I on Si(100) and by Koleske and Gates[381,388] for Br on both Si(100) and Si(111). From Si(100) the abstraction was studied for temperatures of 300–600 K and the removal rate was highest for I, followed by Br and Cl.[386,387] For surface temperatures below 600 K, the removal rate for both surfaces was first order in atomic hydrogen flux and in halogen surface coverage and exhibited a near-zero activation energy.[386,388] On Si(111), however, the rate is also first order in the surface hydrogen coverage, suggesting that different mechanisms are operative on the two surfaces. For Si(100) an Eley–Rideal (ER) mechanism was suggested,[386,388] while a hydrogen transfer (HT) mechanism was suggested for Si(111),[388] and schematics showing the two mechanisms are shown in Figure 55. Interestingly, Koleske and Gates[381] found that for higher temperatures (above 673 K), the removal rate is first order in both the surface hydrogen and the halogen coverage for Si(100) as well as for Si(111). Furthermore, the removal was now activated with E_{act} = 45 and 43 kcal/mol for Si(100) and Si(111), respectively, interpreted in terms of a

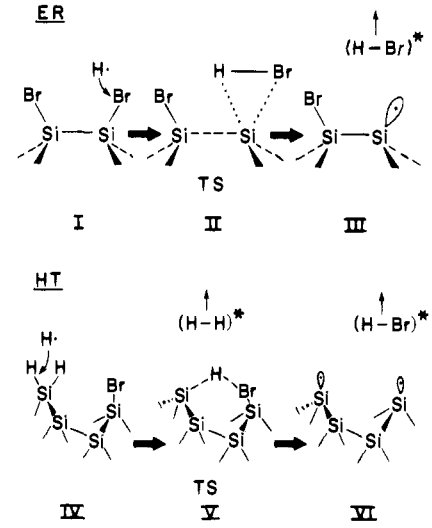

Figure 55. Schematic drawings of Eley–Rideal (ER, top), and hydrogen transfer (HT, bottom) mechanisms.[388]

thermal HBr desorption process. This process beginning at 720 K had also been observed in temperature-programmed desorption studies of Br/Si(100) after atomic hydrogen exposure.[386]

IX. Concluding Remarks

In this review the major recent results for the thermal reactions of hydrogen and the main group elements on silicon surfaces have been presented. We have focused on reactions occurring directly at the silicon surface and on reactions where an understanding of the individual steps has been pursued. Other major areas of research on silicon surfaces include photochemical reactions and reactions of the transition metals and their compounds, as may be inferred from the supplementary bibliography (Appendix 2).

Despite the extensive research on silicon surfaces, the field of semiconductor surface chemistry is still in its early stages, and many questions that have been addressed have not yet been answered conclusively. However, one commonly observed trend is that lattice energy effects control the surface chemistry through reconstruction and strain relief processes.

New exciting results in semiconductor surface chemistry are likely to be spurred by the desire for higher device density in electronic device fabrication, and to be closely connected to the development of new atomic resolution experimental techniques.

Acknowledgments

H. Neergaard Waltenburg acknowledges partial support from the Danish Research Academy. We thank the Office of Naval Research for support of this activity.

Appendix 1. Surface Science Measurement Techniques

Surface science employs a wide variety of surface measurement techniques which give thermodynamic, kinetic, structural, electronic and dynamical information about the character of the surface species.

Because of the complexity of chemical bonding effects on silicon surfaces, it has proven desirable to use a combination of measurement techniques, and this is very common in the best research work on surfaces. The following lists all of the techniques employed by the workers referenced in this review and gives a brief explanation of the physical principles of each.

Acronym Name

AES Auger Electron Spectroscopy

Atoms in the near-surface region are ionized in their core levels, followed by relaxation in a radiationless process, where one electron from an outer level fills the core hole and a second outer level electron leaves with the excess kinetic energy. The energy of the departing electron depends only on the energies of the involved electronic levels (i.e., it is independent of the source and energy of the excitation), and thus each element has its own characteristic set of Auger electron energies. See: Briggs, D.; Seah, M. P., Eds. *Practical Surface Analysis*; Wiley: New York, 1983.

ESDIAD Electron-Stimulated Desorption Ion Angular Distribution

Surface species are electronically excited by electron impact and both positive and negative ions as well as electronically and vibrationally excited species can be ejected. The angular distribution is closely correlated with the surface orientation of the chemical bond being broken. The thermal broadening of the angular distribution can be used to infer the dynamical behavior of the surface bond. See: Ramsier, R. D.; Yates, J. T., Jr. *Surf. Sci. Rep.* **1991**, *12*, 243.

HREELS High-Resolution Electron Energy Loss Spectroscopy

Vibrational modes of surface species are excited by a monoergetic electron beam. The spectrum of reflected electrons is collected and displays peaks at loss energies (relative to the peak of elastically scattered electrons) characteristic of the vibrational modes. See: Ibach, H.; Mills, D. L. *Electron Energy Loss Spectroscopy and Surface Vibrations*; Academic: New York, 1982.

IRAS Infrared Reflection Absorption Spectroscopy

Infrared light is reflected from the surface at glancing angles, exciting vibrational modes of surface species. See: Hayden, B. E. In *Vibrational Spectroscopy of Molecules on Surfaces*; Yates, J. T., Jr., Madey, T. E., Eds.; Plenum: New York, 1987; pp 267–344.

ISS Ion Scattering Spectrometry

Also known as low-energy ion scattering (LEIS). A monoenergetic, well-collimated beam of ions (0.1–10 keV) strikes the surface and the energy distribution of ions scattered in some particular angle is measured. The mass, i.e., chemical identity, and number of surface atoms is obtained from the energy and intensity, respectively, of peaks in the spectrum. See: Buck, T. M. In *Methods of Surface Analysis*; Czanderna, A. W., Ed.; Elsevier: New York, 1975; pp 75–102.

LEED Low-Energy Electron Diffraction

The long-range ordering of the surface is probed by diffraction of electrons with energies in the range of 20–500 eV. See: Van Hove, M. A.; Weinberg, W. H.; Chan, C.-M. *Low-Energy Electron Diffraction*; Springer: New York, 1986.

LEEM Low-Energy Electron Microscopy

Low-energy electrons reflected of the surface are used for imaging of the surface. The low electron energy gives very high surface sensitivity, while the resolution is limited to observation of larger structures such as steps. See: Bauer, E. In *Chemistry and Physics of Solid Surfaces VIII*; Vanselow, R.; Howe, R., Eds.; Springer: Berlin, 1990; pp 267–287.

LITD Laser-Induced Thermal Desorption

The species desorbing from the surface are monitored by mass spectrometry as the crystal temperature is increased rapidly (1000 K in <100 ns) by a laser pulse. See: Hall, R. B.; Bares, S. J. In *Chemistry and Structure at Interfaces*; Hall, R. B., Ellis, A. B., Eds.; VCH: Weinheim, Germany, 1986; pp 85–149.

NEXAFS Near-Edge X-ray Absorption Fine Structure

Described under SEXAFS.

NRA Nuclear Reaction Analysis

Also known as nuclear microanalysis. The surface is bombarded by high-energy charged particles (protons or He nuclei) and a nuclear reaction occurs. The emitted particles are collected, and using known cross sections, the number of reacting surface atoms can be determined. This technique is especially valuable for determination of hydrogen coverage. See: Feldman, L. C. In *Ion Spectroscopies for Surface Analysis*; Czanderna, A. W., Hercules, D. M., Eds.; Plenum: New York, 1991; pp 311–361.

PES Photoelectron Spectroscopy

Originally known as electron spectroscopy for chemical analysis (ESCA). The surface atoms are photoionized by UV (UV PES, UPS) or X-ray (X-ray PES, XPS) radiation, and the kinetic energy distribution of the photoelectrons is measured. This in turn gives the binding energies of the electronic levels, which will depend on the initial charge state and the chemical environment of the atom in the surface. The photoelectron energies are also influenced by polarization effects in the medium surrounding the ionized atom. Using angle-resolved measurements (ARPES), the dispersion of the individual electron bands may be obtained. See: Siegbahn, K.; et al. *Electron Spectroscopy for Chemical Analysis*; Almquist and Wiksells: Stockholm, 1967.

RHEED Reflection High-Energy Electron Diffraction

Structural information is obtained from electron diffraction, and enhanced surface sensitivity is ob-

tained by using grazing incidence. See: Ino, S. In *Reflection High-Energy Electron Diffraction and Reflection Electron Imaging of Surfaces*; Larsen, P. K., Dobson, P. J., Eds.; Plenum: New York, 1988; pp 3–28.

SEXAFS Surface X-ray Absorption Fine Structure

The surface atoms are ionized by X-ray radiation, and the dependence of the absorption coefficient on photon energy above the ionization threshold is measured. Surface sensitivity is obtained by measuring the absorption coefficient indirectly, commonly by detecting the electron yield. The energy dependence stems from interference effects of the ejected electron, which will scatter at the surrounding atoms, and thus coordination numbers and interatomic distances are available from Fourier transformation of the absorption coefficient. For the energy region very close to the ionization threshold, the terms near-edge EXAFS (NEXAFS) or X-ray absorption near-edge structures (XANES) are used. See: Stöhr, J. In *X-ray Absorption: Principles, Applications, Techniques of EXAFS, SEXAFS, and XANES*; Koningsberger, D. C., Prins, R., Eds.; Wiley: New York, 1988; pp 443–571.

SHG Second Harmonic Generation

The surface is irradiated with laser light of frequency ω, and the radiation emitted with frequency 2ω is detected. The emission will be enhanced when there is resonance with an absorption band of the adsorbates, and thus by varying the frequency of the incoming light, a spectrum from the adsorbed molecules is obtained. The method works only for atoms bound in noncentrosymmetric sites such as those at the surface. Furthermore, surface symmetries may be deduced by taking advantage of the polarization of the laser radiation. See: Shen, Y. R. In *Chemistry and Structure at Interfaces*; Hall, R. B.; Ellis, A. B., Eds.; VCH: Weinheim, Germany, 1986; pp 151–196.

SIMS Secondary Ion Mass Spectroscopy

The surface is bombarded with high-energy ions, causing sputtering of atomic and molecular ions and neutrals, which are detected by mass spectroscopy. The technique can be used for depth profiling, when multiple layers are removed, or for surface analysis (often termed static SIMS or SSIMS), when only a fraction of a layer is removed. See: Benninghoven, A.; Rüdenauer, F. G.; Werner, H. W. *Secondary Ion Mass Spectroscopy: Basic Concepts, Instrumental Aspects, Applications, and Trends*; Wiley: New York, 1987.

STM Scanning Tunneling Microscopy

The local electronic structure of the surface is probed by scanning a biased tip across the surface. Electrons will tunnel between the tip and the surface, and the tunneling current depends on the electrical potential and the tip–surface separation. Topographs are obtained from the spatial distribution of the tunneling current. See: Chen, C. J. *Introduction to Scanning Tunneling Microscopy*; Oxford University: New York, 1993.

STS Scanning Tunneling Spectroscopy

Closely related to STM. The relative derivative of the tunneling current with respect to the tip bias ($(dI/I)/(dV/V)$) is probed at specific surface sites, and this quantity has been shown to be representative of the local density of electronic states. See: Chen, C. J. *Introduction to Scanning Tunneling Microscopy*; Oxford University: New York, 1993; pp 295–312.

TED Transmission Electron Diffraction

A high-energy (10 keV) electron beam is transmitted through a thinned area of the crystal, and the diffracted electrons are collected. The relative intensities of the diffracted beams are very sensitive to the lateral positions of the surface atoms. See: Thomas, G.; Goringe, M. J. *Transmission Electron Microscopy of Materials*; Wiley: New York, 1981.

TOF-SARS Time-of-Flight Scattering and Recoiling Spectroscopy

This is a combination of ISS and SIMS. Ions and neutrals from scattering of the incoming noble gas ions and from recoiled surface species are detected by the time-of-flight technique. See: Grizzi, O.; Bu, M. S.; Rabalais, J. W. In *Chemistry and Physics of Solid Surfaces VIII*; Vanselow, R.; Howe, R., Eds.; Springer: Berlin, 1990; pp 213–238.

TPD Temperature-Programmed Desorption

The species desorbing from the surface are monitored with a mass spectrometer while the crystal temperature is increased at a controlled rate, which is usually linear with time and in the range 1–10 K/s. See: Yates, J. T., Jr. In *Methods of Experimental Physics 22*; Park, R. L., Lagally, M. G., Eds.; Academic: Orlando, 1985; pp 425–464.

UPS Ultraviolet Photoelectron Spectroscopy

Described under PES.

XPS X-ray Photoelectron Spectroscopy

Described under PES.

XSW X-ray Standing Wave Interferometry

An X-ray standing wave field at a crystal surface is excited through interference between an incident X-ray plane wave and the Bragg diffracted wave scattered from the crystal below the surface. The intensity of the standing wave field has the periodicity of the bulk diffracting planes. Variation of the incident beam angle through the range corresponding to total Bragg reflection and comparison to theory, allows determination of the position of adsorbate atoms relative to the substrate lattice. See: Golovchenko, J. A.; Batterman, B. W.; Brown, W. L. *Phys. Rev. B* **1974**, *10*, 4239–4242.

Appendix 2. Supplementary Bibliography

The following is a list of recent references to surface layers on silicon arranged by periodic groups and

compound types. In contrast to the periodic group designation used in the body of the review, here we employ the new periodic group designation for better classification. References that naturally fall into more than one category are listed in all appropriate categories, and for quick access a directory of the category headings is at the front of this review.

Hydrogen

Effect of Hydrogen on Surface Roughening during Si Homoepitaxial Growth; Adams, D. P.; Yalisove, S. M.; Eaglesham, D. J. *Appl. Phys. Lett.* **1993**, *63*, 3571−3573.

Si Crystal Growth Mediated by Synchrotron Radiation Stimulated Hydrogen Desorption; Akazawa, H.; Utsumi, Y.; Urisu, T.; Nagase, M. *Phys. Rev. B* **1993**, *47*, 15946−15949.

Chemical Equilibration of Plasma Deposited Amorphous Silicon with Thermally Generated Atomic Hydrogen; An, I.; Li, Y. M.; Wronski, C. R.; Collins, R. W. *Phys. Rev. B* **1993**, *48*, 4464−4472.

Silver Induced Formation of Si(111)-$\sqrt{3}\times\sqrt{3}$ Structure from Hydrogenated Amorphous Silicon Film; Ashtikar, M. S.; Sharma, G. L. *Solid State Commun.* **1994**, *91*, 831−834.

Detection of Hydrogen Plasma Induced Defects in Si by Positron Annihilation; Asokakumar, P.; Stein, H. J.; Lynn, K. G. *Appl. Phys. Lett.* **1994**, *64*, 1684−1686.

Microstructure of Nanosize Hydrogenated Crystalline Silicon Studied by Scanning Tunneling Microscopy; Bai, C. L.; Wang, Z. H.; Dai, C. C.; Zhang, P. C.; He, Y. L. *J. Vac. Sci. Technol. B* **1994**, *12*, 1823−1826.

The Role of Hydrogen in Silicon Liquid Phase Epitaxy; Bergmann, R.; Kurianski, J. *Mater. Lett.* **1993**, *17*, 137−140.

Electrochemically Prepared Si(111) 1×1-H Surface; Bitzer, T.; Gruyters, M.; Lewerenz, H. J.; Jacobi, K. *Appl. Phys. Lett.* **1993**, *63*, 397−399.

Si2p Core-Level Chemical Shifts at the H/Si(111)-(1×1) Surface; Blase, X.; Dasilva, A. J. R.; Zhu, X. J.; Louie, S. G. *Phys. Rev. B* **1994**, *50*, 8102−8105.

Desorption and Other Effects of Pulsed Laser Annealing of Hydrogen Implanted Silicon; Boivin, R.; Terreault, B. *J. Appl. Phys.* **1993**, *73*, 1943−1951.

Scanning Tunneling Microscopy of the Interaction of Hydrogen with Silicon Surfaces; Boland, J. J. *Adv. Phys.* **1993**, *42*, 129−171.

Light Scattering by Acoustic Phonons in Unhydrogenated and Hydrogenated Amorphous Silicon; Bustarret, E.; Thomsen, C.; Stutzmann, M.; Asano, A.; Summonte, C. *J. Non-Cryst. Solids* **1993**, *166*, 927−930.

Infrared Spectroscopy of Semiconductor Surfaces—H-Terminated Silicon Surfaces; Chabal, Y. J. *J. Mol. Struct.* **1993**, *292*, 65−80.

The Interaction of Atomic Hydrogen with Adsorbed Ethylene and Acetylene on Si(100); Chua, L. H.; Jackman, R. B.; Foord, J. S. *Surf. Sci.* **1994**, *315*, 69−80.

Hydrogen Halogen Chemistry on Semiconductor Surfaces; Cohen, S. M.; Hukka, T. I.; Yang, Y. L.; Develyn, M. P. *Thin Solid Films* **1993**, *225*, 155−159.

H Coverage Dependence of Si(001) Homoepitaxy; Copel, M.; Tromp, R. M. *Phys. Rev. Lett.* **1994**, *72*, 1236−1239.

Hydrogenating Silicon Dioxide in an Electron Cyclotron Plasma; Delfino, M.; Tsai, W.; Reynolds, G.; Day, M. E. *Appl. Phys. Lett.* **1993**, *63*, 3426−3428.

Mechanistic Insight into Gas Phase Reactions of H• + Si_2H_6 and Hydrogen Atom Etching of Silicon Surfaces; Dobbs, K. D.; Doren, D. J. *J. Am. Chem. Soc.* **1993**, *115*, 3731−3738.

Vibrational Properties of H/Si(111)-(1×1) Surfaces—Infrared Absorption and Electron Energy Loss Spectroscopic Studies; Dumas, P.; Chabal, Y. J.; Jakob, P. *Appl. Surf. Sci.* **1993**, *65/66*, 580−586.

Effect of H on Si Molecular Beam Epitaxy; Eaglesham, D. J.; Unterwald, F. C.; Luftman, H.; Adams, D. P.; Yalisove, S. M. *J. Appl. Phys.* **1993**, *74*, 6615−6618.

The Role of Hydride Coverage in Surface Limited Thin Film Growth of Epitaxial Silicon and Germanium; Eres, G.; Sharp, J. W. *J. Appl. Phys.* **1993**, *74*, 7241−7250.

Hydrogenation of Boron in Silicon during Low Temperature Gas and Liquid Phase Processing; Filangeri, E. M.; Nishida, T. *J. Appl. Phys.* **1994**, *76*, 332−335.

Temperature Programmed Desorption of Molecular Hydrogen from a Si(100)-2×1 Surface—Theory and Experiment; Flowers, M. C.; Jonathan, N. B. H.; Liu, Y.; Morris, A. *J. Chem. Phys.* **1993**, *99*, 7038−7048.

Positron Trap Sites in the Native Oxide Film Grown on a Hydrogen Terminated Silicon Surface; Fujinami, M.; Chilton, N. B. *Appl. Phys. Lett.* **1993**, *63*, 3458−3460.

Vibrational Energy Relaxation of Si−H Stretching Modes on the H/Si(111)1×1 Surface; Gai, H. D.; Voth, G. A. *J. Chem. Phys.* **1993**, *99*, 740−743.

First Principles Molecular Dynamics Study of Surface Vibrations and Vibrational Mode Coupling on the H/Si(111)1×1 Surface; Gai, H. D.; Voth, G. A. *J. Chem. Phys.* **1994**, *101*, 1734−1737.

Low Energy Electron Beam Enhanced Etching of Si(100)-(2×1) by Molecular Hydrogen; Gillis, H. P.; Clemons, J. L.; Chamberlain, J. P. *J. Vac. Sci. Technol. B* **1992**, *10*, 2729−2733.

Effect of Substrate Photoexcitation on the Dynamics of the Si−H Stretch for Si(111)/H; Guyotsionnest, P. *J. Electron Spectrosc. Relat. Phenom.* **1993**, *64/65*, 1−9.

Silicon Molecular Beam Epitaxy on Hydrogen Plasma Cleaned Substrates; Hansch, W.; Hammerl, E.; Kiunke, W.; Eisele, I.; Ramm, J.; Beck, E. *Jpn. J. Appl. Phys.* **1994**, *33*, 2263−2267.

Vibrational Energy Flow at Stepped H/Si(111)—Phonons, Dipoles and Screening; Harris, A. L.; Kuhnke, K.; Morin, M.; Jakob, P.; Levinos, N. J.; Chabal, Y. J. *Faraday Discuss. Chem. Soc.* **1993**, *96*, 217−226.

Raman Studies of Steric Hindrance and Surface Relaxation of Stepped H-Terminated Silicon Surfaces; Hines, M. A.; Chabal, Y. J.; Harris, T. D.; Harris, A. L. *Phys. Rev. Lett.* **1993**, *71*, 2280−2283.

The Selective Deposition of a Silicon Film on Hydrogenated Amorphous Silicon by Mercury Sensitized Photochemical Vapor Deposition; Hiramatsu,

M.; Ishida, A.; Kamimura, T.; Kawakyu, Y. *Jpn. J. Appl. Phys.* **1993**, *32*, 1781–1783.

Electron Stimulated Desorption of Surface Hydrogen on a Si(100) Surface; Hirose, F.; Sakamoto, H. *Appl. Surf. Sci.* **1994**, *75*, 87–92.

Electron Tunneling Through Ultrathin Gate Oxide Formed on Hydrogen Terminated Si(100) Surfaces; Hiroshima, M.; Yasaka, T.; Miyazaki, S.; Hirose, M. *Jpn. J. Appl. Phys.* **1994**, *33*, 395–398.

Hydrogen Desorption Rate and Surface Hydrogen Coverage during Isothermal Annealing for Si_2H_6-Adsorbed Si(100) Surfaces; Horie, T.; Takakuwa, Y.; Yamaguchi, T.; Miyamoto, N. *J. Cryst. Growth* **1994**, *136*, 344–348.

Basis Modified Hydrogen Atoms as Embedding Atoms in Ab-Initio Chemisorption Cluster Model Calculations on Si Surfaces; Illas, F.; Roset, L.; Ricart, J. M.; Rubio, J. *J. Comput. Chem.* **1993**, *14*, 1534–1544.

Effects of Substrate Temperature and Bias Potential on Hydrogen Plasma Etching of Silicon; Ishii, M.; Nakashima, K.; Hayakawa, T.; Tajima, I.; Yamamoto, M. *J. Vac. Sci. Technol. B* **1994**, *12*, 2342–2346.

Investigation of Hydrogen Plasma Etched Si Surfaces; Ishii, M.; Nakashima, K.; Tajima, I.; Yamamoto, M. *Jpn. J. Appl. Phys.* **1992**, *31*, 4422–4427.

The Initial Stages of Diamond Growth—An Adsorption Study of Hot Filament Activated Methane and Hydrogen on Si(100); Jackman, R. B.; Chua, L. H.; Foord, J. S. *Surf. Sci.* **1993**, *292*, 47–60.

Chemisorption of H, H_2O and C_2H_4 on Si(113)—Implications for the Structure; Jacobi, K.; Myler, U. *Surf. Sci.* **1993**, *284*, 223–235.

Monohydride Structures on Chemically Prepared Silicon Surfaces; Jakob, P.; Chabal, Y. J.; Kuhnke, K.; Christman, S. B. *Surf. Sci.* **1994**, *302*, 49–56.

Imperfections on the Chemically Prepared, Ideally H-Terminated Si(111)-(1×1) Surfaces; Jakob, P.; Chabal, Y. J.; Raghavachari, K.; Dumas, P.; Christman, S. B. *Surf. Sci.* **1993**, *285*, 251–258.

Mechanism of H_2 Desorption from Monohydride Si(100)2×1-H; Jing, Z.; Lucovsky, G.; Whitten, J. L. *Surf. Sci.* **1993**, *296*, 33–37.

Observation of Hydrogen Terminated Silicon(111) Surface by Ultrahigh Vacuum Atomic Force Microscopy; Kageshima, M.; Yamada, H.; Morita, Y.; Tokumoto, H.; Nakayama, K.; Kawazu, A. *Jpn. J. Appl. Phys.* **1993**, *32*, 1321–1323.

Tip Induced Surface Disorder on Hydrogen Terminated Silicon(111) Surface Observed by Ultrahigh Vacuum Atomic Force Microscopy; Kageshima, M.; Yamada, H.; Morita, Y.; Tokumoto, H.; Nakayama, K.; Kawazu, A. *Jpn. J. Appl. Phys.* **1994**, *33*, 3735–3738.

Hydrogen Desorption Kinetics from the Growing Si(100) Surface during Silane Gas Source Molecular Beam Epitaxy; Kim, K. J.; Suemitsu, M.; Miyamoto, N. *Appl. Phys. Lett.* **1993**, *63*, 3358–3360.

Observation of Atomic Steps on Vicinal Si(111) Annealed in Hydrogen Gas Flow by Scanning Tunneling Microscopy; Kitahara, K.; Ueda, O. *Jpn. J. Appl. Phys.* **1993**, *32*, 1826–1829.

Mechanism of Hydrogen Sensing by Platinum Silicon Oxide Silicon MIS Tunneling Diodes; Kobayashi, H.; Kogetsu, Y.; Nakato, Y. *Surf. Sci.* **1994**, *306*, 69–80.

Hydrogen Adsorption on and Desorption from Si—Considerations on the Applicability of Detailed Balance; Kolasinski, K. W.; Nessler, W.; Demeijere, A.; Hasselbrink, E. *Phys. Rev. Lett.* **1994**, *72*, 1356–1359.

Influence of Si Surface Structure on Reaction Mechanism—Atomic Hydrogen Plus Adsorbed Br; Koleske, D. D.; Gates, S. M. *J. Chem. Phys.* **1993**, *98*, 5091–5094.

Kinetics of Atomic Hydrogen Plus Adsorbed Br Reactions on Si(100) and Si(111) Surfaces; Koleske, D. D.; Gates, S. M. *J. Chem. Phys.* **1993**, *99*, 8218–8228.

Atomic H Abstraction of Surface-H on Si—An Eley-Rideal Mechanism; Koleske, D. D.; Gates, S. M.; Jackson, B. *J. Chem. Phys.* **1994**, *101*, 3301–3309.

Facile Abstraction of Chemisorbed-D on Si(100) by Atomic H; Koleske, D. D.; Gates, S. M.; Schultz, J. A. *J. Chem. Phys.* **1993**, *99*, 5619–5622.

Vibrational Energy Transfer Among Adsorbate Modes—Picosecond Dynamics on Stepped H/Si(111); Kuhnke, K.; Morin, M.; Jakob, P.; Levinos, N. J.; Chabal, Y. J.; Harris, A. L. *J. Chem. Phys.* **1993**, *99*, 6114–6125.

Electrolytic Hydrogenation of Silicon—A High Resolution Electron Energy Loss Spectroscopy Investigation; Lewerenz, H. J.; Bitzer, T.; Gruyters, M.; Jacobi, K. *J. Electrochem. Soc.* **1993**, *140*, 44–46.

Planar Basis Pseudopotential Calculations of the Si(001)2×1 Surface with and Without Hydrogen Passivation; Li, G. W.; Chang, Y. C. *Phys. Rev. B* **1993**, *48*, 12032–12036.

First Principles Study of Steps on the Si(111)-H Surface; Li, X. P.; Vanderbilt, D.; Kingsmith, R. D. *Phys. Rev. B* **1994**, *50*, 4637–4641.

Interaction of Atomic Hydrogen with the Si(100)2×1 Surface; Lu, H.; Wang, X. D.; Bai, C. L.; Hashizume, T.; Sakurai, T. *Appl. Phys. A* **1994**, *58*, 203–209.

Interadsorbate Vibrational Energy Flow on Stepped Vicinal H/Si(111) Surfaces; Morin, M.; Kuhnke, K.; Jakob, P.; Chabal, Y. J.; Levinos, N. J.; Harris, A. L. *J. Electron Spectrosc. Relat. Phenom.* **1993**, *64/65*, 11–21.

Si(111)-$\sqrt{3}\times\sqrt{3}$R30°Si Mediated by Hydrogen Desorption; Morita, Y.; Miki, K.; Tokumoto, H. *Surf. Sci.* **1993**, *298*, 163–168.

Hydrogen Terminated Si(100) Surfaces Investigated by Reflectance Anisotropy Spectroscopy; Muller, A. B.; Reinhardt, F.; Resch, U.; Richter, W.; Rose, K. C.; Rossow, U. *Thin Solid Films* **1993**, *233*, 19–23.

Hydrogen Interactions with Cavities in Helium Implanted Silicon; Myers, S. M.; Follstaedt, D. M.; Stein, H. J.; Wampler, W. R. *Phys. Rev. B* **1993**, *47*, 13380–13394.

Coadsorption of Hydrogen and Deuterium on Si(100) Surfaces Studied by Elastic Recoil Detection Analysis; Naitoh, M.; Morioka, H.; Shoji, F.; Oura, K. *Surf. Sci.* **1993**, *297*, 135–140.

Effect of Atomic and Molecular Hydrogen Irradiation on Ge Surface Segregation during Si Molecular

Beam Epitaxy; Nakagawa, K.; Nishida, A.; Kimura, Y.; Shimada, T. *Jpn. J. Appl. Phys.* **1994**, *33*, 1331–1334.

Effects of Substrate Temperature and Ion Incident Energy on Silicon Surface Cleaning Using a Hydrogen Plasma Excited by Electron Cyclotron Resonance; Nakashima, K.; Ishii, M.; Hayakawa, T.; Tajima, I.; Yamamoto, M. *J. Appl. Phys.* **1993**, *74*, 6936–6940.

In-Situ Process Evaluation during Hydrogen Plasma Etching of A-Si–H Films by Microwave Detected Transient Photoconductivity Measurements; Neitzert, H. C.; Hirsch, W.; Kunst, M. *J. Appl. Phys.* **1993**, *73*, 7446–7452.

Oxidation of Hydrogen Terminated Si Surfaces Studied by Infrared Spectroscopy; Niwano, M.; Kageyama, J.; Kinashi, K.; Sawahata, J.; Miyamoto, N. *Surf. Sci.* **1994**, *301*, 245–249.

Infrared Spectroscopy Study of Initial Stages of Oxidation of Hydrogen Terminated Si Surfaces Stored in Air; Niwano, M.; Kageyama, J.; Kurita, K.; Kinashi, K.; Takahashi, I.; Miyamoto, N. *J. Appl. Phys.* **1994**, *76*, 2157–2163.

Hydrogen Induced Ag Cluster Formation on the Si(111) ($\sqrt{3}\times\sqrt{3}$)R30°-Ag Surface Observed by Scanning Tunneling Microscopy; Ohnishi, H.; Yamamoto, Y.; Katayama, I.; Ohba, Y.; Oura, K. *Jpn. J. Appl. Phys.* **1994**, *33*, 1106–1109.

Surface Hydrogen Effects on Ge Surface Segregation during Silicon Gas Source Molecular Beam Epitaxy; Ohtani, N.; Mokler, S.; Xie, M. H.; Zhang, J.; Joyce, B. A. *Jpn. J. Appl. Phys.* **1994**, *33*, 2311–2316.

Selective Etching of Hydrogenated Amorphous Silicon by Hydrogen Plasma; Otobe, M.; Kimura, M.; Oda, S. *Jpn. J. Appl. Phys.* **1994**, *33*, 4442–4445.

The Role of Hydrogen Radicals in Nucleation and Growth of Nanocrystalline Silicon; Otobe, M.; Oda, S. *J. Non-Cryst. Solids* **1993**, *166*, 993–996.

Elastic Recoil Detection Analysis of Coadsorption of Hydrogen and Deuterium on Clean Si Surfaces; Oura, K.; Naitoh, M.; Morioka, H.; Watamori, M.; Shoji, F. *Nucl. Instrum. Methods Phys. Res. Sect. B* **1994**, *85*, 344–346.

STM Study of Si(111)1×1-H Surfaces Prepared by In-Situ Hydrogen Exposure; Owman, F.; Martensson, P. *Surf. Sci.* **1994**, *303*, 367–372.

Substituent Effects in Silicon Hydrides—Implications for Models of Surface Sites; Pai, S.; Doren, D. *J. Phys. Chem.* **1994**, *98*, 4422–4427.

Semiempirical Total Energy Functional for Silicon-Hydrogen Interactions in Solids; Park, Y. K.; Myles, C. W. *Phys. Rev. B* **1993**, *48*, 17086–17091.

Chemomechanical Polishing of Silicon—Surface Termination and Mechanism of Removal; Pietsch, G. J.; Higashi, G. S.; Chabal, Y. J. *Appl. Phys. Lett.* **1994**, *64*, 3115–3117.

Step Relaxation and Surface Stress at H-Terminated Vicinal Si(111); Raghavachari, K.; Jakob, P.; Chabal, Y. J. *Chem. Phys. Lett.* **1993**, *206*, 156–160.

Low Temperature Epitaxial Growth by Molecular Beam Epitaxy on Hydrogen Plasma Cleaned Silicon Wafers; Ramm, J.; Beck, E.; Dommann, A.; Eisele, I.; Kruger, D. *Thin Solid Films* **1994**, *246*, 158–163.

Cleaning of Silicon Surfaces by Hydrogen Multipolar Microwave Plasma Excited by Distributed Electron Cyclotron Resonance; Raynaud, P.; Pomot, C. *J. Vac. Sci. Technol. B* **1994**, *12*, 574–580.

Kinetics of Hydrogen Desorption in Surface Limited Thin Film Growth of SiGe Alloys; Sharp, J. W.; Eres, G. *Appl. Phys. Lett.* **1993**, *62*, 2807–2809.

Structure of Hydrogen on the Si(100) Surface in the (2×1)-H Monohydride, (1×1)-H Dihydride, and *C*(4×4)-H Phases; Shi, M.; Wang, Y.; Rabalais, J. W. *Phys. Rev. B* **1993**, *48*, 1689–1695.

Monte Carlo Simulation of Surface Reactions in Plasma Enhanced Chemical Vapor Deposition of Hydrogenated Amorphous Silicon Thin Films; Shirafuji, T.; Chen, W. M.; Yamamuka, M.; Tachibana, K. *Jpn. J. Appl. Phys.* **1993**, *32*, 4946–4947.

Direct Photochemical Vapor Deposition of Hydrogenated Amorphous Silicon—Effects of Excitation Wavelengths and Source Gases; Shirafuji, T.; Nakajima, S.; Wang, Y. F.; Genji, T.; Tachibana, K. *Jpn. J. Appl. Phys.* **1993**, *32*, 1546–1557.

Diffusion of Hydrogen Atoms on a Si(111)-(7×7) Reconstructed Surface—Monte Carlo Variational Phase Space Theory; Sorescu, D. C.; Thompson, D. L.; Raff, L. M. *J. Chem. Phys.* **1994**, *101*, 1638–1647.

A Theoretical Study of the Initial Stages of the Hydrogenation of Si(111) 7×7; Stauffer, L.; Minot, C. *Catal. Lett.* **1994**, *23*, 1–11.

Hydrogen Introduction and Hydrogen Enhanced Thermal Donor Formation in Silicon; Stein, H. J.; Hahn, S. K. *J. Appl. Phys.* **1994**, *75*, 3477–3484.

Infrared Spectroscopy of Chemically Bonded Hydrogen at Voids and Defects in Silicon; Stein, H. J.; Myers, S. M.; Follstaedt, D. M. *J. Appl. Phys.* **1993**, *73*, 2755–2764.

Epitaxial Growth of Aluminum Films on Hydrogen Mediated Si(100) Surface; Sugawara, H.; Ueda, K. *Jpn. J. Appl. Phys.* **1994**, *33*, 837–839.

Pitfalls in the Measurement of Metal/p-Si Contacts—The Effect of Hydrogen Passivation; Sullivan, J. P.; Graham, W. R.; Tung, R. T.; Schrey, F. *Appl. Phys. Lett.* **1993**, *62*, 2804–2806.

Study of Sputtering Mechanism of Silicon with Hydrogen Plasma Controlled by Magnetic Field; Sun, Y.; Nishitani, R.; Miyasato, T. *Jpn. J. Appl. Phys.* **1994**, *33*, 263–266.

Temperature Dependent Reaction of RF Hydrogen Plasma with Silicon; Sun, Y.; Nishitani, R.; Miyasato, T. *Jpn. J. Appl. Phys.* **1994**, *33*, 1117–1120.

Epitaxial Growth of Metal Phthalocyanines on Hydrogen Terminated Si(111) Surfaces; Tada, H.; Kawaguchi, T.; Koma, A. *Appl. Surf. Sci.* **1994**, *75*, 93–98.

Removal of Hydrogen from 1×1 Dihydride Passivated Si(100) by Low Energy Rare Gas Ions—Implications for RPCVD; Tesauro, M. R.; Banerjee, S.; Campion, A. *Surf. Sci.* **1994**, *318*, 1171–1174.

Atomic and Electronic Structure of the Si(001) Surface Induced by Hydrogen Adsorption; Uchiyama, T.; Tsukada, M. *Surf. Sci.* **1993**, *295*, 1037–1042.

Theory of Scanning Tunneling Microscopy and Spectroscopy on Hydrogen Adsorbed Si(100) Surface; Uchiyama, T.; Tsukada, M. *J. Vac. Sci. Technol. B* **1994**, *12*, 2205–2208.

Theory of Scanning Tunneling Microscopy and Spectroscopy of the Hydrogen Terminated Si(001)

Surface; Uchiyama, T.; Tsukada, M. *Surf. Sci.* **1994**, *313*, 17–24.

Behaviors of Hydrogen and Oxygen on Claned Silicon Surfaces; Ueda, K. *Jpn. J. Appl. Phys.* **1994**, *33*, 1524–1527.

Desorption Study of a Proton from H/Si(100) by Electron Stimulated Desorption Spectroscopy; Ueda, K.; Kodama, S.; Takano, A. *Surf. Sci.* **1993**, *283*, 195–198.

Energies of Various Configurations of Hydrogen in Silicon; Vandewalle, C. G. *Phys. Rev. B* **1994**, *49*, 4579–4585.

Atomic Force Microscopy and Infrared Spectroscopy Studies of Hydrogen Baked Si Surfaces; Vatel, O.; Verhaverbeke, S.; Bender, H.; Caymax, M.; Chollet, F.; et al. *Jpn. J. Appl. Phys.* **1993**, *32*, 1489–1491.

Energetics of Atomic Hydrogen Diffusion on Si(100); Vittadini, A.; Selloni, A.; Casarin, M. *Surf. Sci.* **1993**, *289*, 625–630.

Hydrogen Uptake into Silicon from an Electron Cyclotron Resonance Plasma; Wampler, W. R.; Barbour, J. C. *J. Vac. Sci. Technol. A* **1994**, *12*, 1978–1983.

Surface Silicon-Deuterium Bond Energy from Gas Phase Equilibration; Wampler, W. R.; Myers, S. M.; Follstaedt, D. M. *Phys. Rev. B* **1993**, *48*, 4492–4497.

Atomic Hydrogen Chemisorption on Si(100)(2×1) Studied by FI-STM; Wang, X. D.; Lu, H.; Hashizume, T.; Pickering, H. W.; Sakurai, T. *Appl. Surf. Sci.* **1993**, *67*, 266–274.

Structure of the Si(100) Surface in the Clean (2×1), (2×1)-H Monohydride, (1×1)-H Dihydride, and *C*(4×4)-H Phases; Wang, Y.; Shi, M.; Rabalais, J. W. *Phys. Rev. B* **1993**, *48*, 1678–1688.

Direct Dimer-by-Dimer Identification of Clean and Monohydride Dimers on the Si(001) Surface by Scanning Tunneling Microscopy; Wang, Y. J.; Bronikowski, M. J.; Hamers, R. J. *J. Vac. Sci. Technol. A* **1994**, *12*, 2051–2057.

Atomic Step Structure on Vicinal H/Si(111) Surface Formed by Hot Water Immersion; Watanabe, S.; Horiuchi, K.; Ito, T. *Jpn. J. Appl. Phys.* **1993**, *32*, 3420–3425.

Oxidation Stages of Clean and H-Terminated Si(001) Surfaces at Room Temperature; Westermann, J.; Nienhaus, H.; Monch, W. *Surf. Sci.* **1994**, *311*, 101–106.

Adsorption of Hydrogen Atoms on the Silicon(111) (1×1) Surface—First-Principles Calculations; Wu, B. R.; Cheng, C. *J. Phys.: Condens. Matter* **1994**, *6*, 1113–1124.

Adsorption of Hydrogen and Disilane on Si(100) and Si-Ge Surfaces; Wu, Y. M.; Nix, R. M. *Surf. Sci.* **1994**, *306*, 59–68.

Synchrotron Radiation X-Ray Photoelectron Spectroscopy Study of Hydrogen Terminated Si Surfaces and Their Oxidation Mechanism; Yamamoto, K.; Hasegawa, M. *J. Vac. Sci. Technol. B* **1994**, *12*, 2493–2499.

Fundamentals of 2-Step Etching Techniques for Ideal Silicon—Hydrogen Termination of Silicon(111); Yang, S. K.; Peter, S.; Takoudis, C. G. *J. Appl. Phys.* **1994**, *76*, 4107–4112.

Film Thickness Reduction of Thermally Annealed Hydrogenated Amorphous Silicon Prepared with Plasma Enhanced Chemical Vapor Deposition; Yang, Y. K.; Shin, J. S.; Hsieh, R. G.; Gan, J. Y. *Appl. Phys. Lett.* **1994**, *64*, 1567–1569.

Pairing and Clustering of Hydrogen on Si(100)2×1—Monte Carlo Studies; Yang, Y. L.; Develyn, M. P. *J. Vac. Sci. Technol. A* **1993**, *11*, 2200–2204.

Atomic H—A Reagent for the Extraction of Chemical Species from Si Surfaces; Yates, J. T.; Cheng, C. C.; Gao, Q.; Colaianni, M. L.; Choyke, W. J. *Thin Solid Films* **1993**, *225*, 150–154.

Effects of Hydrogen and Bias on Single Crystal Al Growth on Vicinal Si by DC Magnetron Sputtering; Yokoyama, S.; Ichikawa, H.; Ichikawa, Y.; Koyanagi, M. *Jpn. J. Appl. Phys.* **1994**, *33*, 459–461.

Model of Hydrogen Diffusion on Si(100); Zhdanov, V. P. *Phys. Rev. B* **1993**, *48*, 14325–14330.

Hydrogen Chemisorption on the Si(111) Surface; Zheng, X. M.; Smith, P. V. *Surf. Sci.* **1993**, *282*, 173–184.

Hydrogen Enhanced Out-Diffusion of Oxygen in Czochralski Silicon; Zhong, L.; Shimura, F. *J. Appl. Phys.* **1993**, *73*, 707–710.

Real-Time, In-Situ Monitoring of Room Temperature Silicon Surface Cleaning Using Hydrogen and Ammonia Plasmas; Zhou, Z. H.; Aydil, E. S.; Gottscho, R. A.; Chabal, Y. J.; Reif, R. *J. Electrochem. Soc.* **1993**, *140*, 3316–3321.

Group 1

Alkali Metals

Angle Resolved Photoemission Study of a Single-Domain Si(001)2×1-Na Surface with Synchrotron Radiation; Abukawa, T.; Kashiwakura, T.; Okane, T.; Takahashi, H.; Suzuki, S.; et al. *Surf. Sci.* **1994**, *303*, 146–152.

Submonolayer Coverage and Monolayer Coverage Structures of K/Si(100); Brodde, A.; Bertrams, T.; Neddermeyer, H. *Phys. Rev. B* **1993**, *47*, 4508–4516.

The Sodium Promoted Nitridation of Si(100)-2×1 Using N_2 Molecular Beams; Bush, T. L.; Hayward, D. O.; Jones, T. S. *Surf. Sci.* **1994**, *313*, 179–187.

A Molecular Beam Study of the Reaction of O_2 with K-Covered Si(100); Bush, T. L.; Jones, T. S.; Hayward, D. O. *Surf. Sci.* **1994**, *309*, 247–252.

Multisite Occupancy at the Alkali Silicon(111) Interface Studied with XSW; Castrucci, P.; Lagomarsino, S.; Scarinci, F.; Giannini, C. *J. Phys. D* **1993**, *26*, 192–196.

Charge Transfer Satellites in KL_{23} XAS Data for K/Si(111)-(2×1)—Evidence for Strong ionic Bonds; Daddato, S.; Ramaker, D. E.; Cosso, R.; Gregory, D.; Morrison, T. P.; et al. *Europhys. Lett.* **1994**, *26*, 85–90.

X-Ray Standing-Wave Study of Alkali Metal Si(111)7×7 Interfaces; Etelaniemi, V.; Michel, E. G.; Materlik, G. *Phys. Rev. B* **1993**, *48*, 12023–12031.

RbBr/Si(111) Interface Studied by the X-Ray Standing-Wave Method; Etelaniemi, V.; Michel, E. G.; Materlik, G. *Surf. Sci.* **1993**, *287*, 288–293.

Na-Promoted Oxidation of Si—The Specific Oxidation Mechanism; Faraci, G.; Larosa, S.; Pennisi, A. R.; Margaritondo, G. *Phys. Rev. B* **1994**, *49*, 2943–2946.

Adsorption of Potassium on the Si(111)$\sqrt{3}\times\sqrt{3}$R30°-B-Surface—Observation of an Insulating Surface at Submonolayer Coverage; Grehk, T. M.; Johansson, L. S. O.; Karlsson, U. O.; Flodstrom, A. S. *Phys. Rev. B* **1993**, *47*, 13887–13890.

Adsorption of Lithium on the Si(111)7×7 Surface Studied with High Resolution Core Level Spectroscopy; Grehk, T. M.; Larsson, C. U. S.; Prince, N. P.; Flodstrom, S. A. *Surf. Sci.* **1993**, *284*, 384–388.

Quantum Size Effect for Na Films on Si(100); Hamawi, A.; Wallden, L. *Surf. Sci.* **1993**, *285*, 93–101.

The Absolute Coverage of K on the Si(111)-3×1-K Surface; Hashizume, T.; Katayama, M.; Jeon, D. R.; Aono, M.; Sakurai, T. *Jpn. J. Appl. Phys.* **1993**, *32*, 1263–1265.

Adsorption Structure of the Na-Saturated Si-(100)2×1 Surface Studied by Field Ion Scanning Tunneling Microscopy Spectroscopy; Hashizume, T.; Motai, K.; Jeon, D. R.; Sakurai, T. *Jpn. J. Appl. Phys.* **1993**, *32*, 1410–1415.

Adsorption Geometry of Na Saturation on the Dimerized Si(100)(2×1) Surface; Hashizume, T.; Motai, K.; Lu, H.; Sakurai, T. *Appl. Surf. Sci.* **1993**, *67*, 261–265.

A Cluster Study of the Stabilities of Adsorption Sites and Charge Transfers at the Na/Si(100) Surface; Hira, A. S.; Lin, P. C.; Ray, A. K. *Phys. Status Solidi B* **1994**, *182*, 331–345.

Interaction of (1×2)-Reconstructed Si(100) and Ag-(110)—Cs Surfaces with C_{60} Overlayers; Hong, H.; Aburano, R. D.; Hirschorn, E. S.; Zschack, P.; Chen, H.; Chiang, T. C. *Phys. Rev. B* **1993**, *47*, 6450–6454.

Sodium-Induced H^+ Ion Resonance on Silicon Surfaces; Hurych, Z.; Soukiassian, P.; Kapoor, S.; Mangat, P. S.; Kim, S. T.; et al. *Surf. Sci.* **1994**, *302*, 293–298.

Structural Transformation of the Si(111)(7×7) To (3×1) Surface Structure Induced by Sodium; Jeon, D.; Hashizume, T.; Wang, X.; Motai, K.; Sakurai, T. *Appl. Surf. Sci.* **1993**, *67*, 257–260.

Scanning Tunneling Microscopy of Oxygen and Sodium Adsorption on the Si(111) Surface; Jeon, D. R.; Hashizume, T.; Sakurai, T. *Jpn. J. Appl. Phys.* **1993**, *32*, 1423–1427.

Electronic Structure of the Na-Adsorbed Si(100)2×1 Surface Studied by Inverse and Direct Angle Resolved Photoemission; Johansson, L. S. O.; Reihl, B. *Phys. Rev. B* **1993**, *47*, 1401–1406.

Alkali Metals on Si(100)2×1—Comparative Study of the Surface Electronic Structures for Li, Na and K Adsorption; Johansson, L. S. O.; Reihl, B. *Surf. Sci.* **1993**, *287*, 524–528.

Surface Reconstructions in the Ag/Si(001) System; Lin, X. F.; Wan, K. J.; Nogami, J. *Phys. Rev. B* **1994**, *49*, 7385–7393.

The Interaction of a Sodium Atom with the Silicon-(111) Surface; Mahapatra, M.; Ray, A. K.; Hira, A. S. *J. Phys.: Condens. Matter* **1993**, *5*, 6543–6554.

Structural Properties of the Na/Si(111)2×1 Surface Studied by Photoemission Extended X-Ray Absorption Fine Structures; Mangat, P. S.; Soukiassian, P.; Huttel, Y.; Hurych, Z. *J. Vac. Sci. Technol. B* **1994**, *12*, 2694–2698.

Determination of the Na/Si(100)2×1 Surface and Interface Geometry by Polarization Dependent Photoemission Extended X-Ray Absorption Fine Structure and Ab-Initio Total Energy Molecular Calculations; Mangat, P. S.; Soukiassian, P.; Schirm, K. M.; Spiess, L.; Tang, S. P.; et al. *Phys. Rev. B* **1993**, *47*, 16311–16321.

Direct Evidence of Occupied States Near the Fermi Level on the Si(100)2×1-K Interface; Martingago, J. A.; Asensio, M. C.; Soria, F.; Aebi, P.; Fasel, R.; et al. *Surf. Sci.* **1994**, *309*, 995–1000.

Adsorption of Rb on Si(211)2×1 Studied by the X-Ray Standing-Wave Technique; Michel, E. G.; Etelaniemi, V.; Materlik, G. *J. Vac. Sci. Technol. A* **1993**, *11*, 1812–1816.

Stability of a Lithium-Drifted Silicon Detector; Miyachi, T.; Ohkawa, S.; Matsuzawa, H.; Otogawa, T.; Kobayashi, N.; Onabe, H. *Jpn. J. Appl. Phys.* **1994**, *33*, 4111–4114.

1st-Principles Molecular Dynamics Study of Alkali Metal Adsorption on a Si(001) Surface; Morikawa, Y.; Kobayashi, K.; Terakura, K. *Surf. Sci.* **1993**, *283*, 377–382.

Oxidation of Si(111)7×7 Using Alkali Metal Atoms—Evidence for Local Promotion Mechanisms; Muscat, A. J.; Rjeb, A.; Roy, D. *Surf. Sci.* **1994**, *302*, 256–262.

Dynamic Study of Alkali Promotion of NO Sticking on Si(100); Namiki, A.; Suzuki, S.; Kato, H.; Nakamura, T.; Suzaki, T. *Surf. Sci.* **1993**, *283*, 9–20.

Low Energy Electron Diffraction as a Direct Identification Technique—Atomic Structures of Ag-Induced and Li-Induced Si(111)-($\sqrt{3}\times\sqrt{3}$)R30°; Over, H.; Huang, H.; Tong, S. Y.; Fan, W. C.; Ignatiev, A. *Phys. Rev. B* **1993**, *48*, 15353–15357.

Na Adsorption on Si(111)-(7×7) Studied by Scanning Tunneling Microscopy and Photoemission; Paggel, J. J.; Haak, H.; Theis, W.; Horn, K. *J. Vac. Sci. Technol. B* **1993**, *11*, 1439–1443.

Detection of Residual Impurities After the Alkali Metal Enhanced Oxidation of Si(100) Surfaces by SIMS and Hall Effect Measurements; Pirug, G.; Muller, O.; Bonzel, H. P. *Appl. Surf. Sci.* **1993**, *70/71*, 644–649.

Spin Correlations in Semiconductor Dangling Bonds—Implications for the Alkali Metal Covered Surfaces; Refolio, M. C.; Rubio, J.; Sancho, M. P. L.; Sancho, J. M. L. *Phys. Rev. B* **1994**, *49*, 4623–4634.

Local Alkali Metal Promoted Oxidation of Si(100)-(2×1) Surfaces—A Generalized Hubbard Model Calculation; Refolio, M. C.; Sancho, J. M. L.; Sancho, M. P. L.; Rubio, J. *Phys. Rev. B* **1994**, *49*, 2629–2636.

Nitric Oxide Adsorption on the Si(111)7×7 Surface—Effect of Potassium Overlayers; Riehlchudoba, M.; Surnev, L.; Soukiassian, P. *Surf. Sci.* **1994**, *306*, 313–326.

Photoemission Study of the Si(111)3×1-K Surface; Sakamoto, K.; Okuda, T.; Nishimoto, H.; Daimon, H.; Suga, S.; et al. *Phys. Rev. B* **1994**, *50*, 1725–1732.

Extended Hubbard Model Analysis of Semiconductor Alkali Interfaces—Implications for the Metallization Problem; Sancho, J. M. L.; Refolio, M. C.; Sancho, M. P. L.; Rubio, J. *Surf. Sci.* **1993**, *285*, 491–497.

Alkali Metal Adsorption on the Si(100) Surface Studied by Low Energy D^+ Scattering; Souda, R.;

Hayami, W.; Aizawa, T.; Ishizawa, Y. *Phys. Rev. B* **1993**, *47*, 9917–9920.

Low Energy D^+ Scattering from Cs and CsCl Adsorbed on the Si(100)2×1 Surface; Souda, R.; Hayami, W.; Aizawa, T.; Ishizawa, Y. *Surf. Sci.* **1993**, *290*, 245–254.

Electronic Properties of Ionic Insulators on Metal and Semiconductor Surfaces—RbCl on Si(100) and W(110); Souda, R.; Hayami, W.; Aizawa, T.; Otani, S.; Ishizawa, Y. *J. Vac. Sci. Technol. A* **1993**, *11*, 535–538.

Potassium Adsorption on Metal and Semiconductor Surfaces Studied by Low Energy D^+ Scattering; Souda, R.; Hayami, W.; Aizawa, T.; Otani, S.; Ishizawa, Y. *Phys. Rev. B* **1993**, *47*, 6651–6660.

Combined Theoretical and Experimental Determination of the Atomic Structure and Adsorption Site of Na on the Si(100)2×1 Surface; Spiess, L.; Mangat, P. S.; Tang, S. P.; Schirm, K. M.; Freeman, A. J.; Soukiassian, P. *Surf. Sci.* **1993**, *289*, 631–637.

Electronic Structure of K/Si(111) Interfaces; Weitering, H. H.; Chen, J.; Dinardo, N. J.; Plummer, E. W. *J. Vac. Sci. Technol. A* **1993**, *11*, 2049–2053.

Electron Correlation, Metallization, and Fermi Level Pinning at Ultrathin K/Si(111) Interfaces; Weitering, H. H.; Chen, J.; Dinardo, N. J.; Plummer, E. W. *Phys. Rev. B* **1993**, *48*, 8119–8135.

Electron Localization and the Nonmetal To Metal Transition at Ultrathin Alkali Metal/Si(111) Interfaces; Weitering, H. H.; Chen, J.; Perezsandoz, R.; Dinardo, N. J. *Surf. Sci.* **1994**, *309*, 978–983.

Variation of Local Charge States and the Local Electrostatic Potential during Oxygen Adsorption on a Caesiated Si(001) Surface Probed with Helium Metastables and Oxygen Molecules; Yamada, K.; Nishigaki, S. *Surf. Sci.* **1993**, *293*, 893–899.

Group 2

Mg

Chemical Interactions and Schottky Barrier Determinations at the Mg/Si(100) Interface Studied Using X-Ray Photoelectron Spectroscopy; Vanbuuren, M. R. J.; Griffiths, C. L.; Vankempen, H. *Surf. Sci.* **1994**, *314*, 172–178.

Epitaxial Silicide Formation in the Mg/Si(111) System; Wigren, C.; Andersen, J. N.; Nyholm, R.; Karlsson, U. O. *Surf. Sci.* **1993**, *289*, 290–296.

Ba

$BaSi_2$ and Thin Film Alkaline-Earth Silicides on Silicon; McKee, R. A.; Walker, F. J.; Conner, J. R.; Raj, R. *Appl. Phys. Lett.* **1993**, *63*, 2818–2820.

Group 4

Ti

Growth Mode of Ti-Thin Films on Si(111) and Double Heteroepitaxial Growth of Epi-Si Epi-C_{54} $TiSi_2$ Si(111); Choi, C. K.; Lee, J. Y.; Lee, Y. P.; Park, H. H.; Jung, S. M.; Kim, K. H. *J. Korean Phys. Soc.* **1993**, *26*, 407–412.

Formation of Epi-C_{49} $TiSi_2$/Si(111) by Solid-Phase Epitaxial Growth; Choi, C. K.; Yang, S. J.; Ryu, J. Y.; Lee, J. Y.; Lee, Y. P.; et al. *J. Korean Phys. Soc.* **1993**, *26*, 148–152.

In-Situ Solid-Phase Epitaxial Growth of C_{49}-$TiSi_2$ on Si(111)-7×7 Substrate; Choi, C. K.; Yang, S. J.; Ryu, J. Y.; Lee, J. Y.; Park, H. H.; et al. *Appl. Phys. Lett.* **1993**, *63*, 485–487.

Diffusion of Elements Implanted in Amorphous Titanium Disilicide; Dheurle, F. M.; Cotte, J.; Gas, P.; Goltz, G.; Stanis, C.; Thomas, O. *Appl. Surf. Sci.* **1993**, *73*, 167–174.

A Transmission Electron Microscopic Study of Titanium Silicides Fabricated by Implantation of Titanium into Silicon and Thermal Annealing; Jin, S.; Wen, X. Y.; Zhang, Z. *Thin Solid Films* **1994**, *249*, 50–53.

Interface Structure and Adhesion of Sputtered Ti Layers on Si—The Effect of Heat-Treatment; Kondo, I.; Yoneyama, T.; Kondo, K.; Takenaka, O.; Kinbara, A. *Thin Solid Films* **1993**, *236*, 236–239.

Growth of Epitaxial $CoSi_2$ Film on Si(100) Substrate—Induced by an Interfacial Ti Layer; Liu, P.; Li, B. Z.; Zhou, Z. Y.; Lin, C. L.; Zou, S. C. *Mater. Lett.* **1993**, *17*, 383–387.

Residual-Stresses and Fracture Properties of Magnetron-Sputtered Ti Films on Si Microelements; Ljungcrantz, H.; Hultman, L.; Sundgren, J. E.; Johansson, S.; Kristensen, N.; et al. *J. Vac. Sci. Technol. A* **1993**, *11*, 543–553.

Detailed In-Situ Monitoring of Film Growth—Application to $TiSi_2$ Chemical Vapor Deposition; Mendicino, M. A.; Seebauer, E. G. *J. Cryst. Growth* **1993**, *134*, 377–385.

Titanium Disilicide on Silicon by Interdiffusion of Titanium and Amorphous Silicon Multilayers—Transmission Electron Microscopy, Spectroscopic Ellipsometry and Resistivity Measurements; Nassiopoulos, A. G.; Tambouris, D.; Frangis, N.; Logothetidis, S.; Georga, S.; et al. *Thin Solid Films* **1994**, *247*, 44–50.

Morphology of $TiSi_2$ and $ZrSi_2$ on Si(100) and (111) Surfaces; Sukow, C. A.; Nemanich, R. J. *J. Mater. Res.* **1994**, *9*, 1214–1227.

On the Influence of Sputter Etch Cleaning on the Silicidation, the Thermal Stability and the Electrical Characteristics of Ti/p-Si Contacts; Vercaemst, A. S.; Vanmeirhaeghe, R. L.; Laflere, W. H.; Cardon, F.; Debosscher, W.; Schreutelkamp, R. J. *Solid-State Electron.* **1993**, *36*, 753–759.

Laser-Assisted Chemical Vapor Deposition of $TiSi_2$—Aspects of Deposition and Etching; Westberg, H.; Boman, M.; Carlsson, J. O. *J. Phys. IV* **1993**, *3*, 225–232.

Zr

Morphology of $TiSi_2$ and $ZrSi_2$ on Si(100) and (111) Surfaces; Sukow, C. A.; Nemanich, R. J. *J. Mater. Res.* **1994**, *9*, 1214–1227.

Group 5

Ta

Si LVV Auger Lineshape Analysis to Study the Oxygen Chemisorption on $TaSi_2$ Thin Film; Sharma,

J. K. N.; Chakraborty, B. R.; Bera, S. *Surf. Interface Anal.* **1993**, *20*, 841–844.

Group 6

Cr

Interfacial Reactions and Silicide Formation in Si/Ni/Si and Si/Cr/Si Sandwich Layers; Zalar, A.; Hofmann, S.; Pimentel, F.; Panjan, P. *Surf. Interface Anal.* **1994**, *21*, 560–565.

Mo

Structure and Performance of Si/Mo Multilayer Mirrors for the Extreme Ultraviolet; Slaughter, J. M.; Schulze, D. W.; Hills, C. R.; Mirone, A.; Stalio, R.; et al. *J. Appl. Phys.* **1994**, *76*, 2144–2156.

W

Processing of W/Si and Si/W Bilayers and Multilayers with Single and Multiple Excimer Laser Pulses; Danna, E.; Luby, S.; Luches, A.; Majova, E.; Martino, M. *Appl. Phys. A* **1993**, *56*, 429–436.

Mechanism of the Reaction of WF_6 and Si; Groenen, P. A. C.; Holscher, J. G. A.; Brongersma, H. H. *Appl. Surf. Sci.* **1994**, *78*, 123–132.

Ultra High Vacuum CVD of W and WSi_2, Films by Si Reduction of WF_6; Jansson, U. *Appl. Surf. Sci.* **1993**, *73*, 51–57.

Structural and Material Properties of Tungsten Silicide Formed at Low Temperature; Singh, A.; Khokle, W. S.; Lal, K. *Vacuum* **1994**, *45*, 867–869.

Chemically Vapor Deposited Tungsten Silicide Films Using Dichlorosilane in a Single Wafer Reactor—Growth, Properties, and Thermal Stability; Telford, S. G.; Eizenberg, M.; Chang, M.; Sinha, A. K.; Gow, T. R. *J. Electrochem. Soc.* **1993**, *140*, 3689–3701.

Metallization of W/Co-Ti/Si and Simultaneous Formation of Diffusion Barrier and Shallow $CoSi_2$ Contact in Normal Flowing Nitrogen Furnace; Yang, F. M.; Peng, J. G.; Huang, T. S.; Huang, S. L.; Chen, M. C. *J. Vac. Sci. Technol. B* **1993**, *11*, 1798–1806.

Group 8

Fe

Geometric and Electronic Structure of Epitaxial Iron Silicides; Alvarez, J.; Deparga, A. L. V.; Hinarejos, J. J.; Delafiguera, J.; Michel, E. G.; et al. *J. Vac. Sci. Technol. A* **1993**, *11*, 929–933.

Initial Stages of the Growth of Fe on Si(111)7×7; Alvarez, J.; Deparga, A. L. V.; Hinarejos, J. J.; Delafiguera, J.; Michel, E. G.; et al. *Phys. Rev. B* **1993**, *47*, 16048–16051.

High Resolution Electron Microscopy Study of α-$FeSi_2$ Heteroepitaxy on Si(111); Berbezier, I.; Chevrier, J.; Derrien, J. *Surf. Sci.* **1994**, *315*, 27–39.

Effects of the Presence of Native Silicon Oxide at the Fe/Si Interface on the Formation of Silicides Studied by Auger Spectroscopy; Chemelli, C.; Dangelo, D.; Girardi, G.; Pizzini, S. *Appl. Surf. Sci.* **1993**, *68*, 173–177.

Reaction of Iron on Silicon; Crecelius, G. *Appl. Surf. Sci.* **1993**, *65/66*, 683–689.

Reaction of Iron and Silicon during Ion Implantation; Crecelius, G.; Radermacher, K.; Dieker, C. *J. Appl. Phys.* **1993**, *73*, 4848–4851.

Surface Structure of β-$FeSi_2$(101) Epitaxially Grown on Si(111); Deparga, A. L. V.; Delafiguera, J.; Prieto, J. E.; Ocal, C.; Miranda, R. *Appl. Phys. A* **1993**, *57*, 477–482.

Dopant Redistribution during the Formation of Iron Silicides; Erlesand, U.; Ostling, M. *Appl. Surf. Sci.* **1993**, *73*, 186–196.

Magnetic Surface Anisotropy at the Iron Silicon Interface; Frait, Z.; Fraitova, D.; Dufour, C.; Mangin, P.; Marchal, G. *IEEE Trans. Magn.* **1994**, *30*, 711–713.

X-Ray Scattering Studies of $FeSi_2$ Films Epitaxially Grown on Si(111); Gay, J. M.; Stocker, P.; Rethore, F. *J. Appl. Phys.* **1993**, *73*, 8169–8178.

Formation of Epitaxial γ-$FeSi_2$ and β-$FeSi_2$ Layers on (111) Si; Grimaldi, M. G.; Franzo, G.; Ravesi, S.; Terrasi, A.; Spinella, C.; Lamantia, A. *Appl. Surf. Sci.* **1994**, *74*, 19–26.

Formation of Epitaxial β-$FeSi_2$ Films on Si(001) as Studied by Medium Energy Ion Scattering; Konuma, K.; Vrijmoeth, J.; Zagwijn, P. M.; Frenken, J. W. M.; Vlieg, E.; Vanderveen, J. F. *J. Appl. Phys.* **1993**, *73*, 1104–1109.

Formation of Ironsilicide on Si(001); Konuma, K.; Vrijmoeth, J.; Zagwijn, P. M.; Vlieg, E.; Vanderveen, J. F. *Appl. Surf. Sci.* **1993**, *70/71*, 564–568.

Surface Electron Diffraction Patterns of β-$FeSi_2$ Films Epitaxially Grown on Silicon; Mahan, J. E.; Lethanh, V.; Chevrier, J.; Berbezier, I.; Derrien, J.; Long, R. G. *J. Appl. Phys.* **1993**, *74*, 1747–1761.

Allotaxial Growth of Epitaxial Si/$FeSi_2$/Si Heterostructures; Muller, O.; Mantl, S.; Radermacher, K.; Bay, H. L.; Crecelius, G.; et al. *Appl. Surf. Sci.* **1993**, *73*, 141–145.

Electronic Structure of γ-$FeSi_2$—Angle Resolved Valence Band Photoemission and Si2p Photoemission; Obrien, W. L.; Tonner, B. P. *Surf. Sci.* **1994**, *312*, 233–238.

β-$FeSi_2$ in (111)Si and in (001)Si Formed by Ion Beam Synthesis; Oostra, D. J.; Bullelieuwma, C. W. T.; Vandenhoudt, D. E. W.; Felten, F.; Jans, J. C. *J. Appl. Phys.* **1993**, *74*, 4347–4353.

Coevaporated Thin Films of Semiconducting β-$FeSi_2$; Powalla, M.; Herz, K. *Appl. Surf. Sci.* **1993**, *65/66*, 482–488.

Surface Morphology and Epitaxy of β-$FeSi_2$ Obtained by Ion Beam Assisted Growth; Ravesi, S.; Terrasi, A.; Lamantia, A. *Nucl. Instrum. Methods Phys. Res. Sect. B* **1993**, *80/81*, 1371–1375.

Epitaxial β-$FeSi_2$, Formed by Fe Deposition on Hot Si(001); Reader, A. H.; Duchateau, J. P. W. B.; Timmers, J.; Hakkens, F. J. G. *Appl. Surf. Sci.* **1993**, *73*, 131–134.

Electron Energy Loss Spectroscopy on $FeSi_2$/Si(111) Heterostructures Grown by Gas Source Molecular Beam Epitaxy; Rosen, B.; Schafer, H. C.; Dieker, C.; Luth, H.; Rizzi, A.; Gerthsen, D. *J. Vac. Sci. Technol. B* **1993**, *11*, 1407–1412.

Structural Approach of the Fe-Si(111) Annealed Interface; Sauvagesimkin, M.; Jedrecy, N.; Waldhauer, A.; Pinchaux, R. *Physica B* **1994**, *198*, 48–54.

Gas Source Molecular Beam Epitaxy of $FeSi_2$/Si-(111) Heterostructures; Schafer, H. C.; Rosen, B.; Moritz, H.; Rizzi, A.; Lengeler, B.; et al. *Appl. Phys. Lett.* **1993**, *62*, 2271–2273.

Ion Beam Assisted Growth of β-$FeSi_2$; Terrasi, A.; Ravesi, S.; Grimaldi, M. G.; Spinella, C. *J. Vac. Sci. Technol. A* **1994**, *12*, 289–294.

Morphological and Structural Studies of β-$FeSi_2$ Films Grown by Ion Beam Assisted Deposition; Terrasi, A.; Ravesi, S.; Spinella, C.; Grimaldi, M. G.; Lamantia, A. *Thin Solid Films* **1994**, *241*, 188–191.

Epitaxial Phase Transitions in the Iron Silicon System; Vonkanel, H.; Onda, N.; Sirringhaus, H.; Mullergubler, E.; Goncalvesconto, S.; Schwarz, C. *Appl. Surf. Sci.* **1993**, *70/71*, 559–563.

Study of the Epitaxy of β-$FeSi_2$ by Codeposition of Fe and Si on Si(111); Wallart, X.; Nys, J. P.; Dehaese, O.; Vincent, G. *Appl. Surf. Sci.* **1993**, *70/71*, 598–602.

Group 9

Co

Growth of Cobalt Overlayers Onto Si(100); Benitez, G.; Carelli, J. L.; Heras, J. M.; Viscido, L. *Surf. Interface Anal.* **1994**, *22*, 214–217.

Scanning Tunneling Microscopy Studies of Nucleation and Growth in a Reactive, Epitaxial System—Co/Si(111); Bennett, P. A.; Parikh, S. A.; Cahill, D. G. *J. Vac. Sci. Technol. A* **1993**, *11*, 1680–1685.

Atomic Structure of Cobalt Silicide Islands Formed by Reactive Epitaxy; Bennett, P. A.; Parikh, S. A.; Lee, M. Y.; Cahill, D. G. *Surf. Sci.* **1994**, *312*, 377–386.

CO Chemisorption on Small Cobalt Particles Deposited on Si(111); Bogdanyi, G.; Zsoldos, Z.; Peto, G.; Guczi, L. *Surf. Sci.* **1994**, *306*, 563–568.

Investigation of the Defect Structure of Thin Single Crystalline $CoSi_2$ (B) Films on Si(111) by Transmission Electron Microscopy; Bullelieuwma, C. W. T.; Vandenhoudt, D. E. W.; Henz, J.; Onda, N.; Vonkanel, H. *J. Appl. Phys.* **1993**, *73*, 3220–3236.

Frustrated Dimers at the $CoSi_2$/Si(001) Interface; Copel, M.; Falta, J. *Phys. Rev. B* **1993**, *48*, 2783–2786.

Direct Observation of 1/2[110] Dislocations Occurring at Steps in Thin Film Type-B $CoSi_2$//Si(111) Interfaces; Daykin, A. C.; Kiely, C. J. *Philos. Mag. A* **1993**, *68*, 1345–1358.

Imaging Misfit Dislocations in Epitaxial $CoSi_2$ Si-(111) Layers Using Quantum Size Microscopy; Kubby, J. A.; Greene, W. J. *Surf. Sci.* **1994**, *311*, 695–702.

Formation and Characterization of Epitaxial $CoSi_2$, on Si(001); Lavia, F.; Spinella, C.; Reader, A. H.; Duchateau, J. P. W. B.; Hakvoort, R. A.; Vanveen, A. *Appl. Surf. Sci.* **1993**, *73*, 108–116.

Scanning Tunneling Microscopy Investigation of the Quantum Size Effect in Epitaxial $CoSi_2$/Si(111); Lee, E. Y.; Sirringhaus, H.; Vonkanel, H. *Phys. Rev. B* **1994**, *50*, 5807–5809.

Growth of Epitaxial $CoSi_2$ Film on Si(100) Substrate—Induced by an Interfacial Ti Layer; Liu, P.; Li, B. Z.; Zhou, Z. Y.; Lin, C. L.; Zou, S. C. *Mater. Lett.* **1993**, *17*, 383–387.

Very Thin $CoSi_2$ Films by Co Sputtering; Maszara, W. P. *Appl. Phys. Lett.* **1993**, *62*, 961–963.

Microstructural Studies of Epitaxial $CoSi_2$ Layers on Silicon Produced by Ion Beam Synthesis and Rapid Thermal Annealing; Meekison, C. D.; Booker, G. R.; Reeson, K. J.; Spraggs, R. S.; Gwilliam, R. M.; Sealy, B. J. *J. Appl. Phys.* **1993**, *74*, 7129–7133.

Initial Stages of Epitaxial $CoSi_2$ Formation on Si-(100) Surfaces; Rangelov, G.; Augustin, P.; Stober, J.; Fauster, T. *Phys. Rev. B* **1994**, *49*, 7535–7542.

In-Situ Study of Epitaxial $CoSi_2$/Si(111) by Ballistic Electron Emission Microscopy; Sirringhaus, H.; Lee, E. Y.; Vonkanel, H. *J. Vac. Sci. Technol. B* **1994**, *12*, 2629–2633.

Threading Dislocations in GaAs on Si Grown with ~1 nm Thick Si Interlayers; Tamura, M.; Saitoh, T.; Palmer, J. E.; Yodo, T. *Appl. Phys. A* **1994**, *58*, 145–155.

Electronic Structure and Stability of Ring Clusters in the Si(111)-($\sqrt{7}\times\sqrt{7}$)Co Surface; Tsai, M. H.; Dow, J. D.; Bennett, P. A.; Cahill, D. G. *Phys. Rev. B* **1993**, *48*, 2486–2492.

Formation of Epitaxial $CoSi_2$ on Si(100)—Role of the Annealing Ambient; Vantomme, A.; Nicolet, M. A.; Bai, G.; Fraser, D. B. *Appl. Phys. Lett.* **1993**, *62*, 243–245.

Growth of Epitaxial $CoSi_2$, on Si(100) Using Si-(100)/Ti/Co Bilayers; Vantomme, A.; Nicolet, M. A.; Bai, G.; Fraser, D. B. *Appl. Surf. Sci.* **1993**, *73*, 117–123.

Epitaxial $CoSi_2$ Films on Si(100) by Solid Phase Reaction; Vantomme, A.; Nicolet, M. A.; Theodore, N. D. *J. Appl. Phys.* **1994**, *75*, 3882–3891.

Study of Co Silicide Formation by Multiple Implantation; Witzmann, A.; Schippel, S.; Zentgraf, A.; Gajduk, P. I. *J. Appl. Phys.* **1993**, *73*, 7250–7260.

Metallization of W/Co-Ti/Si and Simultaneous Formation of Diffusion Barrier and Shallow $CoSi_2$ Contact in Normal Flowing Nitrogen Furnace; Yang, F. M.; Peng, J. G.; Huang, T. S.; Huang, S. L.; Chen, M. C. *J. Vac. Sci. Technol. B* **1993**, *11*, 1798–1806.

Ir

Epitaxial Iridium Silicide Formation during Deposition of Ir on Si(100) at High Temperature Under Ultrahigh Vacuum; Chung, C. K.; Hwang, J. *J. Appl. Phys.* **1994**, *76*, 1937–1939.

Growth and Structure of $IrSi_3$ on Si(111); Lange, D. A.; Gibson, G. A.; Falco, C. M. *J. Appl. Phys.* **1994**, *75*, 2917–2923.

Group 10

Ni

Epitaxial Surface of $NiSi_2$ (001) Studied with Low Energy Electron Diffraction and Scanning Tunneling Microscopy; Becker, R. S.; Becker, A. J.; Sullivan, J.; Tung, R. T. *J. Vac. Sci. Technol. B* **1993**, *11*, 752–755.

Characterization of Ni on Si Wafers—Comparison of Surface Analysis Techniques; Calaway, W. F.; Coon, S. R.; Pellin, M. J.; Gruen, D. M.; Gordon, M.; et al. *Surf. Interface Anal.* **1994**, *21*, 131–137.

Formation of Ultrathin $NiSi_2$ Films and Heteroepitaxial Growth of Epi-$NiSi_2$/Si(111); Choi, C. K.; Boo,

S. E.; Koh, J. D.; Hong, S. R.; Lee, J. Y.; et al. *J. Korean Phys. Soc.* **1994**, *27*, 528–534.

Silicide Growth and Oxygen Effects in Annealed Si Thin Film Ni Single Crystal Structures; John, P. K.; Froelich, H. R.; Rastogi, A. C. *J. Electrochem. Soc.* **1993**, *140*, 2937–2943.

Insitu 2nd Harmonic Generation Measurements during the Electrodeposition of Ni on n-Si(111); Kruger, J.; Sorg, N.; Reif, J.; Kautek, W. *Appl. Surf. Sci.* **1993**, *69*, 388–392.

Imaging Defect Formation in the Template Growth of $NiSi_2$/Si(111)—An Application of Quantum Size Microscopy; Kubby, J. A.; Wang, Y. R.; Greene, W. J. *Phys. Rev. B* **1993**, *48*, 4473–4480.

Structures of Clean and Nickel Containing High Miller Index Surfaces of Silicon; Olshanetsky, B. Z.; Solovyov, A. E.; Dolbak, A. E.; Maslov, A. A. *Surf. Sci.* **1994**, *306*, 327–341.

XPS and XAES Study of Interaction Between Ni and Si(111), SiO_x/Si(111) Supports; Sarapatka, T. J. *J. Electron Spectrosc. Relat. Phenom.* **1993**, *62*, 335–349.

Computer Simulation of $SiMO_x$ and $SiMN_i$ Formed by Low Energy Ion Implantation; Shi, Z. Y.; Lin, C. L.; Zhu, W. H.; Hemment, P. L. F.; Bussmann, U.; Zou, S. C. *Nucl. Instrum. Methods Phys. Res. Sect. B* **1993**, *74*, 210–212.

Clean and Ni-Adsorbed Si(110) Surfaces; Shimaoka, G. *Appl. Surf. Sci.* **1993**, *65/66*, 569–574.

SHG Measurements of N-Si(111) Aqueous Solution Interfaces; Sorg, N.; Kruger, J.; Kautek, W.; Reif, J. *Ber. Bunsen-Ges. Phys. Chem.* **1993**, *97*, 402–406.

Single Crystal Si/$NiSi_2$/Si(100) Structures; Tung, R. T.; Eaglesham, D. J.; Schrey, F.; Sullivan, J. P. *J. Appl. Phys.* **1993**, *73*, 8250–8257.

Structure Determination of the $NiSi_2$(111) Surface with Medium Energy Ion Backscattering from Individual Monolayers; Vrijmoeth, J.; Zagwijn, P. M.; Vlieg, E.; Frenken, J. W. M.; Alkemade, P. F. A. *Surf. Sci.* **1993**, *290*, 255–266.

Ion Beam Synthesis of Buried and Surface Nickel Silicides during a Single Implantation Step; Wu, M. F.; Dewachter, J.; Pattyn, H.; Vanbavel, A. M.; Langouche, G.; et al. *Appl. Surf. Sci.* **1993**, *73*, 246–252.

RBS, RHEED and THEED Studies of $SiMO_x$ and $SiMN_i$ Structures Formed by Ion Beam Synthesis; Yankov, R. A.; Komarov, F. F.; Petrov, S. A. *Vacuum* **1993**, *44*, 1077–1084.

Interfacial Reactions and Silicide Formation in Si/Ni/Si and Si/Cr/Si Sandwich Layers; Zalar, A.; Hofmann, S.; Pimentel, F.; Panjan, P. *Surf. Interface Anal.* **1994**, *21*, 560–565.

Medium Energy Ion Scattering Study of Ni on Ultrathin Films of SiO_2 on Si(111); Zhou, J. B.; Gustafsson, T.; Lin, R. F.; Garfunkel, E. *Surf. Sci.* **1993**, *284*, 67–76.

Enhanced Surface-Interface Recombination and Surface Inversion of Ni Decorated Si/Si(Ge)/Si Heterostructures; Zhou, T. Q.; Buczkowski, A.; Radzimski, Z. J.; Rozgonyi, G. A. *J. Appl. Phys.* **1993**, *73*, 8412–8418.

Pd

Insitu Strain Measurements during the Formation of Palladium Silicide Films; Buaud, P. P.; Dheurle, F. M.; Chevacharoenkul, S.; Irene, E. A. *J. Vac. Sci. Technol. B* **1993**, *11*, 304–310.

Evidence for Pd Bonding with Si Intermediate Oxidation States; Faraci, G.; Larosa, S.; Pennisi, A. R.; Hwu, Y.; Lozzi, L.; Margaritondo, G. *J. Appl. Phys.* **1993**, *73*, 749–754.

Nucleation and Surface Reconstruction of Pd on Si(100) Observed by Scanning Tunneling Microscopy; Itoh, H.; Narui, S.; Tanabe, H.; Ichinokawa, T. *Surf. Sci.* **1993**, *284*, 236–246.

Study of the Pd/Si(100)2×1 System Using Soft X-Rays; Kawamoto, S.; Saitoh, K.; Hirai, M.; Kusaka, M.; Iwami, M. *Surf. Sci.* **1993**, *287*, 151–154.

AES and LEED Studies of Surface Stoichiometry of Palladium Silicide Epilayers on Si(111); Kuznetsov, A. A.; Abramova, S. Y.; Potapova, T. E.; Protopopov, O. D. *J. Electron Spectrosc. Relat. Phenom.* **1994**, *68*, 407–412.

Pt

Scanning Tunneling Microscope and Atomic Force Microscope Observation of Topography of Molecular Beam Epitaxy Grown Pt Films on Cu Buffer Layer and Si(111)-(7×7) Substrate; Nishikawa, K.; Yamamoto, M.; Kurumizawa, T.; Kingetsu, T. *Jpn. J. Appl. Phys.* **1993**, *32*, 2940–2944.

Group 11

Interaction of Copper Catalysts and Si(100) for the Direct Synthesis of Methylchlorosilanes; Floquet, N.; Yilmaz, S.; Falconer, J. L. *J. Catal.* **1994**, *148*, 348–368.

Investigation of the Si(100)2×1/Cu Interface by UPS and Surface Reflectance Spectroscopy; Guillet, S.; Regalado, L. E.; Lopezrios, T.; Cinti, R. *Appl. Surf. Sci.* **1993**, *65/66*, 742–745.

Thermal Behavior of Cu Films on the Si(111) Surface in the Monolayer Regime; Ishigami, R.; Yuhara, J.; Morita, K. *Surf. Sci.* **1994**, *315*, 302–308.

Scanning Tunneling Microscope and Atomic Force Microscope Observation of Topography of Molecular Beam Epitaxy Grown Pt Films on Cu Buffer Layer and Si(111)-(7×7) Substrate; Nishikawa, K.; Yamamoto, M.; Kurumizawa, T.; Kingetsu, T. *Jpn. J. Appl. Phys.* **1993**, *32*, 2940–2944.

On the Surface Segregation of Silicon in Cu_3Si; Samson, Y.; Rousset, J. L.; Bergeret, G.; Tardy, B.; Bertolini, J. G.; Laroze, G. *Appl. Surf. Sci.* **1993**, *72*, 373–379.

Topography and Crystallography of a Pt Film on a Cu Buffer Layer and a Si(111)(7×7) Substrate; Yamamoto, M.; Nishikawa, K.; Kingetsu, T.; Kurumizawa, T.; Kusao, K. *Appl. Surf. Sci.* **1993**, *67*, 275–280.

Ballistic Electron Emission Microscopy Study of the Au/Si(111)7×7 and Au/CaF_2/Si(111)7×7 Interfaces; Cuberes, M. T.; Bauer, A.; Wen, H. J.; Prietsch, M.; Kaindl, G. *Appl. Phys. Lett.* **1994**, *64*, 2300–2302.

X-Ray Photoelectron Diffraction and Spectroscopy of Sputter Deposited or Evaporated Coinage Metals on Si(100); Lamontagne, B.; Sacher, E.; Wertheimer, M. R. *Appl. Surf. Sci.* **1993**, *64*, 205–213.

Silver Induced Formation of Si(111)-$\sqrt{3}\times\sqrt{3}$ Structure from Hydrogenated Amorphous Silicon Film;

Ashtikar, M. S.; Sharma, G. L. *Solid State Commun.* **1994**, *91*, 831–834.

Sudden Beginning of Metallic Behavior at Ag/Si-(100) Interface—A Real-Time Photoreflectance Spectroscopy Investigation; Borensztein, Y.; Alameh, R.; Roy, M. *Phys. Rev. B* **1993**, *48*, 14737–14740.

Observations of the Au/Si(111) System with a High Resolution Ultrahigh Vacuum Scanning Electron Microscope; Endo, A.; Ino, S. *Jpn. J. Appl. Phys.* **1993**, *32*, 4718–4725.

Observation of the Ag/Si(111) System Using a High Resolution Ultra High Vacuum Scanning Electron Microscope; Endo, A.; Ino, S. *Surf. Sci.* **1993**, *293*, 165–182.

Interfacial Reaction in A-Si/Au and A-Si/Cu Thin Film Bilayers; Heald, S. M.; Tan, Z. Q. *Jpn. J. Appl. Phys.* **1993**, *32*, 386–390.

Ultralarge Atomically Flat Template-Stripped Au Surfaces for Scanning Probe Microscopy; Hegner, M.; Wagner, P.; Semenza, G. *Surf. Sci.* **1993**, *291*, 39–46.

A Scanned Angle and Scanned Energy Photoelectron Diffraction Study of $(\sqrt{3}\times\sqrt{3})$R30° Ag on Si(111); Herman, G. S.; Bullock, E. L.; Yamada, M.; Kaduwela, A. P.; Friedman, D. J.; et al. *Surf. Sci.* **1993**, *284*, 23–52.

High Resolution Photoelectron Spectroscopy Study of $(\sqrt{3}\times\sqrt{3})$R30°-Ag on Si(111); Herman, G. S.; Woicik, J. C.; Andrews, A. B.; Erskine, J. L. *Surf. Sci.* **1993**, *290*, 643–648.

Surface Reactivity of Alkylgold(I) Complexes—Substrate Selective Chemical Vapor Deposition of Gold from $RAuP(CH_3)_3$ (R = CH_2CH_3, CH_3) at Remarkably Low Temperatures; Holl, M. M. B.; Seidler, P. F.; Kowalczyk, S. P.; McFeely, F. R. *Inorg. Chem.* **1994**, *33*, 510–517.

Atomic Structure of the Si(111)$(\sqrt{3}\times\sqrt{3})$R30°-Ag Surface; Jia, J. F.; Zhao, R. G.; Yang, W. S. *Phys. Rev. B* **1993**, *48*, 18109–18113.

A Study on the Si(111)-$\sqrt{3}\times\sqrt{3}$-Ag System. 1. Role of the Substrate; Kirchner, E. J. J.; Baerends, E. J.; Vlieg, E. *Surf. Sci.* **1994**, *304*, 12–23.

Cu Precipitation in Oxidized Wafers with and Without a Ge_xSi_{1-x} Heteroepitaxial Layer; Kissinger, G.; Morgenstern, G.; Richter, H. *J. Mater. Res.* **1993**, *8*, 1900–1907.

Intrinsic Stress and Growth of Ag on P-Doped Si-(001)(2×1)—Influence of Dopant Concentration; Koch, R.; Winau, D.; Thurmer, K.; Weber, M.; Rieder, K. H. *Europhys. Lett.* **1993**, *21*, 213–219.

X-Ray Diffraction Study of Si(111)$\sqrt{3}\times\sqrt{3}$-Au; Kuwahara, Y.; Nakatani, S.; Takahasi, M.; Aono, M.; Takahashi, T. *Surf. Sci.* **1994**, *310*, 226–230.

X-Ray Photoelectron Diffraction and Spectroscopy of Sputter Deposited or Evaporated Coinage Metals on Si(100); Lamontagne, B.; Sacher, E.; Wertheimer, M. R. *Appl. Surf. Sci.* **1993**, *64*, 205–213.

Ag on Si(001)—Growth Behavior of the Annealed Surface; Lin, X. F.; Wan, K. J.; Nogami, J. *Phys. Rev. B* **1993**, *47*, 10947–10950.

Ag on the Si(001) Surface—Growth of the 1st Monolayer at Room Temperature; Lin, X. F.; Wan, K. J.; Nogami, J. *Phys. Rev. B* **1993**, *47*, 13491–13497.

Low Temperature Structure and Phase Transitions at the Au/Si (100) Interface; Ma, Z.; Allen, L. H. *Phys. Rev. B* **1993**, *48*, 15484–15487.

Scanning Tunneling Microscopy Investigation of the Nucleation and Growth of Ag/Si(111)-$(\sqrt{3}\times\sqrt{3})$; McComb, D. W.; Moffatt, D. J.; Hackett, P. A.; Williams, B. R.; Mason, B. F. *Phys. Rev. B* **1994**, *49*, 17139–17148.

Direct Observation of the Growth Process of Ag Thin Film on a Hydrogen Terminated Si(111) Surface; Naitoh, M.; Shoji, F.; Oura, K. *Jpn. J. Appl. Phys.* **1992**, *31*, 4018–4019.

$\sqrt{3}\times\sqrt{3}$ Reconstructions of Si(111) and Ge(111) Induced by Ag and Au; Nogami, J.; Wan, K.; Glueckstein, J. C. *Jpn. J. Appl. Phys.* **1994**, *33*, 3679–3682.

Au Adatom Superstructure on the Ag Si(111)-$\sqrt{3}\times\sqrt{3}$-R30° Surface; Nogami, J.; Wan, K. J.; Lin, X. F. *Surf. Sci.* **1994**, *306*, 81–86.

Scanning Tunneling Microscope Observation of Si-(111)-3×1-Ag Structure; Ohnishi, H.; Katayama, I.; Ohba, Y.; Oura, K. J. *Jpn. J. Appl. Phys.* **1994**, *33*, 3683–3687.

Growth Processes of Si(111)-$\sqrt{3}\times\sqrt{3}$-Ag Studied by Scanning Tunneling Microscope; Ohnishi, H.; Katayama, I.; Ohba, Y.; Shoji, F.; Oura, K. *Jpn. J. Appl. Phys.* **1993**, *32*, 2920–2922.

Hydrogen Induced Ag Cluster Formation on the Si-(111) $\sqrt{3}\times\sqrt{3}$ R30°-Ag Surface Observed by Scanning Tunneling Microscopy; Ohnishi, H.; Yamamoto, Y.; Katayama, I.; Ohba, Y.; Oura, K. *Jpn. J. Appl. Phys.* **1994**, *33*, 1106–1109.

Nucleation and Evolution of the Au-Induced 5×2 Structure on Vicinal Si(111); Omahony, J. D.; McGilp, J. F.; Flipse, C. F. J.; Weightman, P.; Leibsle, F. M. *Phys. Rev. B* **1994**, *49*, 2527–2535.

Low Energy Electron Diffraction as a Direct Identification Technique—Atomic Structures of Ag-Induced and Li-Induced Si(111)-$(\sqrt{3}\times\sqrt{3})$R30°; Over, H.; Huang, H.; Tong, S. Y.; Fan, W. C.; Ignatiev, A. *Phys. Rev. B* **1993**, *48*, 15353–15357.

Photoemission Study of Ag on Hydrogenated Amorphous Silicon; Pi, T. W. *Jpn. J. Appl. Phys.* **1993**, *32*, 2818–2823.

Low Temperature, Flux Independent Epitaxy in Ag/Si(111); Roos, K. R.; Tringides, M. C. *Surf. Sci.* **1994**, *302*, 37–48.

1→(1-1) $AgM_{4,5}$ XAS Investigation at the Ag/Si-(111)2×1 Interface; Sancrotti, M.; Duo, L.; Cosso, R.; Daddato, S.; Gregory, D. A.; et al. *Appl. Surf. Sci.* **1993**, *70/71*, 456–460.

Dynamic Observation of Ag Desorption Process on Si(111) Surface by High Temperature Scanning Tunneling Microscopy; Sato, T.; Sueyoshi, T.; Kitamura, S.; Iwatsuki, M. *Jpn. J. Appl. Phys.* **1993**, *32*, 2923–2928.

Restructuring of the Reconstructed Si(111)7×7 Surface by Metal (Au, Ag) Deposition; Shibata, A.; Takayanagi, K. *Jpn. J. Appl. Phys.* **1993**, *32*, 1385–1388.

Wetting of Silicon Single Crystal by Silver and Tin, and Their Interfaces; Sugihara, S.; Okazaki, K.; Suganuma, K. *J. Mater. Sci.* **1993**, *28*, 2455–2458.

Concentration Profiles of Deep Levels Induced by Gold Diffusion in Silicon; Takahashi, M.; Morooka,

M.; Ueda, F.; Hashimoto, F. *Jpn. J. Appl. Phys.* **1994**, *33*, 1713–1716.

Refinement of the Si(111)$\sqrt{3}\times\sqrt{3}$-Ag Structure by Surface X-Ray Diffraction; Takahashi, T.; Nakatani, S. *Surf. Sci.* **1993**, *282*, 17–32.

Structural Correlation Among Different Phases in the Initial Stage of Epitaxial Growth of Au on Si(111); Takami, T.; Fukushi, D. J.; Nakayama, T.; Uda, M.; Aono, M. *Jpn. J. Appl. Phys.* **1994**, *33*, 3688–3695.

Photoemission Study of Au, Ge, and O_2 Deposition on NH_4F Etched Si(111); Terry, J.; Cao, R.; Wigren, C.; Pianetta, P. *J. Vac. Sci. Technol. A* **1994**, *12*, 1869–1875.

Low Energy Electron Microscopy Studies of Ge and Ag Growth on Si(111); Vandergon, A. W. D.; Tromp, R. M.; Reuter, M. C. *Thin Solid Films* **1993**, *236*, 140–145.

Surface Reconstructions in the Ag/Si(111) System; Wan, K. J.; Lin, X. F.; Nogami, J. *Phys. Rev. B* **1993**, *47*, 13700–13712.

Theoretical Calculations of STM Images of the Si(111)$\sqrt{3}\times\sqrt{3}$-Ag and Si(111)$\sqrt{3}\times\sqrt{3}$-Sb Surfaces; Watanabe, S.; Aono, M.; Tsukada, M. *Surf. Sci.* **1993**, *287*, 1036–1040.

Ag on Si(001)(2×1): Formation of a 2×3 Superstructure; Winau, D.; Itoh, H.; Schmid, A. K.; Ichinokawa, T. *J. Vac. Sci. Technol. B* **1994**, *12*, 2082–2085.

Reconstructions and Growth of Ag on Si(001)(2×1); Winau, D.; Itoh, H.; Schmid, A. K.; Ichinokawa, T. *Surf. Sci.* **1994**, *303*, 139–145.

Growth of the Room Temperature Au/Si(111)-(7×7) Interface; Yeh, J. J.; Hwang, J.; Bertness, K.; Friedman, D. J.; Cao, R.; Lindau, I. *Phys. Rev. Lett.* **1993**, *70*, 3768–3771.

Cluster Models Study of Ag Bonding, Migration and Interaction on Si(100)-2×1; Zhou, R. H.; Cao, P. L.; Lee, L. Q. *Surf. Sci.* **1993**, *290*, 649–654.

Group 12

Zn

The Effect of Zn Promoter on Enhanced Diffusion during Catalytic Formation of Methylchlorosilanes; Potochnik, S. J.; Falconer, J. L. *J. Catal.* **1994**, *147*, 101–106.

Group 13

B

Si(001)2×1 Gas Source Molecular Beam Epitaxy from Si_2H_6—Growth Kinetics and Boron Doping; Bramblett, T. R.; Lu, Q.; Hasan, M. A.; Jo, S. K.; Greene, J. E. *J. Appl. Phys.* **1994**, *76*, 1884–1888.

Characterization of the B/Si Surface Electronic Structures; Cao, R.; Yang, X.; Pianetta, P. *J. Vac. Sci. Technol. A* **1993**, *11*, 1817–1822.

Atomic and Electronic Structure of B/Si(100); Cao, R.; Yang, X.; Pianetta, P. *J. Vac. Sci. Technol. B* **1993**, *11*, 1455–1458.

Hydrogenation of Boron in Silicon during Low Temperature Gas and Liquid Phase Processing; Filangeri, E. M.; Nishida, T. *J. Appl. Phys.* **1994**, *76*, 332–335.

Contribution to the Study of the Dynamical Properties of the B-Si(111) $\sqrt{3}\times\sqrt{3}$ Surface—Effect of the Dopant Behavior, from the Infrared to the Visible Energy Range; Fontaine, M.; Layet, J. M. *J. Electron Spectrosc. Relat. Phenom.* **1993**, *64/65*, 201–205.

Characteristics of B-Doped $Si_{1-x}Ge_x$ Growth Rates by Chemical Vapor Deposition Using Si_2H_6, GeH_4, and B_2H_6 Gases; Fujinaga, K.; Karasawa, T. *J. Electrochem. Soc.* **1993**, *140*, 2081–2084.

Dopant Electrical Activity of Si and $Si_{1-x}Ge_x$ Multilayer Structures Doped with Delta-Like Boron Spikes at Different Temperatures; Gaworzewski, P.; Kruger, D.; Kurps, R.; Rucker, H.; Zeindl, H. P. *J. Appl. Phys.* **1994**, *75*, 7869–7875.

Adsorption of Potassium on the Si(111)$\sqrt{3}\times\sqrt{3}$R30°-B-Surface—Observation of an Insulating Surface at Submonolayer Coverage; Grehk, T. M.; Johansson, L. S. O.; Karlsson, U. O.; Flodstrom, A. S. *Phys. Rev. B* **1993**, *47*, 13887–13890.

Influence of Fluorine Preamorphization on the Diffusion and Activation of Low Energy Implanted Boron during Rapid Thermal Annealing; Huang, T. H.; Kinoshita, H.; Kwong, D. L. *Appl. Phys. Lett.* **1994**, *65*, 1829–1831.

Point Defects in n-Type Silicon Implanted with Low Doses of MeV Boron and Silicon Ions; Jagadish, C.; Svensson, B. G.; Hauser, N. *Semicond. Sci. Technol.* **1993**, *8*, 481–487.

Behavior of Boron and Nitrogen in a Surface-Layer of Silicon during Synthesis of Buried Layers by Implantation of N^+ Ions; Kachurin, G. A.; Tyschenko, I. E. *Semiconductor* **1993**, *27*, 658–662.

Defects Produced in Si p+n Diodes by B^+ Implantation at Liquid Nitrogen Temperature or −60 °C; Kase, M.; Kikuchi, Y.; Kimura, M.; Mori, H.; Liebert, R. B. *J. Appl. Phys.* **1994**, *75*, 3358–3364.

Influence of Boron Adsorption Over Si(111) Surface on Si Molecular Beam Epitaxial Growth Studies by Reflection High Energy Electron Diffraction; Kumagai, Y.; Mori, R.; Ishimoto, K.; Hasegawa, F. *Jpn. J. Appl. Phys.* **1994**, *33*, 817–819.

Ion Beam Induced Epitaxy in B-Implanted Silicon Preamorphized with Ge Ions; Kuriyama, K.; Takahashi, H.; Shimoyama, K.; Hayashi, N.; Hasegawa, M.; Kobayashi, N. *Nucl. Instrum. Methods Phys. Res. Sect. B* **1993**, *80/81*, 994–997.

Solid Boron and Antimony Doping of Si and SiGe Grown by Gas Source Molecular Beam Epitaxy; Li, S. H.; Bhattacharya, P. K.; Chung, S. W.; Zhou, J. X.; Gulari, E. *J. Electron. Mater.* **1993**, *22*, 409–412.

Effects of SiH_4, GeH_4, and B_2H_6 on the Nucleation and Deposition of Polycrystalline $Si_{1-x}Ge_x$ Films; Lin, H. C.; Chang, C. Y.; Chen, W. H.; Tsai, W. C.; Chang, T. C.; et al. *J. Electrochem. Soc.* **1994**, *141*, 2559–2563.

Shallow Boron-Doped Layer Formation by Boron Diffusion from Poly-Si Through Thin SiO_2; Miyake, M. *J. Electrochem. Soc.* **1994**, *141*, 1702–1708.

Selective Adsorption of HBO_2 and Sb on a Si Surface Partially Covered with Ultrathin Oxide; Murakami, E.; Kujirai, H.; Kimura, S. *J. Appl. Phys.* **1994**, *76*, 563–568.

Low Temperature Epitaxial Growth of In-Situ B-Doped $Si_{1-x}Ge_x$ Films; Murota, J.; Honma, F.;

Yoshida, T.; Goto, K.; Maeda, T.; et al. *J. Phys. IV* **1993**, *3*, 427–432.

Growth and Characterization of GaSe and GaAs/GaSe on As-Passivated Si(111) Substrates; Palmer, J. E.; Saitoh, T.; Yodo, T.; Tamura, M. *J. Appl. Phys.* **1993**, *74*, 7211–7222.

Picosecond Photoelectron Spectroscopy of Excited States at Si(111) $\sqrt{3}\times\sqrt{3}$R30°-B, Si(111)7×7, Si(100)2×1, and Laser-Annealed Si(111)1×1 Surfaces; Rowe, M. W.; Liu, H. L.; Williams, G. P.; Williams, R. T. *Phys. Rev. B* **1993**, *47*, 2048–2064.

Relation Between Electrical Activation and the B-Induced Strain in Si Determined by Reciprocal Lattice Mapping; Sardela, M. R.; Radamson, H. H.; Ekberg, J. O.; Sundgren, J. E.; Hansson, G. V. *Semicond. Sc. Technol.* **1994**, *9*, 1272–1275.

STM Study of Surface Reconstructions of Si(111)-B; Shen, T. C.; Wang, C.; Lyding, J. W.; Tucker, J. R. *Phys. Rev. B* **1994**, *50*, 7453–7460.

Structural Study of the Si/B($\sqrt{3}\times\sqrt{3}$)R30° Ge_xSi_{1-x}(111) Interface by Spatially Selective Diffraction Anomalous Fine Structure (DAFS); Tweet, D. J.; Akimoto, K.; Hirosawa, I.; Tatsumi, T.; Kimura, H.; et al. *Jpn. J. Appl. Phys.* **1993**, *32*, 203–205.

Al

Angle Resolved Electron Energy Loss Study of Al/Si(111); Akavoor, P.; Glander, G. S.; Kesmodel, L. L.; Burke, K. *Phys. Rev. B* **1993**, *48*, 12063–12071.

Adsorption of Al on Si(100)—A Surface Polymerization Reaction; Brocks, G.; Kelly, P. J.; Car, R. *Phys. Rev. Lett.* **1993**, *70*, 2786–2789.

Aluminum on Si(100)—Growth and Structure of the 1st Layer; Brocks, G.; Kelly, P. J.; Car, R. *J. Vac. Sci. Technol. B* **1994**, *12*, 2705–2708.

Identification of a Moving Phase of Al_2O_3 by Auger Electron Spectroscopy in the Back Aluminized Surface of Si; Chakravarty, B. C.; Arora, N. K.; Singh, S. N.; Das, B. K.; Chakraborty, B. R.; Sen, N. *Appl. Phys. Lett.* **1994**, *64*, 2847–2848.

Electrical Characteristics of Al/SiO_2/n-Si Tunnel Diodes with an Oxide Layer Grown by Rapid Thermal Oxidation; Depas, M.; Vanmeirhaeghe, R. L.; Laflere, W. H.; Cardon, F. *Solid-State Electron.* **1994**, *37*, 433–441.

Laser Direct-Write Al Deposition on Si, GaAs and Diamond from Trialkylamine-Alane Precursors; Foulon, F.; Lehmann, O.; Stuke, M. *Appl. Surf. Sci.* **1993**, *69*, 87–93.

Al-O Interactions in Ion Implanted Crystalline Silicon; Galvagno, G.; Laferla, A.; Spinella, C.; Priolo, F.; Raineri, V.; et al. *J. Appl. Phys.* **1994**, *76*, 2070–2077.

Interaction of Aluminum with Hydrogenated Amorphous Silicon at Low Temperatures; Haque, M. S.; Naseem, H. A.; Brown, W. D. *J. Appl. Phys.* **1994**, *75*, 3928–3935.

Effect of Oxygen Radicals for Epitaxial Growth of Al_2O_3 on Si; Hayama, K.; Ishida, M.; Nakamura, T. *Jpn. J. Appl. Phys.* **1994**, *33*, 496–499.

Interfacial Layers of High Barrier Schottky Diode of Al/n-Type (100)Si Exposed to H_2 Plasma; Iwakuro, H.; Tokonami, M.; Kuroda, T.; Tamaki, S.; Kitatsuji, Y. *Jpn. J. Appl. Phys.* **1993**, *32*, 5487–5495.

Growth and Energetics of Ga and Al Chains on Si(112); Jung, T. M.; Prokes, S. M.; Kaplan, R. *J. Vac. Sci. Technol. A* **1994**, *12*, 1838–1842.

Chemical and Structural Transformations in the Al/Si(111)8×8-N System; Khramtsova, E. A.; Saranin, A. A.; Lifshits, V. G. *Surf. Sci.* **1993**, *295*, 319–324.

Layer-by-Layer Growth of AlAs Buffer Layer for GaAs on Si at Low Temperature by Atomic Layer Epitaxy; Kitahara, K.; Ohtsuka, N.; Ashino, T.; Ozeki, M.; Nakajima, K. *Jpn. J. Appl. Phys.* **1993**, *32*, 236–238.

Reflection High Energy Electron Diffraction of Heteroepitaxy in Chemical Vapor Deposition Reactor—Atomic Layer Epitaxy of GaAs, AlAs and GaP on Si; Kitahara, K.; Ozeki, M.; Nakajima, K. *Jpn. J. Appl. Phys.* **1993**, *32*, 1051–1055.

Al-O Complex Formation in Ion Implanted Czochralski and Floating Zone Si Substrates; Laferla, A.; Torrisi, L.; Galvagno, G.; Rimini, E.; Ciavola, G.; et al. *Appl. Phys. Lett.* **1993**, *62*, 393–395.

High Energy Implants of Aluminum in Czochralski and Floating Zone Grown Silicon Substrates; Laferla, A.; Torrisi, L.; Galvagno, G.; Rimini, E.; Ciavola, G.; et al. *Nucl. Instrum. Methods Phys. Res. Sect. B* **1993**, *74*, 109–112.

Single Crystal Al Growth on Si(111) by Low Temperature Molecular Beam Epitaxy; Miura, Y.; Fujieda, S.; Hirose, K. *Appl. Phys. Lett.* **1993**, *62*, 1751–1753.

Different Fermi Level Pinning Positions Between Epitaxial and Rotational Al/Si Interfaces; Miura, Y.; Fujieda, S.; Hirose, K. *Phys. Rev. B* **1994**, *50*, 4893–4896.

Epitaxial Growth of Aluminum Films on Hydrogen Mediated Si(100) Surface; Sugawara, H.; Ueda, K. *Jpn. J. Appl. Phys.* **1994**, *33*, 837–839.

Improvement of the Interface Between Selectively Deposited Aluminum and Silicon by Annealing; Tani, K.; Nishikawa, S. *Jpn. J. Appl. Phys.* **1994**, *33*, 455–458.

Adsorption and Desorption of $AlCl_3$ on Si(111)7×7 Observed by Scanning Tunneling Microscopy and Atomic Force Microscopy; Uesugi, K.; Takiguchi, T.; Izawa, M.; Yoshimura, M.; Yao, T. *Jpn. J. Appl. Phys.* **1993**, *32*, 6200–6202.

Elastic Strain Gradients and X-Ray Line Broadening Effects as a Function of Temperature in Aluminum Thin Films on Silicon; Venkatraman, R.; Besser, P. R.; Bravman, J. C.; Brennan, S. *J. Mater. Res.* **1994**, *9*, 328–335.

Effects of Hydrogen and Bias on Single Crystal Al Growth on Vicinal Si by DC Magnetron Sputtering; Yokoyama, S.; Ichikawa, H.; Ichikawa, Y.; Koyanagi, M. *Jpn. J. Appl. Phys.* **1994**, *33*, 459–461.

Influence of Sputtering Geometry on Crystallinity of Al(110) Thin Films on Off-Set (100)Si; Yokoyama, S.; Ichikawa, H.; Koyanagi, M. *Jpn. J. Appl. Phys.* **1993**, *32*, 283–286.

LEED-AES Reexamination of the Al/Si(111) γ-Phase; Zotov, A. V.; Khramtsova, E. A.; Ryzhkov, S. V.; Saranin, A. A.; Chub, A. B.; Lifshits, V. G. *Surf. Sci.* **1994**, *316*, 1034–1038.

Ga

Electrical Transport Quantum Effects in the $In_{0.53}Ga_{0.47}As/In_{0.52}Al_{0.48}As$ Heterostructure on Silicon; Georgakilas, A.; Christou, A.; Zekentes, K.; Mercy, J. M.; Konczewicz, L. K.; et al. *J. Appl. Phys.* **1994**, *76*, 1948−1952.

Fluence Dependent Concentration of Low Energy Ga Implanted in Si; Gnaser, H.; Steltmann, J.; Oechsner, H. *Nucl. Instrum. Methods Phys. Res. Sect. B* **1993**, *80/81*, 110−114.

Pb Preadsorption Facilitates Island Formation during Ga Growth on Si(111); Hibino, H.; Shimizu, N.; Sumitomo, K.; Shinoda, Y.; Nishioka, T.; Ogino, T. *J. Vac. Sci. Technol. A* **1994**, *12*, 23−28.

Photochemical Decomposition of Triethylgallium on Si(111) Studied by Means of STM, LEED, AES and Mass Spectroscopy; Inukai, J.; Mizutani, W.; Fukui, K.; Shimizu, H.; Iwasawa, Y. *Jpn. J. Appl. Phys.* **1993**, *32*, 1768−1771.

Ga on Si(112)—Growth and Energetics of Thermal Desorption; Jung, T. M.; Kaplan, R.; Prokes, S. M. *Surf. Sci.* **1993**, *289*, 577−583.

Growth and Energetics of Ga and Al Chains on Si(112); Jung, T. M.; Prokes, S. M.; Kaplan, R. *J. Vac. Sci. Technol. A* **1994**, *12*, 1838−1842.

Microprobe RHEED and SREM Studies of Si MBE on Ga-Adsorbed Si(111) Surface; Nakahara, H.; Ichikawa, M.; Stoyanov, S. *Ultramicroscopy* **1993**, *48*, 417−424.

Lattice Mismatched InGaAs on Silicon Photodetectors Grown by Molecular Beam Epitaxy; Papanicolaou, N. A.; Anderson, G. W.; Iliadis, A. A.; Christou, A. *J. Electron. Mater.* **1993**, *22*, 201−206.

Resolving the Ga Ad-Dimer Location and Orientation on the Si(100) Surface; Qian, Y.; Bedzyk, M. J.; Tang, S.; Freeman, A. J.; Franklin, G. E. *Phys. Rev. Lett.* **1994**, *73*, 1521−1524.

Characterization of Antiphase Domain in GaP on Misoriented (001) Si Substrate Grown by Metalorganic Chemical Vapor Deposition; Soga, T.; Nishikawa, H.; Jimbo, T.; Umeno, M. *Jpn. J. Appl. Phys.* **1993**, *32*, 4912−4915.

Heteroepitaxy of GaSe Layered Semiconductor Compound on Si(111)7×7 Substrate—A van der Waals Epitaxy; Vinh, L. T.; Eddrief, M.; Sebenne, C.; Sacuto, A.; Balkanski, M. *J. Cryst. Growth* **1994**, *135*, 1−10.

Surface Structures of Si(111)/Ga; Zegenhagen, J.; Artacho, E.; Freeland, P. E.; Patel, J. R. *Philos. Mag. B* **1994**, *70*, 731−745.

The Effect of As/Ga Flux Ratio on Si-Doped GaAs Layers Grown by Molecular Beam Epitaxy; Zhang, D. H.; Radhakrishnan, K.; Yoon, S. F. *J. Cryst. Growth* **1994**, *135*, 441−446.

In

Adsorption and Decomposition of Trimethylindium on Si(110); Bu, Y.; Chu, J. C. S.; Shinn, D. W.; Lin, M. C. *Mater. Chem. Phys.* **1993**, *33*, 99−105.

Morphology and Crystalline Perfection of InAs Films on Si(100); Choi, C. H.; Barnett, S. A. *J. Cryst. Growth* **1994**, *137*, 381−387.

The Effect of Temperature and Doping on the Segregation of In during Solid Phase Epitaxial Crystallization of Si; Elliman, R. G.; Fang, Z. W. *J. Appl. Phys.* **1993**, *73*, 3313−3318.

An X-Ray Diffraction Study of the Si(111)($\sqrt{3}\times\sqrt{3}$)-R30° Indium Reconstruction; Finney, M. S.; Norris, C.; Howes, P. B.; Vansilfhout, R. G.; Clark, G. F.; Thornton, J. M. C. *Surf. Sci.* **1993**, *291*, 99−109.

Electrophysical Properties of Surface Phases of In on Si (111); Gasparov, V. A.; Grazhulis, V. A.; Bondarev, V. V.; Bychkova, T. M.; Lifshits, V. G.; Churusov, B. K. *Solid State Commun.* **1993**, *88*, 51−55.

Electrical Transport Quantum Effects in the $In_{0.53}Ga_{0.47}As/In_{0.52}Al_{0.48}As$ Heterostructure on Silicon; Georgakilas, A.; Christou, A.; Zekentes, K.; Mercy, J. M.; Konczewicz, L. K.; et al. *J. Appl. Phys.* **1994**, *76*, 1948−1952.

Indium Adsorption on Silicon Surfaces—A PAC Study; Krausch, G.; Fink, R.; Jacobs, K.; Luckscheiter, B.; Lohmuller, J.; et al. *Surf. Sci.* **1993**, *285*, 81−92.

Reconstruction, Step-Bunching and Faceting of a Vicinal Si(100) Surface Induced by Indium Adsorption; Li, L.; Wei, Y.; Tsong, I. S. T. *Surf. Sci.* **1994**, *304*, 1−11.

Electronic Structure and Morphology of In Oxide-Si(111) Interfaces; Ofner, H.; Kraft, J.; Hofmann, R.; Surnev, S. L.; Netzer, F. P.; et al. *Surf. Sci.* **1994**, *316*, 112−122.

Spectroscopy of Interface States of Indium-Si(111) (4×1) and (1×1)R30° Surfaces; Ofner, H.; Surnev, S. L.; Shapira, Y.; Netzer, F. P. *Surf. Sci.* **1994**, *309*, 315−320.

Lattice Mismatched InGaAs on Silicon Photodetectors Grown by Molecular Beam Epitaxy; Papanicolaou, N. A.; Anderson, G. W.; Iliadis, A. A.; Christou, A. *J. Electron. Mater.* **1993**, *22*, 201−206.

The Structure of the Si(100)-(4×3)In Surface Studied by STM and ICISS; Steele, B. E.; Cornelison, D. M.; Li, L.; Tsong, I. S. T. *Nucl. Instrum. Methods Phys. Res. Sect. B* **1994**, *85*, 414−419.

Observation of Initial Growth of In on Silicon(100) Surface; Zhu, C. X.; Hayashi, T.; Misawa, S. J.; Tsukahara, S. *Jpn. J. Appl. Phys.* **1994**, *33*, 3706−3709.

Group 14

C

Effects of Propane and Methane on Carbonization and Surface Morphology in Heteroepitaxial Growth of β-SiC Films on (100) Si via Chemical Vapor Deposition; Bahavar, B.; Chaudhry, M. I.; McCluskey, R. J. *Appl. Phys. Lett.* **1993**, *63*, 914−916.

Effect of Carbon on Thermal Oxidation of Silicon and Electrical Properties of SiO_2-Si Structures; Beck, R. B.; Brozek, T.; Ruzyllo, J.; Hossain, S. D.; Tressler, R. E. *J. Electron. Mater.* **1993**, *22*, 689−694.

Scanning Tunneling Microscopy Study of the Adsorption of C_{60} Molecules on Si(100)-(2×1) Surfaces; Chen, D.; Gallagher, M. J.; Sarid, D. *J. Vac. Sci. Technol. B* **1994**, *12*, 1947−1951.

Temperature Effects of Adsorption of C_{60} Molecules on Si(111)-(7×7) Surfaces; Chen, D.; Sarid, D. *Phys. Rev. B* **1994**, *49*, 7612−7620.

Conversion of Single Crystal Si(100) to SiC Film by C_2H_2; Chiu, C. C.; Desu, S. B. *J. Mater. Res.* **1993**, *8*, 535–544.

X-Ray Photoelectron Diffraction Observation of β-SiC(001) Obtained by Electron Cyclotron Resonance Plasma Assisted Growth on Si(001); Diani, M.; Bischoff, J. L.; Kubler, L.; Bolmont, D. *Appl. Surf. Sci.* **1993**, *68*, 575–582.

Direct Deposition of Polycrystalline Diamond Films on the Si(100) Mirror Surface by Hot Filament Chemical Vapor Deposition; Gao, C. X.; Zou, G. T.; Jin, Z. S. *Chin. Phys. Lett.* **1994**, *11*, 317–320.

Investigation of Nucleation and Growth Processes of Diamond Films by Atomic Force Microscopy; George, M. A.; Burger, A.; Collins, W. E.; Davidson, J. L.; Barnes, A. V.; Tolk, N. H. *J. Appl. Phys.* **1994**, *76*, 4099–4106.

Binding Energies for Carbon Atoms and Clusters Deposited on the Si(100) Surface; Halicioglu, T. *Thin Solid Films* **1994**, *249*, 78–82.

C_{60} Adsorption on the Si(100)2×1 and Cu(111)1×1 Surfaces; Hashizume, T.; Sakurai, T. *J. Vac. Sci. Technol. B* **1994**, *12*, 1992–1999.

Field Ion Scanning Tunneling Microscopy Study of C_{84} on the Si(100) Surface; Hashizume, T.; Wang, X. D.; Nishina, Y.; Shinohara, H.; Saito, Y.; Sakurai, T. *Jpn. J. Appl. Phys.* **1993**, *32*, 132–134.

Controlled Carbonization of Si(001) Surface Using Hydrocarbon Radicals in Ultrahigh Vacuum; Hatayama, T.; Tarui, Y.; Yoshinobu, T.; Fuyuki, T.; Matsunami, H. *J. Cryst. Growth* **1994**, *136*, 333–337.

Interaction of (1×2) Reconstructed Si(100) and Ag(110)–Cs Surfaces with C_{60} Overlayers; Hong, H.; Aburano, R. D.; Hirschorn, E. S.; Zschack, P.; Chen, H.; Chiang, T. C. *Phys. Rev. B* **1993**, *47*, 6450–6454.

Electron Spin Resonance Study of Diamond-Like Nuclei Produced in an Si Surface Layer by High Dose C Ion Doping; Izumi, T.; Show, Y.; Deguchi, M.; Kitabatake, M.; Hirao, T.; et al. *Thin Solid Films* **1993**, *228*, 285–288.

The Initial Stages of Diamond Growth–An Adsorption Study of Hot Filament Activated Methane and Hydrogen on Si(100); Jackman, R. B.; Chua, L. H.; Foord, J. S. *Surf. Sci.* **1993**, *292*, 47–60.

Classical MD Simulation and Ab-Initio Mixed Basis Band Calculation of C_{60} Adsorbed on Si(100) Surface; Kamiyama, H.; Rafiitabar, H.; Maruyama, Y.; Ohno, K.; Kawazoe, Y. *Sci. Rep. Res. Inst. Tohoku Univ. Ser. A* **1993**, *39*, 7–14.

Electronic Structures of Layered C_{60} and C_{70} on Si(100) Surface; Kawazoe, Y.; Kamiyama, H.; Maruyama, Y.; Ohno, K. *Jpn. J. Appl. Phys.* **1993**, *32*, 1433–1437.

Structure of Layered C_{60} on Si(100) Surface Studied by Abinitio and Classical Molecular Dynamics Simulations; Kawazoe, Y.; Maruyama, Y.; Rafiitabar, H. S.; Ikeda, M.; Kamiyama, H.; Ohno, K. *Mater. Sci. Eng. B* **1993**, *19*, 165–171.

Diamond Nucleation on Unscratched SiO_2 Substrates; Lauten, F. S.; Shigesato, Y.; Sheldon, B. W. *Appl. Phys. Lett.* **1994**, *65*, 210–212.

Reduction of Secondary Defect Density by C-Implant and B-Implant in Ge_xSi_{1-x} Layers Formed by High Dose Ge Implantation in (100) Si; Lombardo, S.; Priolo, F.; Campisano, S. U.; Lagomarsino, S. *Appl. Phys. Lett.* **1993**, *62*, 2335–2337.

Diamond Nucleation by Carbon Fibers on Unscratched Substrate by Hot Filament Chemical Vapor Deposition; Nakamura, Y.; Tamaki, K.; Watanabe, Y.; Hirayama, S. *J. Mater. Res.* **1994**, *9*, 1619–1621.

Nucleation and Growth during the Chemical Vapor Deposition of Diamond on SiO_2 Substrates; Rankin, J.; Boekenhauer, R. E.; Csencsits, R.; Shigesato, Y.; Jacobson, M. W.; Sheldon, B. W. *J. Mater. Res.* **1994**, *9*, 2164–2173.

Fullerene (C_{60}) Adsorption on Si Surfaces; Sakurai, T.; Wang, X. D.; Hashizume, T.; Nishina, Y.; Shinohara, H.; Saito, Y. *Appl. Surf. Sci.* **1993**, *67*, 281–285.

Investigation of Heteroepitaxial Diamond Films by Atomic Force and Scanning Tunneling Microscopy; Schiffmann, K.; Jiang, X. *Appl. Phys. A* **1994**, *59*, 17–22.

Vibrational Modes of C_{60} Fullerene Adsorbed on Si(100)2×1 Surface Studied by High Resolution Electron Energy Loss Spectroscopy; Suto, S.; Kasuya, A.; Ikeno, O.; Horiguchi, N.; Wawro, A.; et al. *Sci. Rep. Res. Inst. Tohoku Univ. Ser. A* **1993**, *39*, 47–50.

Nucleation of Diamond Particles by Hot Filament Chemical Vapor Deposition; Tamaki, K.; Watanabe, Y.; Nakamura, Y.; Hirayama, S. *Thin Solid Films* **1993**, *236*, 115–119.

Kinetic Study of Silicon Carbide Deposited from Methyltrichlorosilane Precursor; Tsai, C. Y.; Desu, S. B.; Chiu, C. C. *J. Mater. Res.* **1994**, *9*, 104–111.

Diamond Epitaxy on a Si(001) Substrate–A Comparison of Structural Models; Verwoerd, W. S. *Surf. Sci.* **1994**, *304*, 24–32.

Kinetic Studies of the Reactions Between Silicon Nitride and Carbon; Wang, H.; Fischman, G. S. *J. Therm. Anal.* **1994**, *41*, 135–146.

Field Ion Scanning Tunneling Microscopy of Metallofullerenes Adsorbed on the Si(100)2×1 Surface; Wang, X. D.; Hashizume, T.; Xue, Q. K.; Shinohara, H.; Saito, Y.; et al. *Jpn. J. Appl. Phys.* **1993**, *32*, 866–868.

Electronic States of Si(001)2×1-C_{60} Surface; Yamaguchi, T. *Jpn. J. Appl. Phys.* **1993**, *32*, 2914–2919.

Electronic States of Fullerenes on Silicon Surfaces; Yamaguchi, T. *Jpn. J. Appl. Phys.* **1994**, *33*, 3667–3672.

Si

Low Temperature Silicon Homoepitaxy by Ultrahigh Vacuum Electron Cyclotron Resonance Chemical Vapor Deposition; Tae, H. S.; Hwang, S. H.; Park, S. J.; Yoon, E.; Whang, K. W. *Appl. Phys. Lett.* **1994**, *64*, 1021–1023.

Ge

Strict Thermal Nitridation Selectivity Between Si and Ge Used as a Chemical Probe of the Outermost Layer of $Si_{1-x}Ge_x$ Alloys and Ge/Si(001) or Si/Ge(001) Heterostructures; Aubel, D.; Diani, M.; Bischoff, J. L.; Bolmont, D.; Kubler, L. *J. Vac. Sci. Technol. B* **1994**, *12*, 2699–2704.

In-Situ Surface Technique Analyses and Ex-Situ Characterization of $Si_{1-x}Ge_x$ Epilayers Grown on Si-

(001)-2×1 by Molecular Beam Epitaxy; Aubel, D.; Diani, M.; Stoehr, M.; Bischoff, J. L.; Kubler, L.; et al. *J. Phys. III* **1994**, *4*, 733–740.

Ballistic Electron Emission Microscopy of Strained $Si_{1-x}Ge_x$ Layers; Bell, L. D.; Milliken, A. M.; Manion, S. J.; Kaiser, W. J.; Fathauer, R. W.; Pike, W. T. *Phys. Rev. B* **1994**, *50*, 8082–8085.

Germanium Segregation Induced Reconstruction of SiGe Layers Deposited on Si(100); Butz, R.; Kampers, S. *Thin Solid Films* **1992**, *222*, 104–107.

Inhomogeneous Pulsed Laser Melting of High Dose Ge-Implanted Silicon; Calcagnile, L.; Grimaldi, M. G.; Baeri, P. *J. Appl. Phys.* **1994**, *76*, 1833–1839.

Ge Chemisorption and Alloying on the Si(111)-(7×7) Surface; Carlisle, J. A.; Miller, T.; Chiang, T. C. *Phys. Rev. B* **1994**, *49*, 13600–13606.

A Study of Oxygen-Implanted $Si_{0.5}Ge_{0.5}$ Alloy by XPS and Thermodynamic Analysis; Castle, J. E.; Liu, H. D.; Saunders, N. *Surf. Interface Anal.* **1993**, *20*, 149–154.

On the Relation Between Low Temperature Epitaxial Growth Conditions and the Surface Morphology of Epitaxial Si and $Si_{1-x}Ge_x$ Layers, Grown in an Ultrahigh Vacuum, Very Low Pressure Chemical Vapor Deposition Reactor; Caymax, M.; Poortmans, J.; Vanammel, A.; Vanhellemont, J.; Libezny, M.; et al. *Thin Solid Films* **1994**, *241*, 335–339.

Atomic Structure of the Ge/Si(100)-(2×1) Surface; Cho, J. H.; Kang, M. H. *Phys. Rev. B* **1994**, *49*, 13670–13673.

Growth Ripples Upon Strained SiGe Epitaxial Layers on Si and Misfit Dislocation Interactions; Cullis, A. G.; Robbins, D. J.; Barnett, S. J.; Pidduck, A. J. *J. Vac. Sci. Technol. A* **1994**, *12*, 1924–1931.

RBS, AES and XPS Analysis of Ion Beam Induced Nitridation of Si and SiGe Alloys; Decoster, W.; Brijs, B.; Bender, H.; Alay, J.; Vandervorst, W. *Vacuum* **1994**, *45*, 389–395.

Ion Beam Mixing and Oxidation of a Si/Ge-Multilayer Under Oxygen Bombardment; Decoster, W.; Brijs, B.; Osiceanu, P.; Alay, J.; Caymax, M.; Vandervorst, W. *Nucl. Instrum. Methods Phys. Res. Sect. B* **1994**, *85*, 911–915.

Defect Induced Intermixing in Thin Si/Ge Superlattices; Dettmer, K.; Kessler, F. R.; Freiman, W.; Beserman, R.; Khait, Y. L. *Appl. Surf. Sci.* **1993**, *65/66*, 501–506.

The Ge Stranski-Krastanov Growth Mode on Si-(001)(2×1) Tested by X-Ray Photoelectron and Auger Electron Diffraction; Diani, M.; Aubel, D.; Bischoff, J. L.; Kubler, L.; Bolmont, D. *Surf. Sci.* **1993**, *291*, 110–116.

X-Ray Photoelectron and Auger Electron Diffraction Probing of Ge Heteroepitaxy on Si (001) 2×1; Diani, M.; Bischoff, J. L.; Kubler, L.; Bolmont, D. *J. Appl. Phys.* **1993**, *73*, 7412–7415.

Thermal Decomposition of Diethylgermane on Si-(100)-(2×1); Du, W.; Keeling, L. A.; Michaelgreenlief, C. *J. Vac. Sci. Technol. A* **1994**, *12*, 2281–2286.

The Role of Hydride Coverage in Surface Limited Thin Film Growth of Epitaxial Silicon and Germanium; Eres, G.; Sharp, J. W. *J. Appl. Phys.* **1993**, *74*, 7241–7250.

2DEG in Strained Si/SiGe Heterostructures; Fang, F. F. *Surf. Sci.* **1994**, *305*, 301–306.

Elastic Stress Relaxation in SiGe Epilayers on Patterned Si Substrates; Fischer, A.; Richter, H. *J. Appl. Phys.* **1994**, *75*, 657–659.

Direct Measurement of the Asymmetric Dimer Buckling of Ge on Si(001); Fontes, E.; Patel, J. R.; Comin, F. *Phys. Rev. Lett.* **1993**, *70*, 2790–2793.

Characteristics of B-Doped $Si_{1-x}Ge_x$ Growth Rates by Chemical Vapor Deposition Using Si_2H_6, GeH_4, and B_2H_6 Gases; Fujinaga, K.; Karasawa, T. *J. Electrochem. Soc.* **1993**, *140*, 2081–2084.

Self-Modulating Sb Incorporation in Si/SiGe Superlattices during Molecular Beam Epitaxial Growth; Fujita, K.; Fukatsu, S.; Usami, N.; Shiraki, Y.; Yaguchi, H.; et al. *Surf. Sci.* **1993**, *295*, 335–339.

Is Low Temperature Growth the Solution to Abrupt $Si/Si_{1-x}Ge_x$ Interface Formation; Fukatsu, S.; Usami, N.; Fujita, K.; Yaguchi, H.; Shiraki, Y.; Ito, R. *J. Cryst. Growth* **1993**, *127*, 401–405.

Dopant Electrical Activity of Si and $Si_{1-x}Ge_x$ Multilayer Structures Doped with Delta-Like Boron Spikes at Different Temperatures; Gaworzewski, P.; Kruger, D.; Kurps, R.; Rucker, H.; Zeindl, H. P. *J. Appl. Phys.* **1994**, *75*, 7869–7875.

Ge Segregation during the Growth of a SiGe Buried Layer by Molecular Beam Epitaxy; Godbey, D. J.; Ancona, M. G. *J. Vac. Sci. Technol. B* **1993**, *11*, 1120–1123.

Concentration Dependence of Ge Segregation during the Growth of a SiGe Buried Layer; Godbey, D. J.; Ancona, M. G. *J. Vac. Sci. Technol. B* **1993**, *11*, 1392–1395.

Asymmetric Sb Dimers on the 1-ML Ge-Terminated Si(100) Surface; Grant, M. W.; Boshart, M. A.; Dieleman, D. J.; Seiberling, L. E. *Surf. Sci.* **1994**, *316*, 1088–1092.

Transmission Ion Channeling Investigation of Ge Adsorbed on the Si(100) Surface at Submonolayer Coverage; Grant, M. W.; Dieleman, D. J.; Boshart, M. A.; Seiberling, L. E. *Phys. Rev. B* **1994**, *49*, 16534–16538.

Growth of Epitaxial Germanium-Silicon Heterostructures by Chemical Vapor Deposition; Greve, D. W. *Mater. Sci. Eng. B* **1993**, *18*, 22–51.

Ge Segregation in SiGe/Si Heterostructures and Its Dependence on Deposition Technique and Growth Atmosphere; Grutzmacher, D. A.; Sedgwick, T. O.; Powell, A.; Tejwani, M.; Iyer, S. S.; et al. *Appl. Phys. Lett.* **1993**, *63*, 2531–2533.

Growth of SiGe/Si Quantum Well Structures by Atmospheric Pressure Chemical Vapor Deposition; Grutzmacher, D. A.; Sedgwick, T. O.; Zaslavsky, A.; Powell, A. R.; Kiehl, R. A.; et al. *J. Electron. Mater.* **1993**, *22*, 303–308.

Polarization Dependence of the Si K-Edge X-Ray Absorption Spectra of Si-Ge Atomic Layer Superlattices; Hitchcock, A. P.; Tyliszczak, T.; Aebi, P.; Feng, X. H.; Lu, Z. H.; et al. *Surf. Sci.* **1994**, *301*, 260–272.

Kinetics of the Low Pressure Chemical Vapor Deposition of Polycrystalline Germanium-Silicon Alloys from SiH_4 and GeH_4; Holleman, J.; Kuiper, A. E. T.; Verweij, J. F. *J. Electrochem. Soc.* **1993**, *140*, 1717–1722.

Formation of Interfacial Dislocation Network in Surfactant Mediated Growth of Ge on Si(111) Investigated by SPA-LEED. 1; Hornvonhoegen, M.; Alfa-

lou, A.; Pietsch, H.; Muller, B. H.; Henzler, M. *Surf. Sci.* **1993**, *298*, 29–42.

The Interplay of Surface Morphology and Strain Relief in Surfactant Mediated Growth of Ge on Si-(111); Hornvonhoegen, M.; Pook, M.; Alfalou, A.; Muller, B. H.; Henzler, M. *Surf. Sci.* **1993**, *284*, 53–66.

In-Situ Investigation of Temperature and Bias Dependent Effects on the Oxide Growth of Si and Ge in an Electron Cyclotron Resonance; Hu, Y. Z.; Wang, Y. Q.; Li, M.; Joseph, J.; Irene, E. A. *J. Vac. Sci. Technol. A* **1993**, *11*, 900–904.

Micro Raman Characterization of Molecular Beam Epitaxial Ge Heterolayers on Si Substrates; Ichimura, M.; Moriguchi, Y.; Usami, A.; Wada, T.; Wakahara, A.; Sasaki, A. *J. Electron. Mater.* **1993**, *22*, 779–784.

Ordered Structure at Si/Ge Interfaces; Ikarashi, N.; Akimoto, K.; Tatsumi, T.; Ishida, K. *Phys. Rev. Lett.* **1994**, *72*, 3198–3201.

High Resolution Transmission Electron Microscopy of Si/Ge Interfacial Structures; Ikarashi, N.; Tatsumi, T.; Ishida, K. *Jpn. J. Appl. Phys.* **1994**, *33*, 1228–1233.

Ge-Dimer Relaxation on Si(100); Jin, J. M.; Lewis, L. J. *Phys. Rev. B* **1994**, *49*, 2201–2204.

Adsorption Sites of Ge Adatoms on Stepped Si(110) Surface; Katircioglu, S.; Erkoc, S. *Surf. Sci.* **1994**, *311*, 703–706.

Solid Source and Gas Source Hybrid Si Molecular Beam Epitaxy for a $Si_{1-x}Ge_x$/Si Single Quantum Well Electroluminescent Device; Kato, Y.; Fukatsu, S.; Shiraki, Y. *J. Electron. Mater.* **1994**, *23*, 47–51.

Hybrid Si Molecular Beam Epitaxial Regrowth for a Strained $Si_{1-x}Ge_x$/Si Single Quantum Well Electroluminescent Device; Kato, Y.; Fukatsu, S.; Usami, N.; Shiraki, Y. *Appl. Phys. Lett.* **1993**, *63*, 2414–2416.

A $Si_{1-x}Ge_x$/Si Single Quantum Well p-i-n Structure Grown by Solid Source and Gas Source Hybrid Si Molecular Beam Epitaxy; Kato, Y.; Fukatsu, S.; Usami, N.; Shiraki, Y. *J. Cryst. Growth* **1994**, *136*, 355–360.

Growth of Ge Thin Films and Islands on the Si-(001) Surface; Khor, K. E.; Dassarma, S. *Phys. Rev. B* **1994**, *49*, 13657–13662.

Control of Deposition Rate in Remote Plasma Enhanced Chemical Vapor Deposition of Ge_xSi_{1-x}/Si Heteroepitaxial Films; Kinosky, D.; Qian, R.; Mahajan, A.; Thomas, S.; Banerjee, S.; et al. *J. Vac. Sci. Technol. B* **1993**, *11*, 1396–1400.

Electrical Effects of Residual Defects in Si After High Energy Implantation of Ge^+ Ions and Annealing; Kogler, R.; Vonborany, J.; Panknin, D.; Skorupa, W. *Nucl. Instrum. Methods Phys. Res. Sect. B* **1994**, *89*, 350–353.

On Transconductance in the p-Channel Si/SiGe Heterojunction Field Effect Transistor; Kovacic, S. J.; Ojha, J. J.; Swoger, J. H.; Simmons, J. G.; Noel, J. P.; Houghton, D. C. *Can. J. Phys.* **1992**, *70*, 963–968.

Fabrication and Characterization of Selectively Grown $Si_{1-x}Ge_x$/Si p^+/n Heterojunctions Using Pulsed Laser Induced Epitaxy and Gas Immersion Laser Doping; Kramer, K. J.; Talwar, S.; Ishida, E.; Weiner, K. H.; Sigmon, T. W. *Appl. Surf. Sci.* **1993**, *69*, 121–126.

Oxygen Incorporation and Oxygen Induced Defect Formation in Thin Si and $Si_{1-x}Ge_x$ Layers on Silicon Grown by Chemical Vapor Deposition at Atmospheric Pressure; Kruger, D.; Morgenstern, T.; Kurps, R.; Bugiel, E.; Quick, C.; Kuhne, H. *J. Appl. Phys.* **1994**, *75*, 7829–7834.

Epitaxial Chemically Vapor Deposited $Si_{1-x}Ge_x$ Thin Film Growth at Very Low Total Pressure; Kuhne, H. *Thin Solid Films* **1993**, *223*, 230–234.

Ion Beam Induced Epitaxy in B-Implanted Silicon Preamorphized with Ge Ions; Kuriyama, K.; Takahashi, H.; Shimoyama, K.; Hayashi, N.; Hasegawa, M.; Kobayashi, N. *Nucl. Instrum. Methods Phys. Res. Sect. B* **1993**, *80/81*, 994–997.

The Chemisorption and Reaction of $GeCl_4$ with Si-(100); Lapianosmith, D. A.; McFeely, F. R. *Thin Solid Films* **1993**, *225*, 187–190.

Synchronization of Nucleation Studied with Monte Carlo Simulations and Applied to $Si_{1-x}Ge_x$ Molecular Beam Epitaxy; Larsson, M. I.; Hansson, G. V. *Surf. Sci.* **1993**, *292*, 98–113.

Progression of Cleavage in Si, Ge, and GaAs; Li, D. G.; McAlpine, N. S.; Haneman, D. *Appl. Surf. Sci.* **1993**, *65/66*, 553–559.

Donor Doping Characteristics of Gas Source Molecular Beam Epitaxial Si and $Si_{1-x}Ge_x$ Using Phosphine; Li, S. H.; Bhattacharya, P. K. *J. Appl. Phys.* **1994**, *76*, 2213–2215.

Molecular Beam Epitaxial Growth of $Si_{1-x}Ge_x$/Si Pseudomorphic Layers Using Disilane and Germanium; Li, S. H.; Bhattacharya, P. K.; Malik, R.; Gulari, E. *J. Electron. Mater.* **1993**, *22*, 793–795.

Reduction of Secondary Defect Density by C-Implant and B-Implant in Ge_xSi_{1-x} Layers Formed by High Dose Ge Implantation in (100) Si; Lombardo, S.; Priolo, F.; Campisano, S. U.; Lagomarsino, S. *Appl. Phys. Lett.* **1993**, *62*, 2335–2337.

Surface Chemistry of Diethylsilane and Diethylgermane on Si(100)—An Atomic Layer Epitaxy Approach; Mahajan, A.; Kellerman, B. K.; Russell, N. M.; Banerjee, S.; Campion, A.; et al. *J. Vac. Sci. Technol. A* **1994**, *12*, 2265–2270.

Microstructure in Molecular Beam Epitaxy Grown Si/Ge Short Period Strained Layer Superlattices; Matsuhata, H.; Miki, K.; Sakamoto, K.; Sakamoto, T.; Yoshida, S. *Phys. Rev. B* **1993**, *47*, 10474–10483.

Large Scale Ab-Initio Study of the Binding and Diffusion of a Ge Adatom on the Si(100) Surface; Milman, V.; Jesson, D. E.; Pennycook, S. J.; Payne, M. C.; Lee, M. H.; Stich, I. *Phys. Rev. B* **1994**, *50*, 2663–2666.

$Si_{1-x}Ge_x$ Alloy Growth on Si(111) Surfaces from Gaseous Hydride Sources; Mokler, S. M.; Joyce, B. A. *Surf. Sci.* **1993**, *298*, 43–49.

Surface Studies during Growth of $Si_{1-x}Ge_x$/Si from Gaseous Si and Ge Hydrides; Mokler, S. M.; Ohtani, N.; Xie, M. H.; Zhang, J.; Joyce, B. A. *J. Vac. Sci. Technol. B* **1993**, *11*, 1073–1076.

Growth Rate Dependence on GeH_4 during Gas Source MBE of Si_xGe_{1-x} Alloys Grown from Si_2H_6 and

GeH_4; Mokler, S. M.; Ohtani, N.; Xie, M. H.; Zhang, X.; Joyce, B. A. *J. Cryst. Growth* **1993**, *127*, 467–471.

Growth Mode of Ge Films on Si(100) Substrate Deposited by Ion Beam Sputtering; Mosleh, N.; Meyer, F.; Schwebel, C.; Pellet, C.; Eizenberg, M. *Thin Solid Films* **1994**, *246*, 30–34.

Low Temperature Epitaxial Growth of In-Situ B-Doped $Si_{1-x}Ge_x$ Films; Murota, J.; Honma, F.; Yoshida, T.; Goto, K.; Maeda, T.; et al. *J. Phys. IV* **1993**, *3*, 427–432.

$Si/Si_{1-x}Ge_x/Si$ Heterostructure Growth by Ultraclean Low Temperature LPCVD for the Fabrication of Novel Heterodevice; Murota, J.; Maeda, T.; Goto, K.; Sakamoto, K.; Aizawa, K.; et al. *J. Phys. IV* **1993**, *3*, 403–410.

Low Temperature Epitaxial Growth of $Si/Si_{1-x}Ge_x/Si$ Heterostructure by Chemical Vapor Deposition; Murota, J.; Ono, S. *Jpn. J. Appl. Phys.* **1994**, *33*, 2290–2299.

Electron Cyclotron Resonance in Silicon Silicon-Germanium Heterostructures; Murphy, S. Q.; Schlesinger, Z.; Nelson, S. F.; Chu, J. O.; Meyerson, B. S. *Appl. Phys. Lett.* **1993**, *63*, 222–224.

Negative Differential Conductivity Measured on a Germanium Layer on Si(001); Mussig, H. J.; Kruger, D.; Hinrich, S.; Hansson, P. O. *Surf. Sci.* **1994**, *314*, 884–888.

Effect of Atomic and Molecular Hydrogen Irradiation on Ge Surface Segregation during Si Molecular Beam Epitaxy; Nakagawa, K.; Nishida, A.; Kimura, Y.; Shimada, T. *Jpn. J. Appl. Phys.* **1994**, *33*, 1331–1334.

Low Temperature Heteroepitaxial Growth of SiGe on Si with Low Pressure Chemical Vapor Deposition; Nakai, K.; Ozeki, M.; Nakajima, K. *J. Cryst. Growth* **1993**, *126*, 285–292.

Surface Hydrogen Effects on Ge Surface Segregation during Silicon Gas Source Molecular Beam Epitaxy; Ohtani, N.; Mokler, S.; Xie, M. H.; Zhang, J.; Joyce, B. A. *Jpn. J. Appl. Phys.* **1994**, *33*, 2311–2316.

Simulation Studies of Ge Surface Segregation during Gas Source MBE Growth of $Si/Si_{1-x}Ge_x$ Heterostructures; Ohtani, N.; Mokler, S. M.; Joyce, B. A. *Surf. Sci.* **1993**, *295*, 325–334.

Transient Growth Rate Change during Gas Source Molecular Beam Epitaxy of $Si_{1-x}Ge_x$ Alloys; Ohtani, N.; Mokler, S. M.; Xie, M. H.; Zhang, J.; Joyce, B. A. *Appl. Phys. Lett.* **1993**, *62*, 2042–2044.

RHEED Investigation of Ge Surface Segregation during Gas Source MBE of $Si/Si_{1-x}Ge_x$ Heterostructures; Ohtani, N.; Mokler, S. M.; Xie, M. H.; Zhang, J.; Joyce, B. A. *Surf. Sci.* **1993**, *284*, 305–314.

Investigation of Surface Reconstruction Domain Behavior during Si-GSMBE; Ohtani, N.; Mokler, S. M.; Zhang, J.; Joyce, B. A. *J. Cryst. Growth* **1993**, *127*, 461–466.

Kinetic Suppression of Islanding in Impurity Mediated Heteroepitaxial Growth of Germanium on Silicon; Osten, H. J. *Appl. Phys. Lett.* **1994**, *64*, 2356–2358.

Surfactant Mediated Growth of Germanium on Silicon (001) with Submonolayer Coverage of Sb and Te; Osten, H. J.; Klatt, J.; Lippert, G.; Bugiel, E.; Higuchi, S. *J. Appl. Phys.* **1993**, *74*, 2507–2511.

Evolution of Surface Morphology and Strain during SiGe Epitaxy; Pidduck, A. J.; Robbins, D. J.; Cullis, A. G.; Leong, W. Y.; Pitt, A. M. *Thin Solid Films* **1992**, *222*, 78–84.

Oxidation of Ultrathin SiGe Layer on Si(001)—Evidence for Inward Movement of Ge; Prabhakaran, K.; Nishioka, T.; Sumitomo, K.; Kobayashi, Y.; Ogino, T. *Jpn. J. Appl. Phys.* **1994**, *33*, 1837–1838.

Growth of Germanium Films on Si(001) Substrates; Roland, C.; Gilmer, G. H. *Phys. Rev. B* **1993**, *47*, 16286–16298.

Thermal Stress Induced Dislocations in Gesi/Si Heterostructures; Roos, B.; Ernst, F. *J. Cryst. Growth* **1994**, *137*, 457–471.

A Surface Kinetics Model for the Growth of $Si_{1-x}Ge_x$ Films from SiH_4/GeH_4 Mixtures; Russell, N. M.; Breiland, W. G. *J. Appl. Phys.* **1993**, *73*, 3525–3530.

Defect Mediated Island Formation in Stranski-Krastanov Growth of Ge on Si(001); Sakai, A.; Tatsumi, T. *Phys. Rev. Lett.* **1993**, *71*, 4007–4010.

Which Surfactant Shall We Choose for the Heteroepitaxy of Ge/Si(001) Questionable—Bi as a Surfactant with Small Self-Incorporation; Sakamoto, K.; Kyoya, K.; Miki, K.; Matsuhata, H.; Sakamoto, T. *Jpn. J. Appl. Phys.* **1993**, *32*, 204–206.

Abrupt Si/Ge/Si(001) Interfaces Fabricated with Bi as a Surfactant; Sakamoto, K.; Matsuhata, H.; Kyoya, K. I.; Miki, K.; Sakamoto, T. *Jpn. J. Appl. Phys.* **1994**, *33*, 2307–2310.

Effect of a Surfactant on the Growth of Si/Ge Heterostructures; Sakamoto, K.; Miki, K.; Sakamoto, T.; Yamaguchi, H.; Oyanagi, H.; et al. *Thin Solid Films* **1992**, *222*, 112–115.

Selective Growth of SiGe Nanostructures by Low Pressure VPE; Schmidt, G.; Langheinrich, W.; Heime, K. *Solid-State Electron.* **1994**, *37*, 587–589.

Structural Ripple Formation in Ge/Sb Multilayers Induced by Laser Irradiation; Serna, R.; Afonso, C. N.; Petfordlong, A. K.; Long, N. J. *Appl. Phys. A* **1994**, *58*, 197–202.

Kinetics of Hydrogen Desorption in Surface Limited Thin Film Growth of SiGe Alloys; Sharp, J. W.; Eres, G. *Appl. Phys. Lett.* **1993**, *62*, 2807–2809.

Role of Ge in SiGe Epitaxial Growth Using Silane Germane Gas Source Molecular Beam Epitaxy; Suemitsu, M.; Kim, K. J.; Miyamoto, N. *J. Vac. Sci. Technol. A* **1994**, *12*, 2271–2275.

Optical Detection of Interdiffusion in Strained $Si_{1-x}Ge_x/Si$ Quantum Well Structures; Sunamura, H.; Fukatsu, S.; Usami, N.; Shiraki, Y. *Jpn. J. Appl. Phys.* **1994**, *33*, 2344–2347.

Structural Characterization of Si/Ge Superlattices Grown on an Si(001) Surface by Molecular Beam Epitaxy; Tamagawa, T.; Shintani, T.; Ueba, H.; Tatsuyama, C.; Nakagawa, K.; Miyao, M. *Thin Solid Films* **1994**, *237*, 282–290.

Photoemission Study of Au, Ge, and O_2 Deposition on NH_4F Etched Si(111); Terry, J.; Cao, R.; Wigren, C.; Pianetta, P. *J. Vac. Sci. Technol. A* **1994**, *12*, 1869–1875.

Layered Heteroepitaxial Growth of Germanium on Si(015) Observed by Scanning Tunneling Microscopy;

Tomitori, M.; Watanabe, K.; Kobayashi, M.; Iwawaki, F.; Nishikawa, O. *Surf. Sci.* **1994**, *301*, 214–222.

Scanning Tunneling Microscopy Scanning Tunneling Spectroscopy Study of Ge and Si Dimers on Si Substrates; Tomitori, M.; Watanabe, K.; Kobayashi, M.; Nishikawa, O. *J. Vac. Sci. Technol. B* **1994**, *12*, 2022–2025.

STM Study of the Ge Growth Mode on Si(001) Substrates; Tomitori, M.; Watanabe, K.; Kobayashi, M.; Nishikawa, O. *Appl. Surf. Sci.* **1994**, *76*, 322–328.

The Influence of Dimerization on the Stability of Ge Hutclusters on Si(001); Tuinstra, F.; Scholte, P. M. L. O.; Rijnders, W. I.; Vandenberg, A. J. *Surf. Sci.* **1994**, *317*, 58–64.

Abrupt Compositional Transition in Luminescent $Si_{1-x}Ge_x$/Si Quantum Well Structures Fabricated by Segregant Assisted Growth Using Sb Adlayer; Usami, N.; Fukatsu, S.; Shiraki, Y. *Appl. Phys. Lett.* **1993**, *63*, 388–390.

Photoluminescence of $Si_{1-x}Ge_x$/Si Quantum Wells with Abrupt Interfaces Formed by Segregant Assisted Growth; Usami, N.; Fukatsu, S.; Shiraki, Y. *Jpn. J. Appl. Phys.* **1994**, *33*, 2304–2306.

Low Energy Electron Microscopy Studies of Ge and Ag Growth on Si(111); Vandergon, A. W. D.; Tromp, R. M.; Reuter, M. C. *Thin Solid Films* **1993**, *236*, 140–145.

Effect of Alloy Composition on Defect Formation in Ge_xSi_{1-x} Si Heterostructures Obtained by Molecular Beam Epitaxy; Vdovin, V. I.; Milvidskii, M. G.; Yugova, T. G.; Lyutovich, K. L.; Saidov, S. M. *J. Cryst. Growth* **1994**, *141*, 109–118.

Surfactant Mediated Epitaxy of Ge on Si(111)—The Role of Kinetics and Characterization of the Ge Layers; Voigtlander, B.; Zinner, A. *J. Vac. Sci. Technol. A* **1994**, *12*, 1932–1937.

Structure of Ge Epilayers on Si(100); Wang, Y.; Bu, H.; Lytle, T. E.; Rabalais, J. W. *Surf. Sci.* **1994**, *318*, 83–88.

Growth and Processing of Relaxed-$Si_{1-x}Ge_x$ Strained-Si Structures for Metal Oxide-Semiconductor Applications; Welser, J.; Hoyt, J. L.; Gibbons, J. F. *Jpn. J. Appl. Phys.* **1994**, *33*, 2419–2422.

Scanning Tunneling Microscopy (STM) Studies of the Chemical Vapor Deposition of Ge on Si(111) from Ge Hydrides and a Comparison with Molecular Beam Epitaxy; Wintterlin, J.; Avouris, P. *J. Chem. Phys.* **1994**, *100*, 687–704.

Profile and Inplane Structures of Self Assembled Monolayers on Ge Si Multilayer Substrates by High Resolution X-Ray Diffraction Employing X-Ray Interferometry Holography; Xu, S.; Fischetti, R. F.; Blasie, J. K.; Peticolas, L. J.; Bean, J. C. *J. Phys. Chem.* **1993**, *97*, 1961–1969.

New Low Pressure Chemical Vapor Deposition Technique for Ge Crystalline Thin Films; Yamamoto, M.; Hanna, J.; Miyauchi, M. *Appl. Phys. Lett.* **1993**, *63*, 2508–2510.

Molecular Dynamics Simulation of the Surface Reconstruction and Strain Relief in $Si_{1-x}Ge_x$/Si(100) Heterostructures; Yu, Q. M.; Clancy, P. *Model. Simul. Mater. Sci. Eng.* **1994**, *2*, 829–844.

Enhanced Surface-Interface Recombination and Surface Inversion of Ni Decorated Si/Si(Ge)/Si Heterostructures; Zhou, T. Q.; Buczkowski, A.; Radzimski, Z. J.; Rozgonyi, G. A. *J. Appl. Phys.* **1993**, *73*, 8412–8418.

Sn

A Study of the Electronic Structure and Schottky Barriers at Reconstructed Sn Si Interfaces; Anyele, H. T.; Cafolla, A. A.; Matthai, C. C. *Appl. Surf. Sci.* **1993**, *70/71*, 433–437.

The Sn/SiO_2 Interface—Tin Oxidation in the Presence of Sodium Oxide; Colaianni, M. L.; Chen, P. J.; Yates, J. T.; Arbab, M. *Appl. Surf. Sci.* **1993**, *68*, 467–475.

Ohmic Contact in Electron Cyclotron Resonance Chemical Vapor Deposition Tin/Si Structure; Harada, Y.; Akahori, T.; Onoda, H. *Jpn. J. Appl. Phys.* **1994**, *33*, 413–418.

Empty States Investigation of Epitaxial Sn/Si(100) Systems; Pedio, M.; Ghisalberti, V.; Ottaviani, C.; Capozi, M.; Lama, F.; et al. *Surf. Sci.* **1994**, *303*, 153–160.

Wetting of Silicon Single Crystal by Silver and Tin, and Their Interfaces; Sugihara, S.; Okazaki, K.; Suganuma, K. *J. Mater. Sci.* **1993**, *28*, 2455–2458.

Pb

Pb Preadsorption Facilitates Island Formation during Ga Growth on Si(111); Hibino, H.; Shimizu, N.; Sumitomo, K.; Shinoda, Y.; Nishioka, T.; Ogino, T. *J. Vac. Sci. Technol. A* **1994**, *12*, 23–28.

Growth Mode and Surface Structures on the Pb/Si(001) System Observed by Scanning Tunneling Microscopy; Itoh, H.; Tanabe, H.; Winau, D.; Schmid, A. K.; Ichinokawa, T. *J. Vac. Sci. Technol. B* **1994**, *12*, 2086–2089.

Surface Conductivity of Si(111) 7 × 7 with Submonolayer Pb Coverages; Suurmeijer, E. P. T. M.; Benedictus, R.; Vanderstadt, A.; Klapwijk, T. M. *Appl. Surf. Sci.* **1993**, *70/71*, 452–455.

LEED I(V) Study of the Si/Pb/Si(111) System; Zhao, H.; Tear, S. P.; Jones, A. H. *Surf. Sci.* **1994**, *309*, 645–649.

Group 15

N

Interaction of Slow N_2^+ Ions with the Si(001) Surface—A Combined Photoemission and LEED Study; Baek, D. H.; Kang, H.; Chung, J. W. *Phys. Rev. B* **1994**, *49*, 2651–2657.

The Sodium Promoted Nitridation of Si(100)-2×1 Using N_2 Molecular Beams; Bush, T. L.; Hayward, D. O.; Jones, T. S. *Surf. Sci.* **1994**, *313*, 179–187.

Silicon Nitride Thin Film Production on Si(111); Colaianni, M. L.; Chen, P. J.; Nagashima, N.; Yates, J. T. *J. Appl. Phys.* **1993**, *73*, 4927–4931.

RBS, AES and XPS Analysis of Ion Beam Induced Nitridation of Si and SiGe Alloys; Decoster, W.; Brijs, B.; Bender, H.; Alay, J.; Vandervorst, W. *Vacuum* **1994**, *45*, 389–395.

Low Energy (3 – 100 eV) Electron Bombardment Induced Nitridation of Thin SiO_2 Films—Physicochemical and Electrical Analyses; Glachant, A.; Garcia, V.; Balland, B.; Bureau, J. C.; Plossu, C.; et al. *Thin Solid Films* **1994**, *238*, 31–36.

Behavior of Boron and Nitrogen in a Surface Layer of Silicon during Synthesis of Buried Layers by Implantation of N^+ Ions; Kachurin, G. A.; Tyschenko, I. E. *Semiconductor* **1993**, *27*, 658–662.

Chemical and Structural Transformations in the Al/Si(111)8×8-N System; Khramtsova, E. A.; Saranin, A. A.; Lifshits, V. G. *Surf. Sci.* **1993**, *295*, 319–324.

Ion Beam Nitridation of a Si(111) Surface—Effects of Ion Reactivity and Thermal Treatment; Kim, B. C.; Kang, H.; Kim, C. Y.; Chung, J. W. *Surf. Sci.* **1994**, *301*, 295–305.

Anisotropic Etching of Silicon Nitride at Low Temperatures by Synchrotron Radiation; Kitamura, O.; Goto, T.; Terakado, S.; Suzuki, S.; Sekitani, T.; Tanaka, K. *Appl. Surf. Sci.* **1994**, *80*, 122–128.

Scanning Tunneling Microscopic Observations of Nonconductive Oxide Surfaces—SiO_2 Thin Films Formed on n-Si(100) and p-Si(100); Komiyama, M.; Kirino, M.; Kurokawa, H. *Jpn. J. Appl. Phys.* **1993**, *32*, 2934–2939.

Very Low Surface Recombination Velocities on 2.5 Ωcm Si Wafers, Obtained with Low Temperature PECVD of Si Oxide and Si Nitride; Leguijt, C.; Lolgen, P.; Eikelboom, J. A.; Amesz, P. H.; Steeman, R. A.; et al. *Sol. Energy Mater. Sol. Cells* **1994**, *34*, 177–181.

An X-Ray Photoelectron Spectroscopy Study of the Thermal Oxidation and Nitridation of Si(100)-2×1 by NO_2; Lutz, F.; Bischoff, J. L.; Kubler, L.; Bolmont, D. *Appl. Surf. Sci.* **1993**, *72*, 427–433.

MeV Ion Channeling Study of SiN_x/Si Interfaces Formed by Various Deposition Methods; Moon, J.; Ito, T.; Hiraki, A. *Appl. Surf. Sci.* **1993**, *70/71*, 53–57.

Estimation of the Thickness of Ultrathin Silicon Nitride Films by X-Ray Photoelectron Spectroscopy; Muto, A.; Mine, T.; Nakazawa, M. *Jpn. J. Appl. Phys.* **1993**, *32*, 3580–3583.

Radiation Effects of Vacuum Ultraviolet Lasers in Amorphous Si_3N_4 Films; Nakamae, K.; Kurosawa, K.; Ohmukai, M.; Katto, M.; Okuda, M.; et al. *Nucl. Instrum. Methods Phys. Res. Sect. B* **1994**, *91*, 659–662.

Silicon Precipitation Induced by Argon Excimer Laser in Surface Layers of Si_3N_4; Ohmukai, M.; Naito, H.; Okuda, M.; Kurosawa, K.; Sasaki, W.; et al. *Jpn. J. Appl. Phys.* **1993**, *32*, 1062–1065.

Kinetic Energy Dependence of N^+ and N^{2+} Reactions with Si(100); Park, K. H.; Kim, B. C.; Kang, H. *Surf. Sci.* **1993**, *283*, 73–77.

Thermally Grown Si_3N_4 Thin Films on Si(100)—Surface and Interfacial Composition; Peden, C. H. F.; Rogers, J. W.; Shinn, N. D.; Kidd, K. B.; Tsang, K. L. *Phys. Rev. B* **1993**, *47*, 15622–15629.

Modification of N-Si(100) Surface by Scanning Tunneling Microscope Tip-Induced Anodization Under Nitrogen Atmosphere; Sugimura, H.; Kitamura, N.; Masuhara, H. *Jpn. J. Appl. Phys.* **1994**, *33*, 143–145.

Comparative Sintering Study on Nonconventional and Commercial Silicon Nitride Powders; Szepvolgyi, J.; Bertoti, I.; Mohaitoth, I.; Gilbart, E.; Riley, F. L.; Patel, M. *J. Mater. Chem.* **1993**, *3*, 279–286.

Electronic Structure of the Nitride Layers Formed on a Si(111) Surface—Angle Resolved Photoemission Study; Tokumitsu, S.; Anazawa, T.; Ozawa, K.; Miyazaki, E.; Edamoto, K.; Kato, H. *Surf. Sci.* **1994**, *317*, 143–151.

Kinetic Studies of the Reactions Between Silicon Nitride and Carbon; Wang, H.; Fischman, G. S. *J. Therm. Anal.* **1994**, *41*, 135–146.

Incorporation of Nitrogen in Si_3N_4-Capped Silicon by CW Ar^+-Laser Melting; Willems, G. J.; Maes, H. E. *J. Appl. Phys.* **1993**, *74*, 5185–5195.

Silicon Nitride Film for High Mobility Thin Film Transistor by Hybrid Excitation Chemical Vapor Deposition; Yamamoto, S.; Migitaka, M. *Jpn. J. Appl. Phys.* **1993**, *32*, 462–468.

P

The Influence of the Solubility Limit on Diffusion of Phosphorus and Arsenic into Silicon; Antoncik, E. *Appl. Phys. A* **1994**, *58*, 117–123.

Investigation of Reoxidation and Phosphorus Behavior in HF-Treated Heavily Doped Silicon Surfaces; Kamiura, Y.; Mizokawa, Y.; Iida, M.; Isobe, Y.; Kawamoto, K. *Jpn. J. Appl. Phys.* **1993**, *32*, 4863–4869.

Phosphorus Direct Doping from Vapor Phase into Silicon for Shallow Junctions; Kiyota, Y.; Nakamura, T.; Muraki, K.; Inada, T. *J. Electrochem. Soc.* **1994**, *141*, 2241–2244.

Controlling the Solid Phase Nucleation of Amorphous Si by Means of a Substrate Step Structure and Local Phosphorus Doping; Moniwa, M.; Kusukawa, K.; Ohkura, M.; Takeda, E. *Jpn. J. Appl. Phys.* **1993**, *32*, 312–317.

Characterization of Antiphase Domain in GaP on Misoriented (001) Si Substrate Grown by Metalorganic Chemical Vapor Deposition; Soga, T.; Nishikawa, H.; Jimbo, T.; Umeno, M. *Jpn. J. Appl. Phys.* **1993**, *32*, 4912–4915.

Nucleation and Crystallization Characteristics of Phosphorus-Doped Amorphous Silicon Slit Nano-Wire; Wada, Y.; Kobayashi, T.; Kure, T.; Yoshimura, T.; Sudou, Y.; et al. *J. Electrochem. Soc.* **1994**, *141*, 1392–1397.

An Atomically Resolved STM Study of the Interaction of Phosphine with the Silicon(001) Surface; Wang, Y. J.; Bronikowski, M. J.; Hamers, R. J. *J. Phys. Chem.* **1994**, *98*, 5966–5973.

Atomic Resolution Study of Overlayer Formation and Interfacial Mixing in the Interaction of Phosphorus with Si(001); Wang, Y. J.; Chen, X. X.; Hamers, R. J. *Phys. Rev. B* **1994**, *50*, 4534–4547.

As

Direct Detection of Atomic Arsenic Desorption from Si(100); Alstrin, A. L.; Strupp, P. G.; Leone, S. R. *Appl. Phys. Lett.* **1993**, *63*, 815–817.

The Influence of the Solubility Limit on Diffusion of Phosphorus and Arsenic into Silicon; Antoncik, E. *Appl. Phys. A* **1994**, *58*, 117–123.

Arsenic Termination of the Si(110) Surface; Biegelsen, D. K.; Bringans, R. D.; Northrup, J. E.; Schabel, M. C.; Swartz, L. E. *Phys. Rev. B* **1993**, *47*, 9589–9596.

Electronic Structure of the Prototypical As-Si(111)-1×1 Surface Investigated by Inverse Photoemission Spectroscopy; Bouzidi, S.; Angot, T.; Coletti, F.; Debever, J. M.; Guyaux, J. L.; Thiry, P. A. *Phys. Rev. B* **1994**, *49*, 16539−16543.

Morphology and Crystalline Perfection of InAs Films on Si(100); Choi, C. H.; Barnett, S. A. *J. Cryst. Growth* **1994**, *137*, 381−387.

Charge Transfer and Electronic Screening at the As/Si(100)-(2×1) and As/Si(111)-(1×1) Surfaces; Cole, R. J.; Evans, J. A.; Weightman, P.; Matthew, J. A. D.; Woolf, D. A.; Westwood, D. I. *Phys. Rev. B* **1994**, *49*, 7528−7534.

Thermal Vibration Amplitudes and Structure of As on Si(001); Franklin, G. E.; Fontes, E.; Qian, Y.; Bedzyk, M. J.; Golovchenko, J. A.; Patel, J. R. *Phys. Rev. B* **1994**, *50*, 7483−7487.

Electrical Transport Quantum Effects in the $In_{0.53}Ga_{0.47}As/In_{0.52}Al_{0.48}As$ Heterostructure on Silicon; Georgakilas, A.; Christou, A.; Zekentes, K.; Mercy, J. M.; Konczewicz, L. K.; et al. *J. Appl. Phys.* **1994**, *76*, 1948−1952.

Codoping Effects of As and Xe on Ion Beam Induced Epitaxial Crystallization of Si; Hasegawa, M.; Kobayashi, N.; Hayashi, N. *Nucl. Instrum. Methods Phys. Res. Sect. B* **1993**, *80/81*, 674−678.

Layer-by-Layer Growth of AlAs Buffer Layer for GaAs on Si at Low Temperature by Atomic Layer Epitaxy; Kitahara, K.; Ohtsuka, N.; Ashino, T.; Ozeki, M.; Nakajima, K. *Jpn. J. Appl. Phys.* **1993**, *32*, 236−238.

Reflection High Energy Electron Diffraction of Heteroepitaxy in Chemical Vapor Deposition Reactor—Atomic Layer Epitaxy of GaAs, AlAs and GaP on Si; Kitahara, K.; Ozeki, M.; Nakajima, K. *Jpn. J. Appl. Phys.* **1993**, *32*, 1051−1055.

Abinition Calculations of Si, As, S, Se, and Cl Adsorption on Si(001) Surfaces; Kruger, P.; Pollmann, J. *Phys. Rev. B* **1993**, *47*, 1898−1910.

Electronic Structures of As/Si(001) 2×1 and Sb/Si-(001) 2×1 Surfaces; Li, G. W.; Chang, Y. C. *Phys. Rev. B* **1994**, *50*, 8675−8680.

Growth and Characterization of GaSe and GaAs/GaSe on As-Passivated Si(111) Substrates; Palmer, J. E.; Saitoh, T.; Yodo, T.; Tamura, M. *J. Appl. Phys.* **1993**, *74*, 7211−7222.

Lattice Mismatched InGaAs on Silicon Photodetectors Grown by Molecular Beam Epitaxy; Papanicolaou, N. A.; Anderson, G. W.; Iliadis, A. A.; Christou, A. *J. Electron. Mater.* **1993**, *22*, 201−206.

Calculation of the Optical-Properties of As Molecules on Si Substrates; Shen, T. H.; Matthai, C. C. *Surf. Sci.* **1993**, *287*, 672−675.

Coaxial Impact Collision Ion Scattering Spectroscopy Measurements of As/Si(100) Structure Prepared by ionized Cluster Beam Method; Shinohara, M.; Saraie, J.; Ishiyama, O.; Ohtani, F.; Mitamura, S. *Jpn. J. Appl. Phys.* **1993**, *32*, 4485−4489.

Cleaning of Si(100) Surface by As ionized Cluster Beam Prior to Epitaxial Growth of GaAs; Shinohara, M.; Saraie, J.; Ohtani, F.; Ishiyama, O.; Ogawa, K.; Asari, M. *J. Appl. Phys.* **1993**, *73*, 7845−7850.

Role of Grain Boundaries in the Epitaxial Realignment of Undoped and As-Doped Polycrystalline Silicon Films; Spinella, C.; Benyaich, F.; Cacciato, A.; Rimini, E.; Fallico, G.; Ward, P. *J. Mater. Res.* **1993**, *8*, 2608−2612.

Threading Dislocations in GaAs on Si Grown with ~1 nm Thick Si Interlayers; Tamura, M.; Saitoh, T.; Palmer, J. E.; Yodo, T. *Appl. Phys. A* **1994**, *58*, 145−155.

Importance of Adsorbate-Adsorbate Interactions for As and Sb Chemisorption on Si(100); Tang, S. P.; Freeman, A. J. *Phys. Rev. B* **1993**, *48*, 8068−8075.

Arsenic Interaction with Vicinal Si(001) Surfaces; Wasserfall, J.; Ranke, W. *Surf. Sci.* **1994**, *315*, 237−247.

The Effect of As/Ga Flux Ratio on Si-Doped GaAs Layers Grown by Molecular Beam Epitaxy; Zhang, D. H.; Radhakrishnan, K.; Yoon, S. F. *J. Cryst. Growth* **1994**, *135*, 441−446.

Sb

Structural and Electrical Study of Epitaxially Realigned Sb-Doped Polycrystalline Si Films; Cacciato, A.; Benyaich, F.; Spinella, C.; Rimini, E.; Fallico, G.; Ward, P. *Mater. Sci. Eng. B* **1993**, *18*, 289−294.

Formation of Buried Sb Dopant Profiles in Silicon by Pulsed Laser Epitaxy; Carolissen, R. J.; Knoesen, D. K.; Sinke, W. C.; Pretorius, R. *J. Mater. Res.* **1993**, *8*, 841−846.

Si(100)2×1+Sb Surfaces Studied with Photoemission and Optical Spectroscopy; Cricenti, A.; Bernhoff, H.; Purdie, D.; Reihl, B. *J. Vac. Sci. Technol. A* **1994**, *12*, 2327−2331.

Occupied and Unoccupied Surface States on the Single-Domain Si(100)-Sb-2×1 Surface; Cricenti, A.; Bernhoff, H.; Reihl, B. *Phys. Rev. B* **1993**, *48*, 10983−10986.

Electronic States on Si(100)2×1-Sb—Existence of 2 Semiconducting Phases; Cricenti, A.; Selci, S.; Felici, A. C.; Ferrari, L.; Chiarotti, G. *Solid State Commun.* **1993**, *86*, 667−670.

Si(100)1×1-Sb and Si(100)2×1-Sb Surfaces Studied with Angle Resolved Photoemission and Surface Differential Reflectivity; Cricenti, A.; Selci, S.; Felici, A. C.; Ferrari, L.; Contini, G.; Chiarotti, G. *Phys. Rev. B* **1993**, *47*, 15745−15749.

Transport Properties of Delta-Doped SiSb Superlattices; Eisele, I.; Wittmann, F.; Lifshits, V. G.; Zotov, A. V.; Ditina, Z. Z.; Ryzhkov, S. V. *Thin Solid Films* **1994**, *238*, 27−30.

Self Modulating Sb Incorporation in Si/SiGe Superlattices during Molecular Beam Epitaxial Growth; Fujita, K.; Fukatsu, S.; Usami, N.; Shiraki, Y.; Yaguchi, H.; et al. *Surf. Sci.* **1993**, *295*, 335−339.

Asymmetric Sb Dimers on the 1-ML Ge-Terminated Si(100) Surface; Grant, M. W.; Boshart, M. A.; Dieleman, D. J.; Seiberling, L. E. *Surf. Sci.* **1994**, *316*, 1088−1092.

Sb Surface Segregation and Doping in Si(100) Grown at Reduced Temperature by Molecular Beam Epitaxy; Hobart, K. D.; Godbey, D. J.; Thompson, P. E.; Simons, D. S. *Appl. Phys. Lett.* **1993**, *63*, 1381−1383.

Sb Surface Segregation during Heavy Doping of Si(100) Grown at Low Temperature by Molecular Beam Epitaxy; Hobart, K. D.; Godbey, D. J.; Thompson, P.

E.; Simons, D. S. *J. Vac. Sci. Technol. B* **1993**, *11*, 1115–1119.

Evaporation of Oxygen Bearing Species from Si Melt and Influence of Sb Addition; Huang, X. M.; Terashima, K.; Sasaki, H.; Tokizaki, E.; Anzai, Y.; Kimura, S. *Jpn. J. Appl. Phys.* **1994**, *33*, 1717–1722.

Evaporation Rates of Oxides from Undoped and Sb-Doped Si Melts Under Atmospheres of Pure Ne, Ar, and Kr; Huang, X. M.; Terashima, K.; Tokizaki, E.; Kimura, S.; Whitby, E. *Jpn. J. Appl. Phys.* **1994**, *33*, 3808–3812.

Growth of Sb on Si(111) Studied by Raman Scattering; Hunger, R.; Blick, N.; Esser, N.; Arens, M.; Richter, W.; et al. *Surf. Sci.* **1994**, *309*, 1061–1065.

Crystal Growth and Electronic Properties of Ultrahigh Vacuum Ion Beam Sputter Deposited Sb-Doped Si(001)2×1; Lee, N. E.; Tomasch, G. A.; Xue, G.; Markert, L. C.; Greene, J. E. *Appl. Phys. Lett.* **1994**, *64*, 1398–1400.

Electronic Structures of As/Si(001) 2×1 and Sb/Si-(001) 2×1 Surfaces; Li, G. W.; Chang, Y. C. *Phys. Rev. B* **1994**, *50*, 8675–8680.

Solid Boron and Antimony Doping of Si and SiGe Grown by Gas Source Molecular Beam Epitaxy; Li, S. H.; Bhattacharya, P. K.; Chung, S. W.; Zhou, J. X.; Gulari, E. *J. Electron. Mater.* **1993**, *22*, 409–412.

Study and Control of Molecule Surface Interaction at the Atomic Level—Sb_4 on Si(001); Mo, Y. W. *J. Vac. Sci. Technol. B* **1994**, *12*, 2231–2236.

Selective Adsorption of HBO_2 and Sb on a Si Surface Partially Covered with Ultrathin Oxide; Murakami, E.; Kujirai, H.; Kimura, S. *J. Appl. Phys.* **1994**, *76*, 563–568.

Theoretical Study of the Electronic Structure of the Si(111)$\sqrt{3}\times\sqrt{3}$Sb Surface; Nagayoshi, H. *Surf. Sci.* **1993**, *282*, 163–172.

Surfactant Mediated Growth of Germanium on Silicon (001) with Submonolayer Coverage of Sb and Te; Osten, H. J.; Klatt, J.; Lippert, G.; Bugiel, E.; Higuchi, S. *J. Appl. Phys.* **1993**, *74*, 2507–2511.

Structural Ripple Formation in Ge/Sb Multilayers Induced by Laser Irradiation; Serna, R.; Afonso, C. N.; Petfordlong, A. K.; Long, N. J. *Appl. Phys. A* **1994**, *58*, 197–202.

Sb-Induced Passivation of the Si(100) Surface; Tang, S.; Freeman, A. J. *Phys. Rev. B* **1993**, *47*, 1460–1465.

Importance of Adsorbate-Adsorbate Interactions for As and Sb Chemisorption on Si(100); Tang, S. P.; Freeman, A. J. *Phys. Rev. B* **1993**, *48*, 8068–8075.

Abrupt Compositional Transition in Luminescent $Si_{1-x}Ge_x$/Si Quantum Well Structures Fabricated by Segregant Assisted Growth Using Sb Adlayer; Usami, N.; Fukatsu, S.; Shiraki, Y. *Appl. Phys. Lett.* **1993**, *63*, 388–390.

Theoretical Calculations of STM Images of the Si-(111)$\sqrt{3}\times\sqrt{3}$-Ag and Si(111)$\sqrt{3}\times\sqrt{3}$-Sb Surfaces; Watanabe, S.; Aono, M.; Tsukada, M. *Surf. Sci.* **1993**, *287*, 1036–1040.

Reaction Pathway for Sb-Dimer Rotation in Conversion of Sb_4 Precursors on Si(001); Yu, B. D.; Oshiyama, A. *Phys. Rev. B* **1994**, *50*, 8942–8945.

Bi

Preparation of Bismuth Silicate Films on Si Wafer by Metalorganic Chemical Vapor Deposition; Kim, J. H.; Tsurumi, T.; Hirano, H.; Kamiya, T.; Mizutani, N.; Daimon, M. *Jpn. J. Appl. Phys.* **1993**, *32*, 135–138.

Adsorption of Bi on Si(001) Surface—An Atomic View; Noh, H. P.; Park, C.; Jeon, D.; Cho, K.; Hashizume, T.; et al. *J. Vac. Sci. Technol. B* **1994**, *12*, 2097–2099.

Scanning Tunneling Microscopy of $\sqrt{3}\times\sqrt{3}$-Bi Reconstruction on the Si(111) Surface; Park, C.; Bakhtizin, R. Z.; Hashizume, T.; Sakurai, T. *Jpn. J. Appl. Phys.* **1993**, *32*, 290–293.

Structure of the Bi/Si(111) Surface by Field Ion Scanning Tunneling Microscopy; Park, C.; Bakhtizin, R. Z.; Hashizume, T.; Sakurai, T. *Jpn. J. Appl. Phys.* **1993**, *32*, 1416–1418.

Ordering of Missing Row Defects Forming $(2\times n)$-Bi Phases on the Si(100) 2×1 Surface Studied by the Scanning Tunneling Microscopy; Park, C.; Bakhtizin, R. Z.; Hashizume, T.; Sakurai, T. *Jpn. J. Appl. Phys.* **1993**, *32*, 528–531.

Adsorption of Bismuth on Si(110) Surfaces Studied by Scanning Tunneling Microscopy; Sakama, H.; Kawazu, A.; Sueyoshi, T.; Sato, T.; Iwatsuki, M. *Jpn. J. Appl. Phys.* **1993**, *32*, 2929–2933.

Bi-Induced Reconstructions on Si(100); Tang, S. P.; Freeman, A. J. *Phys. Rev. B* **1994**, *50*, 1701–1704.

Group 16

O

Kinetics of Oxygen Dissociation on Si(111)7×7 Investigated with Optical 2nd Harmonic Generation; Bratu, P.; Kompa, K. L.; Hofer, U. *Phys. Rev. B* **1994**, *49*, 14070–14073.

Structure Analysis of O_2 and H_2O Chemisorption on a Si(100) Surface; Bu, H.; Rabalais, J. W. *Surf. Sci.* **1994**, *301*, 285–294.

A Molecular Beam Study of the Reaction of O_2 with K-Covered Si(100); Bush, T. L.; Jones, T. S.; Hayward, D. O. *Surf. Sci.* **1994**, *309*, 247–252.

A Study of Oxygen Implanted $Si_{0.5}Ge_{0.5}$ Alloy by XPS and Thermodynamic Analysis; Castle, J. E.; Liu, H. D.; Saunders, N. *Surf. Interface Anal.* **1993**, *20*, 149–154.

The Initial Adsorption of Oxygen on the Si(111)7×7 Surface at 150 K; Dai, D. X.; Zhu, F. R.; Luo, Y. S.; Davoli, I.; Stizza, S. *Appl. Surf. Sci.* **1994**, *78*, 293–297.

Gas Phase Etching of Si(111)-(7×7) Surfaces by Oxygen Observed by Scanning Tunneling Microscopy; Donig, F.; Feltz, A.; Kulakov, M.; Hessel, H. E.; Memmert, U.; Behm, R. J. *J. Vac. Sci. Technol. B* **1993**, *11*, 1955–1961.

Site Specific and State Selective Photofragmentation of Molecular Oxygen on Si(111)-(7×7); Dujardin, G.; Comtet, G.; Hellner, L.; Hirayama, T.; Rose, M.; et al. *Phys. Rev. Lett.* **1994**, *73*, 1727–1730.

Influence of Oxygen on the Formation of Ripples on Si; Elst, K.; Vandervorst, W.; Alay, J.; Snauwaert, J.; Hellemans, L. *J. Vac. Sci. Technol. B* **1993**, *11*, 1968–1981.

Na-Promoted Oxidation of Si—The Specific Oxidation Mechanism; Faraci, G.; Larosa, S.; Pennisi, A. R.; Margaritondo, G. *Phys. Rev. B* **1994**, *49*, 2943–2946.

High Temperature Scanning Tunneling Microscopy Studies on the Interaction of O_2 with Si(111)-(7×7) Surfaces; Feltz, A.; Memmert, U.; Behm, R. J. *Surf. Sci.* **1994**, *314*, 34–56.

Al-O Interactions in Ion Implanted Crystalline Silicon; Galvagno, G.; Laferla, A.; Spinella, C.; Priolo, F.; Raineri, V.; et al. *J. Appl. Phys.* **1994**, *76*, 2070–2077.

An Area Selective and Anisotropic Etching of Si by Synchrotron Radiation Excitation—Effects of Introducing O_2 Molecules; Goto, T.; Kitamura, O.; Terakado, S.; Suzuki, S.; Tanaka, K. *Jpn. J. Appl. Phys.* **1992**, *31*, 4449–4453.

Initial Stage of Oxygen Adsorption Onto a Si(111)-7×7 Surface Studied by Scanning Tunneling Microscopy; Hasegawa, T.; Kohno, M.; Hosoki, S. *Jpn. J. Appl. Phys.* **1994**, *33*, 3702–3705.

Effect of Oxygen Radicals for Epitaxial Growth of Al_2O_3 on Si; Hayama, K.; Ishida, M.; Nakamura, T. *Jpn. J. Appl. Phys.* **1994**, *33*, 496–499.

Theoretical Consideration on Dimer Vacancy Images in the STM Observations of Si(001) Surfaces in Terms of the Adsorption of O_2 Molecules; Hoshino, T.; Tsuda, M.; Oikawa, S.; Ohdomari, I. *Surf. Sci.* **1993**, *291*, 763–767.

Observation of Oxygen Precipitates in CZ-Grown Si Wafers with a Phase Differential Scanning Optical Microscope; Kimura, S. *J. Electrochem. Soc.* **1994**, *141*, 120–122.

Accurate Evaluation Techniques of Interstitial Oxygen Concentrations in Medium Resistivity Si Crystals; Kitagawara, Y.; Tamatsuka, M.; Takenaka, T. *J. Electrochem. Soc.* **1994**, *141*, 1362–1364.

Modeling and Experimental Studies of a Reactive Ion Etcher Using SF_6/O_2 Chemistry; Kopalidis, P. M.; Jorne, J. *J. Electrochem. Soc.* **1993**, *140*, 3037–3045.

Oxygen Incorporation and Oxygen Induced Defect Formation in Thin Si and $Si_{1-x}Ge_x$ Layers on Silicon Grown by Chemical Vapor Deposition at Atmospheric Pressure; Kruger, D.; Morgenstern, T.; Kurps, R.; Bugiel, E.; Quick, C.; Kuhne, H. *J. Appl. Phys.* **1994**, *75*, 7829–7834.

AES Study of Si LVV Bonding States in Various Substoichiometric Oxide Environments; Lang, B.; Khellafi, M. *Surf. Interface Anal.* **1993**, *20*, 827–832.

Multiple Internal Reflection Infrared Spectroscopy of Silicon Surface Structure and Oxidation Process at Room Temperature; Ling, L.; Kuwabara, S.; Abe, T.; Shimura, F. *J. Appl. Phys.* **1993**, *73*, 3018–3022.

Control of the Buried SiO_2 Layer Thickness and Si Defect Density in $SiMO_x$ Substrates—Structural Investigation and Process Optimization; Marsh, C. D.; Nejim, A.; Li, Y.; Booker, G. R.; Hemment, P. L. F.; et al. *Nucl. Instrum. Methods Phys. Res. Sect. B* **1993**, *74*, 197–203.

Oxidation of Si(111)7×7 Using Alkali Metal Atoms—Evidence for Local Promotion Mechanisms; Muscat, A. J.; Rjeb, A.; Roy, D. *Surf. Sci.* **1994**, *302*, 256–262.

Multiphoton Ionization Detection of a SiO Molecule Formed by O_2 Oxidation of a Silicon Surface; Nakamura, K. G.; Kuroki, H.; Kitajima, M. *J. Appl. Phys.* **1994**, *75*, 4261–4263.

Oxidation of Hydrogen Terminated Si Surfaces Studied by Infrared Spectroscopy; Niwano, M.; Kageyama, J.; Kinashi, K.; Sawahata, J.; Miyamoto, N. *Surf. Sci.* **1994**, *301*, 245–249.

Infrared Spectroscopy Study of Initial Stages of Oxidation of Hydrogen Terminated Si Surfaces Stored in Air; Niwano, M.; Kageyama, J.; Kurita, K.; Kinashi, K.; Takahashi, I.; Miyamoto, N. *J. Appl. Phys.* **1994**, *76*, 2157–2163.

Oxidation of Silicon with a Hot Oxygen Beam; Ono, T.; Hiraoka, S.; Suzuki, K. *J. Vac. Sci. Technol. A* **1993**, *11*, 959–963.

Local Alkali Metal Promoted Oxidation of Si(100)-(2×1) Surfaces—A Generalized Hubbard Model Calculation; Refolio, M. C.; Sancho, J. M. L.; Sancho, M. P. L.; Rubio, J. *Phys. Rev. B* **1994**, *49*, 2629–2636.

Electron Stimulated Desorption (ESD) of the O_2 Si-(111) Surface; Sakamoto, K.; Nakatsuji, K.; Daimon, H.; Yonezawa, T.; Suga, S. *Surf. Sci.* **1994**, *306*, 93–98.

A Theoretical Study of the Initial Stages of Si(111)-7×7 Oxidation. 1. The Molecular Precursor; Schubert, B.; Avouris, P.; Hoffmann, R. *J. Chem. Phys.* **1993**, *98*, 7593–7605.

A Theoretical Study of the Initial Stages of Si(111)-7×7 Oxidation. 2. The Dissociated State and Formation of SiO_4; Schubert, B.; Avouris, P.; Hoffmann, R. *J. Chem. Phys.* **1993**, *98*, 7606–7612.

Oxygen Incorporation during Low Temperature Chemical Vapor Deposition Growth of Epitaxial Silicon Films; Schwartz, P. V.; Sturm, J. C. *J. Electrochem. Soc.* **1994**, *141*, 1284–1290.

Effects of Trace Surface Oxidation in Low Temperature Epitaxy Grown from Dichlorosilane; Sedgwick, T. O.; Agnello, P. D.; Grutzmacher, D. A. *J. Electrochem. Soc.* **1993**, *140*, 3684–3688.

Elevated Temperature Oxidation and Etching of the Si(111) 7×7 Surface Observed with Scanning Tunneling Microscopy; Seiple, J.; Pecquet, J.; Meng, Z.; Pelz, J. P. *J. Vac. Sci. Technol. A* **1993**, *11*, 1649–1653.

Si LVV Auger Lineshape Analysis to Study the Oxygen Chemisorption on $TaSi_2$ Thin Film; Sharma, J. K. N.; Chakraborty, B. R.; Bera, S. *Surf. Interface Anal.* **1993**, *20*, 841–844.

Computer Simulation of $SiMO_x$ and $SiMN_i$ Formed by Low Energy Ion Implantation; Shi, Z. Y.; Lin, C. L.; Zhu, W. H.; Hemment, P. L. F.; Bussmann, U.; Zou, S. C. *Nucl. Instrum. Methods Phys. Res. Sect. B* **1993**, *74*, 210–212.

Photoemission Study of Au, Ge, and O_2 Deposition on NH_4F Etched Si(111); Terry, J.; Cao, R.; Wigren, C.; Pianetta, P. *J. Vac. Sci. Technol. A* **1994**, *12*, 1869–1875.

The Initial Stages of the Thermal Oxidation of Si-(001)2×1 Surface Studied by Scanning Tunneling Microscopy; Udagawa, M.; Niwa, M.; Sumita, I. *Jpn. J. Appl. Phys.* **1993**, *32*, 282–285.

Behaviors of Hydrogen and Oxygen on Cleaned Silicon Surfaces; Ueda, K. *Jpn. J. Appl. Phys.* **1994**, *33*, 1524–1527.

Oxidation Stages of Clean and H-Terminated Si-(001) Surfaces at Room Temperature; Westermann, J.; Nienhaus, H.; Monch, W. *Surf. Sci.* **1994**, *311*, 101–106.

Evolution of Surface Morphology of Si(100)-(2×1) during Oxygen Adsorption at Elevated Tempera-

tures; Wurm, K.; Kliese, R.; Hong, Y.; Rottger, B.; Wei, Y.; et al. *Phys. Rev. B* **1994**, *50*, 1567–1574.

Effects of Oxygen Doping on Properties of Microcrystalline Silicon Film Grown Using Rapid Thermal Chemical Vapor Deposition; Xu, X. L.; Misra, V.; Ozturk, M. C.; Wortman, J. J.; Harris, G. S.; et al. *J. Electron. Mater.* **1993**, *22*, 1345–1351.

Variation of Local Charge States and the Local Electrostatic Potential during Oxygen Adsorption on a Caesiated Si(001) Surface Probed with Helium Metastables and Oxygen Molecules; Yamada, K.; Nishigaki, S. *Surf. Sci.* **1993**, *293*, 893–899.

RBS, RHEED and THEED Studies of $SiMO_x$ and $SiMN_i$ Structures Formed by Ion Beam Synthesis; Yankov, R. A.; Komarov, F. F.; Petrov, S. A. *Vacuum* **1993**, *44*, 1077–1084.

Hydrogen Enhanced Out-Diffusion of Oxygen in Czochralski Silicon; Zhong, L.; Shimura, F. *J. Appl. Phys.* **1993**, *73*, 707–710.

S

Vacancy Creation on the Si(111)-7×7 Surface Due to Sulfur Desorption Studied by Scanning Tunneling Microscopy; Koenders, L.; Moriarty, P.; Hughes, G.; Jusko, O. *Surf. Sci.* **1993**, *297*, 113–118.

Ab initio Calculations of Si, As, S, Se, and Cl Adsorption on Si(001) Surfaces; Kruger, P.; Pollmann, J. *Phys. Rev. B* **1993**, *47*, 1898–1910.

Se

Ab-initio Calculations of Si, As, S, Se, and Cl Adsorption on Si(001) Surfaces; Kruger, P.; Pollmann, J. *Phys. Rev. B* **1993**, *47*, 1898–1910.

Growth and Characterization of GaSe and GaAs/GaSe on As-Passivated Si(111) Substrates; Palmer, J. E.; Saitoh, T.; Yodo, T.; Tamura, M. *J. Appl. Phys.* **1993**, *74*, 7211–7222.

Heteroepitaxy of GaSe Layered Semiconductor Compound on Si(111)7×7 Substrate—A van der Waals Epitaxy; Vinh, L. T.; Eddrief, M.; Sebenne, C.; Sacuto, A.; Balkanski, M. *J. Cryst. Growth* **1994**, *135*, 1–10.

Te

Surfactant Mediated Growth of Germanium on Silicon (001) with Submonolayer Coverage of Sb and Te; Osten, H. J.; Klatt, J.; Lippert, G.; Bugiel, E.; Higuchi, S. *J. Appl. Phys.* **1993**, *74*, 2507–2511.

Group 17

F

Surface Cleaning for Si Epitaxy Using Photoexcited Fluorine Gas; Aoyama, T.; Yamazaki, T.; Ito, T. *J. Electrochem. Soc.* **1993**, *140*, 366–371.

ESDIAD Studies of Fluorine and Chlorine Adsorption at Si(100); Bennett, S. L.; Greenwood, C. L.; Williams, E. M. *Surf. Sci.* **1993**, *290*, 267–276.

Influence of Single Atomic Height Steps on F_2 Reactions with Si(100)-2×1; Carter, L. E.; Carter, E. A. *J. Vac. Sci. Technol. A* **1994**, *12*, 2235–2239.

Phenomenological Modeling of Ion Enhanced Surface Kinetics in Fluorine Based Plasma Etching; Gray, D. C.; Tepermeister, I.; Sawin, H. H. *J. Vac. Sci. Technol. B* **1993**, *11*, 1243–1257.

Temperature Dependence of Etching with Molecular Fluorine on Si(111) Surface; Hiroi, M.; Tatsumi, T. *Jpn. J. Appl. Phys.* **1994**, *33*, 2244–2247.

Scanning Tunneling Microscopy Investigations of the Si(111) Topography Produced by Etching in 40% NH_4F—Observation of an Optimum Etch Duration; Hsiao, G. S.; Virtanen, J. A.; Penner, R. M. *Appl. Phys. Lett.* **1993**, *63*, 1119–1121.

Influence of Fluorine Preamorphization on the Diffusion and Activation of Low Energy Implanted Boron during Rapid Thermal Annealing; Huang, T. H.; Kinoshita, H.; Kwong, D. L. *Appl. Phys. Lett.* **1994**, *65*, 1829–1831.

Structure of Polycrystalline Silicon Thin Film Fabricated from Fluorinated Precursors by Layer-by-Layer Technique; Ishihara, S.; He, D. Y.; Shimizu, I. *Jpn. J. Appl. Phys.* **1994**, *33*, 51–56.

Dynamics of Ion Assisted Etching in the Si(100)/XeF_2/Ar^+ System on a Time-Scale 100 μs-1000 s; Joosten, G. J. P.; Vugts, M. J. M.; Spruijt, H. J.; Senhorst, H. A. J.; Beijerinck, H. C. W. *J. Vac. Sci. Technol. A* **1994**, *12*, 636–647.

XeF_2 Etching of Si(111)—The Geometric Structure of the Reaction Layer; Lo, C. W.; Shuh, D. K.; Chakarian, V.; Durbin, T. D.; Varekamp, P. R.; Yarmoff, J. A. *Phys. Rev. B* **1993**, *47*, 15648–15659.

Influence of Electronic-Structure on XeF_2 Etching of Silicon; Lo, C. W.; Shuh, D. K.; Yarmoff, J. A. *J. Vac. Sci. Technol. A* **1993**, *11*, 2054–2058.

Substrate Disorder-Induced by a Surface Chemical-Reaction—The Fluorine Silicon Interaction; Lo, C. W.; Varekamp, P. R.; Shuh, D. K.; Durbin, T. D.; Chakarian, V.; Yarmoff, J. A. *Surf. Sci.* **1993**, *292*, 171–181.

Simulation of Bulk Silicon-Crystals and Si(111) Surfaces with Application to a Study of Fluorine Coverage of the Surfaces; Lutrus, C. K.; Oshiro, T.; Hagen, D. E.; Salk, S. H. S. *Phys. Rev. B* **1993**, *48*, 15086–15091.

Fluorine Termination of Silicon Surface by F_2 and Succeeding Reaction with Water; Nakamura, M.; Takahagi, T.; Ishitani, A. *Jpn. J. Appl. Phys.* **1993**, *32*, 3125–3130.

Formation of Hexafluorosilicate on Si Surface Treated in NH_4F Investigated by Photoemission and Surface Infrared Spectroscopy; Niwano, M.; Kurita, K.; Takeda, Y.; Miyamoto, N. *Appl. Phys. Lett.* **1993**, *62*, 1003–1005.

Effects of Ion Bombardment in Plasma Etching on the Fluorinated Silicon Surface-Layer—Real-Time and Postplasma Surface Studies; Oehrlein, G. S. *J. Vac. Sci. Technol. A* **1993**, *11*, 34–46.

Half Monolayer and Monolayer Chemisorption of Fluorine on the Silicon(002)2×2 Surface; Radny, M. W.; Smith, P. V. *Surf. Sci.* **1994**, *301*, 97–104.

Chemisorption of Fluorine on the Silicon(001)2×1 Surface; Radny, M. W.; Smith, P. V. *Vacuum* **1994**, *45*, 293–296.

Role of Implantation Induced Defects in Surface-Oriented Diffusion of Fluorine in Silicon; Szeles, C.; Nielsen, B.; Asokakumar, P.; Lynn, K. G.; Anderle, M.; et al. *J. Appl. Phys.* **1994**, *76*, 3403–3409.

Chemical-Structure and Reactivity of a Silicon Single-Crystal Surface Fluorinated by Xenon Fluo-

ride; Takahagi, T.; Ishitani, A.; Wakao, S. *J. Appl. Phys.* **1994**, *76*, 3140–3143.

Cl

Mechanism of Cleaning and Etching Si Surfaces with Low Energy Chlorine Ion Bombardment; Bello, I.; Chang, W. H.; Lau, W. M. *J. Appl. Phys.* **1994**, *75*, 3092–3097.

ESDIAD Studies of Fluorine and Chlorine Adsorption at Si(100); Bennett, S. L.; Greenwood, C. L.; Williams, E. M. *Surf. Sci.* **1993**, *290*, 267–276.

Manipulating Chlorine Atom Bonding on the Si-(100)-(2×1) Surface with the STM; Boland, J. J. *Science* **1993**, *262*, 1703–1706.

Ion Assisted Etching of Si with Cl_2—The Effect of Flux Ratio; Coburn, J. W. *J. Vac. Sci. Technol. B* **1994**, *12*, 1384–1389.

Dynamics of Dissociative Chemisorption—Cl_2/Si-(111)-(2×1); Devita, A.; Stich, I.; Gillan, M. J.; Payne, M. C.; Clarke, L. J. *Phys. Rev. Lett.* **1993**, *71*, 1276–1279.

Stimulated Desorption of Cl^+ and the Chemisorption of Cl_2 on Si(111)-7×7 and Si(100)-2×1; Durbin, T. D.; Simpson, W. C.; Chakarian, V.; Shuh, D. K.; Varekamp, P. R.; et al. *Surf. Sci.* **1994**, *316*, 257–266.

Mechanisms of Halogen Chemisorption Upon a Semiconductor Surface—I_2, Br_2, Cl_2, and C_6H_5Cl Chemisorption Upon the Si(100) (2×1) Surface; Flaum, H. C.; Sullivan, D. J. D.; Kummel, A. C. *J. Phys. Chem.* **1994**, *98*, 1719–1731.

Chlorine Bonding Sites and Bonding Configurations on Si(100)-(2×1); Gao, Q.; Cheng, C. C.; Chen, P. J.; Choyke, W. J.; Yates, J. T. *J. Chem. Phys.* **1993**, *98*, 8308–8323.

Comparison of Cl_2 and HCl Adsorption on Si(100)-(2×1); Gao, Q.; Cheng, C. C.; Chen, P. J.; Choyke, W. J.; Yates, J. T. *Thin Solid Films* **1993**, *225*, 140–144.

Supersonic Molecular Beam Scattering of Cl_2 from Clean and Alkali-Covered Si(100)2×1; Geuzebroek, F. H.; Babasaki, Y.; Tanaka, M.; Nakamura, T.; Namiki, A. *Surf. Sci.* **1993**, *297*, 141–150.

Broad Pulsed Ga Ion Beam Assisted Etching of Si with Cl_2; Haraichi, S.; Komuro, M. *Jpn. J. Appl. Phys.* **1993**, *32*, 6168–6172.

Study of the Etching Reaction by Atomic Chlorine Using Molecular Beam Scattering; Karahashi, K.; Matsuo, J.; Horiuchi, K. *Jpn. J. Appl. Phys.* **1994**, *33*, 2252–2254.

Ab-initio Calculations of Si, As, S, Se, and Cl Adsorption on Si(001) Surfaces; Kruger, P.; Pollmann, J. *Phys. Rev. B* **1993**, *47*, 1898–1910.

Cl-Cl Interaction and Chlorine Adsorption Mechanism on Si(100) 2×1; Lee, L. Q.; Cao, P. L. *J. Phys.: Condens. Matter* **1994**, *6*, 6169–6175.

Adsorption of Chlorine on Si(100); Mendicino, M. A.; Seebauer, E. G. *Appl. Surf. Sci.* **1993**, *68*, 285–290.

Barrierless Dimer Breaking at Semiconductor Surfaces by Chlorine Atoms; Ohno, T. *Phys. Rev. Lett.* **1993**, *70*, 962–965.

Chemical Kinetics of Chlorine in Electron Cyclotron Resonance Plasma Etching of Si; Ono, K.; Tuda, M.; Nishikawa, K.; Oomori, T.; Namba, K. *Jpn. J. Appl. Phys.* **1994**, *33*, 4424–4432.

Chlorination and Photodesorption on Si(100) and Si(111); Paulsenboaz, C. M.; Rhodin, T. N.; Lang, C. C. *Appl. Surf. Sci.* **1994**, *80*, 72–78.

Dynamics of Dissociative Chemisorption Cl_2/Si-(111)-2×1; Payne, M. C.; Stich, I.; Devita, A.; Gillan, M. J.; Clarke, L. J. *Faraday Discuss. Chem. Soc.* **1993**, *96*, 151–159.

Si(100)2×1-Cl Structure from X-Ray Absorption Spectroscopy; Purdie, D.; Prakash, N. S.; Purcell, K. G.; Wincott, P. L.; Thornton, G.; Law, D. S. L. *Phys. Rev. B* **1993**, *48*, 2275–2281.

Dynamics of Pulsed Ultraviolet Laser Enhancement of the Chlorine-Si(111) Reaction; Rhodin, T. N.; Paulsenboaz, C.; Obrien, W. L. *Surf. Sci.* **1993**, *283*, 109–116.

First-Order Isothermal Desorption Kinetics of Chlorine on SiH_2Cl_2-Adsorbed Si(100) Surface; Sakamoto, H.; Takakuwa, Y.; Hori, T.; Horie, T.; Miyamoto, N. *Appl. Surf. Sci.* **1994**, *75*, 27–32.

The Interaction of Chlorine with Si(100)2×1 Studied Using Soft X-Ray Photoemission and Photon Stimulated Ion Desorption; Sterratt, D.; Greenwood, C. L.; Williams, E. M.; Muryn, C. A.; Wincott, P. L.; et al. *Surf. Sci.* **1994**, *309*, 269–273.

High Reaction Selectivity on UV Laser-Induced Desorption from Chlorinated Si(111) 7×7 Studied by Scanning Tunneling Microscopy; Suguri, M.; Shudo, K.; Komori, F.; Murata, Y. *J. Phys.: Condens. Matter* **1993**, *5*, 6607–6612.

Precursor and Direct Activated Chemisorption of Chlorine Molecules Onto Si(111) (7×7) and Si(100) (2×1) Surfaces; Sullivan, D. J. D.; Flaum, H. C.; Kummel, A. C. *J. Phys. Chem.* **1993**, *97*, 12051–12060.

Etching of Si with Cl_2 Using an Electron Cyclotron Resonance Source; Sung, K. T.; Pang, S. W. *J. Vac. Sci. Technol. A* **1993**, *11*, 1206–1210.

Characterization of Etch Induced Damage for Si Etched in Cl_2 Plasma Generated by an Electron Cyclotron Resonance Source; Sung, K. T.; Pang, S. W. *J. Vac. Sci. Technol. A* **1994**, *12*, 1346–1350.

Etching of Si Surfaces with Hot Chlorine Beams—Translational and Vibrational Excitation of the Incident Chlorine Particles; Szabo, A.; Engel, T. *J. Vac. Sci. Technol. A* **1994**, *12*, 648–657.

Reactions of Chlorine with Si(100) and Si-(111)—Adsorption and Desorption Kinetics; Szabo, A.; Farrall, P. D.; Engel, T. *Surf. Sci.* **1994**, *312*, 284–300.

Thermal and Direct Etching Mechanisms of Si(100) with a Hyperthermal Chlorine Beam; Szabo, A.; Farrall, P. D.; Engel, T. *J. Appl. Phys.* **1994**, *75*, 3623–3626.

Adsorption and Desorption of $AlCl_3$ on Si(111)7×7 Observed by Scanning Tunneling Microscopy and Atomic Force Microscopy; Uesugi, K.; Takiguchi, T.; Izawa, M.; Yoshimura, M.; Yao, T. *Jpn. J. Appl. Phys.* **1993**, *32*, 6200–6202.

Large Island Formation Versus Single Site Adsorption for Cl_2 Chemisorption Onto Si(111)-(7×7) Surfaces; Yan, C.; Jensen, J. A.; Kummel, A. C. *Phys. Rev. Lett.* **1994**, *72*, 4017–4020.

Halogen Surface Chemistry on Si(100)-(2×1); Yates, J. T.; Cheng, C. C.; Gao, Q.; Choyke, W. J. *Surf. Sci. Rep.* **1993**, *19*, 79–86.

Photon Stimulated Desorption Mechanism of Cl^+ Ions from Cl/Si(111) Surface; Yonezawa, T.; Daimon, H.; Nakatsuji, K.; Sakamoto, K.; Suga, S.; et al. *Jpn. J. Appl. Phys.* **1994**, *33*, 2248–2251.

Velocity Distributions of Nascent $SiCl_n$ (n = 2, 3 and 4) Products Formed from the Reaction of Si(111) with a Cl_2 Beam; Yoshikawa, H.; Shobatake, K. *Chem. Phys. Lett.* **1994**, *223*, 341–346.

Br

The Bonding Characterization of Br on Si(100) 2×1; Cao, P. L.; Zhou, R. H. *J. Phys.: Condens. Matter* **1993**, *5*, 2897–2902.

Layer-by-Layer Etching of Si(100)-2×1 with Br_2—A Scanning Tunneling Microscopy Study; Chander, M.; Li, Y. Z.; Patrin, J. C.; Weaver, J. H. *Phys. Rev. B* **1993**, *47*, 13035–13038.

Patterning of Si(100)—Spontaneous Etching with Br_2; Chander, M.; Li, Y. Z.; Rioux, D.; Weaver, J. H. *Phys. Rev. Lett.* **1993**, *71*, 4154–4157.

RbBr/Si(111) Interface Studied by the X-Ray Standing-Wave Method; Etelaniemi, V.; Michel, E. G.; Materlik, G. *Surf. Sci.* **1993**, *287*, 288–293.

Mechanisms of Halogen Chemisorption Upon a Semiconductor Surface—I_2, Br_2, Cl_2, and C_6H_5Cl Chemisorption Upon the Si(100) (2×1) Surface; Flaum, H. C.; Sullivan, D. J. D.; Kummel, A. C. *J. Phys. Chem.* **1994**, *98*, 1719–1731.

The Bromination Binding of Photosensitive Dyes on Monocrystalline Silicon Surface and Their Surface Photovoltage Spectroscopy; Hao, J. X.; Song, J. H.; Zhang, Z. X.; Cao, Z. X. *Chin. Sci. Bull.* **1994**, *39*, 107–112.

Enhancement of Emission of Si Atoms from Si(100) Surface by Low Rate Br Exposure—A New Model of Dry Etching Based on Defect-Adsorbate Interaction; Kanasaki, J. I.; Yu, I. K.; Nakai, Y.; Itoh, N. *Jpn. J. Appl. Phys.* **1994**, *33*, 2255–2257.

Influence of Si Surface Structure on Reaction Mechanism—Atomic Hydrogen Plus Adsorbed Br; Koleske, D. D.; Gates, S. M. *J. Chem. Phys.* **1993**, *98*, 5091–5094.

Kinetics of Atomic Hydrogen Plus Adsorbed Br Reactions on Si(100) and Si(111) Surfaces; Koleske, D. D.; Gates, S. M. *J. Chem. Phys.* **1993**, *99*, 8218–8228.

Bromine Interaction with Si(100)-2×1—Chemisorption and Initial Stages of Etching; Rioux, D.; Chander, M.; Li, Y. Z.; Weaver, J. H. *Phys. Rev. B* **1994**, *49*, 11071–11079.

Temperature Dependent Surface Morphologies for Br-Etched Si(100)-2×1; Rioux, D.; Pechman, R. J.; Chander, M.; Weaver, J. H. *Phys. Rev. B* **1994**, *50*, 4430–4438.

X-Ray Photoelectron Spectroscopic Study of Si(111) and Si(100) Surfaces with Chemically Adsorbed Bromine; Sekar, K.; Kuri, G.; Mahapatra, D. P.; Dev, B. N.; Ramana, J. V.; et al. *Surf. Sci.* **1994**, *302*, 25–36.

Halogen Surface Chemistry on Si(100)-(2×1); Yates, J. T.; Cheng, C. C.; Gao, Q.; Choyke, W. J. *Surf. Sci. Rep.* **1993**, *19*, 79–86.

I

The Adsorption of I_2 on Si(111)-7×7 Studied by Soft X-Ray Photoemission; Chakarian, V.; Shuh, D. K.; Yarmoff, J. A.; Hakansson, M. C.; Karlsson, U. O. *Surf. Sci.* **1993**, *296*, 383–392.

Halogen Surface Chemistry on Si(100)-(2×1); Yates, J. T.; Cheng, C. C.; Gao, Q.; Choyke, W. J. *Surf. Sci. Rep.* **1993**, *19*, 79–86.

Group 18

Rare Gases

Codoping Effects of As and Xe on Ion Beam Induced Epitaxial Crystallization of Si; Hasegawa, M.; Kobayashi, N.; Hayashi, N. *Nucl. Instrum. Methods Phys. Res. Sect. B* **1993**, *80/81*, 674–678.

Argon Incorporation in Si(100) by Ion Bombardment at 15–100 eV; Lau, W. M.; Bello, I.; Huang, L. J.; Feng, X.; Vos, M.; Mitchell, I. V. *J. Appl. Phys.* **1993**, *74*, 7101–7106.

Quantitative Analysis of Low Energy Xe^+ Ion Bombardment Damage of Si(100) Surfaces Using X-Ray Photoelectron Spectroscopy; Lu, Z. H.; Mitchell, D. F.; Graham, M. J. *Appl. Phys. Lett.* **1994**, *65*, 552–554.

Electrical Properties of He-Implantation Produced Nanocavities in Silicon; Seager, C. H.; Myers, S. M.; Anderson, R. A.; Warren, W. L.; Follstaedt, D. M. *Phys. Rev. B* **1994**, *50*, 2458–2473.

Scanning Tunneling Microscopy Study of Solid Phase Epitaxy Processes of Argon Ion Bombarded Silicon Surface and Recovery of Crystallinity by Annealing; Uesugi, K.; Yoshimura, M.; Yao, T.; Sato, T.; Sueyoshi, T.; Iwatsuki, M. *J. Vac. Sci. Technol. B* **1994**, *12*, 2018–2021.

Rare Earth Metals

Sm

Valency Changeover at the Sm/Si(111)7×7 Interface Through Chemisorption and Epitaxy; Sakho, O.; Desantis, M.; Sacchi, M.; Sirotti, F.; Rossi, G. *Appl. Surf. Sci.* **1993**, *65/66*, 729–734.

Sm-Induced and Yb-Induced Reconstructions of the Si(111) Surface; Wigren, C.; Andersen, J. N.; Nyholm, R.; Gothelid, M.; Hammar, M.; et al. *Phys. Rev. B* **1993**, *48*, 11014–11019.

Formation of Sm Silicides on Si(111)—Composition and Epitaxy; Wigren, C.; Andersen, J. N.; Nyholm, R.; Karlsson, U. O. *Surf. Sci.* **1993**, *293*, 254–259.

Gd

Growth, Characterization and Electrical Properties of Gadolinium Silicide Thin Layers; Travlos, A.; Aloupogiannis, P.; Rokofyllou, E.; Papastaikoudis, C.; Traverse, A.; Weber, G. *Philos. Mag. B* **1993**, *67*, 485–495.

Tb

A Study of the Oxide Grown on Tb and Terbium Silicide by XPS, AES and Xrd; Berning, G. L. P.; Swart, H. C. *Appl. Surf. Sci.* **1994**, *78*, 339–343.

Er

Electrical and Photoelectrical Properties of $ErSi_{1.7}$/Si Junctions; Muret, P.; Vonblanckenhagen, G.; Lefki, K.; Tan, T. A. N.; Lollman, D. *Appl. Surf. Sci.* **1993**, *65/66*, 725–728.

Optical Doping of Silicon with Erbium by Ion Implantation; Polman, A.; Custer, J. S.; Snoeks, E.; Vandenhoven, G. N. *Nucl. Instrum. Methods Phys. Res. Sect. B* **1993**, *80/81*, 653–658.

Growth of Er-Doped Si Films by Electron Cyclotron Resonance Plasma Enhanced Chemical Vapor Deposition; Rogers, J. L.; Varhue, W. J.; Adams, E.; Lavoie, M. A.; Frenette, R. O. *J. Vac. Sci. Technol. A* **1994**, *12*, 2762–2766.

Electronic Structure and Interfacial Geometry of Epitaxial 2-Dimensional Er Silicide on Si(111); Stauffer, L.; Mharchi, A.; Pirri, C.; Wetzel, P.; Bolmont, D.; et al. *Phys. Rev. B* **1993**, *47*, 10555–10562.

$Si/ErSi_{1.7}$ Interfaces and Si Reepitaxy on the $ErSi_{1.7}$/Si Structure; Tan, T. A. N.; Veuillen, J. Y.; Kennou, S.; Magaud, L. *Appl. Surf. Sci.* **1993**, *70/71*, 520–525.

Atomic Structure of Epitaxial Er Silicides Grown on Si(111) Studied by Surface Extended X-Ray Absorption Fine Structure; Tuilier, M. H.; Pirri, C.; Wetzel, P.; Gewinner, G.; Veuillen, J. Y.; Tan, T. A. N. *Surf. Sci.* **1994**, *309*, 710–715.

Interfacial Structure of 2-Dimensional Epitaxial Er Silicide on Si(111); Tuilier, M. H.; Wetzel, P.; Pirri, C.; Bolmont, D.; Gewinner, G. *Phys. Rev. B* **1994**, *50*, 2333–2338.

Conduction Mechanisms in Erbium Silicide Schottky Diodes; Unewisse, M. H.; Storey, J. W. V. *J. Appl. Phys.* **1993**, *73*, 3873–3879.

Electronic Structure of Erbium Silicide Ultra Thin Films; Veuillen, J. Y.; Tan, T. A. N.; Lollman, D. B. B. *Surf. Sci.* **1993**, *293*, 86–92.

Epitaxial Er Silicide Formation on Si(111) in the Monolayer Range; Wetzel, P.; Pirri, C.; Bolmont, D.; Gewinner, G. *Appl. Surf. Sci.* **1993**, *65/66*, 718–724.

Yb

The Growth of Epitaxial Yb Silicide—A Study with STM; Hofmann, R.; Netzer, F. P.; Patchett, A. J.; Barrett, S. D.; Leibsle, F. M. *Surf. Sci.* **1993**, *291*, 402–410.

Sm-Induced and Yb-Induced Reconstructions of the Si(111) Surface; Wigren, C.; Andersen, J. N.; Nyholm, R.; Gothelid, M.; Hammar, M.; et al. *Phys. Rev. B* **1993**, *48*, 11014–11019.

Adsorption Site Determination of Ordered Yb on Si(111) Surfaces; Wigren, C.; Andersen, J. N.; Nyholm, R.; Karlsson, U. O.; Nogami, J.; et al. *Phys. Rev. B* **1993**, *47*, 9663–9668.

Hydrides

Silanes

Species-Specific Growth-Kinetics and Film Properties in Synchrotron Radiation Excited Si Growth with Disilane; Akazawa, H.; Utsumi, Y.; Nagase, M. *Appl. Surf. Sci.* **1994**, *80*, 299–303.

Growth-Kinetics of Micrometer-Size Silicon Lines Produced by Decomposition of Silane Using a Laser Direct-Writing Technique; Boughaba, S.; Auvert, G.; Pauleau, Y. *J. Appl. Phys.* **1994**, *75*, 3635–3642.

Si(001)2×1 Gas Source Molecular Beam Epitaxy from Si_2H_6—Growth-Kinetics and Boron Doping; Bramblett, T. R.; Lu, Q.; Hasan, M. A.; Jo, S. K.; Greene, J. E. *J. Appl. Phys.* **1994**, *76*, 1884–1888.

Adsorption and Dissociation of Disilane on Si(001) Studied by STM; Bronikowski, M. J.; Wang, Y. J.; McEllistrem, M. T.; Chen, D.; Hamers, R. J. *Surf. Sci.* **1993**, *298*, 50–62.

Study of Growth-Kinetics in Silicon Gas Source Molecular Beam Epitaxy with Disilane Using RHEED Intensity Oscillations; Butzke, S.; Werner, K.; Trommel, J.; Radelaar, S.; Balk, P. *Thin Solid Films* **1993**, *228*, 27–31.

Modeling Silicon Epitaxial Growth with SiH_2Cl_2; Coon, P. A.; Wise, M. L.; George, S. M. *J. Cryst. Growth* **1993**, *130*, 162–172.

Adsorption and Reactions of Diethylsilane on Si(100); Darlington, B.; Foster, M.; Campion, A. *Surf. Sci.* **1994**, *304*, 407–412.

Mechanistic Insight into Gas-Phase Reactions of $H^{\cdot} + Si_2H_6$ and Hydrogen-Atom Etching of Silicon Surfaces; Dobbs, K. D.; Doren, D. J. *J. Am. Chem. Soc.* **1993**, *115*, 3731–3738.

Interaction of Copper-Catalysts and Si(100) for the Direct Synthesis of Methylchlorosilanes; Floquet, N.; Yilmaz, S.; Falconer, J. L. *J. Catal.* **1994**, *148*, 348–368.

Numerical Evaluation of Silicon-Thin Film Growth from $SiHCl_3$-H_2 Gas-Mixture in a Horizontal Chemical Vapor Deposition Reactor; Habuka, H.; Katayama, M.; Shimada, M.; Okuyama, K. *Jpn. J. Appl. Phys.* **1994**, *33*, 1977–1985.

Effect of Heating SiH_4 on the Plasma Chemical Vapor Deposition of Hydrogenated Amorphous Silicon; Hishikawa, Y.; Sasaki, M.; Tsuge, S.; Tsuda, S. *Jpn. J. Appl. Phys.* **1994**, *33*, 4373–4376.

Kinetics of the Low Pressure Chemical Vapor Deposition of Polycrystalline Germanium-Silicon Alloys from SiH_4 and GeH_4; Holleman, J.; Kuiper, A. E. T.; Verweij, J. F. *J. Electrochem. Soc.* **1993**, *140*, 1717–1722.

Hydrogen Desorption Rate and Surface Hydrogen Coverage during Isothermal Annealing for Si_2H_6-Adsorbed Si(100) Surfaces; Horie, T.; Takakuwa, Y.; Yamaguchi, T.; Miyamoto, N. *J. Cryst. Growth* **1994**, *136*, 344–348.

Conditions for Successful Low Temperature Growth of Hydrogenated Amorphous Silicon Film from Silyl Radicals Conformed to Layer-Growth Mode; Kawasaki, M.; Suzuki, H.; Kawaguchi, Y. *Appl. Surf. Sci.* **1994**, *80*, 310–315.

Hydrogen Desorption Kinetics from the Growing Si(100) Surface during Silane Gas Source Molecular Beam Epitaxy; Kim, K. J.; Suemitsu, M.; Miyamoto, N. *Appl. Phys. Lett.* **1993**, *63*, 3358–3360.

Photoirradiation Effects on Surface-Reactions in Si Monolayer Overgrowth by Si_2H_6 Source MBE; Koide, Y.; Zaima, S.; Okada, M.; Yasuda, Y. *Appl. Surf. Sci.* **1994**, *80*, 304–309.

Thermal Reactions of Disilane on Si(100) Studied by Synchrotron-Radiation Photoemission; Lin, D. S.; Miller, T.; Chiang, T. C.; Tsu, R.; Greene, J. E. *Phys. Rev. B* **1993**, *48*, 11846–11850.

Effects of SiH_4, GeH_4, and B_2H_6 on the Nucleation and Deposition of Polycrystalline $Si_{1-x}Ge_x$ Films; Lin, H. C.; Chang, C. Y.; Chen, W. H.; Tsai, W. C.; Chang, T. C.; et al. *J. Electrochem. Soc.* **1994**, *141*, 2559–2563.

Si Atomic Layer Epitaxy Based on Si_2H_6 and Remote He Plasma Bombardment; Mahajan, A.; Irby, J.; Kinosky, D.; Qian, R.; Thomas, S.; et al. *Thin Solid Films* **1993**, *225*, 177–182.

Surface Chemistry of Diethylsilane and Diethylgermane on Si(100)—An Atomic Layer Epitaxy Approach; Mahajan, A.; Kellerman, B. K.; Russell, N. M.; Banerjee, S.; Campion, A.; et al. *J. Vac. Sci. Technol. A* **1994**, *12*, 2265–2270.

Adsorption of $TiCl_4$, SiH_4, and HCl on Si(100)—Application to $TiSi_2$ Chemical Vapor Deposition and Si Etching; Mendicino, M. A.; Seebauer, E. G. *J. Electrochem. Soc.* **1993**, *140*, 1786–1793.

Growth-Rate Dependence on GeH_4 during Gas Source MBE of Si_xGe_{1-x} Alloys Grown from Si_2H_6 and GeH_4; Mokler, S. M.; Ohtani, N.; Xie, M. H.; Zhang, X.; Joyce, B. A. *J. Cryst. Growth* **1993**, *127*, 467–471.

Metal Impurity Evaluation in Silane Gas from the Qualification of Poly-Si Layers; Morin, M.; Koyanagi, M.; Friedt, J. M.; Hirose, M. *J. Electrochem. Soc.* **1994**, *141*, 274–277.

Si Deposition from Chlorosilanes. 1. Deposition Modeling; Narusawa, U. *J. Electrochem. Soc.* **1994**, *141*, 2072–2077.

Si Deposition from Chlorosilanes. 2. Numerical-Analysis of Thermofluid Effects on Deposition; Narusawa, U. *J. Electrochem. Soc.* **1994**, *141*, 2078–2083.

Effects of SiH_2Cl_2 on Low Temperature (≤200 °C) Si Epitaxy by Photochemical Vapor Deposition; Oshima, T.; Sano, M.; Yamada, A.; Konagai, M.; Takahashi, K. *Appl. Surf. Sci.* **1994**, *80*, 215–219.

On the Homogeneous Chemistry of the Thermal Decomposition of Methyltrichlorosilane—Thermodynamic Analysis and Kinetic Modeling; Papasouliotis, G. D.; Sotirchos, S. V. *J. Electrochem. Soc.* **1994**, *141*, 1599–1611.

The Effect of Zn Promoter on Enhanced Diffusion during Catalytic Formation of Methylchlorosilanes; Potochnik, S. J.; Falconer, J. L. *J. Catal.* **1994**, *147*, 101–106.

Adsorption and Decomposition of Diethylsilane and Diethyldichlorosilane by Si(100)(2×1) and Si(111)-(1×1); Schmidt, J.; Stuhlmann, C.; Ibach, H. *Surf. Sci.* **1994**, *302*, 10–24.

Effects of Trace Surface Oxidation in Low Temperature Epitaxy-Grown from Dichlorosilane; Sedgwick, T. O.; Agnello, P. D.; Grutzmacher, D. A. *J. Electrochem. Soc.* **1993**, *140*, 3684–3688.

Photoelectron Intensity Oscillation during Chemical Vapor Deposition on Si(100) Surface with Si_2H_6; Takakuwa, Y.; Enta, Y.; Yamaguchi, T.; Hori, T.; Niwano, M.; et al. *Appl. Phys. Lett.* **1994**, *64*, 2013–2015.

Growth Defect Observation with Pyramidal Hillock and Reduction by Photoexcited Hydrogen in Si CVD with SiH_2Cl_2; Takakuwa, Y.; Mazumder, M. K.; Miyamoto, N. *J. Electrochem. Soc.* **1994**, *141*, 2567–2572.

Chemically Vapor Deposited Tungsten Silicide Films Using Dichlorosilane in a Single-Wafer Reactor—Growth, Properties, and Thermal Stability; Telford, S. G.; Eizenberg, M.; Chang, M.; Sinha, A. K.; Gow, T. R. *J. Electrochem. Soc.* **1993**, *140*, 3689–3701.

Synchrotron-Radiation Assisted Si Epitaxial Growth—Comparison of Growth-Characteristics Between Si_2H_6 and SiH_2Cl_2 Gases; Urisu, T.; Akutsu, T.; Kuchitsu, K. *Appl. Phys. Lett.* **1993**, *62*, 2821–2823.

Synchrotron Radiation Assisted Si Epitaxial Growth Using Si_2H_6 and SiH_2Cl_2 Gases—Properties in the Low Temperature Region; Urisu, T.; Takahashi, J.; Utsumi, Y.; Akutsu, T.; Kuchitsu, K. *J. Electrochem. Soc.* **1994**, *141*, 1562–1565.

An Atomically Resolved Scanning Tunneling Microscopy Study of the Thermal Decomposition of Disilane on Si(001); Wang, Y. J.; Bronikowski, M. J.; Hamers, R. J. *Surf. Sci.* **1994**, *311*, 64–100.

Evidence for Non-Hydrogen Desorption Limited Growth of Si from Disilane at Very-Low Temperatures in Gas Source Molecular Beam Epitaxy; Werner, K.; Butzke, S.; Radelaar, S.; Balk, P. *J. Cryst. Growth* **1994**, *136*, 338–343.

Adsorption of Hydrogen and Disilane on Si(100) and Si-Ge Surfaces; Wu, Y. M.; Nix, R. M. *Surf. Sci.* **1994**, *306*, 59–68.

Nitrogen Hydrides

A Photoemission Study of Ammonia Adsorption on Si(100)2×1 and Si(111)2×1 Surfaces; Bischoff, J. L.; Kubler, L.; Bolmont, D.; Sebenne, C. A.; Lacharme, J. P.; et al. *Surf. Sci.* **1993**, *293*, 35–40.

Contrasted Behavior of Si(001) and Si(111) Surfaces with Respect to NH_3 Adsorption and Thermal Nitridation—A N1s and Si2p Core Level Study with Synchrotron Radiation; Dufour, G.; Rochet, F.; Roulet, H.; Sirotti, F. *Surf. Sci.* **1994**, *304*, 33–47.

Real-Time, In-Situ Monitoring of Room Temperature Silicon Surface Cleaning Using Hydrogen and Ammonia Plasmas; Zhou, Z. H.; Aydil, E. S.; Gottscho, R. A.; Chabal, Y. J.; Reif, R. *J. Electrochem. Soc.* **1993**, *140*, 3316–3321.

Surface Chemistry of N_2H_4 on Si(100)-2×1; Bu, Y.; Lin, M. C. *Surf. Sci.* **1994**, *311*, 385–394.

The 308 nm Laser Photodissociation of HN_3 Adsorbed on Si(111)-7×7; Bu, Y.; Lin, M. C. *Surf. Sci.* **1994**, *301*, 118–128.

Spectroscopy and Reactions of Hydrazoic Acid on Silicon Single Crystal Surfaces. 3. HN_3 and DN_3 on Si(111)(7×7); Chu, J. C. S.; Bu, Y.; Lin, M. C. *Surf. Sci.* **1993**, *284*, 281–290.

PH_3

Adsorption and Dissociation of PH_3 on Si(100) 2×1 and Si(111) 7×7—Theoretical Study; Cao, P. L.; Lee, L. Q.; Dai, J. J.; Zhou, R. H. *J. Phys.: Condens. Matter* **1994**, *6*, 6103–6109.

An Atomically Resolved STM Study of the Interaction of Phosphine with the Silicon(001) Surface;

Wang, Y. J.; Bronikowski, M. J.; Hamers, R. J. *J. Phys. Chem.* **1994**, *98*, 5966–5973.

AsH_3

Arsine Absorption on Si(100) 2×1—A Photoemission and Scanning Tunneling Microscopy Study; Kipp, L.; Bringans, R. D.; Biegelsen, D. K.; Swartz, L. E.; Hicks, R. F. *Phys. Rev. B* **1994**, *50*, 5448–5455.

H_2O

Water Adsorption on the Si(110) Surface; Alhayek, I.; Katircioglu, S. *Surf. Sci.* **1993**, *286*, 92–96.

Insitu Observation of Water Adsorption on Si(100) with Scanning Tunneling Microscopy; Andersohn, L.; Kohler, U. *Surf. Sci.* **1993**, *284*, 77–90.

Influence of Capillary Condensation of Water on Nanotribology Studied by Force Microscopy; Binggeli, M.; Mate, C. M. *Appl. Phys. Lett.* **1994**, *65*, 415–417.

Structure Analysis of O_2 and H_2O Chemisorption on a Si(100) Surface; Bu, H.; Rabalais, J. W. *Surf. Sci.* **1994**, *301*, 285–294.

The Mechanism of Ion Desorption from H_2O/Si(100) by O1s Electron Excitation; Ikeura, H.; Sekiguchi, T.; Tanaka, K.; Obi, K.; Ueno, N.; Honma, K. *Jpn. J. Appl. Phys.* **1993**, *32*, 246–248.

Chemisorption of H, H_2O and C_2H_4 on Si(113)—Implications for the Structure; Jacobi, K.; Myler, U. *Surf. Sci.* **1993**, *284*, 223–235.

Early Stages of H_2O Adsorption on Clean Si(100); Lacharme, J. P.; Sebenne, C.; Cherif, S. M.; Chikhi, M.; Safta, N.; Zaibi, M. A. *Appl. Surf. Sci.* **1993**, *65/66*, 598–602.

An Oxygen K-Edge NEXAFS Study of H_2O Adsorption on Si(111); Lindsay, R.; Wincott, P. L.; Muryn, C. A.; Thornton, G.; Frigo, S. P.; et al. *Jpn. J. Appl. Phys.* **1993**, *32*, 347–349.

The Growth of Ice Clusters on the Si(100)(2×1)-H(D) Surface—Electron Energy Loss Spectroscopy and Thermal Desorption Studies; Takagi, N.; Minami, N.; Furukawa, T.; Nishijima, M. *Surf. Sci.* **1993**, *297*, 43–47.

Auger Electron Spectroscopy Electron Beam Induced Damage of a H_2O-Covered Si(100) Surface; Viscido, L.; Heras, J. M. *J. Vac. Sci. Technol. A* **1993**, *11*, 175–179.

Atomic Step Structure on Vicinal H/Si(111) Surface Formed by Hot Water Immersion; Watanabe, S.; Horiuchi, K.; Ito, T. *Jpn. J. Appl. Phys.* **1993**, *32*, 3420–3425.

H_2O_2

Chemical Treatment Effects of Si Surfaces in NH_4-OH H_2O_2 H_2O Solutions Studied by Spectroscopic Ellipsometry; Adachi, S.; Utani, K. *Jpn. J. Appl. Phys.* **1993**, *32*, 1189–1191.

Influence of HF-H_2O_2 Treatment on Si(100) and Si(111) Surfaces; Graf, D.; Bauermayer, S.; Schnegg, A. *J. Appl. Phys.* **1993**, *74*, 1679–1683.

HF

Electronic-Properties of the HF-Passivated Si(111) Surface during the Initial Oxidation in Air; Dittrich, T.; Angermann, H.; Fussel, W.; Flietner, H. *Phys. Status Solidi A* **1993**, *140*, 463–470.

Reaction of NH_4F/HF Solutions on Si(100) and Si(111) Surfaces; Graf, D.; Bauermayer, S.; Schnegg, A. *J. Vac. Sci. Technol. A* **1993**, *11*, 940–944.

Preferential Local Dissolution of Indented Silicon (111) Surface by Aqueous-Solutions of HF with Varying pH; Katayama, K.; Senna, M. *Solid State Ionics* **1994**, *73*, 127–137.

Spectroscopic Ellipsometry Studies of HF Treated Si(100) Surfaces; Yao, H.; Woollam, J. A.; Alterovitz, S. A. *Appl. Phys. Lett.* **1993**, *62*, 3324–3326.

Effects of Predeposition HF/NH_4F Treatments on the Electrical-Properties of SiO_2/Si Structures Formed by Low Temperature Plasma Assisted Oxidation and Deposition Processes; Yasuda, T.; Ma, Y.; Chen, Y. L.; Lucovsky, G.; Maher, D. *J. Vac. Sci. Technol. A* **1993**, *11*, 945–951.

In-Situ Internal-Reflection Infrared Study of Aqueous Hydrofluoric-Acid and Ultraviolet Ozone Treated Silicon(100) Surfaces; Zazzera, L.; Evans, J. F. *J. Vac. Sci. Technol. A* **1993**, *11*, 934–939.

Electron Desorption Study of HF Etched Si(100); Craig, J. H.; Cariss, C.; Craig, M. J. *J. Vac. Sci. Technol. A* **1993**, *11*, 554–556.

Effect of Surface Treatments After HF Etching on Oxidation of Si; Egawa, M.; Ikoma, H. *Jpn. J. Appl. Phys.* **1994**, *33*, 943–949.

Influence of HF-H_2O_2 Treatment on Si(100) and Si(111) Surfaces; Graf, D.; Bauermayer, S.; Schnegg, A. *J. Appl. Phys.* **1993**, *74*, 1679–1683.

Characterization of HF-Treated Si(111) Surfaces; Konishi, T.; Uesugi, K.; Takaoka, K.; Kawano, S.; Yoshimura, M.; Yao, T. *Jpn. J. Appl. Phys.* **1993**, *32*, 3131–3134.

Local Modification of HF-Treated Silicon (100) Surface and Its Characterization by Scanning Tunneling Microscopy and Spectroscopy; Perezmurano, F.; Barniol, N.; Aymerich, X. *J. Vac. Sci. Technol. B* **1993**, *11*, 651–657.

Anisotropic Etching Versus Interaction of Atomic Steps—Scanning Tunneling Microscopy Observations on HF/NH_4F-Treated Si(111); Pietsch, G. J.; Kohler, U.; Henzler, M. *J. Appl. Phys.* **1993**, *73*, 4797–4807.

UltraHigh Vacuum Surface Analysis of Silicon (100) Treated in Aqueous Hydrofluoric Acid and Buffered Hydrofluoric Acid Solutions; Sauer, D. E.; Stuve, E. M. *Appl. Surf. Sci.* **1994**, *78*, 47–55.

HF-Treated (111), (110) and (100) Si Surfaces Studied by Spectroscopic Ellipsometry; Utani, K.; Adachi, S. *Jpn. J. Appl. Phys.* **1993**, *32*, 3572–3576.

HF-Treated and NH_4OH-Treated (111)Si Surfaces Studied by Spectroscopic Ellipsometry; Utani, K.; Suzuki, T.; Adachi, S. *J. Appl. Phys.* **1993**, *73*, 3467–3471.

On the Electrical Impedance Due to the Anodic Dissolution of Silicon in HF Solutions; Vanmaekelbergh, D.; Searson, P. C. *J. Electrochem. Soc.* **1994**, *141*, 697–702.

HCl

Comparison of Cl_2 and HCl Adsorption on Si(100)-(2×1); Gao, Q.; Cheng, C. C.; Chen, P. J.; Choyke, W. J.; Yates, J. T. *Thin Solid Films* **1993**, *225*, 140–144.

Adsorption of $TiCl_4$, SiH_4, and HCl on Si(100)—Application to $TiSi_2$ Chemical Vapor Deposi-

tion and Si Etching; Mendicino, M. A.; Seebauer, E. G. *J. Electrochem. Soc.* **1993**, *140*, 1786–1793.

HBr

Optimization of an Electron Cyclotron Resonance Plasma Etch Process for N+ Polysilicon–HBr Process Chemistry; Tipton, G. D.; Blain, M. G.; Westerfield, P. L.; Trutna, L. S.; Maxwell, K. L. *J. Vac. Sci. Technol. B* **1994**, *12*, 416–421.

Oxides

O_3

Infrared Spectroscopic Study of Initial Stages of Ultraviolet Ozone Oxidation of Si(100) and Si(111) Surfaces; Niwano, M.; Kageyama, J.; Kinashi, K.; Miyamoto, N.; Honma, K. *J. Vac. Sci. Technol. A* **1994**, *12*, 465–470.

Native Oxide Growth and Organic Impurity Removal on Si Surface with Ozone Injected Ultrapure Water; Ohmi, T.; Isagawa, T.; Kogure, M.; Imaoka, T. *J. Electrochem. Soc.* **1993**, *140*, 804–810.

CO

CO Chemisorption on Small Cobalt Particles Deposited on Si(111); Bogdanyi, G.; Zsoldos, Z.; Peto, G.; Guczi, L. *Surf. Sci.* **1994**, *306*, 563–568.

Interaction of CO with Silicon Single Crystal Surfaces Studied by HREELS, UPS and TPD; Yue, B.; Lin, M. C. *Surf. Sci.* **1993**, *298*, 94–100.

SiO_2

The Effects of Polishing Damage and Oxygen Concentration on Gate Oxide Integrity in Silicon-Crystals; Abe, T.; Kato, Y. *Jpn. J. Appl. Phys.* **1993**, *32*, 1879–1883.

Modifications in the Si Valence-Band After Ion Beam-Induced Oxidation; Alay, J. L.; Vandervorst, W. *J. Vac. Sci. Technol. A* **1994**, *12*, 2420–2424.

SiO_x Surface Stoichiometry by XPS—A Comparison of Various Methods; Alfonsetti, R.; Desimone, G.; Lozzi, L.; Passacantando, M.; Picozzi, P.; Santucci, S. *Surf. Interface Anal.* **1994**, *22*, 89–92.

Investigation of Native-Oxide Growth on HF-Treated Si(111) Surfaces by Measuring the Surface-State Distribution; Angermann, H.; Dittrich, T.; Flietner, H. *Appl. Phys. A* **1994**, *59*, 193–197.

Growth and Characterization of Room Temperature Anodic SiO_2 Films; Bardwell, J. A.; Clark, K. B.; Mitchell, D. F.; Bisaillion, D. A.; Sproule, G. I.; et al. *J. Electrochem. Soc.* **1993**, *140*, 2135–2138.

Effect of Carbon on Thermal Oxidation of Silicon and Electrical-Properties of SiO_2-Si Structures; Beck, R. B.; Brozek, T.; Ruzyllo, J.; Hossain, S. D.; Tressler, R. E. *J. Electron. Mater.* **1993**, *22*, 689–694.

2nd-Harmonic Generation in Si–SiO_2 Heterostructures Formed by Chemical, Thermal, and Plasma Assisted Oxidation and Deposition Processes; Bjorkman, C. H.; Shearon, C. E.; Ma, Y.; Yasuda, T.; Lucovsky, G.; et al. *J. Vac. Sci. Technol. A* **1993**, *11*, 964–970.

Influence of Surface-Roughness on the Electrical-Properties of Si–SiO_2 Interfaces and on 2nd-Harmonic Generation at These Interfaces; Bjorkman, C. H.; Yasuda, T.; Shearon, C. E.; Ma, Y.; Lucovsky, G.; et al. *J. Vac. Sci. Technol. B* **1993**, *11*, 1521–1527.

Mechanism of Submonolayer Oxide Formation on Silicon Surfaces Upon Thermal Oxidation; Borman, V. D.; Gusev, E. P.; Lebedinski, Y. Y.; Troyan, V. I. *Phys. Rev. B* **1994**, *49*, 5415–5423.

Effects of the Presence of Native Silicon Oxide at the Fe/Si Interface on the Formation of Silicides Studied by Auger Spectroscopy; Chemelli, C.; Dangelo, D.; Girardi, G.; Pizzini, S. *Appl. Surf. Sci.* **1993**, *68*, 173–177.

Hydrogenating Silicon Dioxide in an Electron Cyclotron Plasma; Delfino, M.; Tsai, W.; Reynolds, G.; Day, M. E. *Appl. Phys. Lett.* **1993**, *63*, 3426–3428.

Electrical Characteristics of Al/SiO_2/n-Si Tunnel-Diodes with an Oxide Layer Grown by Rapid Thermal Oxidation; Depas, M.; Vanmeirhaeghe, R. L.; Laflere, W. H.; Cardon, F. *Solid-State Electron.* **1994**, *37*, 433–441.

Etching Rate Characterization of SiO_2 and Si Using Ion Energy Flux and Atomic Fluorine Density in a CF_4/O_2/Ar Electron Cyclotron Resonance Plasma; Ding, J.; Jenq, J. S.; Kim, G. H.; Maynard, H. L.; Hamers, J. S.; et al. *J. Vac. Sci. Technol. A* **1993**, *11*, 1283–1288.

Effect of Surface Treatments After HF Etching on Oxidation of Si; Egawa, M.; Ikoma, H. *Jpn. J. Appl. Phys.* **1994**, *33*, 943–949.

Optical 2nd-Harmonic Generation—A Probe of Atomic-Structure and Bonding at Si–SiO_2 Interfaces, and Other Chemically-Modified Si Surfaces; Emmerichs, U.; Meyer, C.; Bakker, H. J.; Wolter, F.; Kurz, H.; et al. *J. Vac. Sci. Technol. B* **1994**, *12*, 2484–2492.

Sensitivity of 2nd-Harmonic Generation to Space-Charge Effects at Si(111) Electrolyte and Si(111)/SiO_2 Electrolyte Interfaces; Fischer, P. R.; Daschbach, J. L.; Gragson, D. E.; Richmond, G. L. *J. Vac. Sci. Technol. A* **1994**, *12*, 2617–2624.

Surface 2nd-Harmonic Studies of Si(111)/Electrolyte and Si(111)/SiO_2/Electrolyte Interfaces; Fischer, P. R.; Daschbach, J. L.; Richmond, G. L. *Chem. Phys. Lett.* **1994**, *218*, 200–205.

Time-Dependent Dielectric-Breakdown of Thin Silicon Oxide Using Dense Contact Electrification; Fukano, Y.; Hontani, K. J.; Uchihashi, T.; Okusako, T.; Chayahara, A.; et al. *Jpn. J. Appl. Phys.* **1994**, *33*, 3756–3760.

Scanning Force Tunneling Microscopy as a Novel Technique for the Study of Nanometer-Scale Dielectric-Breakdown of Silicon Oxide Layer; Fukano, Y.; Sugawara, Y.; Yamanishi, Y.; Oasa, T.; Morita, S. *Jpn. J. Appl. Phys.* **1993**, *32*, 290–293.

Time Evolution of Contact-Electrified Electron Dissipation on Silicon Oxide Surface Investigated Using Noncontact Atomic Force Microscope; Fukano, Y.; Uchihashi, T.; Okusako, T.; Chayahara, A.; Sugawara, Y.; et al. *Jpn. J. Appl. Phys.* **1994**, *33*, 379–382.

The Mechanism of the Anodic-Oxidation of Silicon in Acidic Fluoride Solutions Revisited; Gerischer, H.; Allongue, P.; Kieling, V. C. *Ber. Bunsen-Ges. Phys. Chem.* **1993**, *97*, 753–756.

Low Energy (3–100 eV) Electron Bombardment Induced Nitridation of Thin SiO_2 Films—Physicochemical and Electrical Analyses; Glachant,

A.; Garcia, V.; Balland, B.; Bureau, J. C.; Plossu, C.; et al. *Thin Solid Films* **1994**, *238*, 31–36.

Damage to Si Substrates during SiO_2 Etching—A Comparison of Reactive Ion Etching and Magnetron Enhanced Reactive Ion Etching; Gu, T.; Ditizio, R. A.; Fonash, S. J.; Awadelkarim, O. O.; Ruzyllo, J.; et al. *J. Vac. Sci. Technol. B* **1994**, *12*, 567–573.

In-Situ Infrared Study of Surface Oxide Formation on Gas Evaporated Si Microcrystals; Hayashi, S.; Kawata, S.; Kim, H. M.; Yamamoto, K. *Jpn. J. Appl. Phys.* **1993**, *32*, 4870–4877.

(311) Facets of Selectively Grown Epitaxial Si Layers on SiO_2-Patterned Si(100) Surfaces; Hirayama, H.; Hiroi, M.; Ide, T. *Phys. Rev. B* **1993**, *48*, 17331–17336.

Electron Tunneling Through Ultrathin Gate Oxide Formed on Hydrogen Terminated Si(100) Surfaces; Hiroshima, M.; Yasaka, T.; Miyazaki, S.; Hirose, M. *Jpn. J. Appl. Phys.* **1994**, *33*, 395–398.

Si/SiO_2 Interface—New Structures and Well-Defined Model Systems; Holl, M. M. B.; McFeely, F. R. *Phys. Rev. Lett.* **1993**, *71*, 2441–2444.

2-Dimensional Growth and Decomposition of Initial Thermal SiO_2 Layer on Si(100); Horie, T.; Takakuwa, Y.; Miyamoto, N. *Jpn. J. Appl. Phys.* **1994**, *33*, 4684–4690.

Probing Inhomogeneous Lattice Deformation at Interface of $Si(111)/SiO_2$ by Optical 2nd Harmonic Reflection and Raman Spectroscopy; Huang, J. Y. *Jpn. J. Appl. Phys.* **1994**, *33*, 3878–3886.

Evaporation Rates of Oxides from Undoped and Sb-Doped Si Melts Under Atmospheres of Pure Ne, Ar, and Kr; Huang, X. M.; Terashima, K.; Tokizaki, E.; Kimura, S.; Whitby, E. *Jpn. J. Appl. Phys.* **1994**, *33*, 3808–3812.

Inverse Modeling of Impact Ionization Rate Through Comparison of Monte Carlo Simulation of Si Metal Oxide-Semiconductor Device Characteristics and Experimental Results; Imanaga, S.; Hane, K.; Hayafuji, Y. *J. Appl. Phys.* **1993**, *74*, 5859–5866.

The Sputtering of SiO_2 and Its Dependence on Oxygen Partial Pressure; Jacobsson, H.; Holmen, G. *Nucl. Instrum. Methods Phys. Res. Sect. B* **1993**, *82*, 291–300.

Optical Functions and Transparent Thin Films of $SrTiO_3$, $BaTiO_3$, and Siox Determined by Spectroscopic Ellipsometry; Jellison, G. E.; Boatner, L. A.; Lowndes, D. H.; McKee, R. A.; Godbole, M. *Appl. Opt.* **1994**, *33*, 6053–6058.

Scanning Tunneling Microscopy of Oxygen and Sodium Adsorption on the Si(111) Surface; Jeon, D. R.; Hashizume, T.; Sakurai, T. *Jpn. J. Appl. Phys.* **1993**, *32*, 1423–1427.

The Mesoscopic and Microscopic Structural Consequences from Decomposition and Desorption of Ultrathin Oxide Layers on Si(100) Studied by Scanning Tunneling Microscopy; Johnson, K. E.; Wu, P. K.; Sander, M.; Engel, T. *Surf. Sci.* **1993**, *290*, 213–231.

Origin of Dark Regions in Scanning Tunneling Microscopy Images Formed by Thermal Oxidation of Si(111) Surface; Kageshima, H.; Ono, Y.; Tabe, M.; Ohno, T. *Jpn. J. Appl. Phys.* **1994**, *33*, 4070–4074.

Ultra Low Temperature Growth of High Integrity Gate Oxide Films by Low Energy Ion Assisted Oxidation; Kawai, Y.; Konishi, N.; Watanabe, J.; Ohmi, T. *Appl. Phys. Lett.* **1994**, *64*, 2223–2225.

Native Oxide Removal on Si Surfaces by NF_3-Added Hydrogen and Water Vapor Plasma Downstream Treatment; Kikuchi, J.; Iga, M.; Ogawa, H.; Fujimura, S.; Yano, H. *Jpn. J. Appl. Phys.* **1994**, *33*, 2207–2211.

Silicon Surface Imperfection Probed with a Novel X-Ray Diffraction Technique and Its Influence on the Reliability of Thermally Grown Silicon Oxide; Kitano, T.; Hasegawa, E.; Tsukiji, M.; Akimoto, K.; Kimura, S.; et al. *Jpn. J. Appl. Phys.* **1993**, *32*, 1581–1583.

Mechanism of Hydrogen Sensing by Platinum Silicon Oxide Silicon MIS Tunneling Diodes; Kobayashi, H.; Kogetsu, Y.; Nakato, Y. *Surf. Sci.* **1994**, *306*, 69–80.

Scanning Tunneling Microscopic Observations of Nonconductive Oxide Surfaces—SiO_2 Thin Films Formed on n-Si(100) and p-Si(100); Komiyama, M.; Kirino, M.; Kurokawa, H. *Jpn. J. Appl. Phys.* **1993**, *32*, 2934–2939.

Modification of Silicon Dioxide by Hydrogen and Deuterium Plasmas at Room Temperature; Kuroda, T.; Iwakuro, H. *Jpn. J. Appl. Phys.* **1993**, *32*, 1273–1276.

Real-Time Ellipsometric Observation of Refractive Index Change Under Ultra Thin Oxide Film Growth; Kuroki, H.; Kawabe, T.; Kitajima, M. *Solid State Commun.* **1993**, *88*, 785–788.

Real-Time Observation of Ultrathin Silicon Oxide Film Growth Using Rapid Ellipsometry; Kuroki, H.; Nakamura, K. G.; Kamioka, I.; Kawabe, T.; Kitajima, M. *J. Vac. Sci. Technol. A* **1994**, *12*, 1431–1434.

Silicon Wafer Orientation Dependence in the Initial Plasma Oxidation Processes; Kuroki, H.; Nakamura, K. G.; Kawabe, T.; Kitajima, M. *Solid State Commun.* **1993**, *88*, 487–489.

AES Study of Si LVV Bonding States in Various Substoichiometric Oxide Environments; Lang, B.; Khellafi, M. *Surf. Interface Anal.* **1993**, *20*, 827–832.

An AES Study of Intrinsic and Ion Induced Structure in the SiO_2-Si System; Lang, B.; Sefsaf, B.; Allan, G. *Appl. Surf. Sci.* **1994**, *81*, 17–26.

Very Low Surface Recombination Velocities on 2.5 Ohm-cm Si Wafers, Obtained with Low Temperature PECVD of Si Oxide and Si Nitride; Leguijt, C.; Lolgen, P.; Eikelboom, J. A.; Amesz, P. H.; Steeman, R. A.; et al. *Sol. Energy Mater. Sol. Cells* **1994**, *34*, 177–181.

Measurements of Thin Oxide Films of $SiO_2/Si(100)$; Lennard, W. N.; Massoumi, G. R.; Mitchell, I. V.; Tang, H. T.; Mitchell, D. F.; Bardwell, J. A. *Nucl. Instrum. Methods Phys. Res. Sect. B* **1994**, *85*, 42–46.

H-1 Nuclear Magnetic Resonance of Thermally Grown Silicon Dioxide Films; Levy, D. H.; Gleason, K. K. *J. Electrochem. Soc.* **1993**, *140*, 797–800.

Multiple Internal Reflection Infrared Spectroscopy of Silicon Surface Structure and Oxidation Process at Room Temperature; Ling, L.; Kuwabara, S.; Abe, T.; Shimura, F. *J. Appl. Phys.* **1993**, *73*, 3018–3022.

$SiO_2/Si(100)$ Interface Studied by Al Kα X-Ray and Synchrotron Radiation Photoelectron Spectroscopy; Lu, Z. H.; Graham, M. J.; Jiang, D. T.; Tan, K. H. *Appl. Phys. Lett.* **1993**, *63*, 2941–2943.

Formation of Si–SiO_2 Stacked Gate Structures by Plasma Assisted and Rapid Thermal Processing—Improved Device Performance Through Process Integration; Lucovsky, G.; Wortman, J. J.; Yasuda, T.; Xu, X. L.; Misra, V.; et al. *J. Vac. Sci. Technol. B* **1994**, *12*, 2839–2847.

SiO_2/Si Interfacial Structure on Vicinal Si(100) Studied with 2nd Harmonic Generation; Lupke, G.; Bottomley, D. J.; Vandriel, H. M. *Phys. Rev. B* **1993**, *47*, 10389–10394.

Nanoscale Patterning and Oxidation of H-Passivated Si(100)-2×1 Surfaces with an Ultrahigh Vacuum Scanning Tunneling Microscope; Lyding, J. W.; Shen, T. C.; Hubacek, J. S.; Tucker, J. R.; Abeln, G. C. *Appl. Phys. Lett.* **1994**, *64*, 2010–2012.

Control of the Buried SiO_2 Layer Thickness and Si Defect Density in $SiMO_x$ Substrates—Structural Investigation and Process Optimization; Marsh, C. D.; Nejim, A.; Li, Y.; Booker, G. R.; Hemment, P. L. F.; et al. *Nucl. Instrum. Methods Phys. Res. Sect. B* **1993**, *74*, 197–203.

Film Thickness Measurements of SiO_2 by XPS; Mitchell, D. F.; Clark, K. B.; Bardwell, J. A.; Lennard, W. N.; Massoumi, G. R.; Mitchell, I. V. *Surf. Interface Anal.* **1994**, *21*, 44–50.

Shallow Boron-Doped Layer Formation by Boron Diffusion from Poly-Si Through Thin SiO_2; Miyake, M. *J. Electrochem. Soc.* **1994**, *141*, 1702–1708.

Strain Evaluation at Si/SiO_2 Interface Using the Electroreflectance Method; Morifuji, M.; Yongwattanasoontorn, P.; Taniguchi, K.; Hamaguchi, C.; Ozawa, Y. *Jpn. J. Appl. Phys.* **1993**, *32*, 2735–2739.

Stable-Unstable Phase Transition of Densely Contract Electrified electrons on Thin Silicon Oxide; Morita, S.; Sugawara, Y.; Fukano, Y.; Uchihashi, T.; Okusako, T.; et al. *Jpn. J. Appl. Phys.* **1993**, *32*, 1852–1854.

In-Situ Auger Electron Spectroscopy of Silicon Thin Films Fabricated Using Arf Excimer Laser-Induced Chemical Vapor Deposition and the Oxidation Process; Mutoh, K.; Takeyama, S.; Yamada, Y.; Miyata, T. *Appl. Surf. Sci.* **1994**, *80*, 459–464.

Si K X-Ray Absorption Spectra of Single Crystal Si and Amorphous SiO_2; Nagashima, N.; Nakano, A.; Ogata, K.; Tamura, M.; Sugawara, K.; Hayakawa, K. *Phys. Rev. B* **1993**, *48*, 18257–18260.

Multiphoton ionization Detection of a SiO Molecule Formed by O_2 Oxidation of a Silicon Surface; Nakamura, K. G.; Kuroki, H.; Kitajima, M. *J. Appl. Phys.* **1994**, *75*, 4261–4263.

Evaluation of Photoemitted Current from SiO_2 Film on Silicon during Synchrotron Radiation Irradiation; Nara, Y.; Moscheni, F.; Sugita, Y.; Horiuchi, K.; Ito, T. *Jpn. J. Appl. Phys.* **1992**, *31*, 4454–4458.

Damage Free Selective Etching of Si Native Oxides Using NH_3/NF_3 and SF_6/H_2O Down Flow Etching; Nishino, H.; Hayasaka, N.; Okano, H. *J. Appl. Phys.* **1993**, *74*, 1345–1348.

Atomic Order Planarization of Ultrathin SiO_2/Si-(001) Interfaces; Niwa, M.; Kouzaki, T.; Okada, K.; Udagawa, M.; Sinclair, R. *Jpn. J. Appl. Phys.* **1994**, *33*, 388–394.

Atomic Scale Planarization of SiO_2/Si(001) Interfaces; Niwa, M.; Udagawa, M.; Okada, K.; Kouzazki, T.; Sinclair, R. *Appl. Phys. Lett.* **1993**, *63*, 675–677.

Ultraviolet Induced Deposition of SiO_2 Film from Tetraethoxysilane Spin Coated on Si; Niwano, M.; Kinashi, K.; Saito, K.; Miyamoto, N.; Honma, K. *J. Electrochem. Soc.* **1994**, *141*, 1556–1561.

Photoemission Study of Synchrotron Radiation Induced Reactions of TeOs Adsorbed on Silicon Surface; Niwano, M.; Miyamoto, N.; Simons, J. K.; Frigo, S. P.; Rosenberg, R. A. *Appl. Surf. Sci.* **1994**, *80*, 403–408.

Periodic Changes in SiO_2/Si(111) Interface Structures with Progress of Thermal Oxidation; Ohishi, K.; Hattori, T. *Jpn. J. Appl. Phys.* **1994**, *33*, 675–678.

Growth of Native Oxide and Accumulation of Organic Matter on Bare Si Wafer in Air; Okada, C.; Kobayashi, H.; Takahashi, I.; Ryuta, J.; Shingyouji, T. *Jpn. J. Appl. Phys.* **1993**, *32*, 1031–1033.

Scanning Tunneling Microscopy Observation of Thermal Oxide Growth on Si(111)7×7 Surfaces; Ono, Y.; Tabe, M.; Kageshima, H. *Phys. Rev. B* **1993**, *48*, 14291–14300.

Chemically Prepared Oxides on Si(001)—An XPS Study; Prabhakaran, K.; Kobayashi, Y.; Ogino, T. *Surf. Sci.* **1993**, *290*, 239–244.

O 1s Investigation of SiO_2/Si Interface Formation Using an Alkali Metal Promoter; Riehlchudoba, M.; Nishigaki, S.; Huttel, Y.; Semond, F.; Brun, P.; Soukiassian, P. *Appl. Surf. Sci.* **1993**, *65/66*, 840–846.

Dynamic Observations of Interface Motion during the Oxidation of Silicon; Ross, F. M.; Gibson, J. M.; Twesten, R. D. *Surf. Sci.* **1994**, *310*, 243–266.

High Intensity Hydrogen Lamp Employing Helicon Wave Plasma and Its Application to Si and SiO_2 Etching; Sadakuni, G.; Kojima, A.; Sakaue, H.; Horike, Y. *Appl. Surf. Sci.* **1994**, *80*, 495–501.

Very Thin Silicon Dioxide Film Thickness Determination Using Transmission Electron Microscopy, Spectroscopic Ellipsometry and X-Ray Photoelectron Spectroscopy; Saoudi, R.; Hollinger, G.; Gagnaire, A.; Ferret, P.; Pitaval, M. *J. Phys. III* **1993**, *3*, 1479–1488.

XPS and XAES Study of Interaction Between Ni and Si(111), SiO_x/Si(111) Supports; Sarapatka, T. J. *J. Electron Spectrosc. Relat. Phenom.* **1993**, *62*, 335–349.

A Theoretical Study of the Initial Stages of Si(111)-7×7 Oxidation. 1. The Molecular Precursor; Schubert, B.; Avouris, P.; Hoffmann, R. *J. Chem. Phys.* **1993**, *98*, 7593–7605.

A Theoretical Study of the Initial Stages of Si(111)-7×7 Oxidation. 2. The Dissociated State and Formation of SiO_4; Schubert, B.; Avouris, P.; Hoffmann, R. *J. Chem. Phys.* **1993**, *98*, 7606–7612.

Effects of Trace Surface Oxidation in Low Temperature Epitaxy Grown from Dichlorosilane; Sedgwick, T. O.; Agnello, P. D.; Grutzmacher, D. A. *J. Electrochem. Soc.* **1993**, *140*, 3684–3688.

Elevated Temperature Oxidation and Etching of the Si(111) 7×7 Surface Observed with Scanning

Tunneling Microscopy; Seiple, J.; Pecquet, J.; Meng, Z.; Pelz, J. P. *J. Vac. Sci. Technol. A* **1993**, *11*, 1649–1653.

Scanning Tunneling Microscopy Study of Oxide Nucleation and Oxidation Induced Roughening at Elevated Temperatures on the Si(001)-(2×1) Surface; Seiple, J. V.; Pelz, J. P. *Phys. Rev. Lett.* **1994**, *73*, 999–1002.

Deposition Characteristics and Properties of SiO_2 Films Prepared by Reactive Sputtering in Hydrogen-Argon, Oxygen-Argon and Nitrogen-Argon Mixtures; Serikawa, T.; Shirai, S. *Jpn. J. Appl. Phys.* **1994**, *33*, 4465–4468.

Higher Frequency Shifts of a Surface Vibration Mode Accompanied by Native Oxide Growth on Silicon in Air; Shirai, H. *Jpn. J. Appl. Phys.* **1994**, *33*, 94–97.

Generation Aspects of the Delocalized Intrinsic Ex Defect in Thermal SiO_2; Stesmans, A.; Scheerlinck, F. *J. Appl. Phys.* **1994**, *75*, 1047–1058.

Spatial Distribution and Its Phase Transition of Densely Contact Electrified electrons on a Thin Silicon Oxide; Sugawara, Y.; Morita, S.; Fukano, Y.; Uchihashi, T.; Okusako, T.; et al. *Jpn. J. Appl. Phys.* **1994**, *33*, 70–73.

Spatial Distributions of Densely Contact Electrified Charges on a Thin Silicon Oxide; Sugawara, Y.; Morita, S.; Fukano, Y.; Uchihashi, T.; Okusako, T.; et al. *Jpn. J. Appl. Phys.* **1994**, *33*, 74–77.

Roughness Evaluation of Thermally Oxidized Si(111) Surfaces by Scanning Force Microscopy; Suzuki, M.; Homma, Y.; Kudoh, Y.; Yabumoto, N. *Jpn. J. Appl. Phys.* **1993**, *32*, 1419–1422.

X-Ray Diffraction Evidence for Epitaxial Microcrystallinity in Thermally Oxidized SiO_2 Thin Films on the Si(001) Surface; Takahashi, I.; Shimura, T.; Harada, J. *J. Phys.: Condens. Matter* **1993**, *5*, 6525–6536.

X-Ray Photoelectron Spectroscopy and X-Ray Absorption Near-Edge Spectroscopy Study of SiO_2/Si(100); Tao, Y.; Lu, Z. H.; Graham, M. J.; Tay, S. P. *J. Vac. Sci. Technol. B* **1994**, *12*, 2500–2503.

Heat Treatment and Steaming Effects of Silicon Oxide Upon Electron Dissipation on Silicon Oxide Surface; Uchihashi, T.; Okusako, T.; Sugawara, Y.; Yamanishi, Y.; Oasa, T.; Morita, S. *Jpn. J. Appl. Phys.* **1994**, *33*, 1128–1130.

The Initial Stages of the Thermal Oxidation of Si(001)2×1 Surface Studied by Scanning Tunneling Microscopy; Udagawa, M.; Niwa, M.; Sumita, I. *Jpn. J. Appl. Phys.* **1993**, *32*, 282–285.

Local Ordering and Lateral Growth of Initial Thermal Oxide of Si(001); Udagawa, M.; Niwa, M.; Sumita, I. *Jpn. J. Appl. Phys.* **1994**, *33*, 375–378.

Oxide Growth at a Si Surface and Role of Radiation Effects; Verdi, L.; Miotello, A.; Kelly, R. *Nucl. Instrum. Methods Phys. Res. Sect. B* **1994**, *91*, 648–653.

Oxide Growth at a Si Surface; Verdi, L.; Miotello, A.; Kelly, R. *Thin Solid Films* **1994**, *241*, 383–387.

A Study of Si(111) Surface Oxidation by Temperature Programmed Desorption; Watanabe, K.; Hirayama, H. *Surf. Sci.* **1994**, *317*, 1125–1128.

Interactions of Water with Trisiloxane Rings. 2. Theoretical Analysis; West, J. K.; Wallace, S. *J. Non-Cryst. Solids* **1993**, *152*, 109–117.

Effects of Predeposition HF/NH_4F Treatments on the Electrical Properties of SiO_2/Si Structures Formed by Low Temperature Plasma Assisted Oxidation and Deposition Processes; Yasuda, T.; Ma, Y.; Chen, Y. L.; Lucovsky, G.; Maher, D. *J. Vac. Sci. Technol. A* **1993**, *11*, 945–951.

Modeling and Characterization of Interface State Parameters and Surface Recombination Velocity at Plasma Enhanced Chemical Vapor Deposited SiO_2-Si Interface; Yasutake, K.; Chen, Z.; Pang, S. K.; Rohatgi, A. *J. Appl. Phys.* **1994**, *75*, 2048–2054.

ESR Study of Natural Oxidation Processes of HF-Treated Silicon-(111) Surfaces; Yokogawa, K.; Mizutani, T. *Jpn. J. Appl. Phys.* **1993**, *32*, 635–637.

Scaling Analysis of SiO_2/Si Interface Roughness by Atomic Force Microscopy; Yoshinobu, T.; Iwamoto, A.; Iwasaki, H. *Jpn. J. Appl. Phys.* **1994**, *33*, 383–387.

Dielectric Loss Function of Si and SiO_2 from Quantitative Analysis of REELS Spectra; Yubero, F.; Tougaard, S.; Elizalde, E.; Sanz, J. M. *Surf. Interface Anal.* **1993**, *20*, 719–726.

Buried Metal Layer Enhanced Infrared Reflection Absorption Spectroscopy for Photoreactions Induced by Synchrotron Radiation on SiO_2 Surfaces; Zhang, Y.; Sato, S.; Ohshima, H.; Hattori, T.; Urisu, T. *Appl. Surf. Sci.* **1994**, *80*, 422–427.

Medium Energy Ion Scattering Study of Ni on Ultrathin Films of SiO_2 on Si(111); Zhou, J. B.; Gustafsson, T.; Lin, R. F.; Garfunkel, E. *Surf. Sci.* **1993**, *284*, 67–76.

Characterization of SiO_2 Layers on Si Wafers Using Atomic Force Microscopy; Zunigasegundo, A.; Ruiz, F.; Vazquezlopez, C.; Gonzalezhernandez, J.; Torresdelgado, G.; Tsu, D. V. *J. Vac. Sci. Technol. A* **1994**, *12*, 2572–2576.

SiO

Laser Studies of the Reactivity of SiO with the Surface of a Depositing Film; Buss, R. J.; Ho, P.; Weber, M. E. *Plasma Chem. Plasma Process.* **1993**, *13*, 61–76.

Siloxanes

Photo Excited Effects and the Growth Mechanism on Epitaxially Grown Al_2O_3(100) on Si(100); Ishida, M.; Yoshizu, T.; Hayama, K.; Nakamura, T. *Appl. Surf. Sci.* **1994**, *80*, 356–360.

On the Chemical Reaction Mode of Polysilicon Deposition from Silane; Kuhne, H. *Cryst. Res. Technol.* **1993**, *28*, 39–52.

Ultraviolet Induced Deposition of SiO_2 Film from Tetraethoxysilane Spin Coated on Si; Niwano, M.; Kinashi, K.; Saito, K.; Miyamoto, N.; Honma, K. *J. Electrochem. Soc.* **1994**, *141*, 1556–1561.

Photoemission Study of Synchrotron Radiation Induced Reactions of TeOs Adsorbed on Silicon Surface; Niwano, M.; Miyamoto, N.; Simons, J. K.; Frigo, S. P.; Rosenberg, R. A. *Appl. Surf. Sci.* **1994**, *80*, 403–408.

Synchrotron Radiation Induced Reactions of Tetraethoxysilane on Si Studied by Photoemission Spec-

troscopy; Niwano, M.; Simons, J. K.; Frigo, S. P.; Rosenberg, R. A. *J. Appl. Phys.* **1994**, *75*, 7304–7309.

High Fluidity Deposition of Silicon by Plasma Enhanced Chemical Vapor Deposition Using Si_2H_6 or SiH_4; Shin, H.; Hashimoto, M.; Okamoto, K.; Miyazaki, S.; Hirose, M. *Jpn. J. Appl. Phys.* **1993**, *32*, 3081–3084.

Nitrogen Oxides

Dynamic Study of Alkali Promotion of NO Sticking on Si(100); Namiki, A.; Suzuki, S.; Kato, H.; Nakamura, T.; Suzaki, T. *Surf. Sci.* **1993**, *283*, 9–20.

Nitric Oxide Adsorption on the Si(111)7×7 Surface—Effect of Potassium Overlayers; Riehlchudoba, M.; Surnev, L.; Soukiassian, P. *Surf. Sci.* **1994**, *306*, 313–326.

Growth Rate and Characterization of Silicon Oxide Films Grown in N_2O Atmosphere in a Rapid Thermal Processor; Lange, P.; Bernt, H.; Hartmannsgruber, E.; Naumann, F. *J. Electrochem. Soc.* **1994**, *141*, 259–263.

Auger Electron Spectroscopy Study of the Interaction of NO_2 with Si(100); Bhat, M.; Kamath, A.; Kwong, D. L.; Sun, Y. M.; White, J. M. *Appl. Phys. Lett.* **1994**, *65*, 1314–1316.

Oxynitrides

Electronic Promotion of Silicon Oxynitridation at Room Temperature by Alkali Metal Catalysts; Glachant, A.; Soukiassian, P.; Kim, S. T.; Hurych, Z. *Appl. Surf. Sci.* **1993**, *65/66*, 847–853.

Surface Stoichiometry Determination of SiO_xN_y Thin Films by Means of XPS; Lozzi, L.; Passacantando, M.; Picozzi, P.; Santucci, S.; Tomassi, G.; et al. *Surf. Interface Anal.* **1994**, *22*, 190–192.

Nitrogen Content of Oxynitride Films on Si(100); Tang, H. T.; Lennard, W. N.; Zinkeallmang, M.; Mitchell, I. V.; Feldman, L. C.; et al. *Appl. Phys. Lett.* **1994**, *64*, 3473–3475.

Study of Process-Dependent Electron Trapping Characteristics of Thin Nitrided Oxides; Yang, B. L.; Wong, H.; Cheng, Y. C. *Solid-State Electron.* **1994**, *37*, 481–486.

$SrTiO_3$

Optical Functions and Transparent Thin Films of $SrTiO_3$, $BaTiO_3$, and SiO_x Determined by Spectroscopic Ellipsometry; Jellison, G. E.; Boatner, L. A.; Lowndes, D. H.; McKee, R. A.; Godbole, M. *Appl. Opt.* **1994**, *33*, 6053–6058.

Roles of Buffer Layers in Epitaxial Growth of $SrTiO_3$ Films on Silicon Substrates; Moon, B. K.; Ishiwara, H. *Jpn. J. Appl. Phys.* **1994**, *33*, 1472–1477.

Ta_2O_5

Sputter Depth Profiling Analysis of Ta_2O_5 on Si Without Preferential Sputtering by Energetic Oxygen-Ion Beams; Moon, D. W.; Kim, K. J. *Appl. Phys. Lett.* **1993**, *62*, 3094–3096.

CeO_2

Reaction and Regrowth Control of CeO_2 on Si(111) Surface for the Silicon on Insulator Structure; Chikyow, T.; Bedair, S. M.; Tye, L.; Elmasry, N. A. *Appl. Phys. Lett.* **1994**, *65*, 1030–1032.

Deposition of CeO_2 on Si(111) Studied by LEED, AES, XPS and RBS; Guillaume, C. E.; Vermeersch, M.; Sporken, R.; Verbist, J. J.; Mathot, S.; Demortier, G. *Surf. Interface Anal.* **1994**, *22*, 186–189.

Stripe Shaped Faceted Morphology and Domain Structure of Epitaxial CeO_2(110) Layers on Si(100) Substrates; Inoue, T.; Ohsuna, T.; Obara, Y.; Yamamoto, Y.; Satoh, M.; Sakurai, Y. *J. Cryst. Growth* **1993**, *131*, 347–351.

$BaTiO_3$

Interactions Between Ferroelectric $BaTiO_3$ and Si; Jia, Q. X.; Chang, L. H.; Anderson, W. A. *J. Electron. Mater.* **1994**, *23*, 551–556.

Optical Functions and Transparent Thin Films of $SrTiO_3$, $BaTiO_3$, and SiO_x Determined by Spectroscopic Ellipsometry; Jellison, G. E.; Boatner, L. A.; Lowndes, D. H.; McKee, R. A.; Godbole, M. *Appl. Opt.* **1994**, *33*, 6053–6058.

Surface Morphologies of $BaTiO_3$ Thin Films by Atomic Force Microscopy; Yoon, Y. S.; Yoon, Y. K.; Lee, J. Y.; Yom, S. S. *Jpn. J. Appl. Phys.* **1994**, *33*, 4075–4079.

TiO_2

Structural Properties of Titanium Dioxide Films Grown on p-Si by Metal Organic Chemical Vapor Deposition at Low Temperature; Yoon, Y. S.; Kang, W. N.; Yom, S. S.; Kim, T. W.; Jung, M.; et al. *Thin Solid Films* **1994**, *238*, 12–14.

Nitrides

Oxynitrides

Electronic Promotion of Silicon Oxynitridation at Room Temperature by Alkali Metal Catalysts; Glachant, A.; Soukiassian, P.; Kim, S. T.; Hurych, Z. *Appl. Surf. Sci.* **1993**, *65/66*, 847–853.

Surface Stoichiometry Determination of SiO_xN_y Thin Films by Means of XPS; Lozzi, L.; Passacantando, M.; Picozzi, P.; Santucci, S.; Tomassi, G.; et al. *Surf. Interface Anal.* **1994**, *22*, 190–192.

Nitrogen Content of Oxynitride Films on Si(100); Tang, H. T.; Lennard, W. N.; Zinkeallmang, M.; Mitchell, I. V.; Feldman, L. C.; et al. *Appl. Phys. Lett.* **1994**, *64*, 3473–3475.

Study of Process-Dependent Electron Trapping Characteristics of Thin Nitrided Oxides; Yang, B. L.; Wong, H.; Cheng, Y. C. *Solid-State Electron.* **1994**, *37*, 481–486.

c-BN

Atomic Structure Calculations for Epitaxy of c-BN on Si(001); Verwoerd, W. S.; Osuch, K.; Badziag, P. *Surf. Sci.* **1994**, *312*, 221–232.

Phosphides

PH_3

Adsorption and Dissociation of PH_3 on Si(100) 2×1 and Si(111) 7×7—Theoretical Study; Cao, P. L.; Lee,

L. Q.; Dai, J. J.; Zhou, R. H. *J. Phys.: Condens. Matter* **1994**, *6*, 6103–6109.

An Atomically Resolved STM Study of the Interaction of Phosphine with the Silicon(001) Surface; Wang, Y. J.; Bronikowski, M. J.; Hamers, R. J. *J. Phys. Chem.* **1994**, *98*, 5966–5973.

InP

InP on Si(111)—Accommodation of Lattice Mismatch and Structural Properties; Krost, A.; Heinrichsdorff, F.; Bimberg, D.; Cerva, H. *Appl. Phys. Lett.* **1994**, *64*, 769–771.

Silicon Carbide

Equilibrium Predictions of the Role of Organosilicon Compounds in the Chemical Vapor Deposition of Silicon Carbide; Allendorf, M. D. *J. Electrochem. Soc.* **1993**, *140*, 747–753.

Low Temperature Impurity Diffusion in SiC—Planar Quantum Size p-n-Junctions and n-p-n Transistor Structures; Bagraev, N. T.; Klyachkin, L. E.; Sukhanov, V. L. *Solid-State Electron.* **1993**, *36*, 1741–1747.

Effects of Propane and Methane on Carbonization and Surface Morphology in Heteroepitaxial Growth of β-SiC Films on (100) Si Via Chemical Vapor Deposition; Bahavar, B.; Chaudhry, M. I.; McCluskey, R. J. *Appl. Phys. Lett.* **1993**, *63*, 914–916.

Atomic Force Microscopy Study of the Microroughness of SiC Thin Films; Blouin, M.; Guay, D.; Elkhakani, M. A.; Chaker, M.; Boily, S.; Jean, A. *Thin Solid Films* **1994**, *249*, 38–43.

Conversion of Single Crystal Si(100) to SiC Film by C_2H_2; Chiu, C. C.; Desu, S. B. *J. Mater. Res.* **1993**, *8*, 535–544.

Electron Cyclotron Resonance Plasma Ion Beam Effects on the Formation of SiC on Si(001) Characterized by In-Situ Photoemission; Diani, M.; Aubel, D.; Bischoff, J. L.; Kubler, L.; Bolmont, D. *Thin Solid Films* **1994**, *241*, 305–309.

X-Ray Photoelectron Diffraction Observation of β-SiC(001) Obtained by Electron Cyclotron Resonance Plasma Assisted Growth on Si(001); Diani, M.; Bischoff, J. L.; Kubler, L.; Bolmont, D. *Appl. Surf. Sci.* **1993**, *68*, 575–582.

Neutral Ion Figuring of Chemical Vapor Deposited SiC; Fawcett, S. C.; Drueding, T. W.; Bifano, T. G. *Opt. Eng.* **1994**, *33*, 967–974.

Microscopic Mechanisms of Accurate Layer-by-Layer Growth of β-SiC; Hara, S.; Meguro, T.; Aoyagi, Y.; Kawai, M.; Misawa, S.; et al. *Thin Solid Films* **1993**, *225*, 240–243.

Mass Spectrometry Detection of SiH_m and CH_m Radicals from SiH_4-CH_4-H_2 RF Discharges Under High Temperature Deposition Conditions of Silicon Carbide; Kaenune, P.; Perrin, J.; Guillon, J.; Jolly, J. *Jpn. J. Appl. Phys.* **1994**, *33*, 4303–4307.

Growth Mechanism of 6H-SiC in Step Controlled Epitaxy; Kimoto, T.; Nishino, H.; Yoo, W. S.; Matsunami, H. *J. Appl. Phys.* **1993**, *73*, 726–732.

Simulations and Experiments of SiC Heteroepitaxial Growth on Si(001) Surface; Kitabatake, M.; Deguchi, M.; Hirao, T. *J. Appl. Phys.* **1993**, *74*, 4438–4445.

Scanning Auger Microscopy Study of Heterogeneous Growth of SiC Film on Si(100) by Reaction with a C_2H_2 Beam; Kusunoki, I. *Jpn. J. Appl. Phys.* **1993**, *32*, 2074–2077.

Atomic Level Epitaxy of 3C-SiC by Low Pressure Vapor Deposition with Alternating Gas Supply; Nagasawa, H.; Yamaguchi, Y. *Thin Solid Films* **1993**, *225*, 230–234.

Heteroepitaxial Growth and ESR Evaluation of 3C-SiC; Nagasawa, H.; Yamaguchi, Y.; Izumi, T.; Tonosaki, K. *Appl. Surf. Sci.* **1993**, *70/71*, 542–545.

Interface Modification and Characterization of Silicon Carbide Platelets Coated with Alumina Particles; Pei, P. T.; Kelly, J. F.; Malghan, S. G. *Colloids Surf. A* **1993**, *70*, 277–287.

Spectroscopic Study of SiC-Like Structures Formed on Polycrystalline Silicon Sheets during Growth; Pivac, B.; Furic, K.; Milun, M.; Valla, T.; Borghesi, A.; Sassella, A. *J. Appl. Phys.* **1994**, *75*, 3586–3592.

Effect of Oxygen Atom Bombardment on the Reflectance of Silicon Carbide Mirrors in the Extreme Ultraviolet Region; Seely, J. F.; Holland, G. E.; Hunter, W. R.; McCoy, R. P.; Dymond, K. F.; Corson, M. *Appl. Opt.* **1993**, *32*, 1805–1810.

Preliminary Soft X-Ray Studies of β-SiC; Shek, M. L.; Miyano, K. E.; Dong, Q. Y.; Callcott, T. A.; Ederer, D. L. *J. Vac. Sci. Technol. A* **1994**, *12*, 1079–1084.

Kinetic Study of Silicon Carbide Deposited from Methyltrichlorosilane Precursor; Tsai, C. Y.; Desu, S. B.; Chiu, C. C. *J. Mater. Res.* **1994**, *9*, 104–111.

Oxidation of Carbon/Carbon Composite Coated with SiC-(Si/$ZrSi_2$)-$ZrSi_2$; Wei, W. C. J.; Wu, T. M. *Carbon* **1994**, *32*, 605–613.

Atomic Structure of β-SiC(100) Surfaces—A Study Using the Tersoff Potential; Yan, H.; Hu, X.; Jonsson, H. *Surf. Sci.* **1994**, *316*, 181–188.

Halogen Compounds

Alkyl Halides

Analysis of Fluorocarbon Film Deposited by Highly Selective Oxide Etching; Akimoto, T.; Furuoya, S.; Harasima, K.; Ikawa, E. *Jpn. J. Appl. Phys.* **1994**, *33*, 2151–2156.

Fluorocarbon High Density Plasmas. 8. Study of the Ion Flux Composition at the Substrate in Electron Cyclotron Resonance Etching Processes Using Fluorocarbon Gases; Kirmse, K. H. R.; Wendt, A. E.; Oehrlein, G. S.; Zhang, Y. *J. Vac. Sci. Technol. A* **1994**, *12*, 1287–1292.

Smoothing of the Si Surface Using CF_4/O_2 Down Flow Etching; Nishino, H.; Hayasaka, N.; Horioka, K.; Shiozawa, J.; Nadahara, S.; et al. *J. Appl. Phys.* **1993**, *74*, 1349–1353.

X-Ray Photoelectron Spectroscopy Study of Low Energy CF^+ Ion Interactions with Silicon; Chang, W. H.; Bello, I.; Lau, W. M. *J. Vac. Sci. Technol. A* **1993**, *11*, 1221–1225.

Etching Rate Characterization of SiO_2 and Si Using Ion Energy Flux and Atomic Fluorine Density in a CF_4/O_2/Ar Electron Cyclotron Resonance Plasma; Ding, J.; Jenq, J. S.; Kim, G. H.; Maynard, H. L.; Hamers, J. S.; et al. *J. Vac. Sci. Technol. A* **1993**, *11*, 1283–1288.

Decomposition of Gaseous Dielectrics (CF_4, SF_6) by a Nonequilibrium Plasma—Mechanisms, Kinetics, Mass Spectrometric Studies and Interactions with

Polymeric Targets; Khairallah, Y.; Khonsariarefi, F.; Amouroux, J. *Pure Appl. Chem.* **1994**, *66*, 1353–1362.

Fluorocarbon High Density Plasmas. 1. Fluorocarbon Film Deposition and Etching Using CF_4 and CHF_3; Oehrlein, G. S.; Zhang, Y.; Vender, D.; Haverlag, M. *J. Vac. Sci. Technol. A* **1994**, *12*, 323–332.

Near-Surface Residue Formation in CF_4/H_2 Reactive Ion Etching of Silicon; Potter, G. E.; Morrison, G. H.; Charvat, P. K.; Ruoff, A. L. *J. Vac. Sci. Technol. B* **1992**, *10*, 2398–2406.

Direct Evidence for β-Hydride Elimination on Si(100); Keeling, L. A.; Chen, L.; Greenlief, C. M.; Mahajan, A.; Bonser, D. *Chem. Phys. Lett.* **1994**, *217*, 136–141.

$SiCl_4$

The Adsorption and Surface Reaction of $SiCl_4$ on Si(100)-(2×1); Gao, Q.; Dohnalek, Z.; Cheng, C. C.; Choyke, W. J.; Yates, J. T. *Surf. Sci.* **1994**, *302*, 1–9.

NH_4F

Step Edge Structures on Si(112) and (113) Surfaces Treated in NH_4F Solution; Fujita, K.; Hirashita, N. *Jpn. J. Appl. Phys.* **1994**, *33*, 399–403.

Corrugated Structures on Si(110) Surfaces Treated in Ammonium Fluoride Solutions; Fujita, K.; Hirashita, N. *Jpn. J. Appl. Phys.* **1994**, *33*, 1145–1148.

Reaction of NH_4F/HF Solutions on Si(100) and Si(111) Surfaces; Graf, D.; Bauermayer, S.; Schnegg, A. *J. Vac. Sci. Technol. A* **1993**, *11*, 940–944.

Separation of Charge Transfer and Surface Recombination Processes by Simultaneous Measurement of Photocurrent and Excess Microwave Conductivity Profiles of Si(111) in NH_4F; Lewerenz, H. J.; Schlichthorl, G. *J. Appl. Phys.* **1994**, *75*, 3544–3547.

Wet Chemical Etching of Si(100) Surfaces in Concentrated NH_4F Solution—Formation of (2×1)H Reconstructed Si(100) Terraces Versus (111) Faceting; Neuwald, U.; Hessel, H. E.; Feltz, A.; Memmert, U.; Behm, R. J. *Surf. Sci.* **1993**, *296*, 8–14.

Anisotropic Etching Versus Interaction of Atomic Steps—Scanning Tunneling Microscopy Observations on HF/NH_4F-Treated Si(111); Pietsch, G. J.; Kohler, U.; Henzler, M. *J. Appl. Phys.* **1993**, *73*, 4797–4807.

Effects of Predeposition HF/NH_4F Treatments on the Electrical Properties of SiO_2/Si Structures Formed by Low Temperature Plasma Assisted Oxidation and Deposition Processes; Yasuda, T.; Ma, Y.; Chen, Y. L.; Lucovsky, G.; Maher, D. *J. Vac. Sci. Technol. A* **1993**, *11*, 945–951.

SF_6

Decomposition of Gaseous Dielectrics (CF_4, SF_6) by a Nonequilibrium Plasma—Mechanisms, Kinetics, Mass Spectrometric Studies and Interactions with Polymeric Targets; Khairallah, Y.; Khonsariarefi, F.; Amouroux, J. *Pure Appl. Chem.* **1994**, *66*, 1353–1362.

Modeling and Experimental Studies of a Reactive Ion Etcher Using SF_6/O_2 Chemistry; Kopalidis, P. M.; Jorne, J. *J. Electrochem. Soc.* **1993**, *140*, 3037–3045.

CaF_2

Comparative Study of Hypersonic Dynamics in CaF_2 and SrF_2 Films on Si(111); Aleksandrov, V. V.; Potapova, J. B.; Diakonov, A. M.; Yakovlev, N. L. *Thin Solid Films* **1994**, *237*, 25–28.

Inverse Photoemission Spectroscopy of Electron Irradiated Epitaxial CaF_2 on Si(111); Bouzidi, S.; Angot, T.; Langlais, V.; Debever, J. M.; Sporken, R.; et al. *Surf. Sci.* **1994**, *309*, 1038–1044.

Radiation Damage of Epitaxial CaF_2 Overlayers on Si(111) Studied by Photon Stimulated Desorption—Formation of Surface-F Centers; Chakarian, V.; Durbin, T. D.; Varekamp, P. R.; Yarmoff, J. A. *J. Vac. Sci. Technol. A* **1994**, *12*, 2159–2163.

Ballistic Electron Emission Microscopy Study of the Au/Si(111)7×7 and Au/CaF_2/Si(111)7×7 Interfaces; Cuberes, M. T.; Bauer, A.; Wen, H. J.; Prietsch, M.; Kaindl, G. *Appl. Phys. Lett.* **1994**, *64*, 2300–2302.

Probing the CaF_2 Density of States at Au/CaF_2/n-Si(111) Interfaces with Photoelectron Spectroscopy and Ballistic Electron Emission Microscopy; Cuberes, M. T.; Bauer, A.; Wen, H. J.; Prietsch, M.; Kaindl, G. *J. Vac. Sci. Technol. B* **1994**, *12*, 2646–2652.

X-Ray Crystal Truncation Rod Scattering from MBE Grown (CaF_2-SrF_2)-Si(111) Superlattices; Harada, J.; Itoh, Y.; Shimura, T.; Takahashi, I.; Alvarez, J. C.; Sokolov, N. S. *Appl. Surf. Sci.* **1994**, *75*, 263–268.

2-Dimensional Structural Modulation in Epitaxial CaF_2 Overlayers on Si(111); Huang, K. G.; Zegenhagen, J.; Phillips, J. M.; Patel, J. R. *Phys. Rev. Lett.* **1994**, *72*, 2430–2433.

High Resolution Electron Microscopy of Epitaxial Layers and Interfaces in the CaF_2/Si(100) and CaF_2/Si/CaF_2/Si(100) Heterosystems; Kiselev, A. N.; Velichko, A. A.; Okomelchenko, I. A. *J. Cryst. Growth* **1993**, *129*, 163–172.

A Microstructural Study of Crystalline Defects in PbSe/BaF_2/CaF_2 on (111)Si Grown by Molecular Beam Epitaxy; Mathet, V.; Galtier, P.; Nguyenvandau, F.; Padeletti, G.; Olivier, J. *J. Cryst. Growth* **1993**, *132*, 241–249.

Preparation and Characterization of MBE Grown Si/CaF_2 Heterostructures; Rossek, U.; Mader, M.; Tempel, A. *Cryst. Res. Technol.* **1993**, *28*, 899–907.

Sm^{2+} Photoluminescence and X-Ray Scattering Studies of A-Type and B-Type Epitaxial CaF_2 Layers on Si(111); Sokolov, N. S.; Hirai, T.; Kawasaki, K.; Ohmi, S. I.; Tsutsui, K.; et al. *Jpn. J. Appl. Phys.* **1994**, *33*, 2395–2400.

SrF_2

Comparative Study of Hypersonic Dynamics in CaF_2 and SrF_2 Films on Si(111); Aleksandrov, V. V.; Potapova, J. B.; Diakonov, A. M.; Yakovlev, N. L. *Thin Solid Films* **1994**, *237*, 25–28.

$TiCl_4$

Adsorption of $TiCl_4$, SiH_4, and HCl on Si(100)—Application to $TiSi_2$ Chemical Vapor Deposition and Si Etching; Mendicino, M. A.; Seebauer, E. G. *J. Electrochem. Soc.* **1993**, *140*, 1786–1793.

LaF_3

Photoemission Study of the Growth of the LaF_3 Si(111) Interface; Malten, C.; Cramm, S.; Colbow, K. M.; Eberhardt, W. *J. Vac. Sci. Technol. A* **1994**, *12*, 418–422.

Semiconductor Films

SiC

Equilibrium Predictions of the Role of Organosilicon Compounds in the Chemical Vapor Deposition of Silicon Carbide; Allendorf, M. D. *J. Electrochem. Soc.* **1993**, *140*, 747–753.

Low Temperature Impurity Diffusion in SiC—Planar Quantum Size p-n-Junctions and n-p-n Transistor Structures; Bagraev, N. T.; Klyachkin, L. E.; Sukhanov, V. L. *Solid-State Electron.* **1993**, *36*, 1741–1747.

Effects of Propane and Methane on Carbonization and Surface Morphology in Heteroepitaxial Growth of β-SiC Films on (100) Si Via Chemical Vapor Deposition; Bahavar, B.; Chaudhry, M. I.; McCluskey, R. J. *Appl. Phys. Lett.* **1993**, *63*, 914–916.

Atomic Force Microscopy Study of the Microroughness of SiC Thin Films; Blouin, M.; Guay, D.; Elkhakani, M. A.; Chaker, M.; Boily, S.; Jean, A. *Thin Solid Films* **1994**, *249*, 38–43.

Conversion of Single Crystal Si(100) to SiC Film by C_2H_2; Chiu, C. C.; Desu, S. B. *J. Mater. Res.* **1993**, *8*, 535–544.

Electron Cyclotron Resonance Plasma Ion Beam Effects on the Formation of SiC on Si(001) Characterized by In-Situ Photoemission; Diani, M.; Aubel, D.; Bischoff, J. L.; Kubler, L.; Bolmont, D. *Thin Solid Films* **1994**, *241*, 305–309.

X-Ray Photoelectron Diffraction Observation of β-SiC(001) Obtained by Electron Cyclotron Resonance Plasma Assisted Growth on Si(001); Diani, M.; Bischoff, J. L.; Kubler, L.; Bolmont, D. *Appl. Surf. Sci.* **1993**, *68*, 575–582.

Neutral Ion Figuring of Chemical Vapor Deposited SiC; Fawcett, S. C.; Drueding, T. W.; Bifano, T. G. *Opt. Eng.* **1994**, *33*, 967–974.

Microscopic Mechanisms of Accurate Layer-by-Layer Growth of β-SiC; Hara, S.; Meguro, T.; Aoyagi, Y.; Kawai, M.; Misawa, S.; et al. *Thin Solid Films* **1993**, *225*, 240–243.

Mass Spectrometry Detection of SiH_m and CH_m Radicals from SiH_4-CH_4-H_2 RF Discharges Under High Temperature Deposition Conditions of Silicon Carbide; Kaenune, P.; Perrin, J.; Guillon, J.; Jolly, J. *Jpn. J. Appl. Phys.* **1994**, *33*, 4303–4307.

Growth Mechanism of 6H-SiC in Step Controlled Epitaxy; Kimoto, T.; Nishino, H.; Yoo, W. S.; Matsunami, H. *J. Appl. Phys.* **1993**, *73*, 726–732.

Simulations and Experiments of SiC Heteroepitaxial Growth on Si(001) Surface; Kitabatake, M.; Deguchi, M.; Hirao, T. *J. Appl. Phys.* **1993**, *74*, 4438–4445.

Scanning Auger Microscopy Study of Heterogeneous Growth of SiC Film on Si(100) by Reaction with a C_2H_2 Beam; Kusunoki, I. *Jpn. J. Appl. Phys.* **1993**, *32*, 2074–2077.

Atomic Level Epitaxy of 3C-SiC by Low Pressure Vapor Deposition with Alternating Gas Supply; Nagasawa, H.; Yamaguchi, Y. *Thin Solid Films* **1993**, *225*, 230–234.

Heteroepitaxial Growth and ESR Evaluation of 3C-SiC; Nagasawa, H.; Yamaguchi, Y.; Izumi, T.; Tonosaki, K. *Appl. Surf. Sci.* **1993**, *70/71*, 542–545.

Interface Modification and Characterization of Silicon Carbide Platelets Coated with Alumina Particles; Pei, P. T.; Kelly, J. F.; Malghan, S. G. *Colloids Surf. A* **1993**, *70*, 277–287.

Spectroscopic Study of SiC-Like Structures Formed on Polycrystalline Silicon Sheets during Growth; Pivac, B.; Furic, K.; Milun, M.; Valla, T.; Borghesi, A.; Sassella, A. *J. Appl. Phys.* **1994**, *75*, 3586–3592.

Effect of Oxygen Atom Bombardment on the Reflectance of Silicon Carbide Mirrors in the Extreme Ultraviolet Region; Seely, J. F.; Holland, G. E.; Hunter, W. R.; McCoy, R. P.; Dymond, K. F.; Corson, M. *Appl. Opt.* **1993**, *32*, 1805–1810.

Preliminary Soft X-Ray Studies of β-SiC; Shek, M. L.; Miyano, K. E.; Dong, Q. Y.; Callcott, T. A.; Ederer, D. L. *J. Vac. Sci. Technol. A* **1994**, *12*, 1079–1084.

Kinetic Study of Silicon Carbide Deposited from Methyltrichlorosilane Precursor; Tsai, C. Y.; Desu, S. B.; Chiu, C. C. *J. Mater. Res.* **1994**, *9*, 104–111.

Oxidation of Carbon/Carbon Composite Coated with SiC-(Si/$ZrSi_2$)-$ZrSi_2$; Wei, W. C. J.; Wu, T. M. *Carbon* **1994**, *32*, 605–613.

Atomic Structure of β-SiC(100) Surfaces—A Study Using the Tersoff Potential; Yan, H.; Hu, X.; Jonsson, H. *Surf. Sci.* **1994**, *316*, 181–188.

Si

Low Temperature Silicon Homoepitaxy by Ultrahigh Vacuum Electron Cyclotron Resonance Chemical Vapor Deposition; Tae, H. S.; Hwang, S. H.; Park, S. J.; Yoon, E.; Whang, K. W. *Appl. Phys. Lett.* **1994**, *64*, 1021–1023.

Chemical Equilibration of Plasma Deposited Amorphous Silicon with Thermally Generated Atomic Hydrogen; An, I.; Li, Y. M.; Wronski, C. R.; Collins, R. W. *Phys. Rev. B* **1993**, *48*, 4464–4472.

Silver Induced Formation of Si(111)-$\sqrt{3}\times\sqrt{3}$ Structure from Hydrogenated Amorphous Silicon Film; Ashtikar, M. S.; Sharma, G. L. *Solid State Commun.* **1994**, *91*, 831–834.

Light Scattering by Acoustic Phonons in Unhydrogenated and Hydrogenated Amorphous Silicon; Bustarret, E.; Thomsen, C.; Stutzmann, M.; Asano, A.; Summonte, C. *J. Non-Cryst. Solids* **1993**, *166*, 927–930.

Density of Amorphous Si; Custer, J. S.; Thompson, M. O.; Jacobson, D. C.; Poate, J. M.; Roorda, S.; et al. *Appl. Phys. Lett.* **1994**, *64*, 437–439.

Interaction of Aluminum with Hydrogenated Amorphous Silicon at Low Temperatures; Haque, M. S.; Naseem, H. A.; Brown, W. D. *J. Appl. Phys.* **1994**, *75*, 3928–3935.

Effect of Heating SiH_4 on the Plasma Chemical Vapor Deposition of Hydrogenated Amorphous Silicon; Hishikawa, Y.; Sasaki, M.; Tsuge, S.; Tsuda, S. *Jpn. J. Appl. Phys.* **1994**, *33*, 4373–4376.

The Chemisorption and Reaction of Diethylsilane on Silicon(100) and Silicon(111) Surfaces; Lapianosmith, D. A.; Himpsel, F. J.; Terminello, L. J. *J. Appl. Phys.* **1993**, *74*, 5842–5849.

Excimer Laser Assisted RF Glow Discharge Deposition of Amorphous and Microcrystalline Silicon Thin Films; Layadi, N.; Icabarrocas, P. R.; Gerri, M.; Marine, W.; Spousta, J. *Appl. Phys. A* **1994**, *58*, 507–512.

Selective Etching of Hydrogenated Amorphous Silicon by Hydrogen Plasma; Otobe, M.; Kimura, M.; Oda, S. *Jpn. J. Appl. Phys.* **1994**, *33*, 4442−4445.

Ordering of Amorphous Silicon during Solid Phase Epitaxy Studied by Scanning Tunneling Microscopy; Terovanesyan, E.; Manassen, Y.; Shachal, D. *Phys. Rev. B* **1994**, *50*, 8020−8023.

Density Changes and Viscous Flow during Structural Relaxation of Amorphous Silicon; Volkert, C. A. *J. Appl. Phys.* **1993**, *74*, 7107−7113.

Film Thickness Reduction of Thermally Annealed Hydrogenated Amorphous Silicon Prepared with Plasma Enhanced Chemical Vapor Deposition; Yang, Y. K.; Shin, J. S.; Hsieh, R. G.; Gan, J. Y. *Appl. Phys. Lett.* **1994**, *64*, 1567−1569.

c-BN

Atomic Structure Calculations for Epitaxy of c-BN on Si(001); Verwoerd, W. S.; Osuch, K.; Badziag, P. *Surf. Sci.* **1994**, *312*, 221−232.

III–V Semiconductors

Low Temperature GaAs Epitaxial Growth on Si-(100) by Molecular Beam Epitaxy and the Postgrowth Rapid Thermal Annealing; Chiang, T. Y.; Liu, E. H.; Yew, T. R. *J. Cryst. Growth* **1994**, *135*, 469−475.

Growth of GaAs Light Modulators on Si by Gas Source Molecular Beam Epitaxy for 850 nm Optical Interconnects; Cunningham, J. E.; Goossen, K. W.; Walker, J. A.; Jan, W.; Santos, M.; Miller, D. A. B. *J. Vac. Sci. Technol. B* **1994**, *12*, 1246−1250.

Monolithically Integrated AlGaAs/InGaAs Laser Diode, p-n Photodetector and GaAs-MESFET Grown on Si Substrate; Egawa, T.; Jimbo, T.; Umeno, M. *Jpn. J. Appl. Phys.* **1993**, *32*, 650−653.

Heteroepitaxy of CdTe on GaAs and Silicon Substrates; Faurie, J. P.; Sporken, R.; Chen, Y. P.; Lange, M. D.; Sivananthan, S. *Mater. Sci. Eng. B* **1993**, *16*, 51−56.

Generation and Annihilation of Antiphase Domain Boundaries in GaAs on Si Grown by Molecular Beam Epitaxy; Georgakilas, A.; Stoemenos, J.; Tsagaraki, K.; Komninou, P.; Flevaris, N.; et al. *J. Mater. Res.* **1993**, *8*, 1908−1921.

GaAs Formation by Reduction of As_2O_3 and Ga_2O_3 at SiO_2/GaAs Oxides/GaAs Interfaces; Jimenez, I.; Moreno, M.; Martingago, J. A.; Asensio, M. C.; Sacedon, J. L. *J. Vac. Sci. Technol. A* **1994**, *12*, 1170−1175.

MOCVD Grown CdZnTe/GaAs/Si Substrates for Large Area HgCdTe Irfpas; Johnson, S. M.; Vigil, J. A.; James, J. B.; Cockrum, C. A.; Konkel, W. H.; et al. *J. Electron. Mater.* **1993**, *22*, 835−842.

X-Ray Standing Wave Analysis of GaAs/Si Interface; Kawamura, T.; Takenaka, H.; Uneta, M.; Oshima, M.; Fukuda, Y.; et al. *Jpn. J. Appl. Phys.* **1993**, *32*, 622−625.

Effects of Insitu Thermal Annealing on Defects Associated with GaAs/Ge Interface in GaAs/Ge/Si Heterostructure; Kim, D. K.; Lee, B. T.; Woo, Y. D.; Kang, T. W.; Paek, M. C. *Mater. Lett.* **1993**, *16*, 26−28.

Reflection High Energy Electron Diffraction of Heteroepitaxy in Chemical Vapor Deposition Reactor—Atomic Layer Epitaxy of GaAs, AlAs and GaP on Si; Kitahara, K.; Ozeki, M.; Nakajima, K. *Jpn. J. Appl. Phys.* **1993**, *32*, 1051−1055.

Effects of Post-Diffusion Annealing on Zn-Diffused GaAs-Si; Ky, N. H.; Ganiere, J. D.; Reinhart, F. K.; Blanchard, B.; Pfister, J. C. *J. Appl. Phys.* **1993**, *74*, 5493−5500.

Progression of Cleavage in Si, Ge, and GaAs; Li, D. G.; McAlpine, N. S.; Haneman, D. *Appl. Surf. Sci.* **1993**, *65/66*, 553−559.

Quasi-2-Dimensional Plasmons of a Single Delta-Doped Layer in GaAs Studied by High Resolution Electron Energy Loss Spectroscopy; Lohe, C.; Leuther, A.; Forster, A.; Luth, H. *Phys. Rev. B* **1993**, *47*, 3819−3826.

Charge-Balanced Heteroepitaxial Growth of GaAs on Si; Maehashi, K.; Hasegawa, S.; Nakashima, H. *Jpn. J. Appl. Phys.* **1993**, *32*, 642−645.

Effects of SiAsBeAs Interface Structure on the Initial Stages of GaAs MBE Growth on Si(111); Maehashi, K.; Hasegawa, S.; Nakashima, H. *J. Cryst. Growth* **1993**, *127*, 98−101.

Improvements in the Heteroepitaxial Growth of GaAs on Si by MOVPE; Marschner, T.; Stolz, W.; Gobel, E. O.; Phillipp, F.; Muller, M.; Lorberth, J. *Mater. Sci. Eng. B* **1993**, *21*, 266−269.

GaAs Heteroepitaxy on an Epitaxial Si Surface with a Low Temperature Process; Mori, H.; Tachikawa, M.; Sugo, M.; Itoh, Y. *Appl. Phys. Lett.* **1993**, *63*, 1963−1965.

Misorientation in GaAs on Si Grown by Migration Enhanced Epitaxy; Nozawa, K.; Horikoshi, Y. *Jpn. J. Appl. Phys.* **1993**, *32*, 626−631.

Growth and Characterization of GaSe and GaAs/GaSe on As-Passivated Si(111) Substrates; Palmer, J. E.; Saitoh, T.; Yodo, T.; Tamura, M. *J. Appl. Phys.* **1993**, *74*, 7211−7222.

Lattice Mismatched InGaAs on Silicon Photodetectors Grown by Molecular Beam Epitaxy; Papanicolaou, N. A.; Anderson, G. W.; Iliadis, A. A.; Christou, A. *J. Electron. Mater.* **1993**, *22*, 201−206.

Correlation Between Initial Growth Planarity and Epilayer Tilting in the Vicinal GaAs/Si System; Riesz, F.; Varrio, J.; Pesek, A.; Lischka, K. *Appl. Surf. Sci.* **1994**, *75*, 248−251.

Deuterium Effusion from Crystalline n-Type GaAs-(Si); Rizk, R.; Theys, B.; Pesant, J. C.; Chevallier, J.; Aucouturier, M.; Pajot, B. *Phys. Rev. B* **1993**, *47*, 15523−15532.

Growth of GaAs Layers on Si Substrates by One-Step Low Pressure Metal-Organic Chemical Vapor Deposition Without High Temperature Thermal Cleaning Treatment; Sato, K.; Togura, K. *Jpn. J. Appl. Phys.* **1993**, *32*, 4656−4660.

Spontaneous Extinction of Twin Surface in GaAs on Si(100) Grown by One-Step Low Pressure Metal-Organic Chemical Vapor Deposition; Sato, K.; Togura, K.; Sato, K. *Jpn. J. Appl. Phys.* **1994**, *33*, 1986−1990.

Cleaning of Si(100) Surface by As ionized Cluster Beam Prior to Epitaxial Growth of GaAs; Shinohara, M.; Saraie, J.; Ohtani, F.; Ishiyama, O.; Ogawa, K.; Asari, M. *J. Appl. Phys.* **1993**, *73*, 7845−7850.

Fabrication of GaAs Nanostructures with a Scanning Tunneling Microscope; Snow, E. S.; Campbell,

P. M.; Shanabrook, B. V. *Appl. Phys. Lett.* **1993**, *63*, 3488–3490.

Minority Carrier Properties of GaAs on Si Grown by Metalorganic Chemical Vapor Deposition; Soga, T.; Jimbo, T.; Umeno, M. *Jpn. J. Appl. Phys.* **1994**, *33*, 1494–1498.

GaAs Single-Domain Growth on Exact (100) Si Substrate; Sprung, K. R.; Wilke, K.; Heymann, G.; Varrio, J.; Pessa, M. *Appl. Phys. Lett.* **1993**, *62*, 2711–2712.

Time Dependence of the Laser-Induced Femtosecond Lattice Instability of Si and GaAs—Role of Longitudinal Optical Distortions; Stampfli, P.; Bennemann, K. H. *Phys. Rev. B* **1994**, *49*, 7299–7305.

Continuous GaAs Film Growth on Epitaxial Si Surface in Initial Stage of GaAs/Si Heteroepitaxy; Tachikawa, M.; Mori, H.; Sugo, M.; Itoh, Y. *Jpn. J. Appl. Phys.* **1993**, *32*, 1252–1255.

Improved CdTe Layers on GaAs and Si Using Atomic Layer Epitaxy; Wang, W. S.; Ehsani, H.; Bhat, I. *J. Electron. Mater.* **1993**, *22*, 873–878.

Effect of ionization and Acceleration of As-Source Beam on Low Temperature Epitaxial Growth of GaAs on Exact (100)Si; Yun, S. J.; Kim, K.; Yoo, M. C. *Appl. Surf. Sci.* **1993**, *70/71*, 536–541.

Low Temperature Epitaxial Growth of GaAs on on-Axis (100) Si Using ionized Source Beam Epitaxy; Yun, S. J.; Yoo, M. C.; Kim, K. *J. Appl. Phys.* **1993**, *74*, 2866–2869.

The Effect of As/Ga Flux Ratio on Si-Doped GaAs Layers Grown by Molecular Beam Epitaxy; Zhang, D. H.; Radhakrishnan, K.; Yoon, S. F. *J. Cryst. Growth* **1994**, *135*, 441–446.

Chemical States of the GaAs/Si Interface; Zhou, H. J.; Ho, W. *J. Vac. Sci. Technol. A* **1994**, *12*, 1114–1119.

InP on Si(111)—Accommodation of Lattice Mismatch and Structural Properties; Krost, A.; Heinrichsdorff, F.; Bimberg, D.; Cerva, H. *Appl. Phys. Lett.* **1994**, *64*, 769–771.

II–VI Semiconductors

Direct Molecular Beam Epitaxial Growth of ZnTe(100) and CdZnTe(100)/ZnTe(100) on Si(100) Substrates; Delyon, T. J.; Roth, J. A.; Wu, O. K.; Johnson, S. M.; Cockrum, C. A. *Appl. Phys. Lett.* **1993**, *63*, 818–820.

Atomic Rearrangement at the Interface of Annealed ZnSe Films Grown on Vicinal Si(001) Substrates; Romano, L. T.; Bringans, R. D.; Knall, J.; Biegelsen, D. K.; Garcia, A.; et al. *Phys. Rev. B* **1994**, *50*, 4416–4423.

CdTe

Structure of CdTe(111)B Grown by MBE on Misoriented Si(001); Chen, Y. P.; Sivananthan, S.; Faurie, J. P. *J. Electron. Mater.* **1993**, *22*, 951–957.

CdTe Rotation Growth on Silicon Substrates by Metalloorganic Chemical Vapor Deposition; Ebe, H.; Takigawa, H. *Mater. Sci. Eng. B* **1993**, *16*, 57–59.

Heteroepitaxy of CdTe on GaAs and Silicon Substrates; Faurie, J. P.; Sporken, R.; Chen, Y. P.; Lange, M. D.; Sivananthan, S. *Mater. Sci. Eng. B* **1993**, *16*, 51–56.

Improved CdTe Layers on GaAs and Si Using Atomic Layer Epitaxy; Wang, W. S.; Ehsani, H.; Bhat, I. *J. Electron. Mater.* **1993**, *22*, 873–878.

TiO_2

Structural Properties of Titanium Dioxide Films Grown on p-Si by Metal Organic Chemical Vapor Deposition at Low Temperature; Yoon, Y. S.; Kang, W. N.; Yom, S. S.; Kim, T. W.; Jung, M.; et al. *Thin Solid Films* **1994**, *238*, 12–14.

Organic Molecules

Ethylene Adsorption and Decomposition on Si(100) 2×1—A Semiempirical Quantum Chemical Study; Cao, P. L.; Zhou, R. H. *J. Phys.: Condens. Matter* **1993**, *5*, 2887–2896.

Molecular Dynamics with Combined Quantum and Empirical Potentials—C_2H_2 Adsorption on Si(100); Carmer, C. S.; Weiner, B.; Frenklach, M. *J. Chem. Phys.* **1993**, *99*, 1356–1372.

An STM Study of the Chemisorption of C_2H_4 on Si(001)(2×1); Mayne, A. J.; Avery, A. R.; Knall, J.; Jones, T. S.; Briggs, G. A. D.; Weinberg, W. H. *Surf. Sci.* **1993**, *284*, 247–256.

Hydrocarbon Surface Chemistry on Si(100); Cheng, C. C.; Taylor, P. A.; Wallace, R. M.; Gutleben, H.; Clemen, L.; et al. *Thin Solid Films* **1993**, *225*, 196–202.

Conversion of Single Crystal Si(100) to SiC Film by C_2H_2; Chiu, C. C.; Desu, S. B. *J. Mater. Res.* **1993**, *8*, 535–544.

The Interaction of Atomic Hydrogen with Adsorbed Ethylene and Acetylene on Si(100); Chua, L. H.; Jackman, R. B.; Foord, J. S. *Surf. Sci.* **1994**, *315*, 69–80.

A Theoretical Study of the Structures of Propylene Adsorbed on the Si(100)-(2×1) Surface; Craig, B. I. *Surf. Sci.* **1993**, *298*, 87–93.

Mechanisms of Halogen Chemisorption Upon a Semiconductor Surface—I_2, Br_2, Cl_2, and C_6H_5Cl Chemisorption Upon the Si(100) (2×1) Surface; Flaum, H. C.; Sullivan, D. J. D.; Kummel, A. C. *J. Phys. Chem.* **1994**, *98*, 1719–1731.

Adsorption and Reactions of Ethylsilane on Si(100); Foster, M.; Darlington, B.; Scharff, J.; Campion, A. *Surf. Sci.* **1994**, *315*, 947–952.

Controlled Carbonization of Si(001) Surface Using Hydrocarbon Radicals in UltraHigh Vacuum; Hatayama, T.; Tarui, Y.; Yoshinobu, T.; Fuyuki, T.; Matsunami, H. *J. Cryst. Growth* **1994**, *136*, 333–337.

Adsorption of Ethylene on the Si(100)-(2×1) Surface; Huang, C.; Widdra, W.; Weinberg, W. H. *Surf. Sci.* **1994**, *315*, 953–958.

The Initial Stages of Diamond Growth—An Adsorption Study of Hot Filament Activated Methane and Hydrogen on Si(100); Jackman, R. B.; Chua, L. H.; Foord, J. S. *Surf. Sci.* **1993**, *292*, 47–60.

Chemisorption of H, H_2O and C_2H_4 on Si(113)—Implications for the Structure; Jacobi, K.; Myler, U. *Surf. Sci.* **1993**, *284*, 223–235.

Reaction of Si+ (P-2) with Acetylene and with Ethylene—Examination of the Potential Energy Surfaces for Adducts $SiC_2H_2^+$ and $SiC_2H_4^+$; Ketvirtis, A. E.; Bohme, D. K.; Hopkinson, A. C. *THEOCHEM J. Mol. Struct.* **1994**, *119*, 1–17.

Tunneling Electron Induced Adsorption of Pyridine on a Hydrogen Terminated Silicon Surface; Komiyama, M.; Kirino, M. *J. Vac. Sci. Technol. B* **1994**, *12*, 1866–1868.

Topographic and Spectroscopic Analysis of Ethylene Adsorption on Si(111)7×7 by STM and STS; Piancastelli, M. N.; Motta, N.; Sgarlata, A.; Balzarotti, A.; Decrescenzi, M. *Phys. Rev. B* **1993**, *48*, 17892–17896.

An Investigation of the Ar^+ Ion Enhanced Reaction of CCl_4 on Si(100) by Secondary Ion Mass Spectroscopy; Wee, A. T. S.; Huan, C. H. A.; Tan, K. L.; Tan, R. S. K. *J. Mater. Sci.* **1994**, *29*, 4037–4042.

Reaction of CH_4 and CH_3F with Si(111); Yang, H.; Jing, Z.; Whitten, J. L. *J. Electron Spectrosc. Relat. Phenom.* **1994**, *69*, 23–29.

Total Energy Calculations for Acetylene Adsorption and Decomposition on Si(100)-2×1; Zhou, R. H.; Cao, P. L.; Lee, L. Q. *Phys. Rev. B* **1993**, *47*, 10601–10606.

Structural Analysis of Epitaxial Films of Metal Phthalocyanines on Hydrogen Terminated Si(111) Surfaces; Kawaguchi, T.; Tada, H.; Koma, A. *J. Appl. Phys.* **1994**, *75*, 1486–1492.

Properties of Heterojunction of Si/Poly(3-Methylthiophene) as a Function of Polymerization Condition; Kokado, H.; Hosokawa, F.; Hoshino, K. *Jpn. J. Appl. Phys.* **1993**, *32*, 189–194.

Catalytic Dehydrogenation and Thermal Chemistry of Cyclohexene and 1-Methyl-1,4-Cyclohexadiene on Si(111)7×7; Macpherson, C. D.; Hu, D. Q.; Doan, M.; Leung, K. T. *Surf. Sci.* **1994**, *310*, 231–242.

Chemisorption of 11H-Eicosafluoroundecanoic Acid Monomolecular Film from a Liquid Phase Onto Si(111) Surface—Study by X-Ray Photoelectron Spectroscopy; Mitsuya, M. *Langmuir* **1994**, *10*, 1635–1637.

Measurement of Organic Matter on Si Wafer by Thermal Desorption Spectroscopy; Okada, C.; Takahashi, I.; Kobayashi, H.; Ryuta, J.; Shingyouji, T. *Jpn. J. Appl. Phys.* **1993**, *32*, 1186–1188.

Epitaxial Growth of Metal-Phthalocyanines on Hydrogen Terminated Si(111) Surfaces; Tada, H.; Kawaguchi, T.; Koma, A. *Appl. Surf. Sci.* **1994**, *75*, 93–98.

Photodecomposition of Adsorbed Methoxy Species by UV Light and Formaldehyde Adsorption on Si(111) Studied by XPS and UPS; Tanaka, K.; Matsuzaki, S.; Toyoshima, I. *J. Phys. Chem.* **1993**, *97*, 5673–5677.

Thermochemistry of the Reaction of Si+((2)P) with Methanol—A G_2 Molecular Orbital Study; Luna, A.; Yanez, M. *J. Phys. Chem.* **1993**, *97*, 10659–10669.

Photodecomposition of Adsorbed Methoxy Species by UV Light and Formaldehyde Adsorption on Si(111) Studied by XPS and UPS; Tanaka, K.; Matsuzaki, S.; Toyoshima, I. *J. Phys. Chem.* **1993**, *97*, 5673–5677.

Analysis of Fluorocarbon Film Deposited by Highly Selective Oxide Etching; Akimoto, T.; Furuoya, S.; Harasima, K.; Ikawa, E. *Jpn. J. Appl. Phys.* **1994**, *33*, 2151–2156.

Fluorocarbon High Density Plasmas. 8. Study of the Ion Flux Composition at the Substrate in Electron Cyclotron Resonance Etching Processes Using Fluorocarbon Gases; Kirmse, K. H. R.; Wendt, A. E.; Oehrlein, G. S.; Zhang, Y. *J. Vac. Sci. Technol. A* **1994**, *12*, 1287–1292.

Smoothing of the Si Surface Using CF_4/O_2 Down Flow Etching; Nishino, H.; Hayasaka, N.; Horioka, K.; Shiozawa, J.; Nadahara, S.; et al. *J. Appl. Phys.* **1993**, *74*, 1349–1353.

X-Ray Photoelectron Spectroscopy Study of Low Energy CF^+ Ion Interactions with Silicon; Chang, W. H.; Bello, I.; Lau, W. M. *J. Vac. Sci. Technol. A* **1993**, *11*, 1221–1225.

Etching Rate Characterization of SiO_2 and Si Using Ion Energy Flux and Atomic Fluorine Density in a $CF_4/O_2/Ar$ Electron Cyclotron Resonance Plasma; Ding, J.; Jenq, J. S.; Kim, G. H.; Maynard, H. L.; Hamers, J. S.; et al. *J. Vac. Sci. Technol. A* **1993**, *11*, 1283–1288.

Decomposition of Gaseous Dielectrics (CF_4, SF_6) by a Nonequilibrium Plasma—Mechanisms, Kinetics, Mass Spectrometric Studies and Interactions with Polymeric Targets; Khairallah, Y.; Khonsariarefi, F.; Amouroux, J. *Pure Appl. Chem.* **1994**, *66*, 1353–1362.

Fluorocarbon High Density Plasmas. 1. Fluorocarbon Film Deposition and Etching Using CF_4 and CHF_3; Oehrlein, G. S.; Zhang, Y.; Vender, D.; Haverlag, M. *J. Vac. Sci. Technol. A* **1994**, *12*, 323–332.

Near-Surface Residue Formation in CF_4/H_2 Reactive Ion Etching of Silicon; Potter, G. E.; Morrison, G. H.; Charvat, P. K.; Ruoff, A. L. *J. Vac. Sci. Technol. B* **1992**, *10*, 2398–2406.

Direct Evidence for β-Hydride Elimination on Si(100); Keeling, L. A.; Chen, L.; Greenlief, C. M.; Mahajan, A.; Bonser, D. *Chem. Phys. Lett.* **1994**, *217*, 136–141.

Ultraviolet Laser Chemistry of Adsorbed Dimethylcadmium Molecules; Varakin, V. N.; Lunchev, V. A.; Simonov, A. P. *High Energy Chem.* **1994**, *28*, 406–411.

Silicon Compounds

Silanes

Species-Specific Growth-Kinetics and Film Properties in Synchrotron Radiation Excited Si Growth with Disilane; Akazawa, H.; Utsumi, Y.; Nagase, M. *Appl. Surf. Sci.* **1994**, *80*, 299–303.

Growth-Kinetics of Micrometer-Size Silicon Lines Produced by Decomposition of Silane Using a Laser Direct-Writing Technique; Boughaba, S.; Auvert, G.; Pauleau, Y. *J. Appl. Phys.* **1994**, *75*, 3635–3642.

Si(001)2×1 Gas Source Molecular Beam Epitaxy from Si_2H_6—Growth-Kinetics and Boron Doping; Bramblett, T. R.; Lu, Q.; Hasan, M. A.; Jo, S. K.; Greene, J. E. *J. Appl. Phys.* **1994**, *76*, 1884–1888.

Adsorption and Dissociation of Disilane on Si(001) Studied by STM; Bronikowski, M. J.; Wang, Y. J.; McEllistrem, M. T.; Chen, D.; Hamers, R. J. *Surf. Sci.* **1993**, *298*, 50–62.

Study of Growth-Kinetics in Silicon Gas Source Molecular Beam Epitaxy with Disilane Using RHEED Intensity Oscillations; Butzke, S.; Werner, K.; Trommel, J.; Radelaar, S.; Balk, P. *Thin Solid Films* **1993**, *228*, 27–31.

Modeling Silicon Epitaxial Growth with SiH_2Cl_2; Coon, P. A.; Wise, M. L.; George, S. M. *J. Cryst. Growth* **1993**, *130*, 162–172.

Adsorption and Reactions of Diethylsilane on Si(100); Darlington, B.; Foster, M.; Campion, A. *Surf. Sci.* **1994**, *304*, 407–412.

Mechanistic Insight into Gas-Phase Reactions of $H^{\bullet}$ + Si_2H_6 and Hydrogen-Atom Etching of Silicon Surfaces; Dobbs, K. D.; Doren, D. J. *J. Am. Chem. Soc.* **1993**, *115*, 3731–3738.

Interaction of Copper-Catalysts and Si(100) for the Direct Synthesis of Methylchlorosilanes; Floquet, N.; Yilmaz, S.; Falconer, J. L. *J. Catal.* **1994**, *148*, 348–368.

Numerical Evaluation of Silicon-Thin Film Growth from $SiHCl_3$-H_2 Gas-Mixture in a Horizontal Chemical Vapor Deposition Reactor; Habuka, H.; Katayama, M.; Shimada, M.; Okuyama, K. *Jpn. J. Appl. Phys.* **1994**, *33*, 1977–1985.

Effect of Heating SiH_4 on the Plasma Chemical Vapor Deposition of Hydrogenated Amorphous Silicon; Hishikawa, Y.; Sasaki, M.; Tsuge, S.; Tsuda, S. *Jpn. J. Appl. Phys.* **1994**, *33*, 4373–4376.

Kinetics of the Low Pressure Chemical Vapor Deposition of Polycrystalline Germanium-Silicon Alloys from SiH_4 and GeH_4; Holleman, J.; Kuiper, A. E. T.; Verweij, J. F. *J. Electrochem. Soc.* **1993**, *140*, 1717–1722.

Hydrogen Desorption Rate and Surface Hydrogen Coverage during Isothermal Annealing for Si_2H_6-Adsorbed Si(100) Surfaces; Horie, T.; Takakuwa, Y.; Yamaguchi, T.; Miyamoto, N. *J. Cryst. Growth* **1994**, *136*, 344–348.

Conditions for Successful Low Temperature Growth of Hydrogenated Amorphous Silicon Film from Silyl Radicals Conformed to Layer-Growth Mode; Kawasaki, M.; Suzuki, H.; Kawaguchi, Y. *Appl. Surf. Sci.* **1994**, *80*, 310–315.

Hydrogen Desorption Kinetics from the Growing Si(100) Surface during Silane Gas Source Molecular Beam Epitaxy; Kim, K. J.; Suemitsu, M.; Miyamoto, N. *Appl. Phys. Lett.* **1993**, *63*, 3358–3360.

Photoirradiation Effects on Surface-Reactions in Si Monolayer Overgrowth by Si_2H_6 Source MBE; Koide, Y.; Zaima, S.; Okada, M.; Yasuda, Y. *Appl. Surf. Sci.* **1994**, *80*, 304–309.

Thermal Reactions of Disilane on Si(100) Studied by Synchrotron-Radiation Photoemission; Lin, D. S.; Miller, T.; Chiang, T. C.; Tsu, R.; Greene, J. E. *Phys. Rev. B* **1993**, *48*, 11846–11850.

Effects of SiH_4, GeH_4, and B_2H_6 on the Nucleation and Deposition of Polycrystalline $Si_{1-x}Ge_x$ Films; Lin, H. C.; Chang, C. Y.; Chen, W. H.; Tsai, W. C.; Chang, T. C.; et al. *J. Electrochem. Soc.* **1994**, *141*, 2559–2563.

Si Atomic Layer Epitaxy Based on Si_2H_6 and Remote He Plasma Bombardment; Mahajan, A.; Irby, J.; Kinosky, D.; Qian, R.; Thomas, S.; et al. *Thin Solid Films* **1993**, *225*, 177–182.

Surface Chemistry of Diethylsilane and Diethylgermane on Si(100)—An Atomic Layer Epitaxy Approach; Mahajan, A.; Kellerman, B. K.; Russell, N. M.; Banerjee, S.; Campion, A.; et al. *J. Vac. Sci. Technol. A* **1994**, *12*, 2265–2270.

Adsorption of $TiCl_4$, SiH_4, and HCl on Si(100)—Application to $TiSi_2$ Chemical Vapor Deposition and Si Etching; Mendicino, M. A.; Seebauer, E. G. *J. Electrochem. Soc.* **1993**, *140*, 1786–1793.

Growth-Rate Dependence on GeH_4 during Gas Source MBE of Si_xGe_{1-x} Alloys Grown from Si_2H_6 and GeH_4; Mokler, S. M.; Ohtani, N.; Xie, M. H.; Zhang, X.; Joyce, B. A. *J. Cryst. Growth* **1993**, *127*, 467–471.

Metal Impurity Evaluation in Silane Gas from the Qualification of Poly-Si Layers; Morin, M.; Koyanagi, M.; Friedt, J. M.; Hirose, M. *J. Electrochem. Soc.* **1994**, *141*, 274–277.

Si Deposition from Chlorosilanes. 1. Deposition Modeling; Narusawa, U. *J. Electrochem. Soc.* **1994**, *141*, 2072–2077.

Si Deposition from Chlorosilanes. 2. Numerical-Analysis of Thermofluid Effects on Deposition; Narusawa, U. *J. Electrochem. Soc.* **1994**, *141*, 2078–2083.

Effects of SiH_2Cl_2 on Low Temperature (≤200 °C) Si Epitaxy by Photochemical Vapor Deposition; Oshima, T.; Sano, M.; Yamada, A.; Konagai, M.; Takahashi, K. *Appl. Surf. Sci.* **1994**, *80*, 215–219.

On the Homogeneous Chemistry of the Thermal Decomposition of Methyltrichlorosilane—Thermodynamic Analysis and Kinetic Modeling; Papasouliotis, G. D.; Sotirchos, S. V. *J. Electrochem. Soc.* **1994**, *141*, 1599–1611.

The Effect of Zn Promoter on Enhanced Diffusion during Catalytic Formation of Methylchlorosilanes; Potochnik, S. J.; Falconer, J. L. *J. Catal.* **1994**, *147*, 101–106.

Adsorption and Decomposition of Diethylsilane and Diethyldichlorosilane by Si(100)(2×1) and Si(111)-(1×1); Schmidt, J.; Stuhlmann, C.; Ibach, H. *Surf. Sci.* **1994**, *302*, 10–24.

Effects of Trace Surface Oxidation in Low Temperature Epitaxy-Grown from Dichlorosilane; Sedgwick, T. O.; Agnello, P. D.; Grutzmacher, D. A. *J. Electrochem. Soc.* **1993**, *140*, 3684–3688.

Photoelectron Intensity Oscillation during Chemical Vapor Deposition on Si(100) Surface with Si_2H_6; Takakuwa, Y.; Enta, Y.; Yamaguchi, T.; Hori, T.; Niwano, M.; et al. *Appl. Phys. Lett.* **1994**, *64*, 2013–2015.

Growth Defect Observation with Pyramidal Hillock and Reduction by Photoexcited Hydrogen in Si CVD with SiH_2Cl_2; Takakuwa, Y.; Mazumder, M. K.; Miyamoto, N. *J. Electrochem. Soc.* **1994**, *141*, 2567–2572.

Chemically Vapor Deposited Tungsten Silicide Films Using Dichlorosilane in a Single-Wafer Reactor—Growth, Properties, and Thermal Stability; Telford, S. G.; Eizenberg, M.; Chang, M.; Sinha, A. K.; Gow, T. R. *J. Electrochem. Soc.* **1993**, *140*, 3689–3701.

Synchrotron-Radiation Assisted Si Epitaxial Growth—Comparison of Growth-Characteristics Between Si_2H_6 and SiH_2Cl_2 Gases; Urisu, T.; Akutsu, T.; Kuchitsu, K. *Appl. Phys. Lett.* **1993**, *62*, 2821–2823.

Synchrotron Radiation Assisted Si Epitaxial Growth Using Si_2H_6 and SiH_2Cl_2 Gases—Properties in the Low Temperature Region; Urisu, T.; Takahashi, J.;

Utsumi, Y.; Akutsu, T.; Kuchitsu, K. *J. Electrochem. Soc.* **1994**, *141*, 1562–1565.

An Atomically Resolved Scanning Tunneling Microscopy Study of the Thermal Decomposition of Disilane on Si(001); Wang, Y. J.; Bronikowski, M. J.; Hamers, R. J. *Surf. Sci.* **1994**, *311*, 64–100.

Evidence for Non-Hydrogen Desorption Limited Growth of Si from Disilane at Very-Low Temperatures in Gas Source Molecular Beam Epitaxy; Werner, K.; Butzke, S.; Radelaar, S.; Balk, P. *J. Cryst. Growth* **1994**, *136*, 338–343.

Adsorption of Hydrogen and Disilane on Si(100) and Si-Ge Surfaces; Wu, Y. M.; Nix, R. M. *Surf. Sci.* **1994**, *306*, 59–68.

$SiCl_4$

The Adsorption and Surface Reaction of $SiCl_4$ on Si(100)-(2×1); Gao, Q.; Dohnalek, Z.; Cheng, C. C.; Choyke, W. J.; Yates, J. T. *Surf. Sci.* **1994**, *302*, 1–9.

Siloxanes

Photo Excited Effects and the Growth Mechanism on Epitaxially Grown Al_2O_3(100) on Si(100); Ishida, M.; Yoshizu, T.; Hayama, K.; Nakamura, T. *Appl. Surf. Sci.* **1994**, *80*, 356–360.

On the Chemical Reaction Mode of Polysilicon Deposition from Silane; Kuhne, H. *Cryst. Res. Technol.* **1993**, *28*, 39–52.

Ultraviolet Induced Deposition of SiO_2 Film from Tetraethoxysilane Spin Coated on Si; Niwano, M.; Kinashi, K.; Saito, K.; Miyamoto, N.; Honma, K. *J. Electrochem. Soc.* **1994**, *141*, 1556–1561.

Photoemission Study of Synchrotron Radiation Induced Reactions of TeOs Adsorbed on Silicon Surface; Niwano, M.; Miyamoto, N.; Simons, J. K.; Frigo, S. P.; Rosenberg, R. A. *Appl. Surf. Sci.* **1994**, *80*, 403–408.

Synchrotron Radiation Induced Reactions of Tetraethoxysilane on Si Studied by Photoemission Spectroscopy; Niwano, M.; Simons, J. K.; Frigo, S. P.; Rosenberg, R. A. *J. Appl. Phys.* **1994**, *75*, 7304–7309.

High Fluidity Deposition of Silicon by Plasma Enhanced Chemical Vapor Deposition Using Si_2H_6 or SiH_4; Shin, H.; Hashimoto, M.; Okamoto, K.; Miyazaki, S.; Hirose, M. *Jpn. J. Appl. Phys.* **1993**, *32*, 3081–3084.

Salts

NaOH

Probing by In-Situ Scanning Tunneling Microscopy the Influence of an Organic Additive on Si Etching in NaOH; Allongue, P.; Bertagna, V.; Kieling, V.; Gerischer, H. *J. Vac. Sci. Technol. B* **1994**, *12*, 1539–1542.

Etching of Silicon in NaOH Solutions. 2. Electrochemical Studies of n-Si(111) and n-Si(100) and Mechanism of the Dissolution; Allongue, P.; Costakieling, V.; Gerischer, H. *J. Electrochem. Soc.* **1993**, *140*, 1018–1026.

The Surface of Si(111) during Etching in NaOH Studied by FTIR Spectroscopy in the ATR Technique; Rappich, J.; Lewerenz, H. J.; Gerischer, H. *J. Electrochem. Soc.* **1993**, *140*, 187–189.

NH_4F

Step Edge Structures on Si(112) and (113) Surfaces Treated in NH_4F Solution; Fujita, K.; Hirashita, N. *Jpn. J. Appl. Phys.* **1994**, *33*, 399–403.

Corrugated Structures on Si(110) Surfaces Treated in Ammonium Fluoride Solutions; Fujita, K.; Hirashita, N. *Jpn. J. Appl. Phys.* **1994**, *33*, 1145–1148.

Reaction of NH_4F/HF Solutions on Si(100) and Si-(111) Surfaces; Graf, D.; Bauermayer, S.; Schnegg, A. *J. Vac. Sci. Technol. A* **1993**, *11*, 940–944.

Separation of Charge Transfer and Surface Recombination Processes by Simultaneous Measurement of Photocurrent and Excess Microwave Conductivity Profiles of Si(111) in NH_4F; Lewerenz, H. J.; Schlichthorl, G. *J. Appl. Phys.* **1994**, *75*, 3544–3547.

Wet Chemical Etching of Si(100) Surfaces in Concentrated NH_4F Solution—Formation of (2×1)H Reconstructed Si(100) Terraces Versus (111) Faceting; Neuwald, U.; Hessel, H. E.; Feltz, A.; Memmert, U.; Behm, R. J. *Surf. Sci.* **1993**, *296*, 8–14.

Anisotropic Etching Versus Interaction of Atomic Steps—Scanning Tunneling Microscopy Observations on HF/NH_4F-Treated Si(111); Pietsch, G. J.; Kohler, U.; Henzler, M. *J. Appl. Phys.* **1993**, *73*, 4797–4807.

Effects of Predeposition HF/NH_4F Treatments on the Electrical Properties of SiO_2/Si Structures Formed by Low Temperature Plasma Assisted Oxidation and Deposition Processes; Yasuda, T.; Ma, Y.; Chen, Y. L.; Lucovsky, G.; Maher, D. *J. Vac. Sci. Technol. A* **1993**, *11*, 945–951.

NH_4OH

Chemical Treatment Effects of Si Surfaces in NH_4-OH H_2O_2 H_2O Solutions Studied by Spectroscopic Ellipsometry; Adachi, S.; Utani, K. *Jpn. J. Appl. Phys.* **1993**, *32*, 1189–1191.

Chemical Treatment Effect of Si Surfaces in 1 NH_4-OH:X H_2O_2:5 H_2O Solutions Studied by Spectroscopic Ellipsometry; Suzuki, T.; Adachi, S. *Jpn. J. Appl. Phys.* **1994**, *33*, 2689–2691.

HF-Treated and NH_4OH-Treated (111)Si Surfaces Studied by Spectroscopic Ellipsometry; Utani, K.; Suzuki, T.; Adachi, S. *J. Appl. Phys.* **1993**, *73*, 3467–3471.

Special Topics

Defects

On the Influence of Extrinsic Point Defects on Irradiation Induced Point Defect Distributions in Silicon; Vanhellemont, J.; Romanorodriguez, A. *Appl. Phys. A* **1994**, *58*, 541–549.

Photoetching

New Microfabrication Technique by Synchrotron Radiation Excited Etching—Use of Noncontact Mask on a Submicrometer Scale; Terakado, S.; Goto, T.; Ogura, M.; Kaneda, K.; Kitamura, O.; Suzuki, S. *Appl. Phys. Lett.* **1994**, *64*, 1659–1661.

References

(1) Walsh, R. *Acc. Chem. Res.* **1981**, *14*, 246.

(2) Bozack, M. J.; Choyke, W. J.; Muehlhoff, L.; Yates, J. T., Jr. *J. Appl. Phys.* **1986**, *60*, 3750–3754.
(3) Schlier, R. E.; Farnsworth, H. E. *J. Chem. Phys.* **1959**, *30*, 917.
(4) Levine, J. D. *Surf. Sci.* **1973**, *34*, 90–107.
(5) Chadi, D. J. *Phys. Rev. Lett.* **1979**, *43*, 43–47.
(6) Haneman, D. *Rep. Prog. Phys.* **1987**, *50*, 1045–1086.
(7) Jedrecy, N.; Sauvage-Simkin, M.; Pinchaux, R.; Massies, J.; Greiser, N.; Etgens, V. H. *Surf. Sci.* **1990**, *230*, 197–204.
(8) Lin, D.-S.; Miller, T.; Chiang, T.-C. *Phys. Rev. Lett.* **1991**, *67*, 2187–2190.
(9) Landemark, E.; Karlsson, C. J.; Chao, Y.-C.; Uhrberg, R. I. G. *Phys. Rev. Lett.* **1992**, *69*, 1588–1591.
(10) Landemark, E.; Karlsson, C. J.; Chao, Y.-C.; Uhrberg, R. I. G. *Surf. Sci.* **1993**, *287/288*, 529–533.
(11) Weakliem, P. C.; Smith, G. W.; Carter, E. A. *Surf. Sci.* **1990**, *232*, L219–L223.
(12) Dabrowski, J.; Scheffler, M. *Appl. Surf. Sci.* **1992**, *56–58*, 15–19.
(13) Roberts, N.; Needs, R. J. *Surf. Sci.* **1990**, *236*, 112–121.
(14) Krüger, P.; Pollmann, J. *Phys. Rev. B* **1993**, *47*, 1898–1910.
(15) Northrup, J. E. *Phys. Rev. B* **1993**, *47*, 10032–10035.
(16) Lander, J. J.; Morrison, J. *J. Chem. Phys.* **1962**, *37*, 729–746.
(17) Cardillo, M. J.; Lambert, W. R. *Surf. Sci.* **1986**, *168*, 724–733.
(18) Tabata, T.; Aruga, T.; Murata, Y. *Surf. Sci.* **1987**, *179*, L63-L70.
(19) Wolkow, R. A. *Phys. Rev. Lett.* **1992**, *68*, 2636–2639.
(20) Hamers, R. J.; Tromp, R. M.; Demuth, J. E. *Phys. Rev. B* **1986**, *34*, 5343–5357.
(21) Wiesendanger, R.; Bürgler, D.; Tarrach, G.; Güntherodt, H.-J. *Surf. Sci.* **1990**, *232*, 1–5.
(22) Wiesendanger, R.; Bürgler, D.; Tarrach, G.; Güntherodt, H.-J.; Shvets, L. V.; Coey, J. M. D. *Surf. Sci.* **1992**, *274*, 93–98.
(23) Chadi, D. J. *Phys. Rev. Lett.* **1987**, *59*, 1691–1694.
(24) Alerhand, O. L.; Vanderbilt, D.; Meade, R. D.; Joannopoulos, J. D. *Phys. Rev. Lett.* **1988**, *61*, 1973–7976.
(25) Poon, T. W.; Yip, S.; Ho, P. S.; Abraham, F. F. *Phys. Rev. Lett.* **1990**, *65*, 2161–2164.
(26) Vilfan, I. *Surf. Sci.* **1993**, *289*, L604–L608.
(27) Alerhand, O. L.; Nihat Berker, A.; Joannopoulos, J. D.; Vanderbilt, D.; Hamers, R. J.; Demuth, J. E. *Phys. Rev. Lett.* **1990**, *64*, 2406–2409.
(28) Salanon, B.; Barbier, L.; Lapajoulade, J. *Appl. Surf. Sci.* **1993**, *65/66*, 575–579.
(29) Tong, X.; Bennett, P. A. *Phys. Rev. Lett.* **1991**, *67*, 101–104.
(30) Schröder-Bergen, E.; Ranke, W. *Surf. Sci.* **1991**, *259*, 323–338.
(31) Barbier, L.; Lapujoulade, J. *Surf. Sci.* **1991**, *253*, 303–312.
(32) Aumann, C. E.; de Miguel, J. J.; Kariotis, R.; Lagally, M. G. *Surf. Sci.* **1992**, *275*, 1–15.
(33) de Miguel, J. J.; Aumann, C. E.; Kariotis, R.; Lagally, M. G. *Phys. Rev. Lett.* **1991**, *67*, 2830–2833.
(34) Takayanagi, K.; Tanishiro, Y.; Takahashi, S.; Takahashi, M. *Surf. Sci.* **1985**, *164*, 367–392.
(35) Vanderbilt, D. *Phys. Rev. B* **1987**, *36*, 6209–6212.
(36) Uhrberg, R. I. G.; Landemark, E.; Johansson, L. S. O. *Phys. Rev. B* **1989**, *39*, 13525–13528.
(37) Feenstra, R. M.; Lutz, M. A. *Surf. Sci.* **1991**, *243*, 151–165.
(38) Garni, B.; Savage, D. E.; Lagally, M. G. *Surf. Sci.* **1990**, *235*, L324–L328.
(39) Ohdomari, I. *Surf. Sci.* **1990**, *227*, L125-L129.
(40) Verwoerd, W. S.; Osuch, K. *Surf. Sci.* **1991**, *256*, L593–L597.
(41) Pandey, K. C. *Phys. Rev. Lett.* **1981**, *47*, 1913–1917.
(42) Pandey, K. C. *Phys. Rev. Lett.* **1982**, *49*, 223–226.
(43) Northrup, J. E.; Cohen, M. L. *Phys. Rev. Lett.* **1982**, *49*, 1349–1352.
(44) Tsong, T. T.; Feng, D. L.; Liu, H. M. *Surf. Sci.* **1988**, *199*, 421–438.
(45) Ranke, W. *Phys. Rev. B* **1990**, *41*, 5243–5250.
(46) Xing, Y. R.; Zhang, J. P.; Wu, J. A.; Liu, C. Z.; Wang, C. H. *Surf. Sci.* **1990**, *232*, L215–L218.
(47) Myler, U.; Althainz, P.; Jacobi, K. *Surf. Sci.* **1991**, *251/252*, 607–611.
(48) Olshanetsky, B. Z.; Solovyov, A. E.; Dolbak, A. E.; Maslov, A. A. *Surf. Sci.* **1994**, *306*, 327–341.
(49) Knall, J.; Pethica, J. B.; Todd, J. D.; Wilson, J. H. *Phys. Rev. Lett.* **1991**, *66*, 1733–1736.
(50) Hadley, M. J.; Tear, S. P.; Röttger, B.; Neddermeyer, H. *Surf. Sci.* **1993**, *280*, 258–264.
(51) Wei, J.; Williams, E. D.; Park, R. L. *Surf. Sci.* **1991**, *250*, L368–L372.
(52) Shimaoka, G. *Appl. Surf. Sci.* **1993**, *65/66*, 569–574.
(53) Dolbak, A. E.; Olshanetsky, B. Z.; Stenin, S. I.; Teys, S. A.; Gavrilova, T. A. *Surf. Sci.* **1989**, *218*, 37–54.
(54) Olshanetsky, B. Z.; Teys, S. A. *Surf. Sci.* **1990**, *230*, 184–196.
(55) Ampo, H.; Miura, S.; Kato, K.; Ohkawa, Y.; Tamura, A. *Phys. Rev. B* **1986**, *34*, 2329–2335.
(56) Safta, N.; Lacharme, J.-P.; Sébenne, C. A. *Surf. Sci.* **1993**, *287/288*, 312–316.
(57) Hoeven, A. J.; Dijkkamp, D.; Van Loenen, E. J.; Van Hooft, P. J. G. M. *Surf. Sci.* **1989**, *211/212*, 165–172.
(58) Shkrebtii, A. I.; Bertoni, C. M.; Del Sole, R.; Nesterenko, B. A. *Surf. Sci.* **1990**, *239*, 227–234.
(59) Chabal, Y. J. *Physica B* **1991**, *170*, 447–456.
(60) Abrefah, J.; Olander, D. R. *Surf. Sci.* **1989**, *209*, 291–313.
(61) Kratzer, P.; Hammer, B.; Nørskov, J. K. *Chem. Phys. Lett.* **1994**, *229*, 645–649.
(62) Kolasinski, K. W.; Nessler, W.; Bornscheuer, K.; Hasselbrink, E. *J. Chem. Phys.* **1994**, *101*, 7082–7094.
(63) Hickmott, T. W. *J. Chem. Phys.* **1960**, *32*, 810–823.
(64) Smith, J. N.; Fite, W. L. *J. Chem. Phys.* **1962**, *37*, 898–904.
(65) Hsu, W. L. *Appl. Phys. Lett.* **1991**, *59*, 1427–1429.
(66) Bornscheuer, K. H.; Lucas, S. R.; Choyke, W. J.; Partlow, W. D.; Yates, J. T., Jr. *J. Vac. Sci. Technol. A* **1993**, *11*, 2822–2826.
(67) Agrawal, P. M.; Thompson, D. L.; Raff, L. M. *J. Chem. Phys.* **1990**, *92*, 1069–1082.
(68) Sinniah, K.; Sherman, M. G.; Lewis, L. B.; Weinberg, W. H.; Yates, J. T., Jr.; Janda, K. C. *J. Chem. Phys.* **1990**, *92*, 5700–5711.
(69) Froitzheim, H.; Köhler, U.; Lammering, H. *Surf. Sci.* **1985**, *149*, 537–557.
(70) Naitoh, M.; Morioka, H.; Shoji, F.; Oura, K. *Surf. Sci.* **1993**, *297*, 135–140.
(71) Koleske, D. D.; Gates, S. M.; Schultz, J. A. *J. Chem. Phys.* **1993**, *99*, 5619–5622.
(72) Sakurai, T.; Hagstrum, H. D. *Phys. Rev. B* **1976**, *14*, 1593–1596.
(73) Chabal, Y. J.; Raghavachari, K. *Phys. Rev. Lett.* **1985**, *54*, 1055–1058.
(74) Cheng, C. C.; Yates, J. T., Jr. *Phys. Rev. B* **1991**, *43*, 4041–4045.
(75) Boland, J. J. *Surf. Sci.* **1992**, *261*, 17–28.
(76) Oura, K.; Yamane, J.; Umezawa, K.; Naitoh, M.; Shoji, F.; Hanawa, T. *Phys. Rev. B* **1990**, *41*, 1200–1203.
(77) Chabal, Y. J.; Raghavachari, K. *Phys. Rev. Lett.* **1984**, *53*, 282–285.
(78) Wu, Y. M.; Baker, J.; Hamilton, P.; Nix, R. M. *Surf. Sci.* **1993**, *295*, 133–142.
(79) Lu, Z. H.; Griffiths, K.; Norton, P. R.; Sham, T. K. *Phys. Rev. Lett.* **1992**, *68*, 1343–1346.
(80) Gates, S. M.; Kunz, R. R.; Greenlief, C. M. *Surf. Sci.* **1989**, *207*, 364–384.
(81) Wang, Y.; Shi, M.; Rabalais, J. W. *Phys. Rev. B* **1993**, *48*, 1678–1688.
(82) Shi, M.; Wang, Y.; Rabalais, J. W. *Phys. Rev. B* **1993**, *48*, 1689–1695.
(83) Shoji, F.; Kusumara, K.; Oura, K. *Surf. Sci.* **1993**, *280*, L247–L252.
(84) Craig, B. I.; Smith, P. V. *Surf. Sci.* **1990**, *226*, L55–L58.
(85) Nachtigall, P.; Jordan, K. D.; Janda, K. C. *J. Chem. Phys.* **1991**, *95*, 8652–8654.
(86) Batra, I. P. *Phys. Rev. B* **1990**, *41*, 5048–5054.
(87) Zheng, X. M.; Smith, P. V. *Surf. Sci.* **1992**, *279*, 127–136.
(88) Wu, C. J.; Carter, E. A. *Chem. Phys. Lett.* **1991**, *185*, 172–178.
(89) Northrup, J. E. *Phys. Rev. B* **1991**, *44*, 1419–1422.
(90) Nielson, O. H., Ed. *Properties of Silicon*; Inspect: London, 1988.
(91) Selmani, A.; Salahub, D. R. *Surf. Sci.* **1988**, *202*, 269–276.
(92) Sakurai, T.; Hagstrum, H. D. *Phys. Rev. B* **1975**, *12*, 5349–5354.
(93) Ichimiya, A.; Mizuno, S. *Surf. Sci.* **1987**, *191*, L765–L771.
(94) Kobayashi, H.; Edamoto, K.; Onchi, M.; Nishijima, M. *J. Chem. Phys.* **1983**, *78*, 7429–7436.
(95) Greenlief, C. M.; Gates, S. M.; Holbert, P. A. *J. Vac. Sci. Technol. A* **1989**, *7*, 1845–1849.
(96) Culbertson, R. J.; Feldman, L. C.; Silverman, P. J.; Haight, R. *J. Vac. Sci. Technol.* **1982**, *20*, 868–871.
(97) Wallace, R. M.; Taylor, P. A.; Choyke, W. J.; Yates, J. T., Jr. *Surf. Sci.* **1990**, *239*, 1–12.
(98) Karlsson, C. J.; Landemark, E.; Johansson, L. S. O.; Karlsson, U. O.; Uhrberg, R. I. G. *Phys. Rev. B* **1990**, *41*, 1521–1528.
(99) Boland, J. J. *Surf. Sci.* **1991**, *244*, 1–14.
(100) Mortensen, K.; Chen, D. M.; Bedrossian, P. J.; Golovchenko, J. A.; Besenbacher, F. *Phys. Rev. B* **1991**, *43*, 1816–1819.
(101) Landemark, E.; Karlsson, C. J.; Uhrberg, R. I. G. *Phys. Rev. B* **1991**, *44*, 1950–1953.
(102) Owman, F.; Mårtenson, P. *Surf. Sci.* **1994**, *303*, L367–L372.
(103) Greenlief, C. M.; Gates, S. M.; Holbert, P. A. *Chem. Phys. Lett.* **1989**, *159*, 202–206.
(104) Schulze, G.; Henzler, M. *Surf. Sci.* **1983**, *124*, 336–350.
(105) Wise, M. L.; Koehler, B. G.; Gupta, P.; Coon, P. A.; George, S. M. *Surf. Sci.* **1991**, *258*, 166–176.
(106) Höfer, U.; Li, L.; Heinz, T. F. *Phys. Rev. B* **1992**, *45*, 9485–9488.
(107) Sinniah, K.; Sherman, M. G.; Lewis, L. B.; Weinberg, W. H.; Yates, J. T., Jr.; Janda, K. C. *Phys. Rev. Lett.* **1990**, *62*, 567–570.
(108) Boland, J. J. *J. Vac. Sci. Technol. A* **1992**, *10*, 2458–2464.
(109) Uchiyama, T.; Tsukada, M. *Surf. Sci.* **1993**, *295*, L1037–L1042.
(110) Appelbaum, J. A.; Baraff, G. A.; Hamann, D. R. *Phys. Rev. B* **1976**, *14*, 588–601.
(111) D'Evelyn, M. P.; Yang, Y. L.; Sutcu, L. F. *J. Chem. Phys.* **1992**, *96*, 852–855.
(112) Shane, S. F.; Kolasinski, K. W.; Zare, R. N. *J. Chem. Phys.* **1992**, *97*, 1520–1530.
(113) Sheng, J.; Zhang, J. Z. H. *J. Chem. Phys.* **1992**, *97*, 596–604.
(114) Shane, S. F.; Kolasinski, K. W.; Zare, R. N. *J. Chem. Phys.* **1992**, *97*, 3704–3709.

(115) Wicks, G. W. *Crit. Rev. in Solid State Mater. Sci.* **1993**, *18*, 239–260.
(116) Jones, A. C. *Adv. Mater.* **1993**, *5*, 81–87.
(117) Yu, M. L.; Vitkavage, D. J.; Meyerson, B. S. *J. Appl. Phys.* **1986**, *59*, 4032–4037.
(118) Ide, T.; Nishimori, T.; Ichinokawa, T. *Surf. Sci.* **1989**, *209*, 335–344.
(119) Nogami, J.; Baski, A. A.; Quate, C. F. *Phys. Rev. B* **1991**, *44*, 1415–1418.
(120) Baski, A. A.; Nogami, J.; Quate, C. F. *J. Vac. Sci. Technol. A* **1990**, *8*, 245–248.
(121) Bourguignon, B.; Carleton, K. L.; Leone, S. R. *Surf. Sci.* **1988**, *204*, 455–472.
(122) Baski, A. A.; Nogami, J.; Quate, C. F. *Phys. Rev. B* **1991**, *43*, 9316–9319.
(123) Rich, D. H.; Samsavar, A.; Miller, T.; Lin, H. F.; Chiang, T.-C.; Sundgren, J.-E.; Greene, J. E. *Phys. Rev. Lett.* **1987**, *58*, 579–582.
(124) Knall, J.; Sundgren, J.-E.; Hansson, G. V.; Greene, J. E. *Surf. Sci.* **1986**, *166*, 512–538.
(125) Nogami, J.; Baski, A. A.; Quate, C. F. *J. Vac. Sci. Technol. A* **1990**, *8*, 3520–3523.
(126) Li, L.; Wei, Y.; Tsong, I. S. T. *Surf. Sci.* **1994**, *304*, 1–11.
(127) Nishikata, K.; Murakami, K.; Yoshimura, M.; Kawazu, A. *Surf. Sci.* **1992**, *269/270*, 995–999.
(128) Finney, M. S.; Norris, C.; Howes, P. B.; Vlieg, E. *Surf. Sci.* **1992**, *277*, 330–336.
(129) Lyo, I.-W.; Kaxiras, E.; Avouris, P. *Phys. Rev. Lett.* **1989**, *63*, 1261–1264.
(130) Chen, P. J.; Colaianni, M. L.; Yates, J. T., Jr. *J. Appl. Phys.* **1992**, *72*, 3155–3160.
(131) Hamers, R. J. *Phys. Rev. B* **1989**, *40*, 1657–1671.
(132) Chester, M.; Gustafsson, T. *Surf. Sci.* **1992**, *264*, 33–44.
(133) Hirayama, H.; Tatsumi, T.; Aizaki, N. *Surf. Sci.* **1988**, *193*, L47–L52.
(134) Finney, M. S.; Norris, C.; Howes, P. B.; van Silfhout, R. G.; Clark, G. F.; Thornton, J. M. C. *Surf. Sci.* **1993**, *291*, 99–109.
(135) Zegenhagen, J.; Patel, J. R.; Freeland, P.; Chen, D. M.; Golovchenko, J. A.; Bedrossian, P.; Northrup, J. E. *Phys. Rev. B* **1989**, *39*, 1298–1301.
(136) Avouris, P.; Lyo, I.-W.; Bozso, F.; Kaxiras, E. *J. Vac. Sci. Technol. A* **1990**, *8*, 3405–3411.
(137) Yates, J. T., Jr. *J. Phys.: Condens. Matter* **1991**, *3*, S143–S156.
(138) Chen, P. J.; Colaianni, M. L.; Yates, J. T., Jr. *J. Appl. Phys.* **1991**, *70*, 2954–2957.
(139) Kao, Chi-T.; Dubois, L. H.; Nuzzo, R. G. *J. Vac. Sci. Technol. A* **1991**, *9*, 228–231.
(140) Wei, J.; Yates, J. T., Jr. *Crit. Rev. in Surf. Chem.*, submitted for publication.
(141) Verwoerd, W. S. *Surf. Sci.* **1994**, *304*, 24–32.
(142) Ferrer, S.; Comin, F.; Martin, J. A.; Vazquez, L.; Bernard, P. *Surf. Sci.* **1991**, *251/252*, 960–964.
(143) Martín-Gago, J. A.; Fraxedas, J.; Ferrer, S.; Comin, F. *Surf. Sci.* **1992**, *260*, L17–L23.
(144) Bu, Y.; Lin, M. C. *Surf. Sci.* **1993**, *298*, 94–100.
(145) Chamberlain, J. P.; Clemn, J. L.; Pounds, A. J.; Gillis, H. P. *Surf. Sci.* **1994**, *301*, 105–117.
(146) Bozack, M. J.; Taylor, P. A.; Choyke, W. J.; Yates, J. T., Jr. *Surf. Sci.* **1986**, *177*, L933–L937.
(147) Clemen, L.; Wallace, R. M.; Taylor, P. A.; Dresser, M. J.; Choyke, W. J.; Weinberg, W. H.; Yates, J. T., Jr. *Surf. Sci.* **1992**, *268*, 205–216.
(148) Taylor, P. A.; Wallace, R. M.; Cheng, C. C.; Weinberg, W. H.; Dresser, M. J.; Choyke, W. J.; Yates, J. T., Jr. *J. Am. Chem. Soc.* **1992**, *114*, 6754–6760.
(149) Cheng, C. C.; Wallace, R. M.; Taylor, P. A.; Choyke, W. J.; Yates, J. T., Jr. *J. Appl. Phys.* **1990**, *67*, 3693–3699.
(150) Nishijima, M.; Yoshinobu, J.; Tsuda, H.; Onchi, M. *Surf. Sci.* **1987**, *192*, 383–397.
(151) Yoshinobu, J.; Tsuda, H.; Onchi, M.; Nishijima, M. *J. Chem. Phys.* **1987**, *87*, 7332–7340.
(152) Huang, C.; Widdra, W.; Wang, X. S.; Weinberg, W. H. *J. Vac. Sci. Technol. A* **1993**, *11*, 2250–2254.
(153) Widdra, W.; Huang, C.; Briggs, G. A. D.; Weinberg, W. H. *J. Electron Spectrosc. Relat. Phenom.* **1993**, *64/65*, 129–136.
(154) Bu, Y.; Ma, L.; Lin, M. C. *J. Phys. Chem.* **1993**, *97*, 11797–11801.
(155) Bozack, M. J.; Taylor, P. A.; Choyke, W. J.; Yates, J. T., Jr. *Surf. Sci.* **1987**, *179*, 132–142.
(156) Toscano, M. *Surf. Sci.* **1991**, *251/252*, 894–899.
(157) Craig, B. I.; Smith, P. V. *Surf. Sci.* **1992**, *276*, 174–183.
(158) Cheng, C. C.; Choyke, W. J.; Yates, J. T., Jr. *Surf. Sci.* **1990**, *231*, 289–296.
(159) Kiskinova, M.; Yates, J. T., Jr. *Surf. Sci.* **1995**, *325*, 1–10.
(160) Yoshinobu, J.; Tsuda, H.; Onchi, M.; Nishijima, M. *Chem. Phys. Lett.* **1986**, *130*, 170–174.
(161) Yoshinobu, J.; Fukushi, D.; Uda, M.; Nomura, W.; Aono, M. *Phys. Rev. B* **1992**, *46*, 9520–9524.
(162) Chu, S.-Y.; Anderson, A. B. *Surf. Sci.* **1988**, *194*, 55–62.
(163) Weiner, B.; Carmer, C. S.; Frenklach, M. *Phys. Rev. B* **1991**, *43*, 1678–1684.
(164) MacPherson, C. D.; Hu, D. Q.; Doan, M.; Leung, K. T. *Surf. Sci.* **1994**, *310*, 231–242.
(165) Hu, D. Q.; MacPherson, C. D.; Leung, K. T. *Surf. Sci.* **1992**, *273*, 21–30.
(166) Taguchi, Y.; Fujisawa, M.; Nishijima, M. *Chem. Phys. Lett.* **1991**, *178*, 363–368.
(167) MacPherson, C. D.; Hu, D. Q.; Leung, K. T. *Surf. Sci.* **1992**, *276*, 156–165.
(168) Taguchi, Y.; Fujisawa, M.; Takaoka, T.; Okada, T.; Nishijima, M. *J. Chem. Phys.* **1991**, *95*, 6870–6876.
(169) Craig, B. I. *Surf. Sci.* **1993**, *280*, L239–L284.
(170) MacPherson, C. D.; Hu, D. Q.; Leung, K. T. *Solid State Commun.* **1991**, *80*, 217–220.
(171) Weast, R. C., Ed. *CRC Handbook of Chemistry of Physics*, 67th ed.; CRC: Boca Raton, 1986.
(172) Gates, S. M. *Surf. Sci.* **1988**, *195*, 307–329.
(173) Gates, S. M.; Greenlief, C. M.; Beach, D. B.; Holbert, P. A. *J. Chem. Phys.* **1990**, *92*, 3144–3153.
(174) (a) Gates, S. M.; Greenlief, C. M.; Kulkarni, S. K.; Sawin, H. H. *J. Vac. Sci. Technol. A* **1990**, *8*, 2965–2969. (b) Gates, S. M.; Greenlief, C. M.; Beach, D. B. *J. Chem. Phys.* **1990**, *93*, 7493–7503.
(175) Gates, S. M.; Kulkarni, S. K. *Appl. Phys. Lett.* **1992**, *60*, 53–55.
(176) Jones, M. E.; Xia, L.-Q.; Maity, N.; Engstrom, J. R. *Chem. Phys. Lett.* **1994**, *229*, 401–407
(177) Wu, Y. M.; Nix, R. M. *Surf. Sci.* **1994**, *306*, 59–68.
(178) Suda, Y.; Lubben, D.; Motooka, T.; Greene, J. E. *J. Vac. Sci. Technol. A* **1990**, *8*, 61–67.
(179) Uram, K. J.; Jansson, U. *J. Vac. Sci. Technol. B* **1989**, *7*, 1176–1181.
(180) Boland, J. J. *Phys. Rev. B* **1991**, *44*, 1383–1386.
(181) Avouris, P.; Bozso, F. *J. Phys. Chem.* **1990**, *94*, 2243–2245.
(182) Bronikowski, M.; Wang, Y.; McEllistrem, M. T.; Chen, D.; Hamers, R. J. *Surf. Sci.* **1993**, *298*, 50–62.
(183) Lin, D.-S.; Hirschorn, E. S.; Chiang, T.-C.; Tsu, R.; Lubben, D.; Greene, J. E. *Phys. Rev. B* **1992**, *45*, 3494–3498.
(184) Engstrom, J. R.; Hansen, D. A.; Furjanic, M. J.; Xia, L. Q. *J. Chem. Phys.* **1993**, *99*, 4051–4054.
(185) Engstrom, J. R.; Xia, L. Q.; Furjanic, M. J.; Hansen, D. A. *Appl. Phys. Lett.* **1993**, *63*, 1821–1823.
(186) Lin, D. S.; Miller, T.; Chiang, T.-C.; Tsu, R.; Greene, J. E. *Phys. Rev. B* **1993**, *48*, 11846–11850.
(187) Kulkarni, S. K.; Gates, S. M.; Greenlief, C. M.; Sawin, H. H. *Surf. Sci.* **1990**, *239*, 26–35.
(188) Wang, Y. J.; Bronikowski, M. J.; Hamers, R. J. *Surf. Sci.* **1994**, *311*, 64–100.
(189) Kulkarni, S. K.; Gates, S. M.; Scott, B. A.; Sawin, H. H. *Surf. Sci.* **1990**, *239*, 13–25.
(190) Uram, K. J.; Jansson, U. *Surf. Sci.* **1991**, *249*, 105–116.
(191) Gupta, P.; Coon, P. A.; Koehler, B. G.; George, S. M. *J. Chem. Phys.* **1990**, *93*, 2827–2835.
(192) Whitman, L. J.; Joyce, S. A.; Yarmoff, J. A.; McFeely, F. R.; Terminello, L. J. *Surf. Sci.* **1990**, *232*, 297–306.
(193) Gao, Q.; Dohnalek, Z.; Cheng, C. C.; Choyke, W. J.; Yates, J. T., Jr. *Surf. Sci.* **1994**, *302*, 1–9.
(194) Coon, P. A.; Gupta, P.; Wise, M. L.; George, S. M. *J. Vac. Sci. Technol. A* **1992**, *10*, 324–333.
(195) Yarmoff, J. A.; Shuh, D. K.; Durbin, T. D.; Lo, C. W.; Lapiano-Smith, D. A.; McFeely, F. R.; Himpsel, F. J. *J. Vac. Sci. Technol. A* **1992**, *10*, 2303–2307.
(196) Sakamoto, H.; Takakuwa, Y.; Hori, T.; Horie, T.; Miyamoto, N. *Appl. Surf. Sci.* **1994**, *75*, 27–32.
(197) Koleske, D. D.; Gates, S. M.; Beach, D. B. *J. Appl. Phys.* **1992**, *72*, 4073–4082.
(198) Schmidt, J.; Stuhlmann, C.; Ibach, H. *Surf. Sci.* **1994**, *302*, 10–24.
(199) Köhler, U.; Demuth, J. E.; Hamers, R. J. *J. Vac. Sci. Technol. A* **1989**, *7*, 2860–2867.
(200) Hoeven, A. J.; Dijkkamp, D.; Lenssinck, J. M.; van Loenen, E. J. *J. Vac. Sci. Technol. A* **1990**, *8*, 3657–3661.
(201) Heun, S.; Falta, J.; Henzler, M. *Surf. Sci.* **1991**, *243*, 132–140.
(202) Hoeven, A. J.; Dijkkamp, D.; van Loenen, E. J.; Lenssinck, J. M.; Dieleman, J. *J. Vac. Sci. Technol. A* **1990**, *8*, 207–209.
(203) Falta, J.; Henzler, M. *Surf. Sci.* **1992**, *269/270*, 14–21.
(204) Hamers, R. J.; Köhler, U. K.; Demuth *J. Vac. Sci. Technol. A* **1990**, *8*, 195–200.
(205) Mo, Y.-W.; Kariotis, R.; Swartzentruber, B. S.; Webb, M. B.; Lagally, M. G. *J. Vac. Sci. Technol. A* **1990**, *8*, 201–206.
(206) Mo, Y.-W.; Lagally, M. G. *Surf. Sci.* **1991**, *248*, 313–320.
(207) Lu, Y.-T.; Zhang, Z.; Metiu, H. *Surf. Sci.* **1991**, *257*, 199–209.
(208) Mo, Y.-W.; Swartzentruber, B. S.; Kariotis, R.; Webb, M. B.; Lagally, M. G. *Phys. Rev. Lett.* **1989**, *63*, 2393–2396.
(209) Greenlief, C. M.; Wankum, P. C.; Klug, D.-A.; Keeling, L. A. *J. Vac. Sci. Technol. A* **1992**, *10*, 2465–2469.
(210) Coon, P. A.; Wise, M. L.; George, S. M. *Surf. Sci.* **1992**, *278*, 383–396.
(211) Kajiyama, K.; Tanishiro, Y.; Takayanagi, K. *Surf. Sci.* **1989**, *222*, 38–46.
(212) Marée, P. M. J.; Nakagawa, K.; Mulders, F. M.; van der Veen, J. F.; Kavanagh, K. L. *Surf. Sci.* **1987**, *191*, 305–328.

(213) Mo, Y.-W.; Savage, D. E.; Swartzentruber, B. S.; Lagally, M. G. *Phys. Rev. Lett.* **1990**, *65*, 1020–1023.
(214) Diani, M.; Aubel, D.; Bischoff, J. L.; Kubler, L.; Bolmont, D. *Surf. Sci.* **1993**, *291*, 110–116.
(215) Horn-von Hoegen, M.; LeGoues, F. K.; Copel, M.; Reuter, M. C.; Tromp, R. M. *Phys. Rev. Lett.* **1991**, *67*, 1130–1133.
(216) Higuchi, S.; Nakanishi, Y. *Surf. Sci.* **1991**, *254*, L465–L468.
(217) Thornton, J. M. C.; Williams, A. A.; Macdonald, J. E.; van Silfhout, R. G.; Finney, M. S.; Norris, C. *Surf. Sci.* **1992**, *273*, 1–8.
(218) Meyer, G.; Voigtländer, B.; Amer, N. M. *Surf. Sci.* **1992**, *274*, L541–L545.
(219) Copel, M.; Reuter, M. C.; Kaxiras, E.; Tromp, R. M. *Phys. Rev. Lett.* **1989**, *63*, 632–635.
(220) Iwawaki, F.; Tomitori, M.; Nishikawa, O. *Surf. Sci.* **1992**, *266*, 285–288.
(221) Köhler, U.; Jusko, O.; Pietsch, G.; Müller, B.; Henzler, M. *Surf. Sci.* **1991**, *248*, 321–331.
(222) Kajiyama, K.; Tanishiro, Y.; Takayanagi, K. *Surf. Sci.* **1989**, *222*, 47–63.
(223) Stauffer, L.; Van, S.; Bolmont, D.; Koulmann, J. J.; Minot, C. *Surf. Sci.* **1994**, *309*, 274–279.
(224) Heckingbottom, R.; Wood, P. R. *Surf. Sci.* **1973**, *36*, 594–605.
(225) Colaianni, M. L.; Chen, P. J.; Nagashima, N.; Yates, J. T., Jr. *J. Appl. Phys.* **1993**, *73*, 4927–4931.
(226) Delord, J. F.; Schrott, A. G.; Fain, S. C., Jr. *J. Vac. Sci. Technol.* **1980**, *17*, 517–520.
(227) Schrott, A. G.; Fain, S. C., Jr. *Surf. Sci.* **1981**, *111*, 39–52.
(228) Schrott, A. G.; Fain, S. C., Jr. *Surf. Sci.* **1982**, *123*, 204–222.
(229) Nishijima, M.; Kobayashi, H.; Edamoto, K.; Onchi, M. *Surf. Sci.* **1984**, *137*, 473–490.
(230) Khramtsova, E. A.; Saranin, A. A.; Lifshits, V. G. *Surf. Sci.* **1993**, *280*, L259–L262.
(231) Edamoto, K.; Tanaka, S.; Onchi, M.; Nishijima, M. *Surf. Sci.* **1986**, *167*, 285–296.
(232) Schrott, A. G.; Su, Q. X.; Fain, S. C., Jr. *Surf. Sci.* **1982**, *123*, 223–230.
(233) Maillot, C.; Roulet, H.; Dufour, G.; Rochet, F.; Rigo, S. *Appl. Surf. Sci.* **1986**, *26*, 326–334.
(234) Peden, C. H. F.; Rogers, J. W., Jr.; Kidd, K. B.; Tsang, K. L.; Shinn, N. D. *Mater. Res. Soc. Symp. Proc.* **1991**, *204*, 521.
(235) Bozso, F.; Avouris, P. *Phys. Rev. Lett.* **1986**, *57*, 1185–1188.
(236) Tarasova, O. L.; Kotlyar, V. G.; Saranin, A. A.; Khramtsova, E. A.; Lifshits, V. G. *Surf. Sci.* **1994**, *310*, 209–216.
(237) Klauber, C.; Alvey, M. D.; Yates, J. T., Jr. *Surf. Sci.* **1985**, *154*, 139–167.
(238) Bassignana, I. C.; Wagemann, K.; Küppers, J.; Ertl, G. *Surf. Sci.* **1986**, *175*, 22–44.
(239) Hübner, A.; Lucas, S. R.; Partlow, W. D.; Choyke, W. J.; Schaefer, J. A.; Yates, J. T., Jr. *J. Vac. Sci. Technol. A*, in press.
(240) Koehler, B. G.; Coon, P. A.; George, S. M. *J. Vac. Sci. Technol. B* **1989**, *7*, 1303–1310.
(241) Bozso, F.; Avouris, P. *Phys. Rev. B* **1988**, *38*, 3937–3942.
(242) Hlil, E. K.; Kubler, L.; Bischoff, J. L.; Bolmont, D. *Phys. Rev. B* **1987**, *35*, 5913–5916.
(243) Kubler, L.; Hlil, E. K.; Bolmont, D.; Peruchetti, J. C. *Thin Solid Films* **1987**, *149*, 385–392.
(244) Tanaka, S.; Onchi, M.; Nishijima, M. *Surf. Sci.* **1987**, *191*, L756–L764.
(245) Kilday, D. G.; Margaritondo, G.; Frankel, D. J.; Anderson, J.; Lapeyre, G. J. *Phys. Rev. B* **1987**, *35*, 9364–9367.
(246) Fujisawa, M.; Taguchi, Y.; Kuwahara, Y.; Onchi, M.; Nishijima, M. *Phys. Rev. B* **1989**, *39*, 12918–12920.
(247) Dresser, M. J.; Taylor, P. A.; Wallace, R. M.; Choyke, W. J.; Yates, J. T., Jr. *Surf. Sci.* **1989**, *218*, 75–107.
(248) Avouris, P.; Bozso, F.; Hamers, R. J. *J. Vac. Sci. Technol. B* **1987**, *5*, 1387–1392.
(249) Hamers, R. J.; Avouris, P.; Bozso, F. *Phys. Rev. Lett.* **1987**, *59*, 2071–2074.
(250) Hamers, R. J.; Avouris, P.; Bozso, F. *J. Vac. Sci. Technol. A* **1988**, *6*, 508–511.
(251) Chérif, S. M.; Lacharme, J.-P.; Sébenne, C. A. *Surf. Sci.* **1991**, *243*, 113–120.
(252) Chérif, S. M.; Lacharme, J.-P.; Sébenne, C. A. *Surf. Sci.* **1992**, *262*, 33–41.
(253) Avouris, P.; Wolkow, R. *Phys. Rev. B* **1989**, *39*, 5091–5100.
(254) Bischoff, J. L.; Lutz, F.; Bolmont, D.; Kubler, L. *Surf. Sci.* **1991**, *251/252*, 170–174.
(255) Zhou, X.-L.; Flores, C. R.; White, J. M. *Surf. Sci.* **1992**, *268*, L267–L273.
(256) Dufour, G.; Rochet, F.; Roulet, H.; Sirotti, F. *Surf. Sci.* **1994**, *304*, 33–47.
(257) Kubler, L.; Bischoff, J. L.; Bolmont, D. *Phys. Rev. B* **1988**, *38*, 13113–13123.
(258) Zhou, R.-H.; Cao, P.-L.; Fu, S.-B. *Surf. Sci.* **1991**, *249*, 129–137.
(259) Larsson, C. U. S.; Flodström, A. S. *Surf. Sci.* **1991**, *241*, 353–356.
(260) Chen, P. J.; Colaianni, M. L.; Yates, J. T., Jr. *Surf. Sci.* **1992**, *274*, L605–L610.
(261) Larsson, C. U. S.; Andersson, C. B. M.; Prince, N. P.; Flodström, A. S. *Surf. Sci.* **1992**, *271*, 349–354.
(262) Chérif, S. M.; Lacharme, J.-P.; Sébenne, C. A. *Surf. Sci.* **1991**, *251/252*, 737–741.
(263) Colaianni, M. L.; Chen, P. J.; Yates, J. T., Jr. *J. Chem. Phys.* **1992**, *96*, 7826–7837.
(264) Bu, Y.; Shinn, D. W.; Lin, M. C. *Surf. Sci.* **1992**, *276*, 184–199.
(265) Slaughter, E. A.; Gland, J. L. *J. Vac. Sci. Technol. A* **1992**, *10*, 66–68.
(266) Bu, Y.; Chu, J. C. S.; Lin, M. C. *Surf. Sci.* **1992**, *264*, L151–L156.
(267) Taguchi, Y.; Fujisawa, M.; Kuwahara, Y.; Onchi, M.; Nishijima, M. *Surf. Sci.* **1989**, *217*, L413–L416.
(268) Sasse, A. G. B. M.; Lakerveld, D. G.; van Silfhout, A. *Surf. Sci.* **1988**, *195*, L167–L172.
(269) Sasse, A. G. B. M.; Kleinherenbring, P. M.; van Silfhout, A. *Surf. Sci.* **1988**, *199*, 243–260.
(270) Sasse, A. G. B. M.; van Silfhout, A. *Phys. Rev. B* **1989**, *40*, 1773–1782.
(271) Fu, S.-B.; Zhou, R.-H.; Cao, P.-L.; Tang, J.-C. *Surf. Sci.* **1991**, *247*, L224–L228.
(272) Bu, Y.; Lin, M. C. *Surf. Sci.* **1994**, *311*, 385–394.
(273) Jonathan, N. B. H.; Knight, P. J.; Morris, A. *Surf. Sci.* **1992**, *275*, L640–L644.
(274) Chu, J. C. S.; Bu, Y.; Lin, M. C. *Surf. Sci.* **1993**, *284*, 281–290.
(275) Shimura, F. *Semiconductor Silicon Crystal Technology*; Academic Press: San Diego, 1989.
(276) Yu, M. L.; Meyerson, B. S. *J. Vac. Sci. Technol. A* **1984**, *2*, 446–449.
(277) Meyerson, B. S.; Yu, M. L. *J. Electrochem. Soc.* **1984**, *131*, 2366–2368.
(278) van Bommel, A. J.; Meyer, F. *Surf. Sci.* **1967**, *8*, 381–398.
(279) van Bommel, A. J.; Crombeen, J. E. *Surf. Sci.* **1973**, *36*, 773–777.
(280) Chen, P. J.; Colaianni, M. L.; Wallace, R. M.; Yates, J. T., Jr. *Surf. Sci.* **1991**, *244*, 177–184.
(281) Colaianni, M. L.; Chen, P. J.; Yates, J. T., Jr. *J. Vac. Sci. Technol. A* **1994**, *12*, 2995–2998.
(282) Olmstead, M. A.; Bringans, R. D.; Uhrberg, R. I. G.; Bachrach, R. Z. *Phys. Rev. B* **1986**, *34*, 6041–6044.
(283) Uhrberg, R. I. G.; Bringans, R. D.; Bachrach, R. Z.; Northrup, J. E. *Phys. Rev. Lett.* **1986**, *56*, 520–523.
(284) Bringans, R. D.; Uhrberg, R. I. G.; Olmstead, M. A.; Bachrach, R. Z. *Phys. Rev. B* **1986**, *34*, 7447–7450.
(285) Becker, R. S.; Klitsner, T.; Vickers, J. S. *J. Microsc.* **1988**, *152*, 157–165.
(286) Bringans, R. D.; Biegelsen, D. K.; Swartz, L.-E. *Phys. Rev. B* **1991**, *44*, 3054–3063.
(287) Alerhand, O. L.; Wang, J.; Joannopoulos, J. D.; Kaxiras, E.; Becker, R. S. *Phys. Rev. B* **1991**, *44*, 6534–6537.
(288) Tromp, R. M.; Denier van der Gon, A. W.; Reuter, M. C. *Phys. Rev. Lett.* **1992**, *68*, 2313–2316.
(289) Yu, B. D.; Oshiyama, A. *Phys. Rev. Lett.* **1993**, *71*, 585–588.
(290) Uhrberg, R. I. G.; Bringans, R. D.; Olmstead, M. A.; Bachrach, R. Z. *Phys. Rev. B* **1987**, *35*, 3945–3951.
(291) Patel, J. R.; Golovchenko, J. A.; Freeland, P. A.; Gossmann, H.-J. *Phys. Rev. B* **1987**, *36*, 7715–7717.
(292) Ohno, T. R.; Williams, E. D. *J. Vac. Sci. Technol. B* **1990**, *8*, 874–883.
(293) Becker, R. S.; Swartzentruber, B. S.; Vickers, J. S.; Hybertsen, M. S.; Louie, S. G. *Phys. Rev. Lett.* **1988**, *60*, 116–119.
(294) Nogami, J.; Baski, A. A.; Quate, C. F. *Appl. Phys. Lett.* **1991**, *58*, 475–477.
(295) Hanada, T.; Kawai, M. *Surf. Sci.* **1991**, *242*, 137–142.
(296) Rich, D. H.; Miller, T.; Franklin, G. E.; Chiang, T.-C. *Phys. Rev. B* **1989**, *39*, 1438–1441.
(297) Rich, D. H.; Leibsle, F. M.; Samsavar, A.; Hirschorn, E. S.; Miller, T.; Chiang, T.-C. *Phys. Rev. B* **1989**, *39*, 12758–12763.
(298) Fan, W. C.; Ignatiev, A.; Wu, N. J. *Surf. Sci.* **1990**, *235*, 169–174.
(299) Richter, M.; Woicik, J. C.; Nogami, J.; Pianetta, P.; Miyano, K. E.; Baski, A. A.; Kendelewicz, T.; Bouldin, C. E.; Spicer, W. E.; Quate, C. F.; Lindau, I. *Phys. Rev. Lett.* **1990**, *65*, 3417–3420.
(300) Richter, M.; Woicik, J. C.; Pianetta, P.; Miyano, K. E.; Kendelewicz, T.; Bouldin, C. E.; Spicer, W. E.; Lindau, I. *J. Vac. Sci. Technol. A* **1991**, *9*, 1951–1955.
(301) Grant, M. W.; Lyman, P. F.; Hoogenraad, J. H.; Seiberling, L. E. *Surf. Sci.* **1992**, *279*, L180–L184.
(302) Wan, K. J.; Guo, T.; Ford, W. K.; Hermanson, J. C. *Surf. Sci.* **1992**, *261*, 69–87.
(303) Balk, P., Ed. *The Si–SiO_2 System*; Materials Science Monographs 32; Elsevier: New York, 1988.
(304) Engel, T. *Surf. Sci. Rep.* **1993**, *18*, 91–144.
(305) Wormeester, H.; Keim, E. G.; van Silfhout, A. *Surf. Sci.* **1992**, *271*, 340–348.
(306) Engstrom, J. R.; Bonser, D. J.; Engel, T. *Surf. Sci.* **1992**, *268*, 238–264.
(307) Zheng, X. M.; Smith, P. V. *Surf. Sci.* **1990**, *232*, 6–16.
(308) Höfer, U.; Morgen, P.; Wurth, W. *Phys. Rev. B* **1989**, *40*, 1130–1145.

(309) Gupta, P.; Mak, C. H.; Coon, P. A.; George, S. M. *Phys. Rev. B* **1989**, *40*, 7739–7749.
(310) Schubert, B.; Avouris, P.; Hoffmann, R. *J. Chem. Phys.* **1993**, *98*, 7593–7605.
(311) Sakamoto, K.; Nakatsuji, K.; Daimon, H.; Yonezawa, T.; Suga, S. *Surf. Sci.* **1994**, *306*, 93–98.
(312) Morgen, P.; Höfer, U.; Wurth, W.; Umbach, E. *Phys. Rev. B* **1989**, *39*, 3720–3734.
(313) Pelz, J. P.; Koch, R. H. *Phys. Rev. B* **1990**, *42*, 3761–3764.
(314) Lyo, I.-W.; Avouris, P.; Schubert, B.; Hoffmann, R. *J. Phys. Chem.* **1990**, *94*, 4400–4403.
(315) Avouris, P.; Lyo, I.-W.; Bozso, F. *J. Vac. Sci. Technol. B* **1991**, *9*, 424–430.
(316) Schubert, B.; Avouris, P.; Hoffmann, R. *J. Chem. Phys.* **1993**, *98*, 7606–7612.
(317) Namiki, A.; Tanimoto, K.; Nakamura, T.; Ohtake, N.; Suzaki, T. *Surf. Sci.* **1989**, *222*, 530–554.
(318) Bu, H.; Rabalais, J. W. *Surf. Sci.* **1994**, *301*, 285–294.
(319) Miyamoto, Y.; Oshiyama, A. *Phys. Rev. B* **1990**, *41*, 12680–12686.
(320) Westermann, J.; Nienhaus, H.; Mönch, W. *Surf. Sci.* **1994**, *311*, 101–106.
(321) Johnson, K. E.; Wu, P. K.; Sander, M.; Engel, T. *Surf. Sci.* **1993**, *290*, 213–231.
(322) Yaguchi, H.; Fujita, K.; Fukatsu, S.; Shiraki, Y.; Ito, R.; Igarashi, T.; Hattori, T. *Surf. Sci.* **1992**, *275*, 395–400.
(323) Avouris, P.; Lyo, I.-W. *Appl. Surf. Sci.* **1992**, *60/61*, 426–436.
(324) Smith, P. V.; Wander, A. *Surf. Sci.* **1989**, *219*, 77–87.
(325) Tikhov, M.; Surnev, L.; Kiskinova, M. *Surf. Sci.* **1990**, *238*, L463–L466.
(326) Sun, Y.-K.; Bonser, D. J.; Engel, T. *J. Vac. Sci. Technol. A* **1992**, *10*, 2314–2321.
(327) Kobayashi, Y.; Sugii, K. *J. Vac. Sci. Technol. B* **1991**, *9*, 748–751.
(328) Liehr, M.; Lewis, J. E.; Rubloff, G. W. *J. Vac. Sci. Technol. A* **1987**, *5*, 1559–1562.
(329) Rubloff, G. W.; Hofmann, K.; Liehr, M.; Young, D. R. *Phys. Rev. Lett.* **1987**, *58*, 2379–2382.
(330) Tromp, R.; Rubloff, G. W.; Balk, P.; LeGoues, F. K.; van Loenen, E. J. *Phys. Rev. Lett.* **1985**, *55*, 2332–2335.
(331) Thiel, P. A.; Madey, T. E. *Surf. Sci. Rep.* **1987**, *7*, 211–385.
(332) Schmeisser, D.; Himpsel, F. J.; Hollinger, G. *Phys. Rev. B* **1983**, *27*, 7813–7816.
(333) Fujiwara, K.; Ogata, H. *Surf. Sci.* **1979**, *86*, 700–705.
(334) Chabal, Y. J.; Christman, S. B. *Phys. Rev. B* **1984**, *29*, 6974–6976.
(335) Nishijima, M.; Edamoto, K.; Kubota, Y.; Tanaka, S.; Onchi, M. *J. Chem. Phys.* **1986**, *84*, 6458–6465.
(336) Fives, K.; McGrath, R.; Stephens, C.; McGovern, I. T.; Cimino, R.; Law, D. S.-L.; Johnson, A. L.; Thornton, G. *J. Phys.: Condens. Matter* **1989**, *1*, SB105–SB109.
(337) Larsson, C. U. S.; Flodström, A. S.; Nyholm, R.; Incoccia, L.; Senf, F. *J. Vac. Sci. Technol. A* **1987**, *5*, 3321–3324.
(338) Oellig, E. M.; Butz, R.; Wagner, H.; Ibach, H. *Solid State Commun.* **1984**, *51*, 7–8.
(339) Schaefer, J. A.; Anderson, J.; Lapeyre, G. J. *J. Vac. Sci. Technol. A* **1985**, *3*, 1443–1447.
(340) Ranke, W.; Xing, Y. R. *Surf. Sci.* **1985**, *157*, 339–352.
(341) Podolsky, B. S.; Ukaintsev, V. A.; Chernov, A. A. *Surf. Sci.* **1991**, *251/252*, 1033–1037.
(342) Koehler, B. G.; Mak, C. H.; George, S. M. *Surf. Sci.* **1989**, *221*, 565–589.
(343) Zhou, X.-L.; Flores, C. R.; White, J. M. *Appl. Surf. Sci.* **1992**, *62*, 223–237.
(344) Schröder-Bergen, E.; Ranke, W. *Surf. Sci.* **1990**, *236*, 103–111.
(345) Chander, M.; Li, Y. Z.; Patrin, J. C.; Weaver, J. H. *Phys. Rev. B* **1993**, *48*, 2493–2499.
(346) Avouris, P.; Lyo, I.-W. *Surf. Sci.* **1991**, *242*, 1–11.
(347) Andersohn, L.; Köhler, U. *Surf. Sci.* **1993**, *284*, 77–90.
(348) Hamers, R. J.; Köhler, U. K. *J. Vac. Sci. Technol. A* **1989**, *7*, 2854–2859.
(349) Hoshino, T.; Tsuda, M.; Oikawa, S.; Ohdomari, I. *Surf. Sci.* **1993**, *291*, 763–767.
(350) Chabal, Y. J. *J. Vac. Sci. Technol. A* **1985**, *3*, 1448–1451.
(351) Johnson, A. L.; Walczak, M. M.; Madey, T. E. *Langmuir* **1988**, *4*, 277–282.
(352) Gao, Q.; Dohnalek, Z.; Cheng, C. C.; Choyke, W. J.; Yates, J. T., Jr. *Surf. Sci.* **1994**, *312*, 261–270.
(353) Larsson, C. U. S.; Johnson, A. L.; Flodström, A. S.; Madey, T. E. *J. Vac. Sci. Technol. A* **1987**, *5*, 842–846.
(354) Kramer, H. M.; Bauer, E. *Surf. Sci.* **1981**, *107*, 1–19.
(355) Matsuo, J.; Karahashi, K.; Sato, A.; Hijiya, S. *Jpn. J. Appl. Phys.* **1992**, *31*, 2025.
(356) Szabó, A.; Farrall, P. D.; Engel, T. *Surf. Sci.* **1994**, *312*, 284–300.
(357) Thornton, G.; Wincott, P. L.; McGrath, R.; McGovern, I. T.; Quinn, F. M.; Norman, D.; Vvedensky, D. D. *Surf. Sci.* **1989**, *211/212*, 959–968.
(358) Bennett, S. L.; Greenwood, C. L.; Williams, E. M. *Surf. Sci.* **1993**, *290*, 267–276.
(359) Gao, Q.; Cheng, C. C.; Chen, P. J.; Choyke, W. J.; Yates, J. T., Jr. *J. Chem. Phys.* **1993**, *98*, 8308–8323.
(360) Sterratt, D.; Greenwood, C. L.; Williams, E. M.; Muryn, C. A.; Wincott, P. L.; Thornton, G.; Román, E. *Surf. Sci.* **1994**, *307–309*, 269–273.
(361) Mendicino, M. A.; Seebauer, E. G. *Appl. Surf. Sci.* **1993**, *68*, 285–290.
(362) Purdie, D.; Prakash, N. S.; Purcell, K. G.; Wincott, P. L.; Thornton, G.; Law, D. S.-L. *Phys. Rev. B* **1993**, *48*, 2275–2281.
(363) Aoto, N.; Ikawa, E.; Kurogi, Y. *Surf. Sci.* **1988**, *199*, 408–420.
(364) Johansson, L. S. O.; Uhrberg, R. I. G.; Lindsay, R.; Wincott, P. L.; Thornton, G. *Phys. Rev. B* **1990**, *42*, 9534–9539.
(365) Cheng, C. C.; Gao, Q.; Choyke, W. J.; Yates, J. T., Jr. *Phys. Rev. B* **1992**, *46*, 12810–12813.
(366) Craig, B. I.; Smith, P. V. *Surf. Sci.* **1993**, *290*, L662–L666.
(367) Lee, L.-Q.; Cao, P.-L. *J. Phys.: Condens. Matter* **1994**, *6*, 6169–6175.
(368) Boland, J. J. *Science* **1993**, *262*, 1703–1706.
(369) Dohnálek, Z.; Gao, Q.; Choyke, W. J.; Yates, J. T., Jr. *J. Chem. Phys.* **1995**, *102*, 2946–2950.
(370) Jackman, R. B.; Ebert, H.; Foord, J. S. *Surf. Sci.* **1986**, *176*, 183–192.
(371) Karahashi, K.; Matsuo, J.; Hijiya, S. *Appl. Surf. Sci.* **1992**, *60/61*, 126–130.
(372) Yonezawa, T.; Daimon, H.; Nakatsuji, K.; Sakamoto, K.; Suga, S. *Appl. Surf. Sci.* **1994**, *80*, 95–99.
(373) Schnell, R. D.; Rieger, D.; Bogen, A.; Himpsel, F. J.; Wandelt, K.; Steinmann, W. *Phys. Rev. B* **1985**, *32*, 8057–8065.
(374) Gupta, P.; Coon, P. A.; Koehler, B. G.; George, S. M. *Surf. Sci.* **1991**, *249*, 92–104.
(375) Citrin, P. H.; Rowe, J. E.; Eisenberger, P. *Phys. Rev. B* **1983**, *28*, 2299–2301.
(376) Boland, J. J.; Villarrubia, J. S. *Phys. Rev. B* **1990**, *41*, 9865–9870.
(377) Villarrubia, J. S.; Boland, J. J. *Phys. Rev. Lett.* **1989**, *63*, 306–309.
(378) Feltz, A.; Memmert, U.; Behm, R. J. *Surf. Sci.* **1994**, *307–309*, 216–222.
(379) Matsuo, J.; Yannick, F.; Karahashi, K. *Surf. Sci.* **1993**, *283*, 52–57.
(380) Engstrom, J. R.; Nelson, M. M.; Engel, T. *Surf. Sci.* **1989**, *215*, 437–500.
(381) Koleske, D. D.; Gates, S. M. *J. Chem. Phys.* **1993**, *99*, 8218–8228.
(382) Michel, E. G.; Pauly, T.; Eteläniemi, V.; Materlik, G. *Surf. Sci.* **1991**, *241*, 111–123.
(383) Bozack, M. J.; Dresser, M. J.; Choyke, W. J.; Taylor, P. A.; Yates, J. T., Jr. *Surf. Sci.* **1987**, *184*, L332–L338.
(384) Wu, C. J.; Carter, E. A. *Phys. Rev. B* **1992**, *45*, 9065–9081.
(385) Li, Y. L.; Pullman, D. P.; Yang, J. J.; Tsekouras, A. A.; Gosalvez, D. B.; Laughlin, K. B.; Zhang, Z.; Schulberg, M. T.; Gladstone, D. J.; McGonigal, M.; Ceyer, S. T. *Phys. Rev. Lett.* **1995**, *74*, 2603–2606.
(386) Cheng, C. C.; Lucas, S. R.; Gutleben, H.; Choyke, W. J.; Yates, J. T., Jr. *J. Am. Chem. Soc.* **1992**, *114*, 1249–1252.
(387) Yates, J. T., Jr.; Cheng, C. C.; Gao, Q.; Colaianni, M. L.; Choyke, W. J. *Thin Solid Films* **1993**, *225*, 150–154.
(388) Koleske, D. D.; Gates, S. M. *J. Chem. Phys.* **1993**, *98*, 5091–5094.
(389) Boland, J. J. *Phys. Rev. Lett.* **1991**, *67*, 1539–1542.

CR940050K